

AD-A275 673



2

DOT/FAA/CT-93/69.II
DOT-VNTSC-FAA-93-13.II

FAA Technical Center
Atlantic City Airport,
NJ 08405

**Damage Tolerance
Assessment Handbook**
Volume II: Airframe Damage Tolerance Evaluation

DTIC
ELECTE
FEB 15 1994
A

Research and
Special Programs
Administration
John A. Volpe National
Transportation Systems Center
Cambridge, MA 02142-1093

Final Report
October 1993

This document has been approved
for public release and its
distribution is unlimited

This document is available to the public
through the National Technical Information
Service Springfield, Virginia 22161

94-05006



U.S. Department of Transportation
Federal Aviation Administration

60 3 14 647

NOTICE

This document is disseminated under the sponsorship of the Department of Transportation in the interest of information exchange. The United States Government assumes no liability for its contents or use thereof.

NOTICE

The United States Government does not endorse products or manufacturers. Trade or manufacturers' names appear herein solely because they are considered essential to the object of this report.

PAGES _____
ARE
MISSING
IN
ORIGINAL
DOCUMENT

REPORT DOCUMENTATION PAGE

Form Approved
OMB No. 0704-0188

Public reporting burden for this collection of information is estimated to average 1 hour per response, including the time for reviewing instructions, searching existing data sources, gathering and maintaining the data needed, and completing and reviewing the collection of information. Send comments regarding this burden estimate or any other aspect of this collection of information, including suggestions for reducing this burden, to Washington Headquarters Services, Directorate for Information Operations and Reports, 1215 Jefferson Davis Highway, Suite 1204, Arlington, VA 22202-4302, and to the Office of Management and Budget, Paperwork Reduction Project (0704-0188), Washington, DC 20503.

1. AGENCY USE ONLY (Leave blank)		2. REPORT DATE October 1993	3. REPORT TYPE AND DATES COVERED June 1990 - Dec. 1992
4. TITLE AND SUBTITLE Damage Tolerance Assessment Handbook Volume II: Airframe Damage Tolerance Evaluation			5. FUNDING NUMBERS FA3H2/A3128
6. AUTHOR(S)			
7. PERFORMING ORGANIZATION NAME(S) AND ADDRESS(ES) U.S. Department of Transportation Research and Special Programs Administration Volpe National Transportation Systems Center Kendall Square, Cambridge, MA 02142			8. PERFORMING ORGANIZATION REPORT NUMBER DOT-VNTSC-FAA-93-13.II
9. SPONSORING/MONITORING AGENCY NAME(S) AND ADDRESS(ES) Federal Aviation Administration Technical Center Atlantic City Airport NJ 08405			10. SPONSORING/MONITORING AGENCY REPORT NUMBER DOT/FAA/CT-93/69.II
11. SUPPLEMENTARY NOTES			
12a. DISTRIBUTION/AVAILABILITY STATEMENT This document is available to the public through the National Technical Information Service, Springfield, VA 22161			12b. DISTRIBUTION CODE
13. ABSTRACT (Maximum 200 words) This "Damage Tolerance Assessment Handbook" consists of two volumes: Volume I introduces the damage tolerance concept with a historical perspective followed by the fundamentals of fracture mechanics and fatigue crack propagation. Various fracture criteria and crack growth rules are studied. Volume II treats exclusively the subject of damage tolerance evaluation of airframes.			
14. SUBJECT TERMS Damage Tolerance, Fracture Mechanics, Crack Initiation, Fracture Toughness, Stress Intensity Factor, Residual Strength, Crack Propagation, Fatigue, Inspection.			15. NUMBER OF PAGES 200
			16. PRICE CODE
17. SECURITY CLASSIFICATION OF REPORT Unclassified	18. SECURITY CLASSIFICATION OF THIS PAGE Unclassified	19. SECURITY CLASSIFICATION OF ABSTRACT Unclassified	20. LIMITATION OF ABSTRACT

PREFACE

The preparation of this Handbook has required the cooperation of numerous individuals from the U.S. Government, universities, and industry. It is the outcome of one of the research programs on the Structural Integrity of Aging Aircraft supported by the Federal Aviation Administration Technical Center and performed at the Volpe Center of the Department of Transportation.

The contributions from the Federal Aviation Administration, the FAA Technical Center, the Department of Defense, and the staff of the Volpe Center are greatly acknowledged.

Please forward all comments and suggestions to :

U.S. Department of Transportation
Office of Systems Engineering, DTS-74
Volpe National Transportation Systems Center
Cambridge, MA 02142

Accession For	
NTIS	DTIC
USDA	USDA
USDA	USDA
By	
Distribution	
Approved for Release	
Dist	Approved for Special
A-1	

METRIC/ENGLISH CONVERSION FACTORS

ENGLISH TO METRIC

LENGTH (APPROXIMATE)

1 inch (in.)	= 2.5 centimeters (cm)
1 foot (ft)	= 30 centimeters (cm)
1 yard (yd)	= 0.9 meter (m)
1 mile (mi)	= 1.6 kilometers (km)

AREA (APPROXIMATE)

1 square inch (sq in., in ²)	= 6.5 square centimeters (cm ²)
1 square foot (sq ft., ft ²)	= 0.09 square meter (m ²)
1 square yard (sq yd., yd ²)	= 0.8 square meter (m ²)
1 square mile (sq mi., mi ²)	= 2.6 square kilometers (km ²)
1 acre	= 0.4 hectares (he) = 4,000 square meters (m ²)

MASS - WEIGHT (APPROXIMATE)

1 ounce (oz)	= 28 grams (gr)
1 pound (lb)	= 45 kilogram (kg)
1 short ton	= 2,000 pounds (lb) = 0.9 tonne (t)

VOLUME (APPROXIMATE)

1 teaspoon (tsp)	= 5 milliliters (ml)
1 tablespoon (tbsp)	= 15 milliliters (ml)
1 fluid ounce (fl oz)	= 30 milliliters (ml)
1 cup (c)	= 0.24 liter (l)
1 pint (pt)	= 0.47 liter (l)
1 quart (qt)	= 0.96 liter (l)
1 gallon (gal)	= 3.8 liters (l)
1 cubic foot (cu ft., ft ³)	= 0.03 cubic meter (m ³)
1 cubic yard (cu yd., yd ³)	= 0.76 cubic meter (m ³)

TEMPERATURE (EXACT)

$$[(x - 32)(5/9)]^{\circ}\text{F} = y^{\circ}\text{C}$$

METRIC TO ENGLISH

LENGTH (APPROXIMATE)

1 millimeter (mm)	= 0.04 inch (in)
1 centimeter (cm)	= 0.4 inch (in)
1 meter (m)	= 3.3 feet (ft)
1 meter (m)	= 1.1 yards (yd)
1 kilometer (km)	= 0.6 mile (mi)

AREA (APPROXIMATE)

1 square centimeter (cm ²)	= 0.16 square inch (sq in., in ²)
1 square meter (m ²)	= 1.2 square yards (sq yd., yd ²)
1 square kilometer (km ²)	= 0.4 square mile (sq mi., mi ²)
1 hectare (he)	= 10,000 square meters (m ²) = 2.5 acres

MASS - WEIGHT (APPROXIMATE)

1 gram (gr)	= 0.036 ounce (oz)
1 kilogram (kg)	= 2.2 pounds (lb)
1 tonne (t)	= 1,000 kilograms (kg) = 1.1 short tons

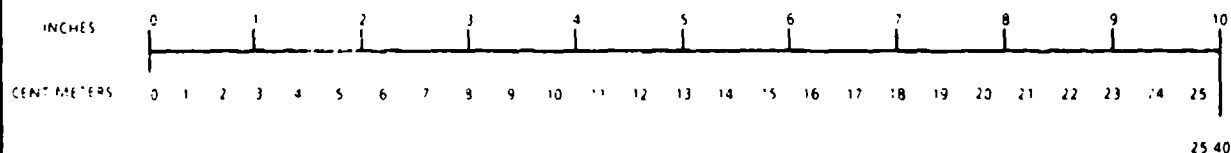
VOLUME (APPROXIMATE)

1 milliliter (ml)	= 0.03 fluid ounce (fl oz)
1 liter (l)	= 2.1 pints (pt)
1 liter (l)	= 1.06 quarts (qt)
1 liter (l)	= 0.26 gallon (gal)
1 cubic meter (m ³)	= 36 cubic feet (cu ft., ft ³)
1 cubic meter (m ³)	= 1.3 cubic yards (cu yd., yd ³)

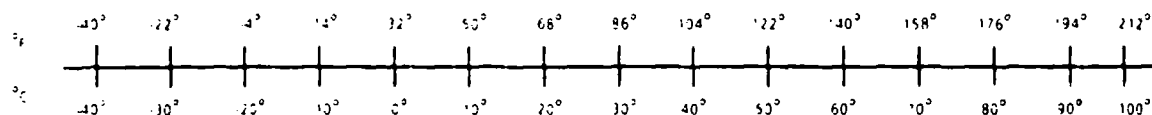
TEMPERATURE (EXACT)

$$[(9/5)y + 32]^{\circ}\text{C} = x^{\circ}\text{F}$$

QUICK INCH-CENTIMETER LENGTH CONVERSION



QUICK FAHRENHEIT-CELSIUS TEMPERATURE CONVERSION



For more exact and broader conversion factors, see NBS Miscellaneous Publication 286, Units of Weights and Measures. Price \$2.50. SD Catalog No. C13-10286.

TABLE OF CONTENTS

1.	INTRODUCTION	1-1
1.1	Historical Perspective	1-2
1.2	Results of Air Force Survey	1-12
1.3	Comparison of Old and New Approaches	1-13
1.3.1	Fatigue Safe-Life Approach	1-16
1.3.2	Damage Tolerance Assessment (DTA) Approach	1-25
2.	FRACTURE MECHANICS	2-1
2.1	Stress Concentration, Fracture and Griffith Theory	2-1
2.1.1	Fracture Modes	2-19
2.2	Extension of Linear Elastic Fracture Mechanics to Metals	2-21
2.2.1	Plastic Zone Size and the Mises-Hencky Yield Criterion	2-24
2.3	Fracture Toughness Testing	2-26
2.3.1	Thickness Effects	2-33
2.3.2	Temperature Effects	2-37
2.4	Failure in the Presence of Large-Scale Yielding	2-38
2.4.1	Resistance Curves	2-39
2.4.1.1	Graphical Construction of Thin-Section Strength Plots ..	2-43
2.4.2	The Net Section Failure Criterion	2-52
2.4.2.1	Failure Mode Determination and the Feddersen Diagram ..	2-54
2.4.3	Crack Opening Displacement	2-56
2.4.4	J-Integral	2-57
2.4.5	Practical Developments	2-58
2.4.6	Strain Energy Density Criterion	2-61
2.4.7	Plastic Collapse Model	2-64
2.5	Internal, Surface, and Corner Cracks	2-66
2.6	Environmental Effects	2-67

TABLE OF CONTENTS (continued)

3.	FATIGUE CRACK PROPAGATION	3-1
3.1	Energy-Based Theory of Crack Propagation	3-1
3.2	Empirical Crack Growth Rate Equations	3-3
3.3	Correlation with Material Properties	3-12
3.4	Crack Growth Life Estimates	3-32
3.4.1	Quick Estimates with Crack Geometry Sums	3-37
3.5	Interaction Effects and Retardation Models	3-38
4.	AIRFRAME DAMAGE TOLERANCE EVALUATION	4-1
4.1	Damage Tolerance Requirements for Transports	4-2
4.1.1	Basic Definitions	4-2
4.1.2	The Damage Tolerance Evaluation Process	4-2
4.1.2.1	Preparation Phase	4-5
4.1.2.2	Evaluation Phase	4-7
4.1.2.3	Inspectability Considerations	4-9
4.2	Identification of Structural Elements and Evaluation Locations	4-10
4.2.1	Wing and Empennage	4-12
4.2.2	Fuselage	4-18
4.3	Load Path Arrangement	4-33
4.3.1	Splices Parallel to the Major Stress Axis	4-34
4.3.2	Stiffeners as Crack Stoppers	4-41
4.3.3	Splices Across the Major Load Axis	4-51
4.3.3.1	Load Concentration and the Benefit of Fastener Flexibility	4-54
4.3.4	Repairs	4-65
4.4	Material Considerations	4-69
4.5	Type and Extent of Damage	4-73
4.6	Analysis and Tests	4-86

TABLE OF CONTENTS (continued)

4.6.1	Load Specification and Stress Analysis	4-86
4.6.1.1	Gust Load Factors (FAR 23.231 and FAR 25.341)	4-92
4.6.2	Residual Strength Evaluation	4-98
4.6.3	Crack Growth Life Evaluation	4-122
4.6.3.1	Modified Safe Life Based on Crack Growth	4-122
4.6.3.2	Damage Tolerance Evaluation Requiring Inspection ...	4-125
4.6.3.2.1	General Considerations for Nondestructive Inspection (NDI) Methodologies and the Inspection Intervals [Reference 4-13]	4-125
4.6.3.2.2	Time to First Inspection and Safe Inspection Interval	4-126
4.6.3.3	Safe Flight Time After Discrete Source Damage	4-129
4.6.3.4	Time to Loss of Fail-Safety	4-131
4.6.3.5	Verification of Crack Growth Life	4-135
4.6.3.5.1	Approximate Estimation of Spectrum Truncation Points	4-141
APPENDIX A - SELECTED STRESS INTENSITY FACTOR FORMULAE		A-1
APPENDIX B - SELECTED RESISTANCE (R-CURVE) PLOTS FOR AIRCRAFT MATERIALS		B-1

LIST OF ILLUSTRATIONS

1-1	Photograph of tanker Schenectady	1-3
1-2	Comet I aircraft, circa 1952	1-3
1-3	Probable Comet failure initiation site	1-4
1-4	USAF Tactical Air Command F-111A circa 1969.	
	(a) F-111 in flight	1-8
	(b) F-111, plan view showing probable failure initiation site	1-8
	(c) Crack in left wing pivot forging of F-111 aircraft	1-8
1-5	An aircraft fuselage failure	
	(a) General view, left side of forward fuselage	1-10
	(b) General view, right side of forward fuselage	1-10
1-6	Examples of distribution and magnitude of service cracking problems	1-14
1-7	Crack initiation, growth and failure mechanisms.	
	(a) 1226 major cracking/failure incidents	1-14
	(b) 64 major cracking/failure incidents	1-14
1-8	Cracking and failure origins	1-15
1-9	Results of a typical fatigue experiment	1-16
1-10	Effect of mean stress	1-18
1-11	Modified Goodman diagram	1-19
1-12	Goodman diagram for 2024-T4 aluminum	1-19
1-13	How the Palmgren-Miner rule is applied	1-21
1-14	Fatigue quality index	1-23
1-15	Uncertainties addressed by safety factor	1-24
1-16	Crack growth in response to cyclic loads	1-26
1-17	Schematic relationship of allowable stress versus crack length	1-26
1-18	Residual strength diagram	1-27
2-1	Circular hole in a large plate	2-2
2-2	Elliptical hole in a large plate	2-3
2-3	Energy principles.	
	(a) Slender rod	2-6
	(b) Uniformly stressed thin plate	2-6
2-4	Energy principles for cracked plate.	
	(a) Initial crack length $2a$	2-9
	(b) Elongated crack length $2(a + \Delta a)$	2-9
2-5	Plate with a center crack	2-11
2-6	Stress components in Irwin's analysis	2-14
2-7	Stress intensity factor formulae for some common geometries.	
	(a) Plate with center crack under tension	2-17
	(b) Plate with edge crack under tension	2-17
2-8	Fracture modes	2-20
2-9	Plastic zone formation ahead of crack tip	2-23

LIST OF ILLUSTRATIONS (continued)

2-10	Refined estimate of plastic zone formation ahead of crack tip	2-23
2-11	Plastic zone approximations based on von Mises criterion	2-25
2-12	The compact tension specimen	2-27
2-13	CTS stress intensity factor versus crack length	2-28
2-14	CTS orientation	2-29
2-15	Load-displacement plot	2-30
2-16	Thickness effect on fracture strength	2-33
2-17	Plane stress-plane strain transition.	
	(a) Three-dimensional plastic zone shape	2-35
	(b) Plastic volume versus thickness	2-35
2-18	Typical fracture surfaces	2-36
2-19	Lateral compression above and below the crack	2-37
2-20	Lateral buckling and tearing	2-38
2-21	Fracture toughness versus temperature	2-39
2-22	Load versus crack extension for different thicknesses	2-40
2-23	Experimental determination of R-curve	2-42
2-24	Dependence of K_{Ic} on crack length	2-43
2-25	K_I and K_{Rc} curves	2-44
2-26	K_I and K_{Rc} curves (logarithmic scale)	2-44
2-27	Overlay of K_I and K_{Rc} curves to determine critical crack length	2-45
2-28	R-Curve for 2024-T3	2-46
2-29	K applied versus crack length	2-47
2-30	Use of critical K to determine critical crack length	2-48
2-31	Critical stress determinations with K_I and K_{Rc} curves	2-49
2-32	K_{Ic} and σ_c vs. a for a 20-inch aluminum panel	2-50
2-33	Effect of surroundings on energy absorption rate.	
	(a) Isolated medium or long crack	2-51
	(b) Short crack	2-51
	(c) One crack tip near edge of a panel	2-51
2-34	Net section failure criterion	2-53
2-35	Net section and R-curve strength curves	2-54
2-36	Illustration of the width effect on thin sheet strength	2-55
2-37	Construction of Feddersen diagram	2-56
2-38	Typical examples of three-dimensional aspects of cracks.	
	(a) Corner crack at a fastener hole	2-60
	(b) Axial crack in an oxygen cylinder	2-60
	(c) Through-crack at a fuselage frame corner detail	2-60
2-39	Strain energy density criterion	2-63
2-40	Definition of critical strain energy density	2-63
2-41	Erdogan's plastic zone model	2-65

LIST OF ILLUSTRATIONS (continued)

2-42	Geometries of surface and corner cracks.	
	(a) Flaw shape parameter for surface flaws	2-68
	(b) Flaw shape parameter for internal flaws	2-68
2-43	Stress intensity factors for surface and corner cracks	2-69
2-44	Deep flaw magnification factor curves	2-70
3-1	Argument for relating fatigue crack growth rate to applied stress intensity factor	3-2
3-2	Effect of cyclic load range on crack growth in Ni-Mo-V alloy steel for released tension loading	3-3
3-3	Alternate definitions of stress cycle	3-5
3-4	Crack growth rate in 7475-T6 aluminum	3-7
3-5	Effect of stress ratio on 7075-T6 aluminum crack growth rate	3-9
3-6	Summary plot of da/dN versus ΔK for six aluminum alloys	3-13
3-7	Summary plot of da/dN versus ΔK for various steel alloys	3-15
3-8	Summary plot of da/dN versus ΔK for five titanium alloys	3-16
3-9	7075-T6 aluminum (0.09 in. thick) crack growth rate properties.	
	(a) Results for $R = 0$ and $R = 0.2$	3-17
	(b) Results for $R = 0.33$ and $R = 0.5$	3-18
	(c) Results for $R = 0.7$ and $R = 0.8$	3-19
3-10	7075-T6 properties (0.2 in. thick) from a different test series	3-22
3-11	2024-T3 aluminum (0.09 in. thick) properties.	
	(a) Results for $R = 0.1$ and $R = 0.11$ (different test series)	3-23
	(b) Results for $R = 0.33$	3-24
	(c) Results for $R = 0.5$	3-25
	(d) Results for $R = 0.7$	3-26
3-12	2014-T6 aluminum (0.25 in. thick) properties at $R = 0$	3-28
3-13	2014-T6 aluminum properties for different thickness and stress ratio	3-30
3-14	Effects of thickness and environment.	
	(a) Effect of thickness on FCP behaviour of 7475-T651 machined from 1-inch plate and tested in dry air	3-31
	(b) A comparison between the FCP rates in dry air and 3.5% NaCl solution for aluminum alloys	3-31
4-1	Structure of requirements and guidelines	4-4
4-2	Structural classification of an airframe	4-13
4-3	Wing box configuration and function	4-15
4-4	Stress in a wing box	4-16
4-5	Simplified fuselage model	4-19
4-6	Stress in a fuselage shell	4-21
4-7	Frame bending	4-23
4-8	Floor cross-beam function	4-23
4-9	Local bending of fuselage at floor	4-24
4-10	Typical bulkhead arrangement	4-26

LIST OF ILLUSTRATIONS (continued)

4-11	Bending stress distributions in a flat circular panel loaded by pressure.	
	(a) Panel model	4-28
	(b) Scaling functions for built-in support	4-28
	(c) Scaling functions for knife-edge support	4-28
4-12	Floor panel and bulkhead evaluation sites	4-29
4-13	Cutaway view of window detail	4-31
4-14	Vickers Viscount circa 1953	4-32
4-15	Static overload after panel failure	4-35
4-16	Damage in a fail-safe panel assembly	4-37
4-17	Ship-lap planks with integral stiffeners	4-37
4-18	Crack model and stress intensity factor	4-39
4-19	Demonstration of crack arrest	4-42
4-20	Fastener design constraints	4-43
4-21	Stringer/skin ratio	4-44
4-22	Definition of fuselage tolerance to discrete source damage	4-46
4-23	Frame collapse mechanism	4-47
4-24	Comparison of old and new design details	4-49
4-25	Offset frame with tear strap	4-50
4-26	Examples of splice details.	
	(a) Lap splice over fuselage stringer	4-52
	(b) Butt splice over fuselage stringer	4-52
	(c) Chordwise butt splice at skin thickness drop in a wing box	4-52
4-27	Examples of pitch change and taper.	
	(a) Lap joint with pitch change between rows	4-53
	(b) Tapered "finger" doubler with outer row pitch doubled	4-53
4-28	Plan view and section of a lap splice model	4-54
4-29	Free-body diagram of left half of splice	4-55
4-30	Re-assembled splice section with stresses and forces summarized	4-55
4-31	Fastener shear model	4-56
4-32	Before and after deformation schematic	4-58
4-33	Load transfer in a bonded lap splice	4-61
4-34	Eccentric bending effects in a lap splice	
	(a) Eccentric bending reduces offset	4-62
	(b) Edge of bend stresses in tension	4-62
4-35	Effect of interference fit	4-63
4-36	Galvanic corrosion	4-64
4-37	Damaged skin with repair patch.	
	(a) Conventional single doubler	4-66
	(b) Stepped inside/outside doubler	4-66
4-38	Rivet load distribution in a single doubler	4-67
4-39	Comparison of rivet load distributions in stepped and single doublers	4-68
4-40	Chip-drag damage in dissimilar metal stack	4-72
4-41	Section through rivet showing debris between faying surfaces	4-74

LIST OF ILLUSTRATIONS (continued)

4-42	Striation mechanism and appearance	4-77
4-43	Derived initial size distribution for average quality cracks	4-78
4-44	Specifications for average quality initial crack	4-79
4-45	Specifications for rogue initial crack	4-79
4-46	Uses of initial crack specifications	4-80
4-47	Effect of access on detectable size.	
	(a) Butt splice	4-82
	(b) Ship-lap splice	4-82
4-48	Crack detectability for different doubler designs.	
	(a) External	4-83
	(b) External/finger	4-83
	(c) Internal/external	4-83
4-49	Examples of crack detection probability curves	4-85
4-50	Airplane load factor for coordinated level turns	4-87
4-51	Example of construction of maneuver spectrum from time history	4-89
4-52	Effect of spanwise location on ground-air-ground cycle	4-91
4-53	L-1011 airplane load factor record	4-94
4-54	Comparison of different counting methods	4-96
4-55	L-1011 exceedance curves for different altitude bands.	
	(a) -500 to 4500 MSL	4-99
	(b) 4500 to 9500 MSL	4-99
	(c) 9500 to 14500 MSL	4-100
	(d) 14500 to 19500 MSL	4-100
	(e) 19500 to 24500 MSL	4-101
	(f) 24500 to 29500 MSL	4-101
	(g) 29500 to 34500 MSL	4-102
	(h) 34500 to 39500 MSL	4-102
	(i) 39500 to 44500 MSL	4-103
4-56	Comparison of composite exceedance curves from four airplanes (all altitudes).	
	(a) L-1011	4-104
	(b) B-727	4-104
	(c) B-747	4-105
	(d) DC-10	4-105
4-57	Panel stress analysis	4-107
4-58	Construction of skin fracture strength plot.	
	(a) R-curve analysis	4-109
	(b) Strength plot	4-109
4-59	Panel strength diagram	4-110
4-60	Panel failure due to stringer overload	4-111
4-61	Panel strength diagram indicating marginal fail-safety	4-112
4-62	Simulated rivet load-displacement curve	4-114
4-63	Basic stress intensity factors used in compatibility model	4-116

LIST OF ILLUSTRATIONS (continued)

4-64	Finite element concept.	
	(a) Bar viewed in natural reference frame	4-118
	(b) Bar viewed in global reference frame	4-118
4-65	Finite element estimate for skin stress intensity factor	4-120
4-66	Use of continuing damage to evaluate safe crack growth life in single path structure.	
	(a) Rogue flaw in a long ligament	4-124
	(b) Rogue flaw in a short ligament	4-124
4-67	Evaluation of bases for time to first inspection and safe inspection interval for multiple path structure	4-128
4-68	Evaluation of safe crack growth life after discrete source damage	4-130
4-69	Two-stage evaluation of pressurized structure	4-132
4-70	Determination of critical crack length for time to loss of crack arrest capability	4-134
4-71	Determination of critical adjacent-bay MSD crack length for time to loss of crack arrest capability	4-135
4-72	Preparation of corner crack test coupon	4-137
4-73	Test spectrum sequences	4-141
4-74	Airplane load factor and the stress spectrum	
	(a) Airplane load factor	4-142
	(b) Stress spectrum	4-142
4-75	Truncation frequency estimation	4-143

LIST OF TABLES

2-1	Properties of some common structural materials	2-31
4-1	Basic definitions	4-3
4-2	Structure classification checklist	4-11
4-3	Metal selection criteria	4-70
4-4	Galvanic series in sea water	4-75
4-5	Currently available NDI methods	4-84
4-6	Expected advances in nondestructive inspection technology	4-85
4-7	Crack growth life evaluation criteria	4-123

CHAPTER 4:

**AIRFRAME
DAMAGE TOLERANCE
EVALUATION**

4. AIRFRAME DAMAGE TOLERANCE EVALUATION

FAR 25.571 establishes the damage tolerance requirements for transport category airplanes. FAR 25.571(a) begins with the statement: *"An evaluation of the strength, detail design, and fabrication must show that catastrophic failure due to fatigue, corrosion, or accidental damage, will be avoided throughout the operational life of the airplane. ..."* This is a good definition of the meaning of airframe damage tolerance. This chapter deals with the application of fracture mechanics and crack propagation concepts to assess how well an airframe will tolerate fatigue cracking, with corrosion effects included where applicable¹, or accidental damage.

Another area for consideration involves repairs. Most major airframe repairs are made in accordance with detailed specifications set forth in the structural repair manual (SRM) published by the manufacturer. Minor repairs are made in accordance with either SRM general guidelines or established metalworking practices. Both major and minor repairs generally involve the application of doubler patches over original skin or spar caps to reinforce areas where fatigue or corrosion damage is anticipated or has been found and removed. Past practice has generally been to design such repairs based on static strength, i.e., to restore the capability of the repaired area to sustain the limit and ultimate loads for which the airframe was originally certified. However, it may be useful to consider the design of airframe repairs from a damage tolerance viewpoint.

How is airframe structure certified for compliance with the damage tolerance requirements? The FAA has established guidelines in Advisory Circular 25.571-1A for manufacturers seeking certification of transport category airplanes. These guidelines are quite general because *"... it is recognized that in such a complex field new design features and methods of fabrication, new approaches to the evaluation, and new configurations could necessitate variations and deviations from the procedures described in this advisory circular. ..."* (AC 25.571, para. 5a).

This chapter discusses the relationships between FAR Part 25, AC 25.571-1A, and some of the more commonly used damage tolerance evaluation methods. It is intended primarily as a training

¹ The effect of corrosion by itself must also be considered. This subject is addressed separately in the FAA Corrosion Control Handbook.

guide for FAA flight standards engineers who are responsible for certification review. Section 4.1 summarizes the regulatory structure and its relation to the logical steps in a damage tolerance evaluation. The succeeding sections develop these steps in detail, with the aid of illustrative examples.

4.1 DAMAGE TOLERANCE REQUIREMENTS FOR TRANSPORTS

4.1.1 Basic Definitions

The definitions of terms given in Table 4-1 are established in AC 25.571-1A. Most of these definitions reflect conventions accepted in the aircraft industry. The reader should become familiar with them to facilitate review of certification documents and discussion with applicants.

4.1.2 The Damage Tolerance Evaluation Process

Figure 4-1 depicts the relations between AC 25.571-1A, the relevant sections of FAR Part 25, and the tasks required in a damage tolerance evaluation. Starting at the upper left, FAR 25.571(a) sets forth a general requirement for evaluation but also provides for exceptions.

The exceptions specified in FAR 25.571(c) are defined on the basis that it may be impractical to design some components for damage tolerance without coming into conflict with other design requirements. In such cases, it is the applicant's responsibility to establish for each exception that a damage tolerance evaluation is impractical because "*... it entails such complications that an effective damage tolerant structure cannot be achieved within the limitations of geometry, inspectability, or good design practice. ...*" (AC 25.571-1A, para. 5a{2}). FAR 25.571{d} also allows an exception for structure subject to sonic damage. All such structures on turbojet aircraft must be evaluated, but the choice between the damage tolerant or safe-life design is left to the applicant's discretion. All exceptions must be qualified as safe-life designs in accordance with paragraph 7 of the AC.

Table 4-1. Basic definitions.

Damage tolerance means that the structure has been evaluated to ensure that should serious fatigue, corrosion, or accidental damage occur within the operational life of the airplane, the remaining structure can withstand reasonable loads without failure or excessive structural deformation until the damage is detected.

Fail-safe means that the structure has been evaluated to assure that catastrophic failure is not probable after fatigue failure or obvious partial failure of a single, principal structural element.

Safe-life means that the structure has been evaluated to be able to withstand the repeated loads of variable magnitude expected during its service life without detectable cracks.

Principal structural elements are those which contribute significantly to carrying flight, ground, and pressurization loads, and whose failure if it remained undetected could result in catastrophic failure of the airplane.

Critical structural elements are those elements whose failure, if remained undetected, would result in catastrophic failure of the airplane.

Primary structure is that structure which carries flight, ground, or pressure loads.

Secondary structure is that structure which carries only air or inertial loads generated on or within the secondary structure.

Single load path is where the applied loads are eventually distributed through a single member within an assembly, the failure of which would result in the loss of the structural integrity of the component involved.

Multiple load path is identified with redundant structures in which (with the failure of individual elements) the applied loads would be safely distributed to other load carrying members.

Reliability refers to detail designs or methodologies which service history has demonstrated to be reliable.

Probability refers to a probability of occurrence of an event consistent with past successful experience.

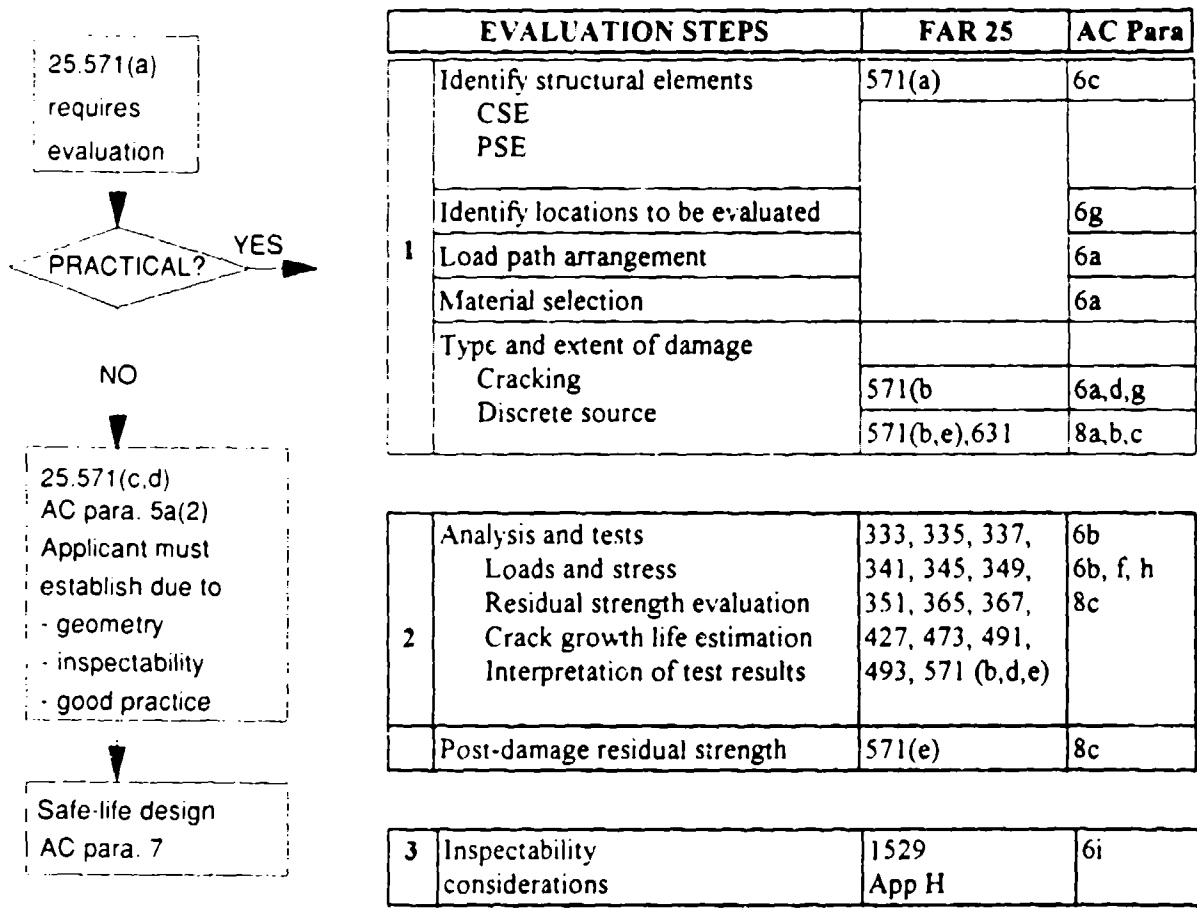


Figure 4-1. Structure of requirements and guidelines.

What makes a good case for an exception? It will be easier to answer this question after discussing the evaluation of structures which can be designed for damage tolerance. The topics of exceptions and fail-safe design will be revisited in the final section of this chapter.

The remainder of Figure 4-1 shows the damage tolerance evaluation process broken down into eight tasks arranged in a logical sequence. The tasks are also grouped into three phases: (1) preparation; (2) evaluation; and (3) inspectability considerations. The regulations and paragraphs of the AC pertinent to each task appear in the two columns at the right.

The illustrated sequence provides a convenient framework for presenting the subject matter but is not unique. Indeed, any damage tolerance specialist picked at random and asked to describe the evaluation process would likely define a different sequence. Such disagreement simply reflects the fact that damage tolerance evaluation is a design process, i.e., an art rather than an exact science. Whatever sequence one uses, its most important function is to serve as a checklist.

Like any design process, damage tolerance evaluation also has an iterative character because the various tasks influence each other. Whether designing or reviewing for compliance, one should be prepared to skip back and forth, revisiting earlier tasks or anticipating the feedback effects of later tasks, to focus attention where most needed.

4.1.2.1 Preparation Phase

The preparation phase has been arranged with the idea in mind that an entire airframe is to be evaluated. Damage tolerant design is usually practical for most of the primary structure in a transport category airframe. Therefore, it is logical to begin by examining the entire airframe to identify its principal structural elements (PSEs) and critical structural elements (CSEs). In general, some level of evaluation is required for all of these elements, with relatively more attention paid to the CSEs.

The degree of attention devoted to a structural element is reflected by the number of locations selected for evaluation. The attention should be proportionate to the perceived consequences of a failure in the element. The locations selected for a CSE should exhaustively cover the possible failure sites. For a PSE, the selection may cover all or nearly all sites if the perceived risk is high, or only one or two typical sites might be selected if the perceived risk is low.

The next three steps, which complete the preparation phase, represent a deeper level in the process of deciding how much attention should be paid to a structural element. Single load path structure evidently poses a greater perceived risk than does multiple load path structure with

built-in crack stoppers. Conversely, a multiple load path structure has more potential sites from which a failure might start.

The effects of material selection are much less obvious but equally important. The advice given to the applicant is simply to consider the use of " ... *Materials and stress levels that, after initiation of cracks, provide a controlled slow rate of crack propagation combined with high residual strength; ...* " (AC 25.571, para. 6a(2)). This is important guidance, but an equally important aspect of material selection is the degree of corrosion protection achieved or, conversely, the potential for corrosion-initiated cracking.

The final preparatory task is to decide upon the type and extent of damage which should be considered for each location to be evaluated. Where are the most likely crack origins? Should more than one crack at a time be considered and, if so, in what sequence? The answers to these questions depend on the load path arrangement and material selection. Additional guidance is available from the service histories of components with similar design features in existing aircraft. "Discrete source" (accidental) damage must also be considered, as specified in FAR 25.571(b)(5) and (e) and discussed in paragraph 8 of the AC. These provisions refer to the kinds of accidental damage which can be caused by bird strikes or uncontained failures of rotating machinery on-board the aircraft.

The documents submitted by an applicant should cover the preparatory data, assumptions, and engineering judgements. The flight standards engineer should review these items to verify that they are reasonable and complete.

All the factors that affect the susceptibility of the PSEs to undetected catastrophic failure should be evaluated. Accessibility, gross stress levels, load path redundancy and strength, susceptibility to corrosion, material selection, etc. all can be rated to determine the overall criticality of a specific PSE. This can minimize the number of PSEs requiring analysis.

4.1.2.2 Evaluation Phase

The evaluation phase consists of the analyses and tests required to demonstrate that each CSE and PSE complies with each applicable damage tolerance criterion. The criteria fall into two general categories: residual strength and life.

For the most severe type and extent of damage anticipated, the residual strength of the damaged structure must exceed the maximum stress which the structure can be reasonably expected to sustain from the time that the damage becomes evident until the airplane can be landed for repair. This category includes assessment of discrete-source damage tolerance and may also include the definition of critical sizes for propagating cracks. Critical sizes are defined as limits beyond which the integrity of the structure cannot be guaranteed.

Under the average stresses repeatedly applied in service, a propagating crack must not reach critical size during the service life of the airplane. The interpretation of this criterion depends on inspectability. If the structure is not inspectable, slow crack growth life from an initial size assumed to represent fabrication damage becomes the determining factor. A similar criterion is also used to establish the time to start inspecting those structures which can be inspected. For inspectable structures, the inspection interval in flights or flight hours is based on slow crack growth life from an initial size assumed to be reliably detectable with high probability, in accordance with the specified inspection procedure.

Both the average repeated stresses (spectra) and the maximum stresses depend on flight and ground loads, which must be established in accordance with the airworthiness standards for the airplane flight envelope and design speeds (FAR 25.333 and 335) and specific conditions defined in the other pertinent sections of Part 25 (see Figure 4-1). The maximum stresses generally correspond to loads specified relative to the airplane's limit-load strength requirements (FAR 25.301{a}). However, the 1.5 factor of safety on limit load specified for the general definition of ultimate load (FAR 25.303) does not apply to the residual strength damage tolerance criteria.

Instead, factors on limit load between 0.7 and 1.1 are specified or recommended for various purposes (FAR 25.571 {b,e} and AC 25.571-1A para. 8c {1,2}).

The stress spectra used for life evaluation are derived from load spectra representing the different phases of typical flights. They may also be used to define maximum stresses for critical crack size determination.

Evaluation of resistance to sonic damage is also required for the affected structure on all transport category airplanes (FAR 25.571 {d}), unless the applicant has chosen the safe-life approach. In either case, sonic stress spectra are necessary for the evaluation.

Separate special consideration must be given to the evaluation of discrete-source damage tolerance. The accident scenarios specified in FAR 25.571 {e} implicitly assume major structural damage, to an extent such that the residual static strength of the damaged area may no longer meet the requirements of FAR 25.301 {a}. It can reasonably be assumed that such an event will be immediately evident to the flight crew, who will quickly execute appropriate emergency procedures, including avoidance of turbulence and restriction to maneuvers well inside the aircraft flight envelope. Since the residual strength criterion for the accident itself is based on unaccelerated flight loads (with a modest factor of safety), further evaluation is required to demonstrate that the airframe can continue to contain the damage under moderately accelerated conditions during altitude recovery and descent to a landing.

The evaluation of residual strength is based upon the fracture and plastic collapse resistance properties of the material and structure described in Chapter 2. The evaluation of slow crack growth life is based upon the crack propagation characteristics described in Chapter 3.

The flight standards engineer should review the sources of data for load and stress spectra and for material and structure properties. The objectives of the review are to verify that the results of supporting tests have been properly interpreted for the purposes of the evaluation and that reliable methods of analysis have been employed. An applicant's evaluation of an entire transport

category airframe contains a large volume of test and analysis reports, typically covering 50 to 150 CSEs and PSEs. In order to be practical and avoid undue delay of the certification process, the flight standards engineer should approach this part of the review as a series of spot checks to assess key questions and issues.

4.1.2.3 Inspectability Considerations

The consideration of inspectability has been placed at the end of the evaluation sequence based on the logic of the design process. How often and by what means a structural element can be inspected depends strongly on the element's design details and its physical relation to other parts of the airframe. The reliability of the information available about these factors may be low at the beginning of the design process and will only approach certainty late in the design cycle, when the configuration is frozen, mock-ups have been built, and production drawings are being issued.

The ultimate objective of this phase is to provide the basis for the manufacturer's recommended inspection program, including compliance with the standards for continued airworthiness (FAR 25.1529 and FAR 25 Appendix H). For a good damage tolerant design, inspectability should be a major consideration. Therefore, it is important to make every effort up front to ensure that splices, joints, or built-up sections are inspectable. The consideration of integral wing skin stiffeners, which way to face channel sections, or various other concepts should be addressed early on. Allowance for access panels where necessary should be done as early as possible. These efforts early in the design cycle will make it easier for the manufacturer to meet the objective of establishing an appropriate inspection program at later stages.

The same inspectability factors should be used to establish the initial crack sizes which are presumed to be reliably detectable for the purposes of evaluating slow crack growth life and defining safe inspection intervals. This will most likely require the applicant to reevaluate some initial crack size assumptions before submitting the final analysis in support of certification. The flight standards engineer should pay close attention to the assumptions, in order to verify that they

are reasonable and consistent with the recommended inspection program and continued airworthiness plan.

4.2 IDENTIFICATION OF STRUCTURAL ELEMENTS AND EVALUATION LOCATIONS

The identification of structural elements should begin with a review of the following four basic definitions repeated from Table 4-1:

Principal structural elements are those which contribute significantly to carrying flight, ground, and pressurization loads, and whose failure, if it remained undetected could result in catastrophic failure of the airplane.

Critical structural elements are those elements whose failure would result in catastrophic failure of the airplane.

Primary structure is that structure which carries flight, ground, or pressure loads.

Secondary structure is that structure which carries only air or inertial loads generated on or within the secondary structure.

These definitions provide some useful guidelines, but they give no easy clues about how to accomplish the identification. Evidently, primary structure ought to consist of PSEs and CSEs, but what should the breakdown be, and what about secondary structure? The answers to these questions depend upon analysis of function and judgement of failure consequences. The approach to getting the answers should begin with a checklist that covers the entire airframe.

Paragraph 6c of AC 25.271-1A provides such a checklist, which is described as containing typical examples of PSEs. That list is expanded and presented in Table 4-2 below as a structure classification checklist. The more general description is used here to allow for designation of CSEs as well as PSEs, and to allow for the classification of as secondary (based on function) but also either PSE or CSE (based on failure consequences).

Table 4-2. Structure classification checklist.*

WING AND EMPENNAGE:

Control surfaces, slats, flaps, |spoilers, and their mechanical systems
and attachments (hinges, tracks, and fittings);
Integrally stiffened plates;
Primary fittings;
Principal splices;
Skin or reinforcement around cutouts or discontinuities;
Skin-stringer combinations,
Spar caps;
Spar webs;
|Spar "kick" details in swept wings.

FUSELAGE:

Circumferential frames and adjacent skin;
Door frames;
Pilot window posts;
Pressure bulkheads;
Skin and any single frame or stiffener around a cutout;
Skin and/or skin splices under circumferential loads;
Skin and/or skin splices under fore-and-aft loads;
Skin around a cutout;
Skin and stiffener combinations under fore-and-aft loads;
Door skins, frames, and latches;
|Floor skins and beams;
Window frames.

LANDING GEAR AND THEIR ATTACHMENTS:

|Trunnions;
|Main struts (inner and outer parts).

ENGINE MOUNTS:

|Struts;
|Thrust links;
|Pitch and yaw reaction force fittings;

|ENGINE CONTAINMENTS AND CASINGS

* From AC 25.571-1A, para. 6c, except as noted.

| Added.

According to T. Swift [4-1], an average of 150 areas are considered critical stress areas and need to be evaluated for crack propagation. The number is often reduced to about 90 PSEs by area similarity. He also proposed the following selection criteria for PSEs:

- Elements in tension or shear
- Low static margin
- High stress concentration
- High load transfer
- High spectrum density
- High stresses in secondary members after primary member failure
- Materials with high crack growth rates
- Areas prone to accidental damage
- Component test results
- Results of full-scale fatigue test

Figure 4-2 illustrates a hypothetical example of a transport airframe classification, based on the checklist. (Some items have been omitted for clarity.) Some of the decisions shown in the figure are obvious and would agree with the classifications assigned by most manufacturers. Others are not obvious and could be classified differently by different manufacturers, depending on factors such as the airframe configuration and airplane flight characteristics. The rationale for various decisions is best made clear by means of illustrative examples. As each example is presented, additional discussion will address the task of identifying locations for evaluation.

4.2.1 Wing and Empennage

The main structural boxes in the wings, horizontal stabilizers, and vertical stabilizer are primary structures which possess generally similar configuration and function. The pressure loads on each corresponding pair of aerodynamic surfaces (upper and lower) are gathered chordwise to the box and then carried spanwise to the fuselage.² The net upward load is the difference between the

² Depending on the design, the load may be routed across the fuselage either through major attachment fittings into heavy frames or via a center "carry-through" box.

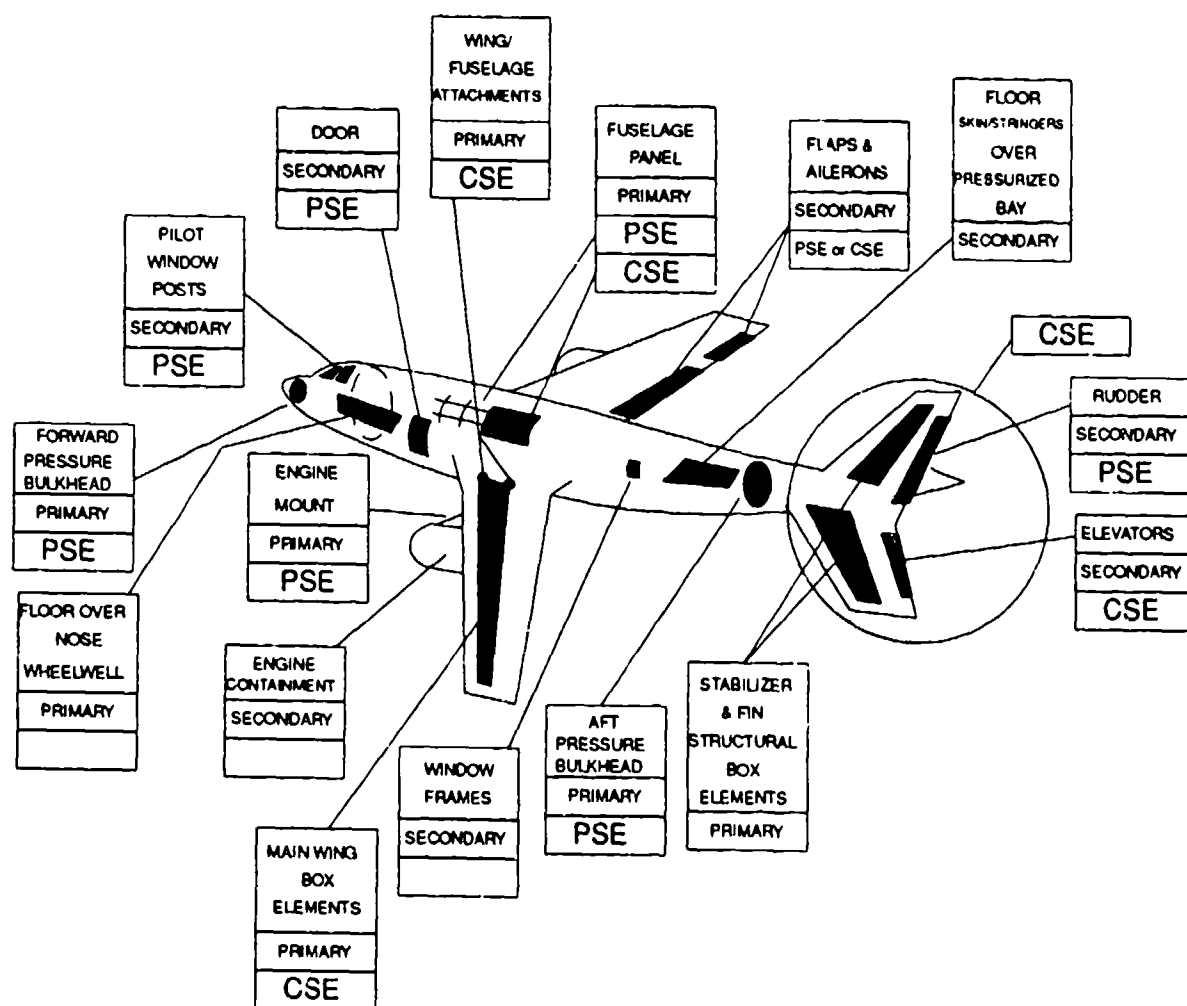


Figure 4-2. Structural classification of an airframe.

aerodynamic lift and the downward acting wing weight (structure, fuel and wing-mounted engines). The box bends and shears upward due to the spanwise load and also twists nose-up

because the center of pressure is offset forward of the elastic axis (Figure 4-3). The aerodynamic drag loading also bends and shears the box aft, but the effect on stresses is small when compared with the effects of upward deflection and twisting.

The resulting stresses are compression in the upper components, tension in the lower components, and shear in the skins and webs. A transport wing box is generally designed to make the most efficient possible use of stressed-skin construction because transport aircraft are designed for high wing loadings to cruise at high speeds. An exploded view of one corner of the box (Figure 4-4) shows how the stresses act on the lower panel (skin, spar caps, and webs). The schematic also shows how the shear associated with twist is carried from the skin through the front spar cap to the front web. (The webs also carry the shear associated with upward bending.) Each fastener participates by exerting equal and opposite bearing loads on the components which it joins.

Similar systems of forces act at splices and repair patches. Spanwise skin splices transfer shear from one skin panel to the next via equal and opposite fastener bearing loads. Chordwise splices transfer both tension (in the lower skin) and shear in a similar manner. Fastener bearing is also the mechanism for diverting some of the skin stress through the doubler in a repair patch.

The wing box lower panel acts as a unit carrying the tension due to bending. A failure of the panel would immediately separate the wing from the aircraft, which would then enter an uncontrollable roll. Thus, the lower panel is an obvious CSE.

What about the empennage? The spars in a stabilizer structural box are often designed to carry a greater proportion of the bending load, in relation to the skins, because the stabilizer dimensions are much smaller and stabilizer loadings are generally much lower than wing loadings.

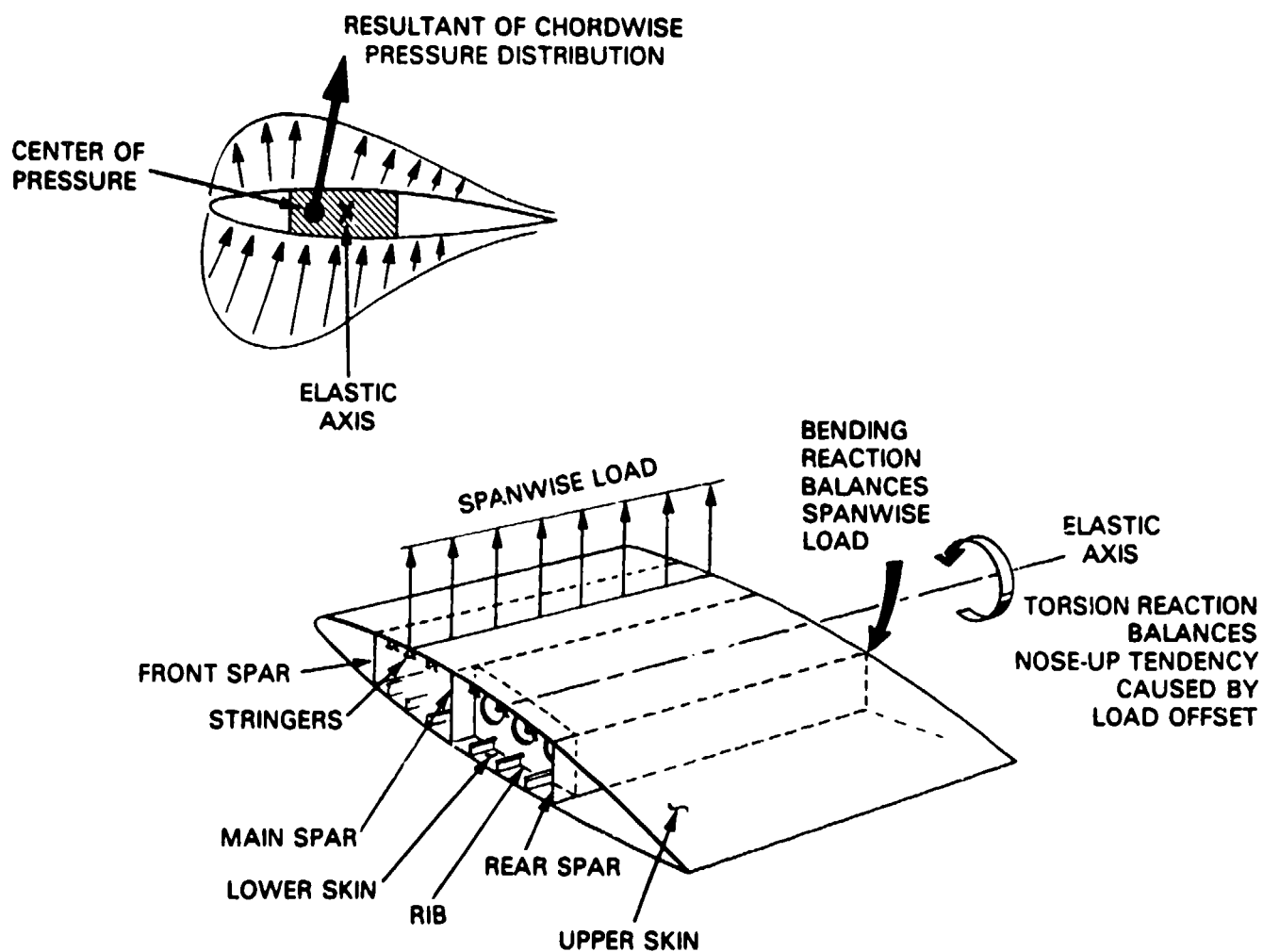


Figure 4-3. Wing box configuration and function.

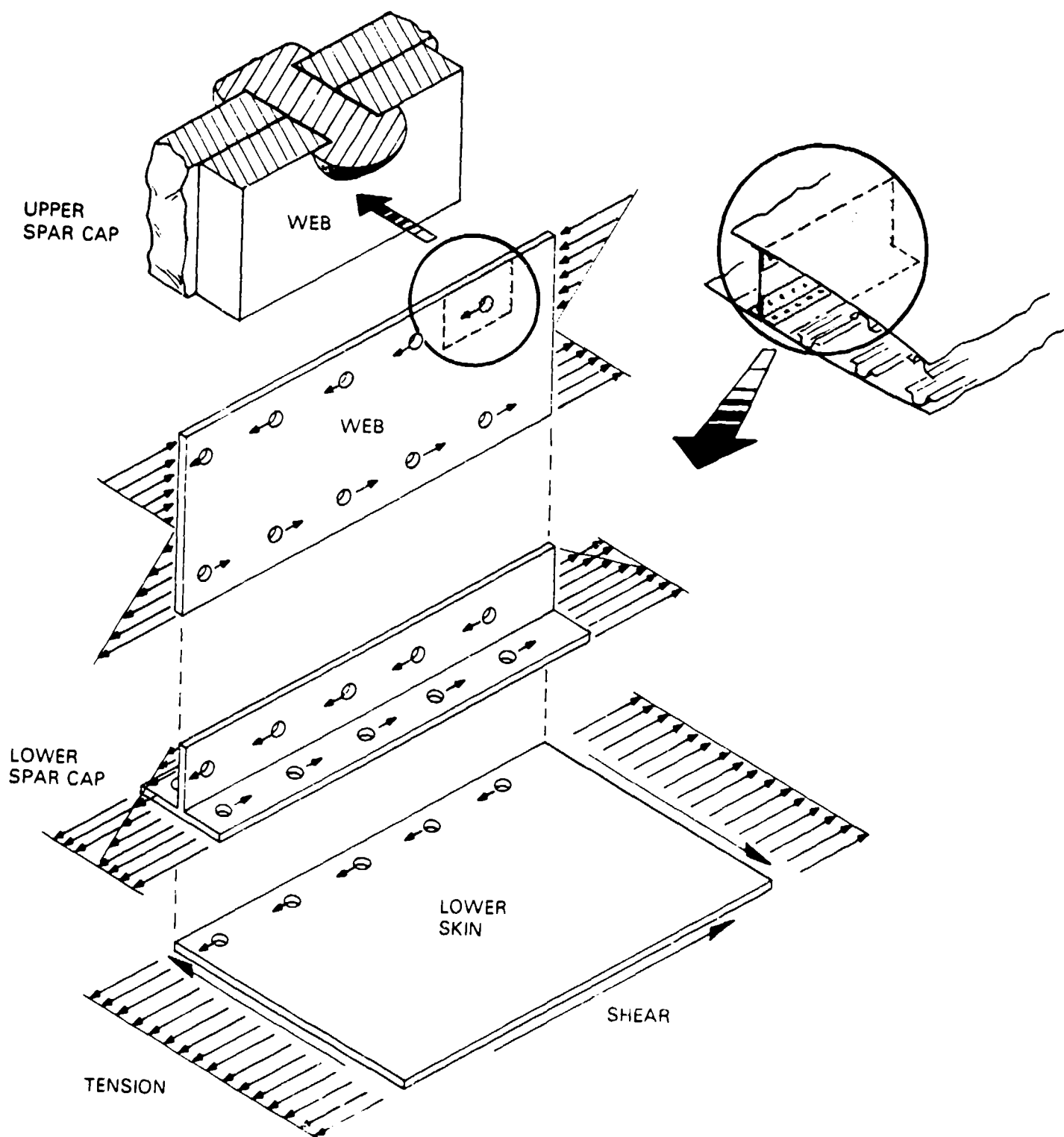


Figure 4-4. Stress in a wing box.

The horizontal stabilizers are normally under down load to maintain pitch trim³, so attention must be paid to the upper panel (or simply the spar caps in a small stabilizer). Loss of one side would cause an immediate nose-down pitch; it is also likely that the damage would prevent control of the elevator on the other side, leaving the aircraft in an unrecoverable dive.

It is not so easy to predict what will happen if the vertical stabilizer fails, since it does not normally bear any significant trim load. The consequent immediate loss of the rudder is serious but not necessarily fatal. Case studies suggest that judgements based on specific aircraft configurations and characteristics (under-wing versus fuselage-mounted engines, coupling between yaw and roll modes, spiral divergence rate, etc.) should determine whether the vertical stabilizer is a PSE or CSE.

The fittings which attach wings and stabilizers to the fuselage continue the carriage of major flight loads. Therefore, these attachments are also primary structure and, for the most part, critical elements.

Conversely, the control surfaces are secondary structure because they carry only their own self-generated air loads. Elevators are obvious CSEs, and rudders can be argued either way, for the same reasons just given in the discussion of primary structure panels. Flaps, slats, ailerons, and spoilers are probably in the PSE category; in any case, the decision should depend on the specific control system design. Do normally operating spoilers provide adequate roll control if one aileron is lost? Can the spoiler control be disabled (spoilers stowed) and the airplane flown with ailerons alone if spoilers are lost on one side? If flaps and/or slats are lost on one side, can the airplane be landed flaps-up, or does the spoiler/aileron system have enough roll control authority to keep the wings level in a partially deployed split-flap situation? Positive answers to questions like these would suggest PSE or lower classification.

³ Unconventional designs with canard stabilizers are loaded upward.

4.2.2 Fuselage

The stressed-skin stiffened shells that form transport aircraft fuselages are primary structures in which panel assemblies again play a major role as structural elements. Most fuselage panels would probably be classified as PSEs, based on the history of aircraft accidents caused by fuselage panel failures. In some cases, the remaining structure prevented in-flight breakup and gave the flight crew enough margin to land at the nearest airport.

How did these fuselages manage to hold together under circumstances that would have led to immediate in-flight breakup, had the failure occurred in a wing box panel? One reason is that a fuselage panel failure quickly relieves the pressurization. A second reason is that the pressure design limit load requirements may lead to structure that is overdesigned for the bending that a damaged fuselage must still continue to carry due to the weight of its own structure plus equipment and payload.

On the fuselage crown at a station over the wing attachments, the axial stress due to bending can approach the magnitude of the pressurization stress. A simplified model, which overestimates the bending stress, is summarized below to illustrate this point. This part of the crown area is usually designed with some local reinforcement, in any case, to accommodate the transfer of major loads between the wing and fuselage.

The ratio of maximum bending stress to pressure hoop stress can be quickly estimated by treating the fuselage as a circular cylinder of radius R , thickness t , and length L loaded by a total weight W distributed uniformly along its length and supported at mid-length, where the wing-fuselage attachments are assumed to be concentrated (Figure 4-5). The effect of stiffeners is neglected. Based on simple beam theory, the maximum bending stress is then given by:

$$\sigma_B = \frac{WL}{8\pi R^2 t} \quad (4-1)$$

The pressure hoop stress is:

$$\sigma_p = \frac{PR}{t} \quad (4-2)$$

where P is the internal pressure. Combining these two formulas leads to the ratio:

$$\frac{\sigma_B}{\sigma_p} = \frac{WL}{8\pi PR^3} \quad (4-3)$$

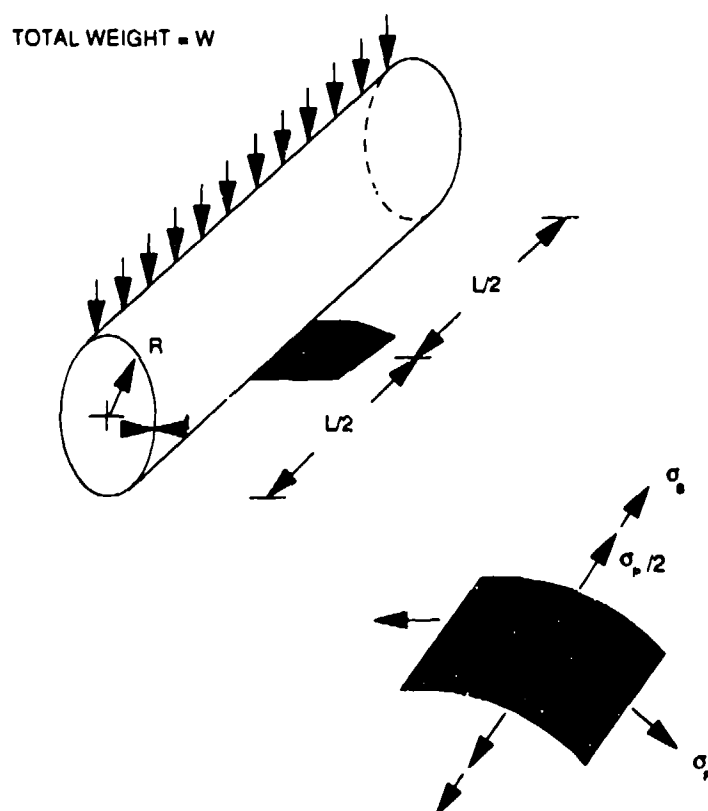


Figure 4-5. Simplified fuselage model

The following results are based on published nominal dimensions and weights of several typical transport airplanes. A pressure $P = 9$ psi was assumed, and the model weight was estimated as:

$$W \cong W_{ZF} - 0.2W_G \quad (4-4)$$

where W_{zf} and W_G are the maximum zero fuel weight and the maximum gross weight respectively.

Model	$W(lb)$	$L(in)$	$R(in)$	σ_B/σ_P
737-300	77,300	1,315	75.4	1.05
747-200B	359,900	2,702	126.5	2.12
757-200	134,000	1,858	74.3	2.68
L-1011-500	236,000	1,970.5	113.5	1.40
DC-9 Super 80	88,600	1,626	64.0	2.43
DC-8 Super 61	111,500	2,249	75.8	2.54

The bending stress is much lower at other locations. At any fuselage station, it decreases in linear proportion to vertical distance below the crown, passing through zero at about the fuselage mid-height and changing to compression in the lower half of the fuselage. It also decreases fore and aft of the wing attachments, in approximate proportion to the square of distance from the station considered to the nose or tail cone. Conversely, the pressurization stresses are approximately constant over the mid-body section, where the fuselage shape is close to a circular cylinder.

The pressure stresses are thus the dominant components over most of the fuselage. The design limit and ultimate load factors for pressurization (FAR 25.365) can thus provide a margin of safety in bending, even after the fuselage has been severely damaged, as long as the aircrew can keep the aircraft close to unaccelerated flight until landing. It is logical to rely on the accident history and to classify most of the pressurized fuselage structure as PSEs. However, the CSE classification should be considered for panels near the wing-fuselage attachments.

Figure 4-6 shows the effect of load distribution between the skin, frames, and stringers in a typical area of a fuselage panel. The skin stresses, shown along the panel edges, vary from maximum values at mid-bay to minimum values over the frames and stringers. The variation is a

consequence of the effect of pressure loading on a stiffened cylinder. If the fuselage were simply a skin, its radius would expand uniformly under pressure. The frames and stringers restrain the expansion to a great extent near their own centerlines and to a decreasing extent toward mid-bay. The maximum pressure stresses at mid-bay are less than the simplified model stresses σ_p and $\sigma_p/2$.

The skin also carries shear stresses, which are generally low compared to the other stresses. Shear associated with fuselage bending is greatest at stations near the wing attachments and at approximately fuselage mid-height, decreasing to zero at the crown and keel. Shear due to twist is approximately independent of location (within the cylindrical portion of the fuselage). The

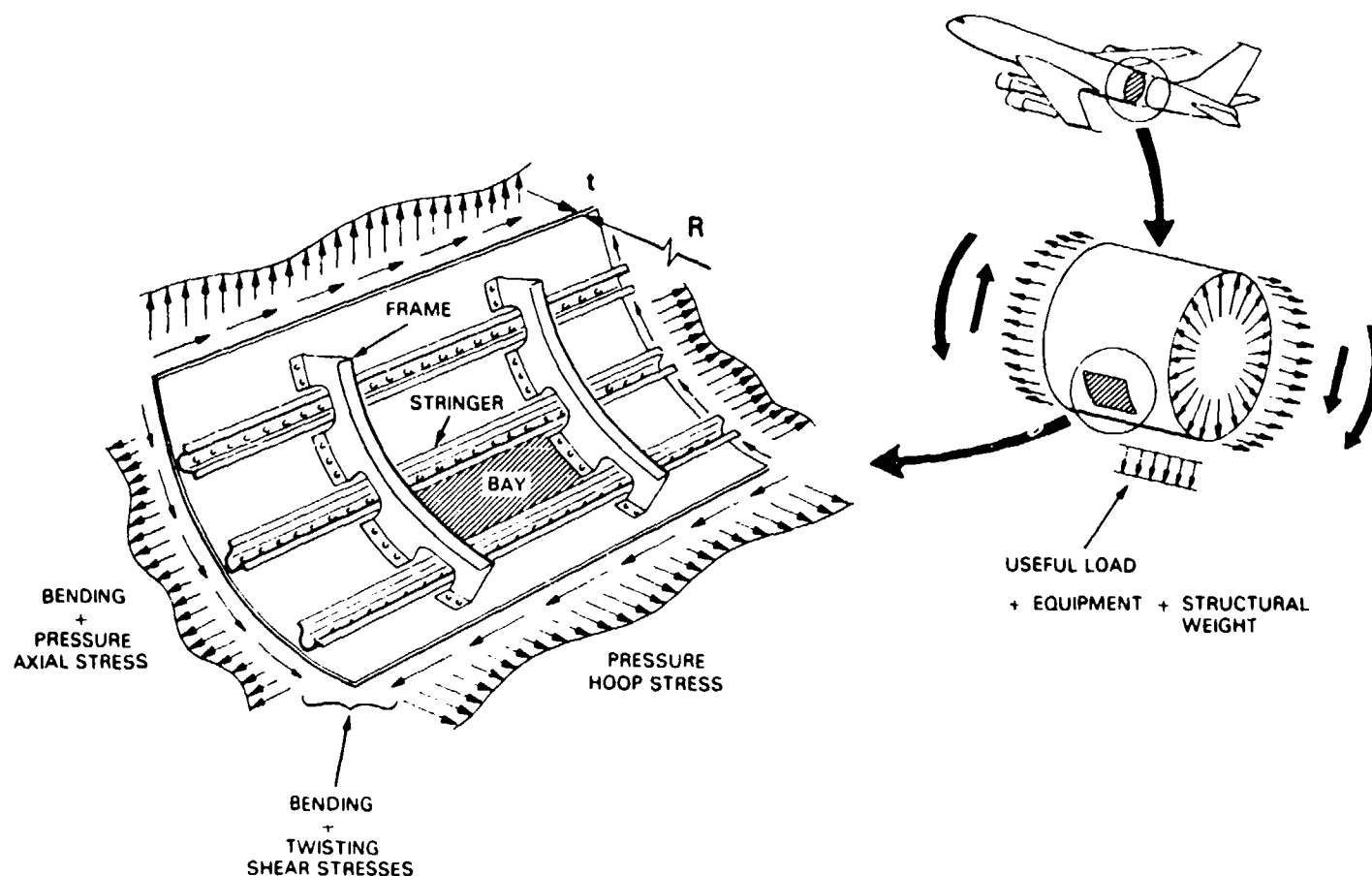


Figure 4-6. Stress in a fuselage shell.

shear due to twist is caused by transient forces, such as vertical stabilizer yaw loads, and is generally much less than the magnitude of shear due to bending.

Only minor fastener bearing loads are encountered over large areas of continuous skin. The minor loads occur mainly near frame-stringer crossovers, where most of the local load transfer between skin and stiffeners takes place as the stiffeners act to restrain the skin expansion. These bearing loads are related to the skin stress variation, which is typically about 30 percent of the nominal skin stress. If the skin in a bay is cracked, of course, the nearby fastener bearing loads must increase in order to redistribute load away from the cracked area to the surrounding stiffeners. A longitudinal crack sheds pressure hoop stress to the adjacent frames; a circumferential crack sheds axial stress to the adjacent stiffeners.

Another important local effect of the restrained expansion phenomenon is secondary bending in the stiffeners. Since the pressure hoop stress generally exceeds the pressure axial stress, longitudinal cracks are of the most concern in a damage tolerance assessment, and frame bending is thus the most important secondary bending effect. Figure 4-7 illustrates a cross-section detail, showing deflections under pressure at an exaggerated scale for clarity. Note that the secondary bending effect tends to concentrate at the stringer crossovers, where cutouts reduce the frame's bending resistance.

The floor structure creates a similar bending effect on a larger scale. The cabin floor is supported in part by cross-beams, which carry the floor loads into the fuselage structure via ties to the frames (Figure 4-8). The floor loads include pressure in those areas of the cabin located above unpressurized cargo bays or wheel wells.

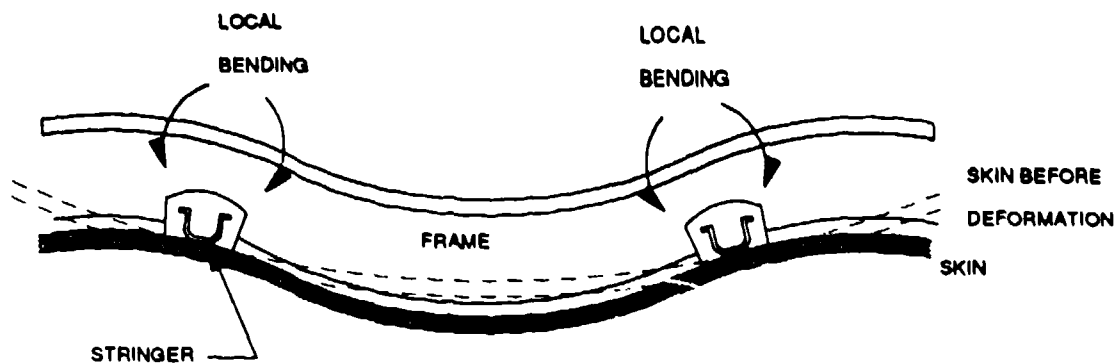


Figure 4-7. Frame bending.

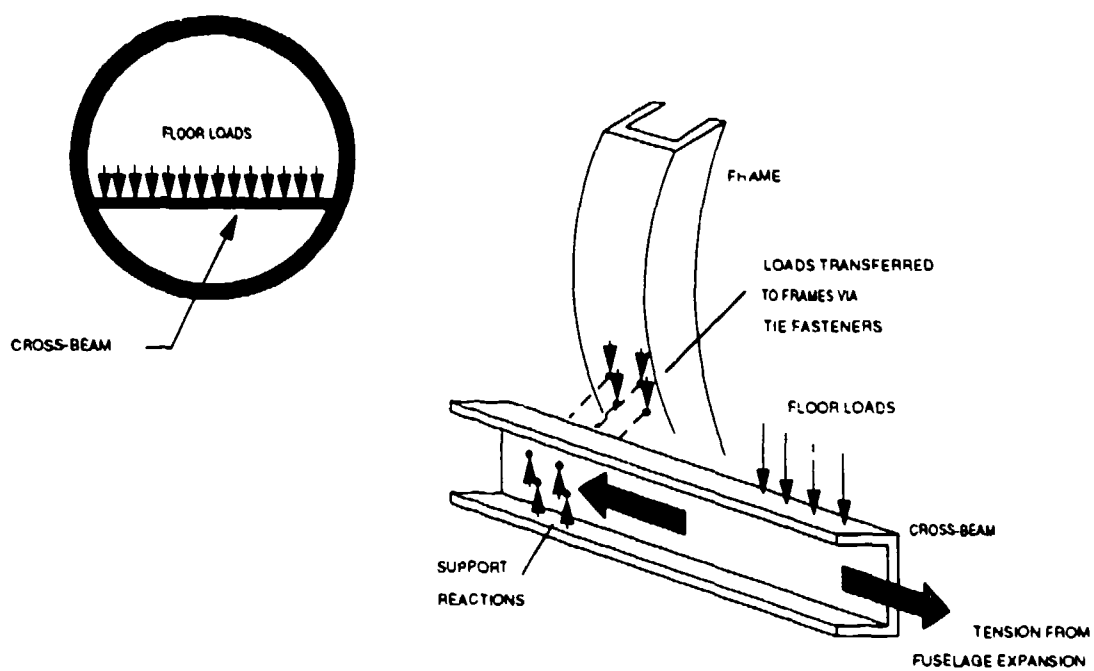


Figure 4-8. Floor cross-beam function.

When the fuselage expands under pressure, it must impose tension on the cross-beams. However, cross-beams are extremely stiff in tension and are able to locally restrain the expansion much more effectively than other parts of the structure. As a result, the skin and frames are bent inward near the floor when the fuselage is pressurized, as depicted in the exaggerated deflection schematic shown in Figure 4-9. This local bending effect also appears as additional fastener bearing loads at the frame tie details.

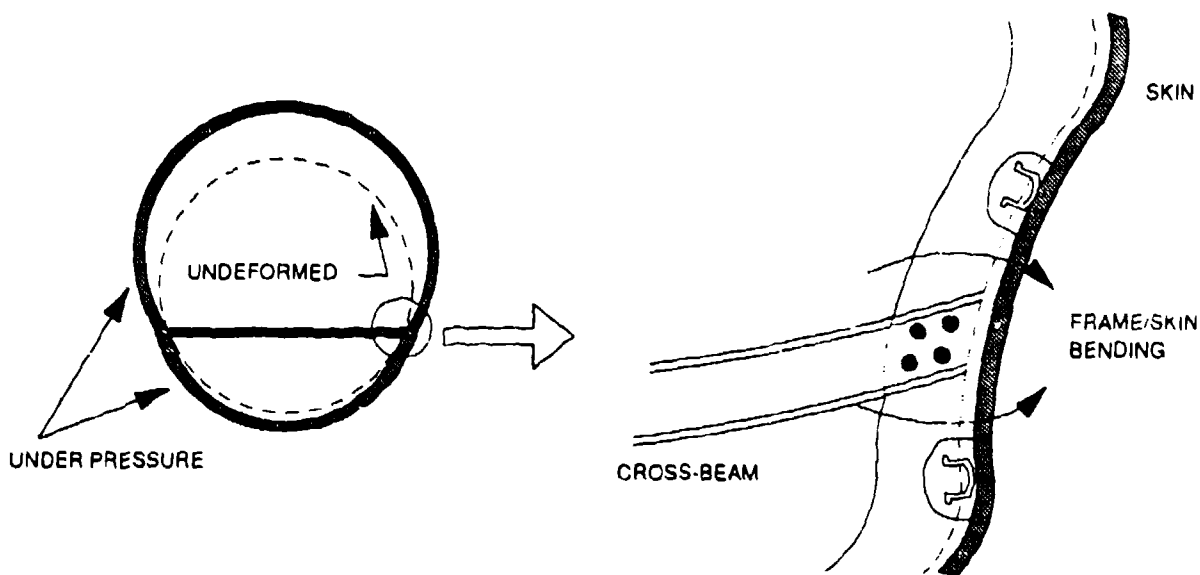


Figure 4-9. Local bending of fuselage at floor.

How should the floor structure be classified? The floor consists of flat panel assemblies (skin, stringers, and cross-beams) that carry mainly passenger and cabin furnishing loads into the fuselage shell. These loads do not appear in the definition of primary structure, so most floor panels would be classified as secondary. Conversely, panels located above unpressurized bays must carry the pressure load and, therefore, should be classified as primary.

Further classification of primary panels as PSEs or CSEs is unlikely without exceptional circumstances peculiar to a specific design. A primary panel fracture is not likely to cause further structural damage to the panel itself before the pressure is relieved. However, the classification should take into account the possible effects of collateral damage.

The meaning of the term "collateral damage" is illustrated by the sequence of events in an accident where a corrosion-cracked nose wheel failed in flight, breaking into a few large fragments. One of the fragments became a discrete damage source when forces from the tire pressure propelled it upward through the cabin floor, causing the cabin pressure to be vented into the wheel well. The wheel well doors, which were not designed for pressurization, were blown open. Two children who had been playing in the aisle when the accident occurred were immediately sucked out of the aircraft. The aircraft was able to return to and land safely at the airport from which it had departed.

The door failure was the collateral damage in this case. As serious as it was, this accident itself would not suggest that the floor panel be classified as a PSE because the door failure did not compromise flight safety. On the other hand, suppose that a similar floor panel failure could damage flight-critical systems, such as hydraulic lines routed through an unpressurized bay. Are the lines adequately protected? Are backup lines routed through a different area? Could the aircraft be flown in a normal manner if these lines were lost? Negative answers to all of these questions would suggest a PSE classification.

Like wings, fuselages must be designed with skin splices to facilitate manufacture from sheet stock of standard width and to allow for practical handling of subassemblies. Circumferential joints are generally designed as butt splices over heavier-than-normal frames; the design may also include internal or external doublers, or provisions for staggering skin and stringer splices. Longitudinal joints are generally located over stringers and may be designed as either reinforced butt splices or lap splices, depending on model and manufacturer. Also, depending on the

manufacturer, splices may be either mechanically fastened and sealed with a nonstructural sealant, or they may be fastened and bonded with a structural adhesive.⁴

The pressure bulkheads are skin-stringer panels that provide end closures for the pressurized volume in the fuselage (Figure 4-10). The forward and intermediate bulkheads are generally flat, and the pressure load creates panel bending stresses. The larger aft bulkhead may be curved, but in that case it is usually a shallow spherical cap which, for practical purposes, can be treated as a flat panel.

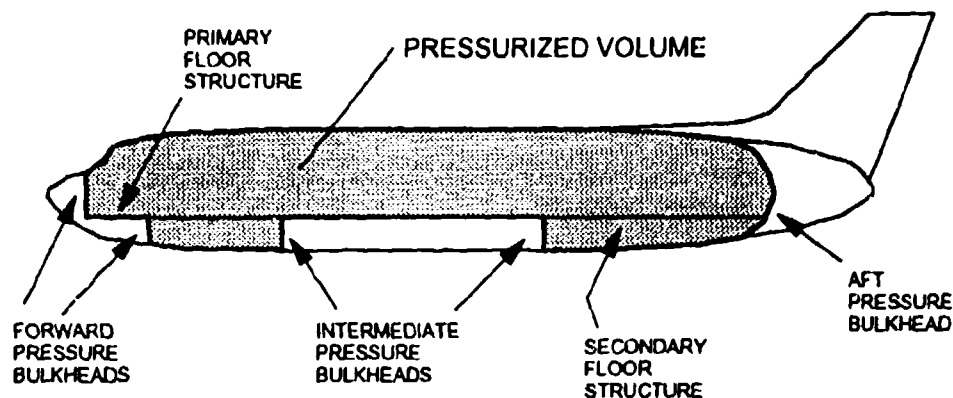


Figure 4-10. Typical bulkhead arrangement.

⁴ Some recent European designs feature splices joined by adhesive bonding alone.

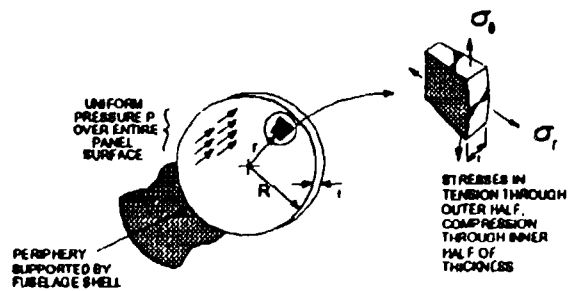
It is useful to represent a full bulkhead by a simplified model, in the present case, an unstiffened circular panel of thickness t supported on its periphery of radius R . Both the location and magnitudes of the maximum bending stresses depend on the support stiffness. The radial (σ_r) and circumferential (σ_θ) stresses at the panel outer surface can be expressed in the form:

$$\sigma_r = P \left(\frac{R}{t} \right)^2 f_r(r) \quad (4-5)$$

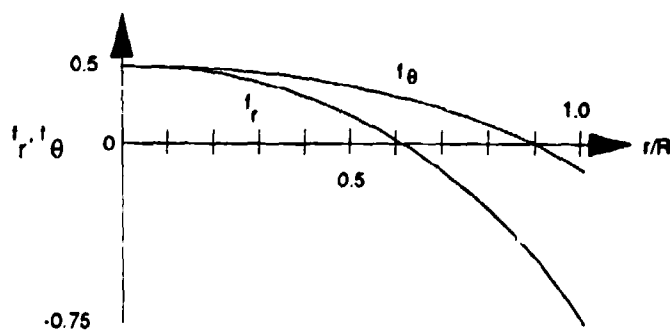
$$\sigma_\theta = P \left(\frac{R}{t} \right)^2 f_\theta(r) \quad (4-6)$$

where f_r and f_θ are scaling functions. Figure 4-11 illustrates the model and the behavior of the scaling functions for two extreme support conditions: built-in (periphery fully restrained against any motion) and knife-edge (periphery fully restrained against linear motion but free to rotate). Note that the stresses vary linearly through the panel thickness, passing through zero at the mid-plane and attaining the maximum compression values $-\sigma_r$, $-\sigma_\theta$ at the inner surface (pressure side). This is similar to the distribution of bending stress over the height of a beam or spar (see Figure 4-4). Note also that, under built-in support conditions, the bending effect reverses near the periphery, i.e., the tensile stresses are on the pressure side.

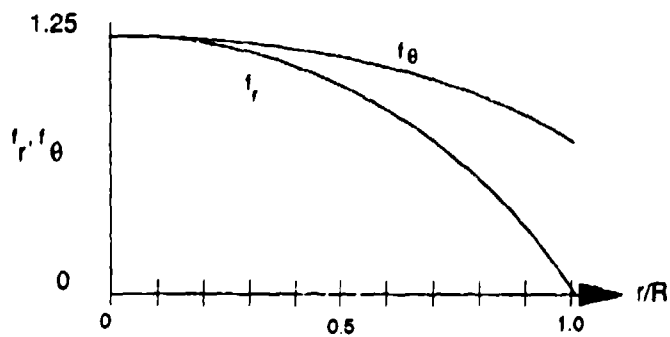
The maximum stresses in an unstiffened panel would be quite high because they are proportional to the square of R/t , which may exceed 200 for typical bulkhead radii and skin thicknesses. Therefore, actual bulkheads are stiffened with stringers to share the bending and reduce the skin stresses to tolerable levels. These structures can have quite complicated geometry; moreover, the structure which supports a bulkhead cannot be realistically approximated by either the knife-edge or built-in idealization. Thus, the reverse bending area is likely to be smaller than would be estimated assuming built-in support, but the actual area can be determined only from a detailed structural stress model.



(a) Panel model.



(b) Scaling functions for built-in support.



(c) Scaling functions for knife-edge support.

Figure 4-11. Bending stress distributions in a flat circular panel loaded by pressure. [4-2]

Floor panels over unpressurized bays are subjected to the same kind of load as pressure bulkheads, but the floor panel stringers are usually on the nonpressure side, whereas bulkhead stringers are often located on the pressure side. Figure 4-12 shows how these two different arrangements lead to different choices of location for damage tolerance evaluation.

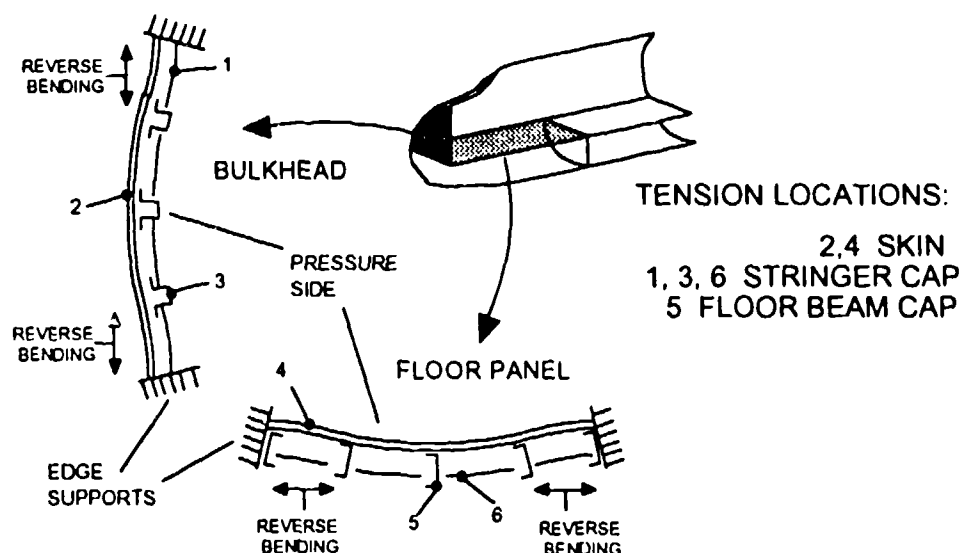


Figure 4-12. Floor panel and bulkhead evaluation sites.

No summary of fuselage structure would be complete without a discussion of doors and windows. All windows and some of the doors are subjected to fuselage pressurization loads. They carry only the pressure on their own surfaces, and this load is passed directly to the fuselage shell. Therefore, doors and windows are secondary structure. If a door or window should fail in flight, the consequences could be serious or even fatal for nearby occupants, but no blowout has ever caused the loss of an aircraft. Therefore, neither doors nor windows need be classified as PSEs.

However, it is important to consider the supporting structure, especially with regard to its effect on the surrounding fuselage panel, which is a PSE or CSE. A simplified window construction

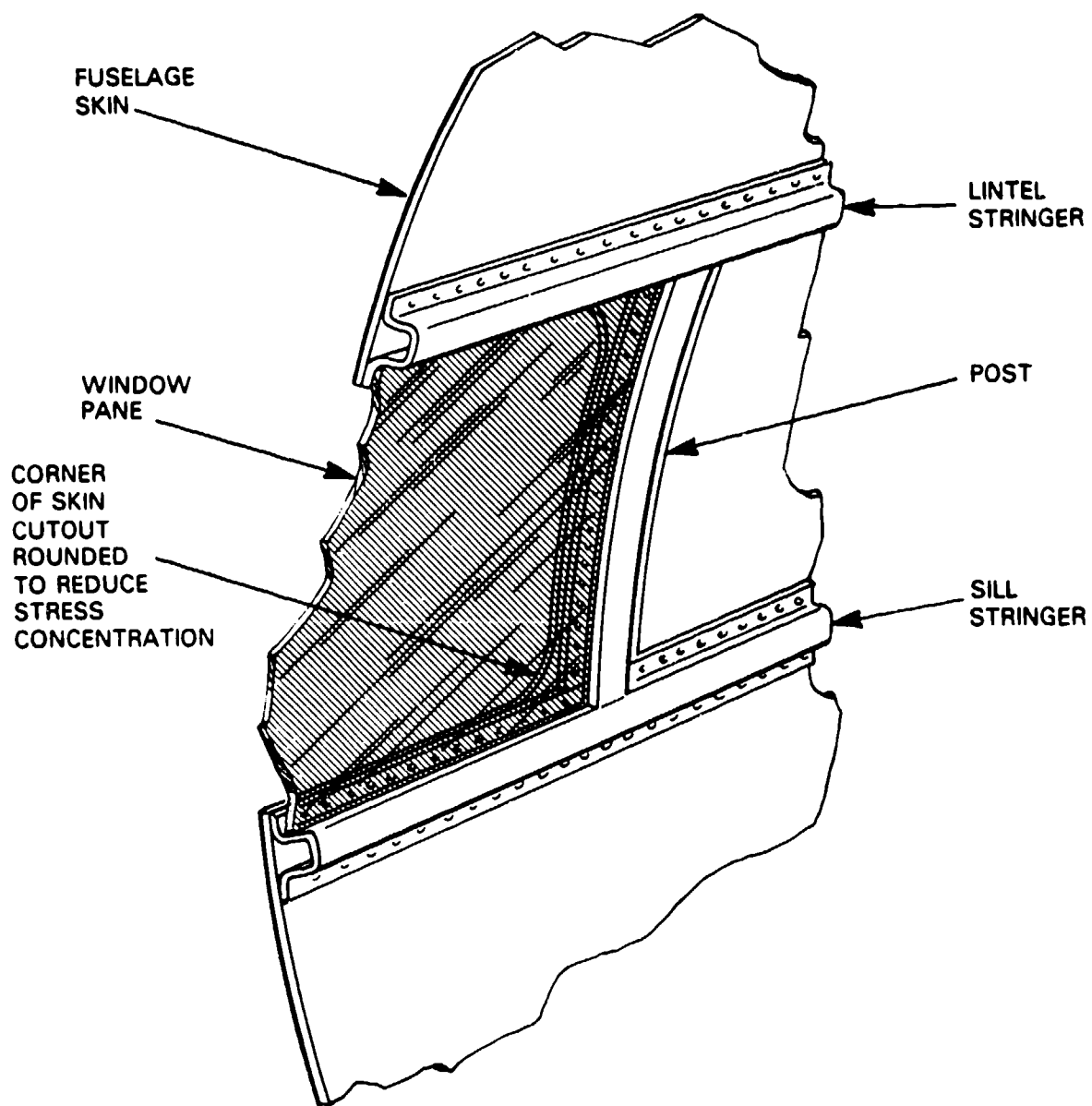


Figure 4-13. Cutaway view of window detail.

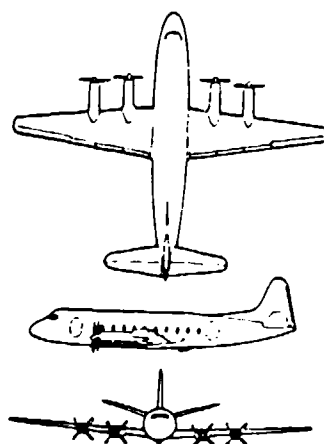
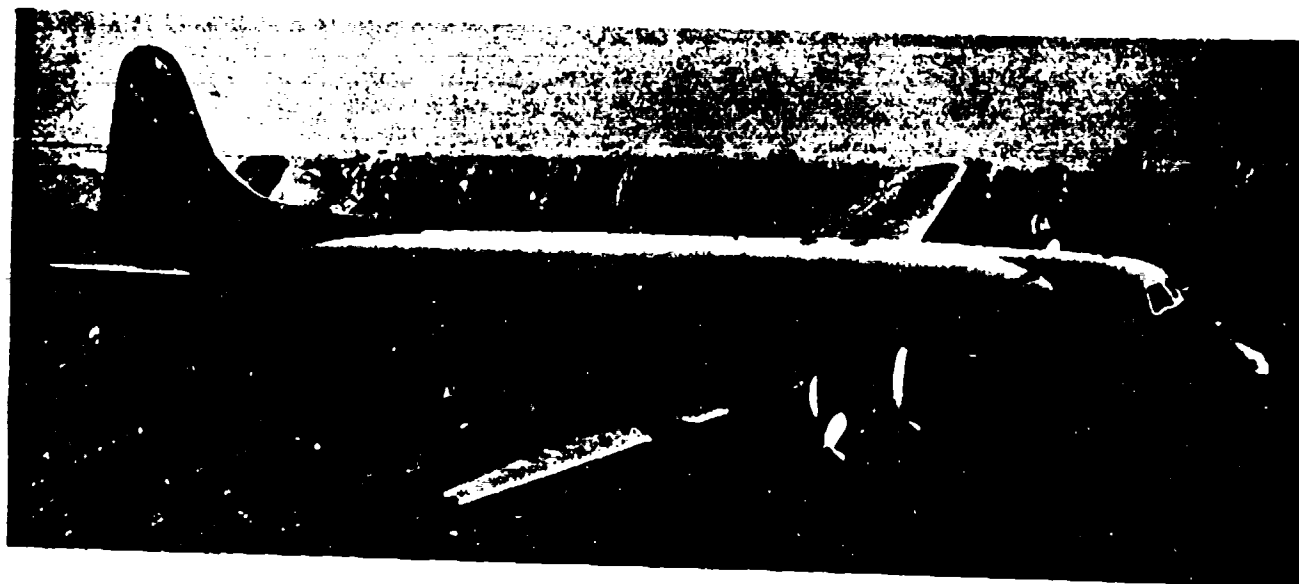


Figure 4-14. Vickers Viscount circa 1953.
[Reprinted from Janes's All the World's Aircraft, 1953-54, p. 100, by permission of Jane's Information Group.]

as ellipses with the ratio of minor to major axis selected to equalize the local axial and hoop stresses. The designers took advantage of the fact that the nominal axial stress is only half the nominal hoop stress. They accepted a larger stress concentration factor on axial stress in order to reduce the factor on hoop stress.

4.3 LOAD PATH ARRANGEMENT

The preceding section included some general discussion of load paths. It is now time to revisit this subject, looking more closely at the details of load path arrangement in examples of typical construction details which may be found in different parts of the airframe. The consideration of load path arrangement necessarily includes local effects; it also leads back to the subject of evaluation sites and forward to inspectability.

The first question to answer about any part of the airframe requiring damage tolerance analysis is whether or not the structure has more than one load path. The basis for the answer is in the following definitions from AC 25.571-1A:

Single load path is where the applied loads are eventually distributed through a single member within an assembly, the failure of which would result in the loss of the structural integrity of the component involved.

Multiple load path is identified with redundant structures in which (with the failure of individual elements) the applied loads would be safely distributed to other load carrying members.

At first glance, the damage tolerance concept might appear to require distinctly different approaches to single and multiple path structure. The two approaches are as follows:

If there is only one load path, then the damage tolerance analysis essentially reduces to the establishment of a life limit which guarantees that no crack will grow to critical size before the

Figure 4-15 illustrates a wing box panel before and after failure together with its two adjacent panels. All three panels are assumed to be of identical design, with strength exactly equal to

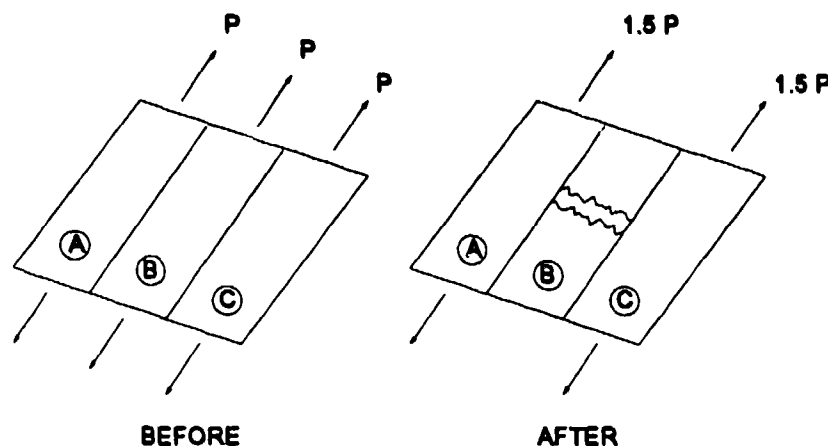


Figure 4-15. Static overload after panel failure.

design ultimate load. The load carrying capacity of the stringers is neglected in this simplified example.

Before failure, each panel carries a load P in the nominal condition (straight and level flight), which is also the condition in which the failure is assumed to occur. In the post-failure state, each adjacent panel must carry a static load of $1.5P$ in the nominal condition. During the failure, which is assumed to be sudden, the extra load of $0.5P$ per panel is assumed to be accompanied by a dynamic factor of 1.5, so that the peak load state per panel is $1.75P$.

The redundancy in the structure can be illustrated by comparing the margins available before, during, and after failure. For the purpose of the comparison, the margin is defined as the ratio of limit or ultimate airplane load factor to the adjacent panel overload factor. If the margin is defined as the ratio of limit or ultimate airplane load factor to panel overload factor, then it gives directly the actual airplane load factor which would impose the limit or ultimate condition on the

structure in the specified state. These margins, summarized in the following table, show that the structure retains some capability to withstand gusts and maneuvers during and after failure.

STATE OF STRUCTURE	LIMIT LOAD FACTOR	ULTIMATE LOAD FACTOR
Intact	2.50	3.75
Post-failure	1.67	2.50
Peak overload	1.43	2.14

The load carrying capacity of any unbroken stringers would make the actual margins during and after failure somewhat greater than the above results. Fortunately, the way in which damage usually occurs in typical panel assemblies tends to leave most of the stringers intact.

Figure 4-16 illustrates a typical chordwise section through a lower panel assembly in a wing box. In this example, fabrication damage or fatigue has occurred at the location of one of the rivets which attaches stringer "1" to skin "B," part of a spanwise butt splice. The most likely consequence is that cracks form in both components, at the intersection of the drill holes with the faying surface. The outcome then depends on the relative rates of crack growth in the skin and stringer. If the stringer crack grows slowly, the panel failure consists of skin B fracture followed immediately by stringer 1 failure. However, stringers 2, 3, and 4 are still available to share the load redistribution with the adjacent skins A and C. Conversely, if the skin crack grows slowly, stringer 1 may fracture without any obvious external sign. Another damage site (say, at stringer 4) might then produce a similar set of cracks, so that the eventual failure of skin B would leave only stringers 2 and 3 to assist the adjacent panels.

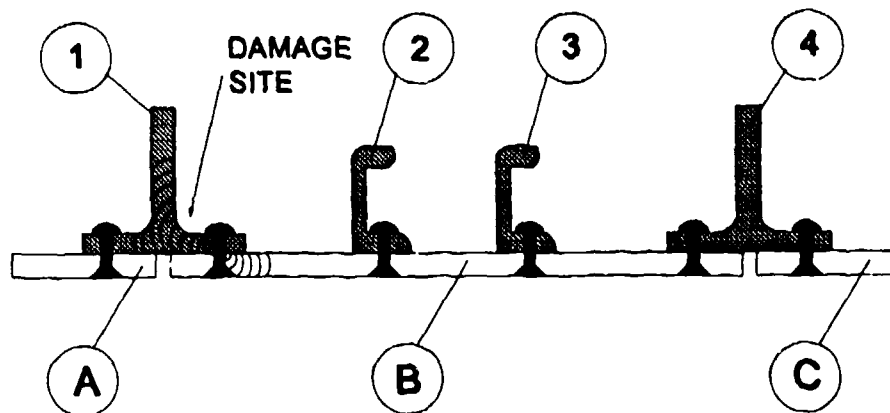


Figure 4-16. Damage in a fail-safe panel assembly.

In contrast to the preceding example, Figure 4-17 illustrates an assembly of planks with integrally machined stiffeners. In the wing root or carry-through area, the high bending loads require heavy skins, and thicknesses from 1/2 to 1-1/2 inches are not uncommon. In such cases, it may be more efficient to produce the stiffened plank by machining it from plate stock, rather than attempting to align and fasten separately made stiffeners.

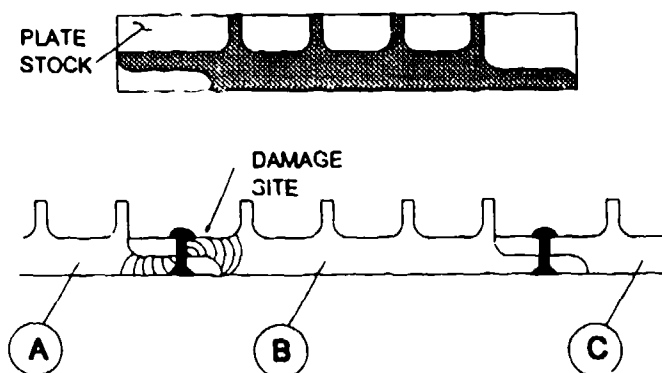


Figure 4-17. Ship-lap planks with integral stiffeners.

Integrally machined planks are inherently less damage tolerant when assembled with ship-lap joints in place of conventional butt splices. In the example shown, the common crack formation affects planks A and B. Whichever fails first, the other can be expected to fail immediately after. Also, the integral character of the stringers means that they too will be lost when a plank fails. The actual structure thus behaves much like the simple model in Figure 4-15, except that in this case two adjacent panels will be required to carry the load redistributed from two failed panels. The static and peak overload factors are thus 2.0 and 2.5, respectively, and the margins are no longer very comfortable:

STATE OF STRUCTURE	LIMIT LOAD FACTOR	ULTIMATE LOAD FACTOR
Intact	2.50	3.75
Post-failure	1.25	1.88
Peak overload	1.00	1.50

The difference in margins for the butt and ship-lap splices can also have a dramatic effect on useful life, especially in planks thick enough to be governed by plane strain fracture toughness. K_{IC} . For example, consider planks made of aluminum with K_{IC} about 20 to 22 ksi $\sqrt{\text{in}}$ and designed for a nominal stress of 13 ksi, a typical 1g stress level for the lower panel in a transport wing box.

For purposes of illustration, we shall consider skin cracks, which will be represented by the stress intensity factor for a single through-crack emanating from one side of a 3/16-inch diameter fastener hole and subjected only to an applied tension. Figure 4-18 illustrates the crack model and the nominal (1g) stress intensity factor. Values of K_I for other stress levels can be obtained by scaling the graph in linear proportion to stress.

A damage tolerance evaluation of the structure might begin with an estimate of the critical crack length for a stress corresponding to the airplane load factor expected (on average) once per flight. A load factor of about 1.5 might be expected on every flight; the corresponding stress is 19.5 ksi, and the critical crack length is about 0.2 inch.

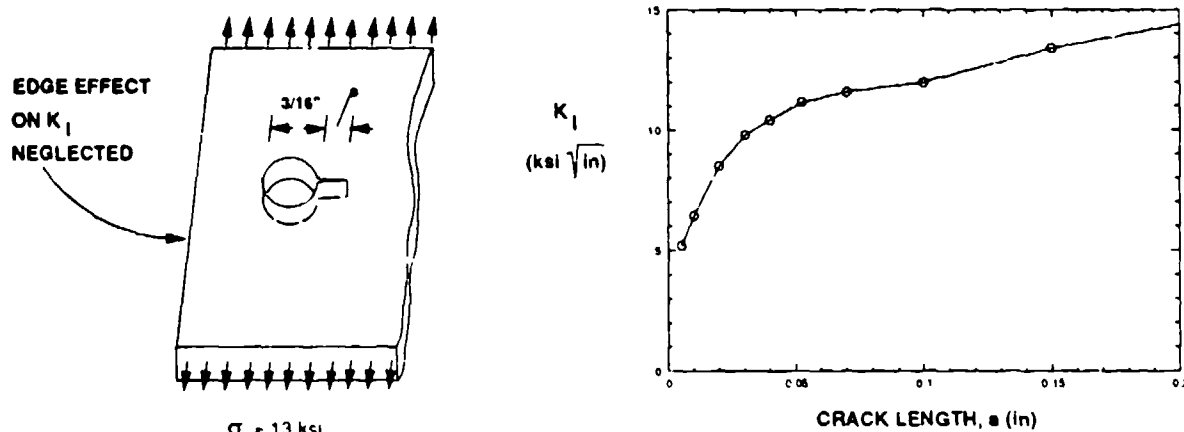


Figure 4-18. Crack model and stress intensity factor.

We might then use this crack length as follows in a determination of the time to the beginning of the periodic inspection program. To guarantee no critical crack in the structure before that time, one might select an initial crack length of 0.02 inch to represent the level of fabrication damage expected for at least one fastener hole in the structure. The time to first inspection would then be based on the slow crack growth life between the crack lengths of 0.02 and 0.2 inch.

Up to this point, the evaluation has proceeded in the conventional manner for multiple path structure. Now, however, consider what might happen if a plank is assumed to fail and the adjacent planks are assumed to contain enough small cracks so that at least one (the "adjacent crack") would be located in the overload area. What would be the critical length of an adjacent crack if it were subjected to peak overload during the first plank failure? Scaling the graph in Figure 4-18 gives the following answers for the two splice details:

Critical Adjacent Crack Lengths
for $K_{IC} = 20 \text{ to } 22 \text{ ksi } \sqrt{\text{in}}$

Design	Peak overload factor	Critical crack length (in.)
Butt splice	1.75	0.07
Ship-lap splice	2.50	0.03

How long would it take for the structure to develop enough cracks of the above lengths so that a first plank failure would be certain to overload an adjacent crack? There must be a large number of cracks in the whole structure to guarantee at least one adjacent crack. Therefore the initial crack length might be set at 0.005 inch to represent average fabrication quality.⁷ The time to reach the postulated condition is then based on the slow crack growth life between the crack lengths of 0.005 and 0.07 or 0.03 inch

The last calculation is vital for thorough evaluation of multiple path structure whenever small critical crack lengths are anticipated. It represents the time at which cracks of large enough size can be present in numbers sufficient to prevent an adjacent plank from containing the first plank failure. Furthermore, the critical adjacent cracks are too small to be detected by ordinary inspection methods. Thus, what was initially a redundant structure has lost its fail-safe character. The time when this occurs is called time to loss of fail-safety or time to widespread cracking. The structure is then described as having entered the widespread cracking or adjacent panel cracking condition.

How long is the time to loss of fail-safety in the example? The answer can be approximated in relative terms, without knowing anything about the service stress spectrum, by calculating and comparing the crack geometry sums with the sum for the time to first inspection. The results can be obtained by summing $1/K_I^4$ (from Figure 4-18) over the respective crack growth intervals:⁸

⁷ Initial flaws from score marks are typically of this size.

⁸ Summing $1/K_I^4$, represents typical crack growth rate properties for aluminum alloys ($da/dN \cong K_I^4$).

4.3.2 Stiffeners as Crack Stoppers

Splices parallel to the major stress axis are effective crack stoppers as long as the structure has not entered the widespread cracking condition. A stiffener attached to a continuous skin can also arrest a running skin fracture under the right conditions.

The following simple experiment will demonstrate the crack-arrest capabilities of stiffeners (Figure 4-19). Inflate two balloons to the same size, using balloons that assume a sausage shape when pressurized. Apply ordinary cellophane tape to one balloon, making two hoops spaced 2 to 3 inches apart. Any tape from 1/4 to 1/2 inch wide will do, as long as it adheres well to the balloon's skin. Quickly cut each balloon with a sharp knife or razor blade, making the cut parallel to the balloon's axis. (The cut in the taped balloon should be made between the "stiffeners.") The balloon with no tape will burst catastrophically, but the tape on the other balloon will arrest the crack and control the deflation.

The crack-stopping experiment works because the much stiffer and stronger tape adheres well to the skin of the balloon. Getting stringers to stop a crack in an aircraft skin depends on analogous characteristics. In a good design, enough of the strain energy released from the skin by the running crack will be diverted into the stringers to reduce the energy available for further extension below the amount needed to create new crack surface.

In the structure, "adherence" means how close to the line of the advancing crack can load be transferred from skin to stringers. In mechanically joined structure, this depends on the fastener pitch and stiffness. Stiffer, more closely spaced fasteners produce better load transfer but other design constraints limit what can be achieved in practice (Figure 4-20). Bonded construction is an alternative approach which generally produces better load transfer than can be obtained from

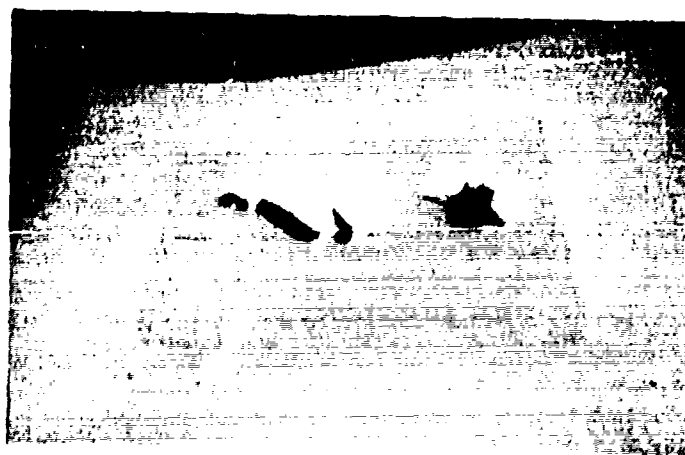
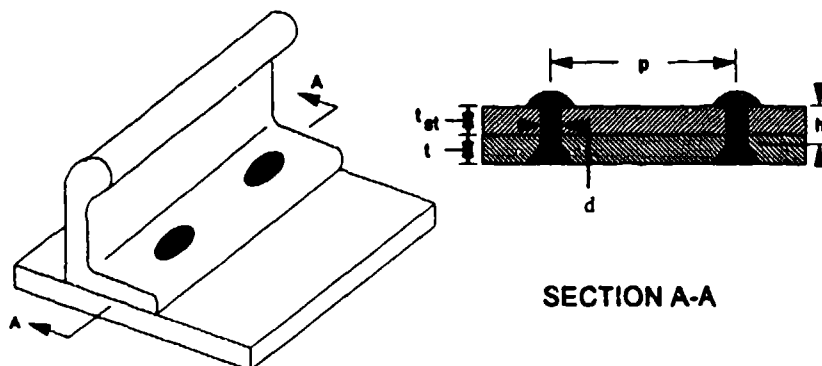


Figure 4-19. Demonstration of crack arrest.



- $t + t_s$ - thick enough to take major tension load
- h - determined by $(t + t_s)$ and fastener type
- d - limited by stringer leg width
- p - enough to prevent interactions of stress concentrations ($p/d \geq 4$)

Figure 4-20. Fastener design constraints.

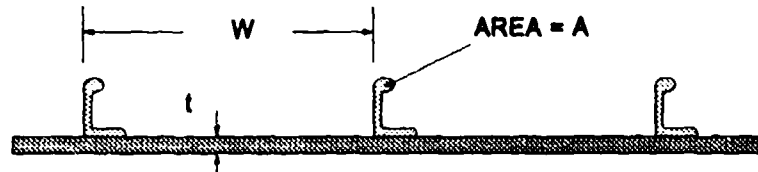
fasteners, provided that the integrity of the bond is maintained.⁹ In this case load transfer improves as the bond layer's thickness decreases and its shear modulus¹⁰ increases.

The stringers provide a route to bypass panel load around the cracked skin. How much load can actually be transferred depends on how stiff the stringers are, relative to the skin. Since both components are normally made of material with the same Young's modulus, the ratio of stringer

⁹ If the designer is reluctant to rely totally on bond integrity, a combination fastened/bonded approach may be adopted. In this case, the bond serves the primary load-transfer function, and the fasteners remain lightly loaded unless the bond is lost.

¹⁰ The engineering shear modulus of an isotropic material can be expressed in terms of Young's modulus and Poisson's ratio as $E/[2(1 + \nu)]$.

to skin area in a typical section determines the stiffness ratio (Figure 4-21). The stiffness ratio can be increased by using heavier stringers and/or by decreasing the bay width between stringers.



$$\text{STIFFNESS RATIO} \approx A/Wt$$

Figure 4-21. Stringer/skin ratio.

The strength available in the bypass route restricts the amount of load that can be transferred. Limits imposed by both the stringers themselves and the attachment design must be considered.

If the local stress in a stringer reaches its ultimate strength before the skin crack is arrested, the stringer fails and cannot divert any more of the strain energy being released by the running crack. A common design practice to guard against stringer failure is to use a material of higher strength. For example, tension panels are often made with 2024-T3 skins and 7075-T6 stringers (ultimate strengths of 50 and 77 ksi, respectively). Since the panel is uniformly stressed when intact, the allowable stress is controlled by the strength of the 2024-T3 alloy, and the extra strength of the 7075-T6 alloy provides a reserve for the stringer.

A basic characteristic of the attachment system is that it is most heavily loaded close to the line of advance of the skin crack. If the concentrated load is high enough to cause local attachment failure, the concentration shifts away from the crack line and decreases as the efficiency of load transfer is reduced. The attachment failure thus progresses away from the crack line to a distance

at which the concentrated load is no longer enough to cause further failure. This distance depends on the shear strength of the fasteners or bond. If the attachment failure distance is long enough, stringer "adherence" is reduced to the point where too little energy is diverted to prevent the crack from running past the intact stringer.¹¹

Like the multiplank panels discussed in Section 4.3.1, the continuous-skin panel is a multiple path structure. As the preceding discussion has shown; however, the multiple path character of the continuous-skin panel is quite different because the independent paths all go through stringers. Continuous skins are found in wing and empennage boxes as well as in fuselages, but fuselage panels require additional consideration because of certain historical factors and the effects of pressurization.

High-altitude piston-engine transports began to come into widespread service in the late 1940s and by the early 1950s there had been a number of incidents and accidents precipitated by propeller blade failures in flight. In a few cases, a blade may have been thrown through the fuselage skin, causing extensive structural damage that brought the airplane close to catastrophic failure.

Concern for prevention of such failures led to the FAA's first damage tolerance regulation, later embodied in FAR 25.571(b)(3)(ii), requiring manufacturers to demonstrate that a pressurized fuselage could arrest a long crack suddenly introduced by a discrete source, under 1g flight loads and 110 percent of normal cabin pressure. The worst case is assumed for test and evaluation purposes, namely: an axial crack (Mode I loading by the pressure hoop stress) located midway between longerons. Different designers have made different assumptions about the initial damage. Today, a crack extending into two frame bays with the central frame also cut is generally assumed (Figure 4-22). The structure is considered to comply with FAR 25.571(b)(3)(ii) if, under the specified conditions, it arrests the skin crack within two frame bays.

¹¹In mechanical attachments, a degree of fastener failure is sometimes intentionally accepted as a compromise, in order to partially unload the stringer and prevent its failure. In such designs, the attachment failure is generally expected to progress no more than 2 to 6 fasteners from the crack line.

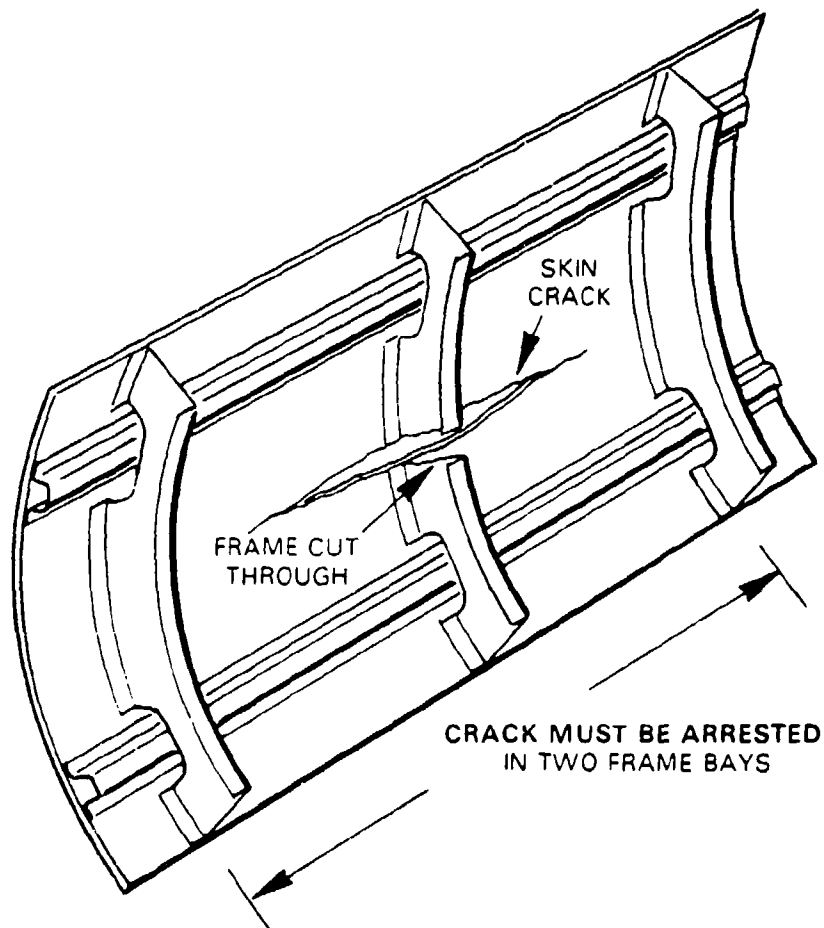


Figure 4-22. Definition of fuselage tolerance to discrete source damage.

Once a fracture has been initiated, the crack runs quite rapidly. In a typical skin fracture, the advance speed builds up to about 1,000 ft/sec in less than 100 microseconds. Thus, the crack reaches the frame at the end of the bay while the fuselage is still almost fully pressurized. Simultaneously, unable to carry the pressure as hoop tension, the cracked skin bulges outward and sheds its load into stringer bending which exacerbates the local frame bending already present

at the stringer crossings (Figure 4-23). The added stress on the reduced frame section at the mousehole may be enough to cause a local frame failure. Even if the frame does not break, it is unable to support further bending in the yielded condition. If the frame section on the crack

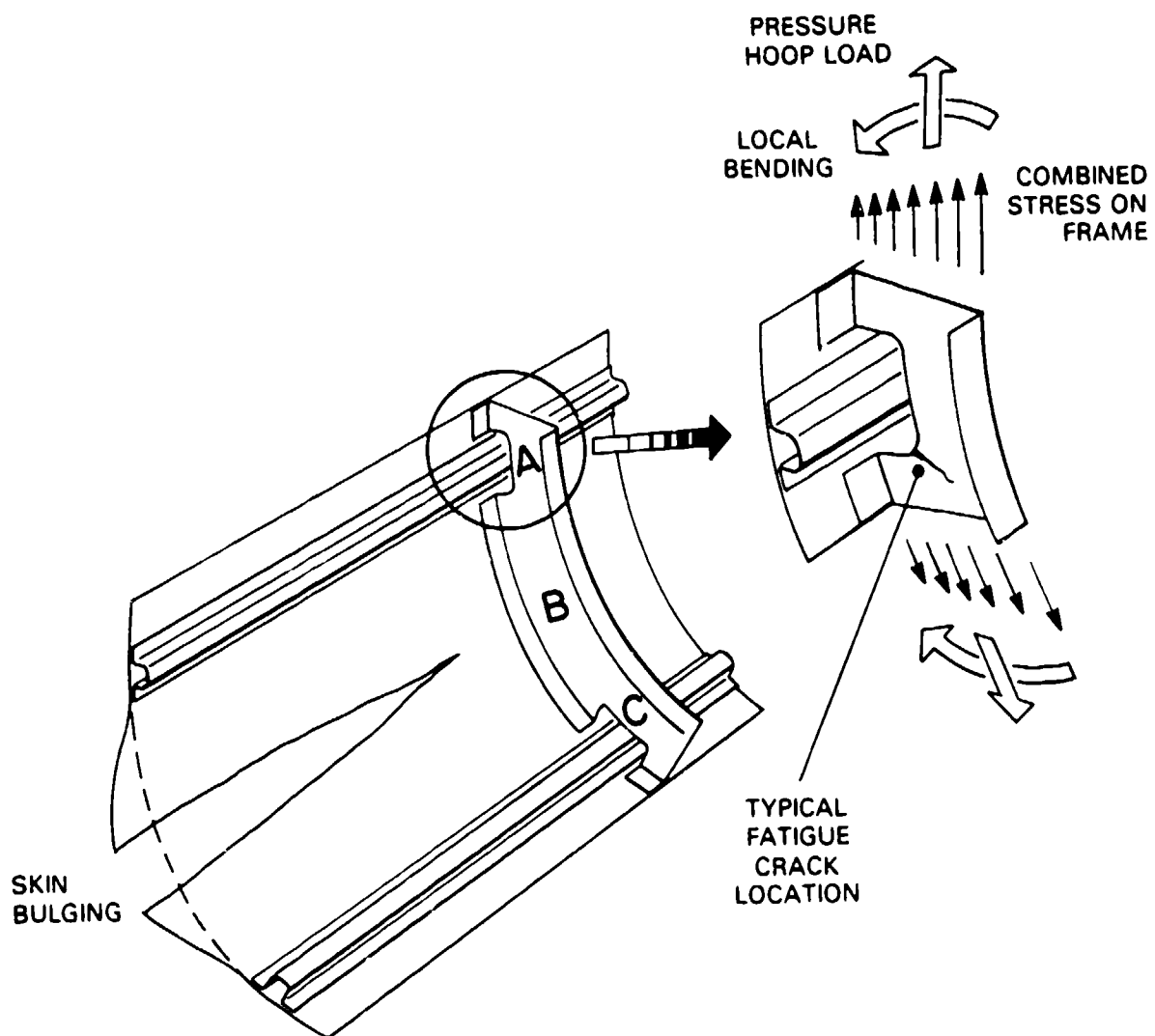


Figure 4-23. Frame collapse mechanism.

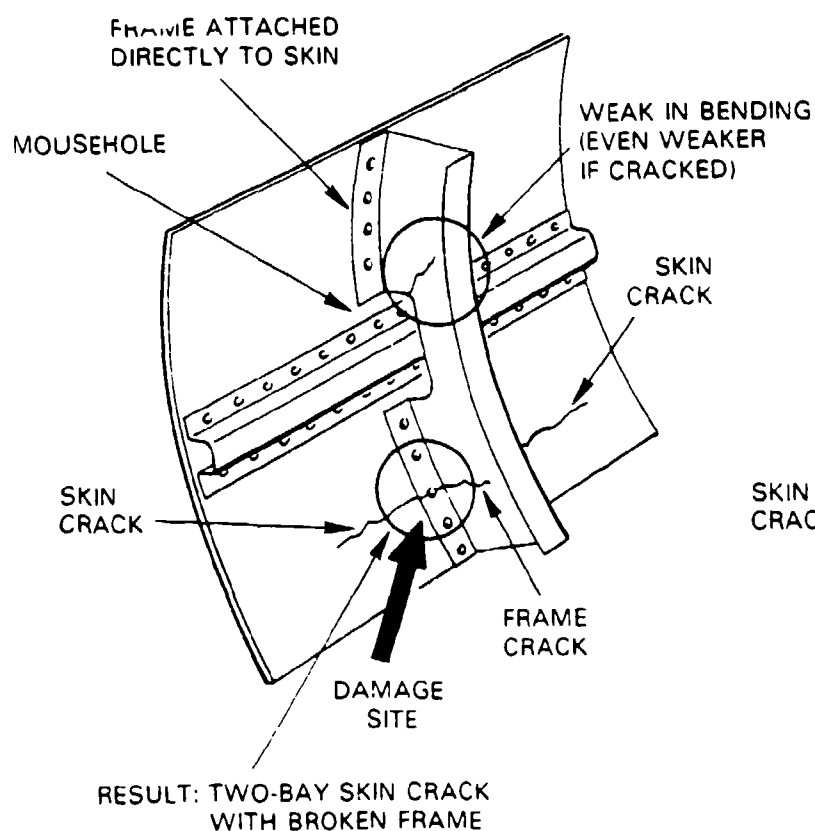
advance line also yields under local overload, the frame acts as if it is hinged at the three points A,B,C shown in the figure. The effects of the skin bulging are then transmitted back to the crack, driving it past the frame.

As more was learned from service experience with pressurized fuselages, designers came to recognize that the practice of attaching frames directly to the skin did not produce the best possible damage tolerance for the least structural weight. In aging airframes, fatigue cracks were frequently found originating at the mousehole corners in the frames. If numbers of such cracks could accumulate in an airframe, then the further reduction of frame bending strength might rob the fuselage of its fail-safe character.

Since there is no convenient way to attach a frame directly to the skin without cutting in mouseholes to let the stringers through, designers began to experiment with offset frames (Figure 4-24). Besides getting rid of the mousehole, offset frame design improved tolerance of single fastener hole fatigue damage. In the older design, a crack at a skin-to-frame fastener could lead to the two-frame-bay crack with a broken central frame (Figure 4-22); an undesirable effect of aging, even though the airframe should be able to contain the damage. Conversely, a similar crack at the skin-to-frame attachment in the new design would leave the frame intact.

Despite its obvious benefits, the offset frame design also has one disadvantage: the shear clip attachments are more flexible and spaced further apart than the older direct fastener system. Thus, while the offset design guards against frame bending failure, it also reduces the diversion of released energy from the skin to the frame. This problem was solved by adding a tear strap to the design. The tear strap is usually about the same thickness as the skin and is attached directly to it (Figure 4-25). In some designs, additional effectiveness may be gained by using a stiffer material for the tear strap (e.g., titanium). In other designs, extra tear straps may be placed in the middle of each frame bay in a trade-off for a lighter frame section.

OLD DESIGN



NEW DESIGN

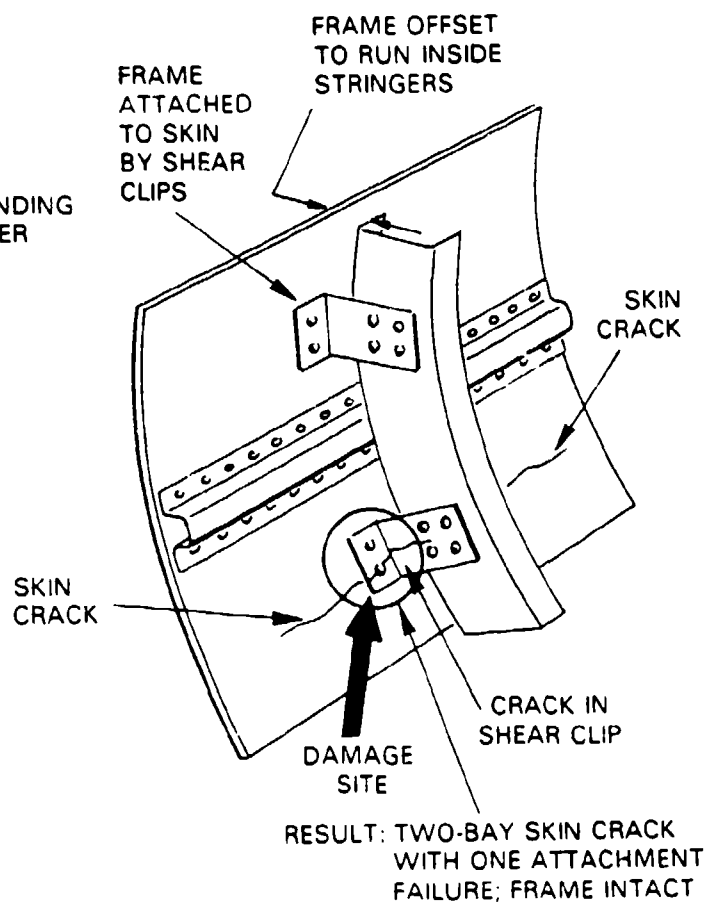


Figure 4-24. Comparison of old and new design details.

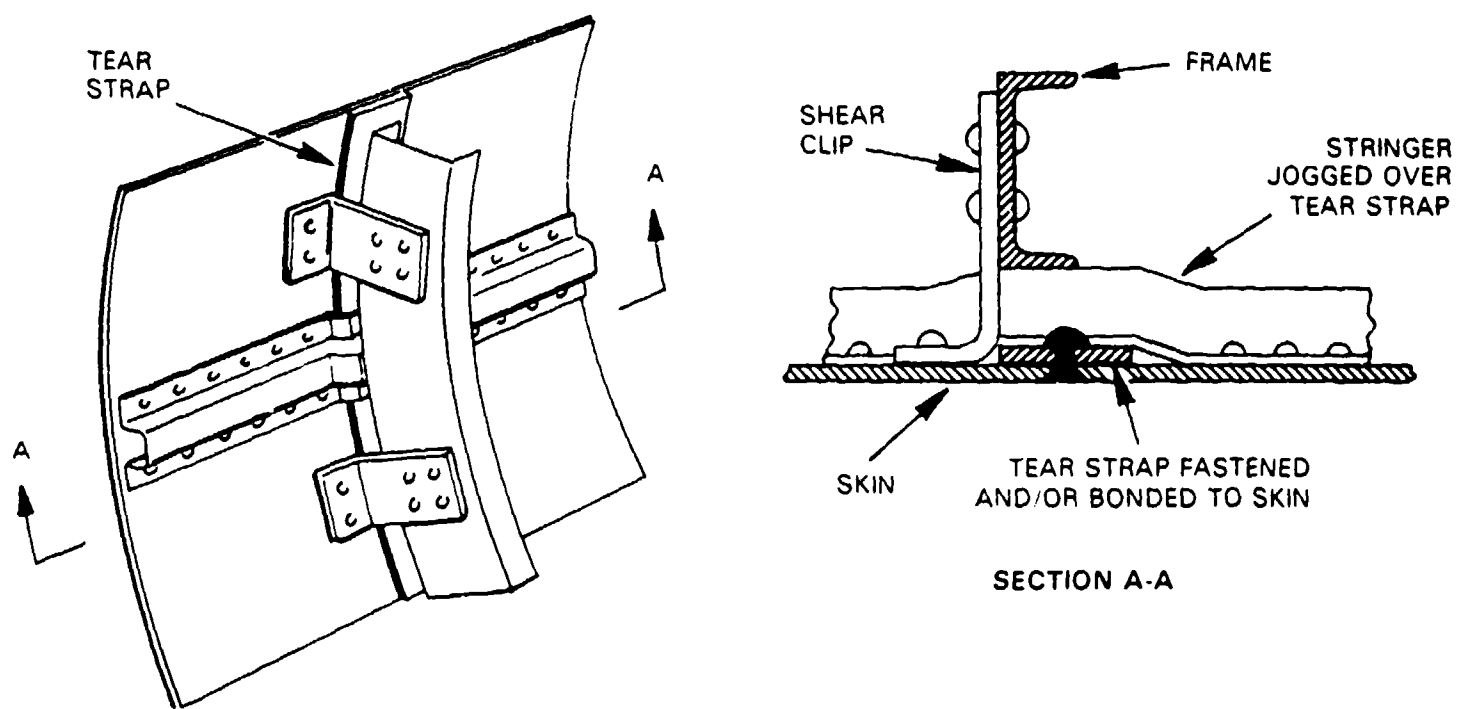


Figure 4-25. Offset frame with tear strap.

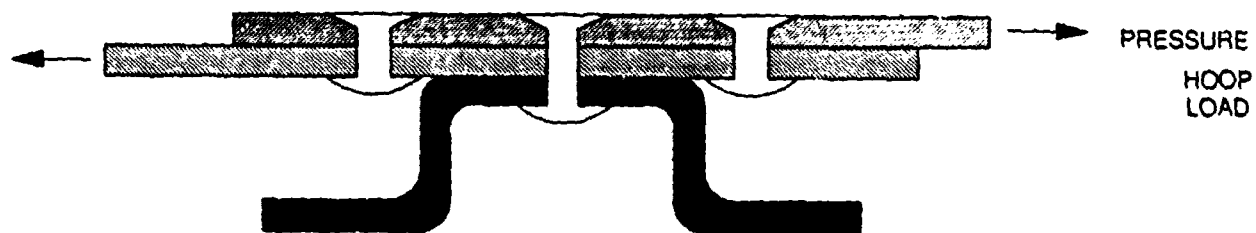
4.3.3 Splices Across the Major Load Axis

When a major load crosses a mechanically joined skin splice, the entire load must be transferred by means of fastener bearing. Crosswise splices are thus more sensitive to fastener detail fatigue than parallel splices, in which fastener bearing transfers only secondary load.

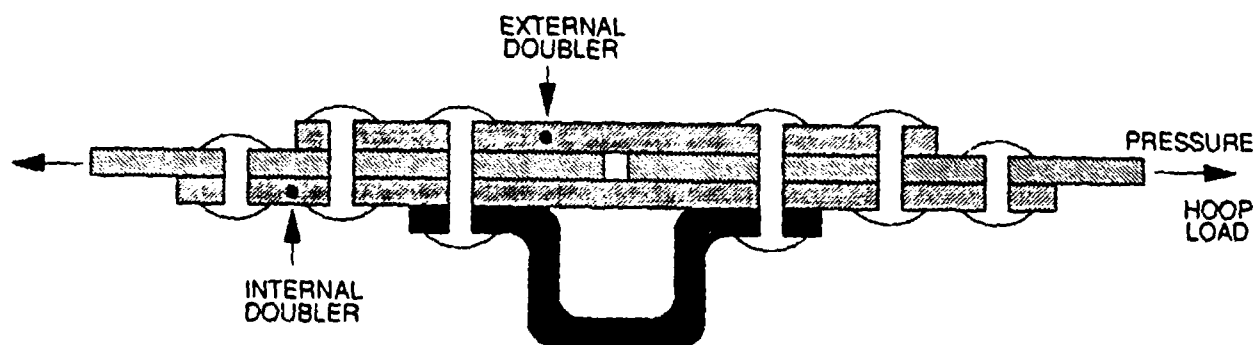
Good fatigue design requires extra material and multiple fastener rows in crosswise splices. Extra material reduces the local skin stress, and multiple fastener rows reduce the bearing stresses. Both factors affect fastener detail fatigue life. Extra material means abrupt change of thickness, a feature which tends to overload the outer fastener rows. The best splice designs employ some combination of the following measures to produce an equitable distribution of fastener bearing loads: (1) multiple fastener rows on each side of the splice; (2) greater fastener pitch in the outer rows; (3) smaller fastener pitch between rows; (4) stepped doublers; (5) doubler taper in the plan view; and (6) fastener flexibility.

Figure 4-26 illustrates cross sections of some possible splice configurations. Examples (a) and (b) show two different approaches to the design of a fuselage skin splice. With three steps and three rows per side, example (b) distributes the bearing loads more evenly than example (a). Example (c) shows how a good load distribution might be achieved where a chordwise splice has been introduced into a wing box to accommodate a drop in the thickness of the lower skin.

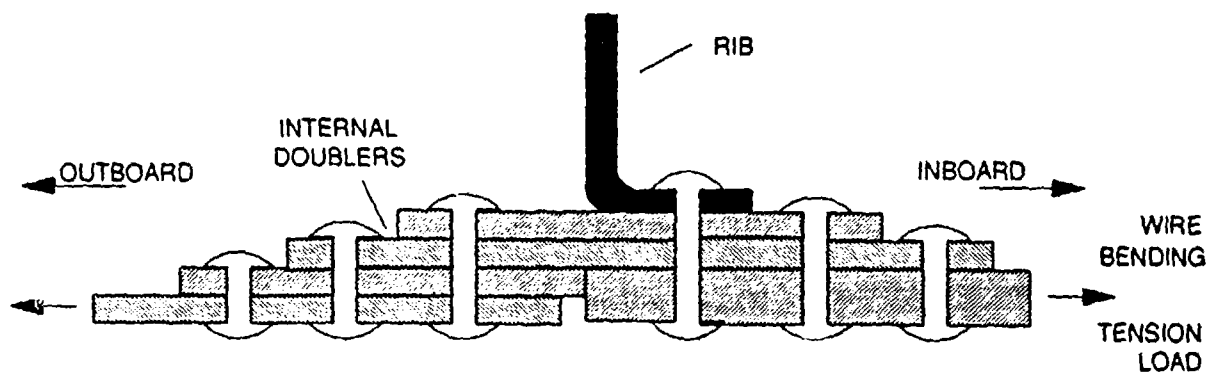
Figure 4-27 illustrates two additional examples. Example (a) shows a lap splice with eight fastener rows. The pitch X_2 between each outer and middle row is less than the pitch X_1 used elsewhere. Example (b) shows a tapered doubler with "finger" edges and outer row pitch twice the pitch of the inner rows.



(a) Lap splice over fuselage stringer.

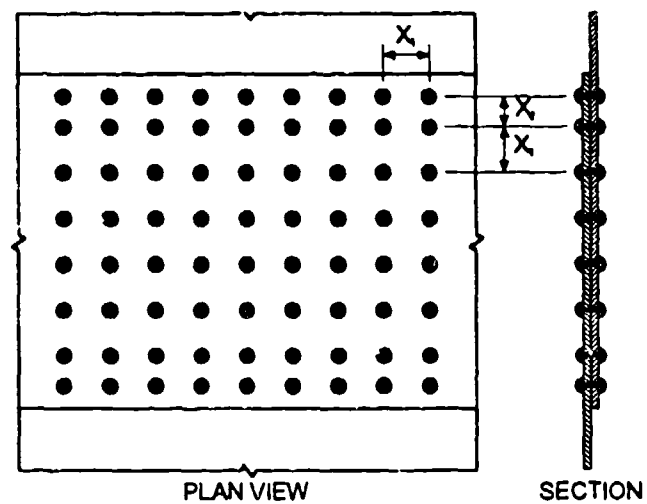


(b) Butt splice over fuselage stringer.

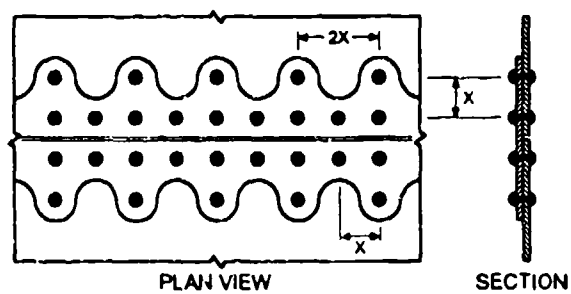


(c) Chordwise butt splice at skin thickness drop in a wing box.

Figure 4-26. Examples of splice details.



(a) Lap joint with pitch change between rows.



(b) Tapered "finger" doubler with outer row pitch doubled.

Figure 4-27. Examples of pitch change and taper.

4.3.3.1 Load Concentration and the Benefit of Fastener Flexibility

A simplified model of a lap splice, Figure 4-28, serves to show how bearing loads concentrate at the outer rows, and also how fastener flexibility reduces the concentration. The model is based on a three-row splice (skins only) with pitch X_1 along the rows and X_2 between rows. One line of fasteners is isolated for analysis as shown below. The total load which the line must transfer is $F = \sigma X_1 t$ (skin stress times area of isolated strip).

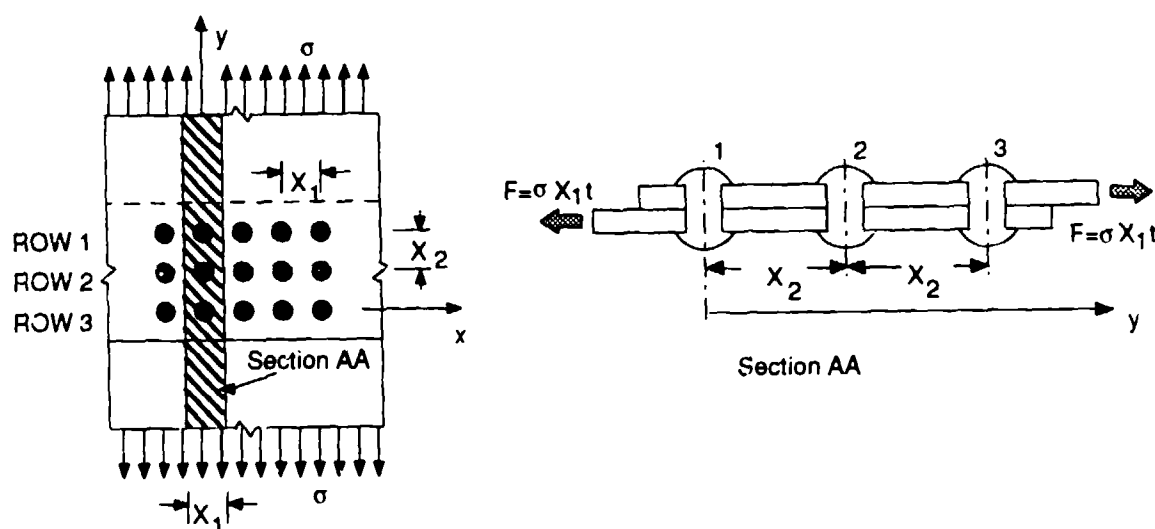


Figure 4-28. Plan view and section of a lap splice model.

In order to focus attention on the character of the load transfer process, we shall assume that each skin ligament is uniformly stressed in tension, and that each fastener is stressed in simple shear.

The total load anywhere in the splice must be $\sigma X_1 t$. The free edges of the skins are unstressed.

Suppose that the upper skin stress is σ_1 between rows 1 and 2. Then the stress in the lower skin between the same rows must be $\sigma - \sigma_1$, and the first fastener has transferred the load $F_1 = C_1 X_1 t$.

See Figure 4-29.

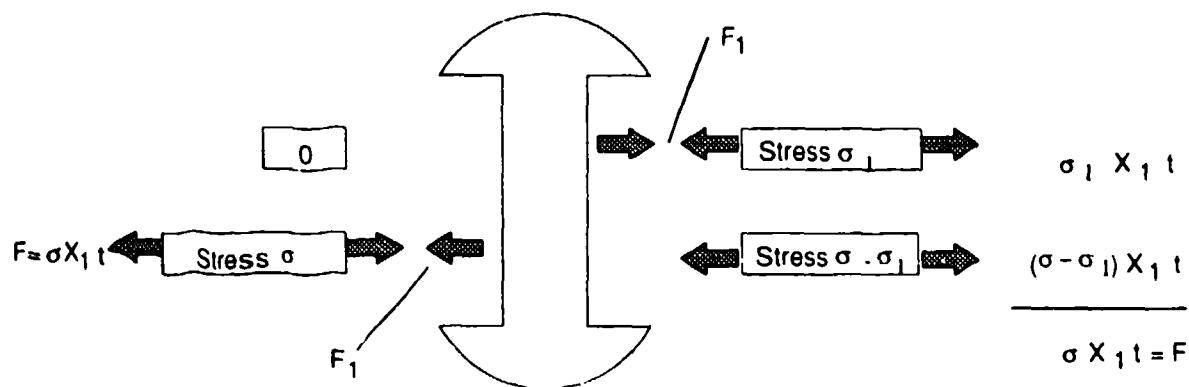


Figure 4-29. Free-body diagram of left half of splice.

A similar analysis of the ligaments between rows 2 and 3 shows that the skin stresses should be reversed (i.e., σ_1 and $\sigma - \sigma_1$ in the lower and upper skins), and also that $F_3 = F_1$. Finally, the load on the middle fastener must be $F_2 = (\sigma - 2\sigma_1) X_1 t$ to reverse the upper and lower skin stresses. The complete picture of skin stresses and fastener bearing loads is shown in Figure 4-30.

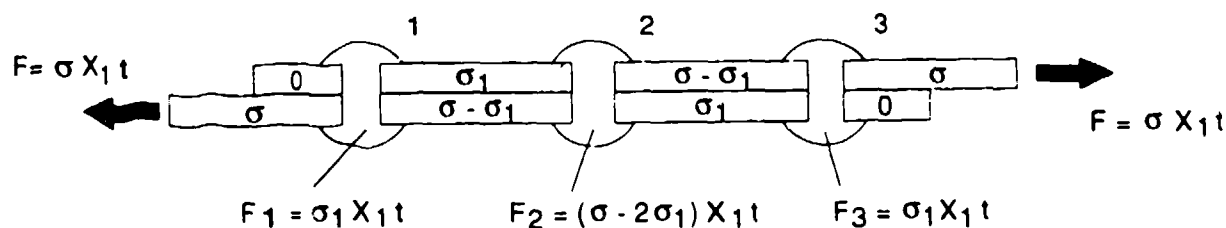


Figure 4-30. Reassembled splice section with stresses and forces summarized.

We have not yet actually found the stresses and bearing loads in the splice. Note that the stress σ_1 can have any value without violating the equilibrium condition anywhere in the splice. The correct value is the one which makes the difference between the upper and lower skin deflections just equal to the fastener shear deflection.

The skin deflections depend on the tensile strain in each ligament, e.g., the upper skin ligament between rows 1 and 2 stretches by the amount $(\sigma_1/E)X_2$. Figure 4-31 summarizes a simple model for fastener shear. The fasteners are assumed to have a shank cross section area A and the same elastic properties as the skins. The bearing forces F_n ($n = 1, 2, 3$) are assumed to cause a simple shear stress $\tau = F_n/A$ in the middle half of the shank. The shear strain $\gamma = 2(1 + \nu)\tau/E$ can also be expressed as $\gamma \cong \Delta y_n/t$ for small deflections, where Δy_n is the fastener shear deflection and t is the skin thickness. Combining these expressions leads to:

$$\Delta y_n = 2(1 + \nu) \frac{F_n t}{EA} \quad (4-7)$$

$$\Delta y_1 = \Delta y_3 = 2(1 + \nu) \frac{t^2}{A} \frac{\sigma_1}{E} X_1$$

$$\Delta y_2 = 2(1 + \nu) \frac{t^2}{A} \frac{\sigma - 2\sigma_1}{E} X_1 \quad (4-8)$$

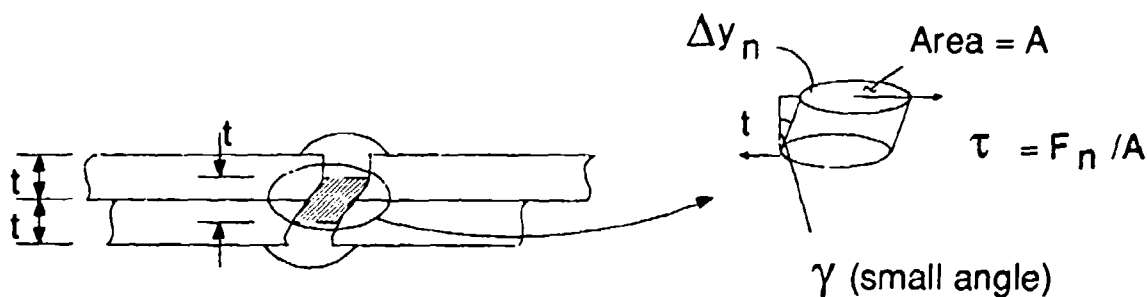


Figure 4-31. Fastener shear model.

Figure 4-32 shows two schematics of the splice as it would appear unloaded and under load. The unstressed parts have been omitted for clarity. Each open rectangle represents a skin ligament, and each shaded rectangle represents the middle half of a fastener shank. The small black circles keep track of the fastener hole centers in the upper and lower skins. (These points should coincide with the fastener centerlines.)

In the unloaded splice, the upper and lower skin points have the same coordinates:

$$y_{U1} = y_{L1} = 0; \quad y_{U2} = y_{L2} = X_2; \quad y_{U3} = y_{L3} = 2X_2 \quad (4-9)$$

For convenience the loaded splice has been aligned so that y_{L1} remains at the y -axis origin. However, $y_{U1} = \Delta y_1$ due to the shear of the first fastener. The deflected coordinates of the other points are:

This coordinate =	Last coordinate +	Unloaded ligament length +	This ligament stretch
y_{U2}	$\Delta y_1 +$	$X_2 +$	$\frac{\sigma_1}{E} X_2$
y_{L2}	$0 +$	$X_2 +$	$\frac{\sigma - \sigma_1}{E} X_2$
y_{U3}	$\Delta y_1 + X_2 + \frac{\sigma_1}{E} X_2 +$	$X_2 +$	$\frac{\sigma - \sigma_1}{E} X_2$
y_{L3}	$X_2 + \frac{\sigma - \sigma_1}{E} X_2 +$	$X_2 +$	$\frac{\sigma_1}{E} X_2$

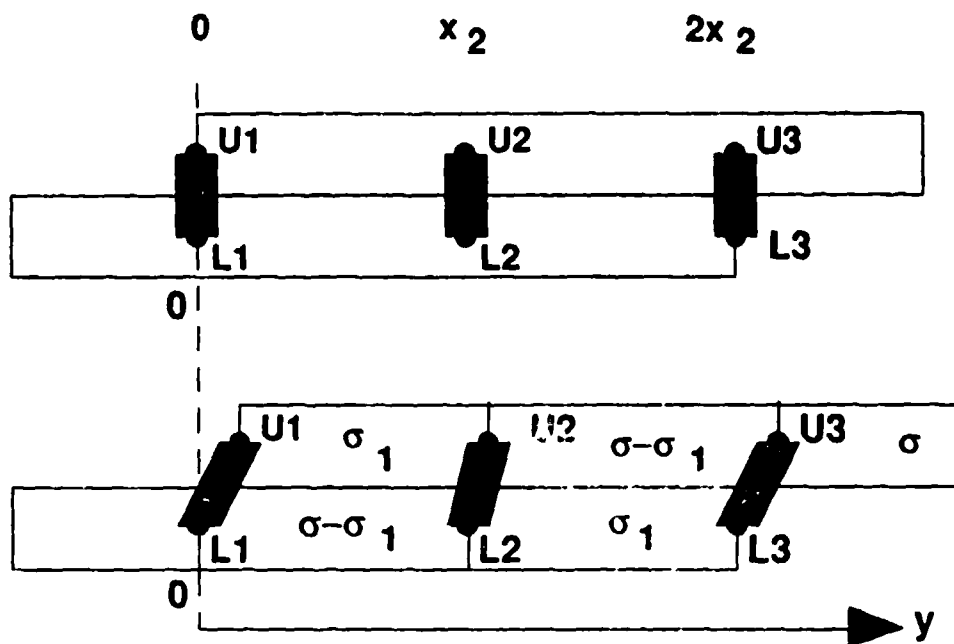


Figure 4-32. Before and after deformation schematic.

The differences between the upper and lower coordinates must agree with the fastener shear. For the third row, this leads to $y_{U3} - y_{L3} = \Delta y_3$, which reduces to the result $\Delta y_3 = \Delta y_1$ obtained earlier. For the middle row,

$$y_{U2} - y_{L2} = \Delta y_1 + \frac{2\sigma_1}{E}X_2 - \frac{\sigma}{E}X_2 = \Delta y_2 \quad (4-10)$$

After substituting the expressions for Δy_1 , Δy_2 derived earlier and rearranging, we can express the solution as:

$$\sigma_1 = \frac{1+\lambda}{2+3\lambda}\sigma \quad (4-11)$$

$$\frac{F_1}{F} = \frac{F_3}{F} = \frac{\sigma_1}{\sigma} \quad \frac{F_2}{F} = 1 - \frac{2\sigma_1}{\sigma} \quad (4-12)$$

where

$$\lambda = 2(1+\nu)\frac{I^2X_1}{AX_2} \quad (4-13)$$

If the fastener is made from a material different from the skins, then:

$$\lambda = 2(1 + \nu_f) \frac{t^2 X_1 E}{A X_2 E_f} \quad (4-14)$$

where E_f , ν_f are the fastener material properties.

The following example represents a skin lap splice in a large transport aircraft:

skin thickness = 0.04" per skin

fasteners - 5/32 dia. AN-426/100° CTSK (driven dia = 0.16"; A = 0.02 in.²)

pitch - 1.00" in both directions

fastener material - aluminum ($\nu = 0.33$)

$$\lambda = 2 \times 1.33 \times (0.04)^2 / 0.02 = 0.213$$

$$\sigma_1 / \sigma = (1 + 0.213) / (2 + 3 \times 0.213) = 0.46$$

Thus, each outer row takes 46% of the splice load, while the middle row takes only 8%. (These numbers exaggerate the load concentration effect somewhat because actual fasteners are more flexible than the simple shear model.)

The foregoing is an example of a compatibility model, i.e., the solution for stresses and bearing forces is determined by enforcing the condition that, under load, the structure's component displacements must be compatible with each other at the junction points. We shall see later that compatibility models also play a major role in the stress analysis of damaged and repaired structures.

The lap splice example above illustrates the basic principle of compatibility analysis. Other splice designs with more fastener rows and/or stepped thickness can be modeled and analyzed in the same way.

Bonded splices behave in a similar but continuous manner. The bond layer is stressed in shear, and the tension is smoothly transferred from one side of the splice to the other. The shear stress peaks at the edges of the splice. A role similar to that of λ in mechanical joints is played by:

$$\beta = \sqrt{2(1 + \nu_b) \frac{E}{E_b} h t} \quad (4-15)$$

for bonded joints, where h is the thickness and E_b, ν_b the elastic properties of the bond layer. For a simple bonded lap splice of length L (Figure 4-33), the shear stress in the bond layer and the tension in the upper skin are given respectively by:

$$\frac{\tau}{\sigma} = \frac{t}{2\beta} \left[\frac{e^{y/\beta}}{e^{L/\beta} - 1} + \frac{e^{-y/\beta}}{1 - e^{-L/\beta}} \right] \quad (4-16)$$

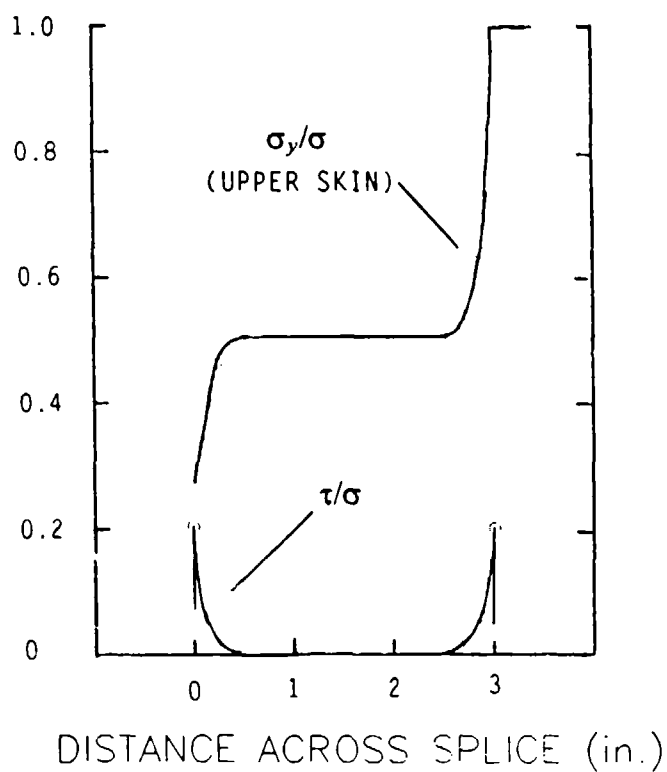
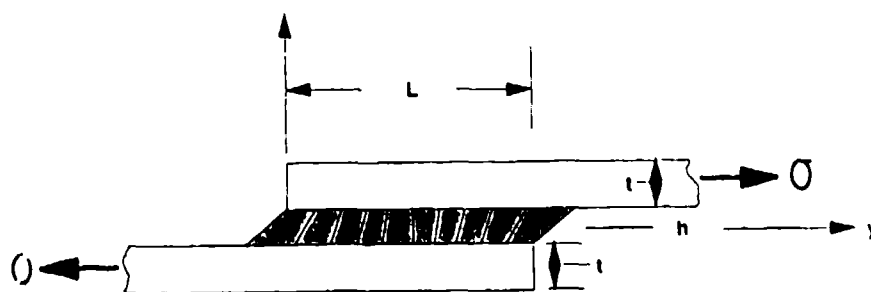
$$\frac{\sigma_u(y)}{\sigma} = \frac{1}{2} \left[\frac{e^{y/\beta} - 1}{e^{L/\beta} - 1} + \frac{1 - e^{-y/\beta}}{1 - e^{-L/\beta}} \right] \quad (4-17)$$

The lower part of Figure 4-33 shows the stress distributions for a 3-inch splice in 0.04-inch thick aluminum skins ($E = 10^7$ psi) with a 0.005-inch thick epoxy bond layer ($E_b = 560,000$ psi, $\nu_b = 0.4$). Note that the average level of shear stress in the bond layer is less than 5 percent of the tensile stress carried by the splice.

A fastened splice is evidently a multiple path structure, whereas a bonded splice has only one load path. Therefore, bonded splices must be designed and fabricated with great care.¹²

Offset splices are also subject to additional stress concentration in the bond layer because of eccentric bending. For example, the offset lines of action of the upper and lower skin tensile loads in the lap splice shown in Figure 4-33 tend to bend the skins, with the result shown in Figure 4-34(a). One result is a buildup of tensile stress across the bond layer, near the edges of the splice. This is called "peel stress," from its tendency to make the bond fail by peeling apart.

¹²See Section 4.4 for discussion of fabrication.



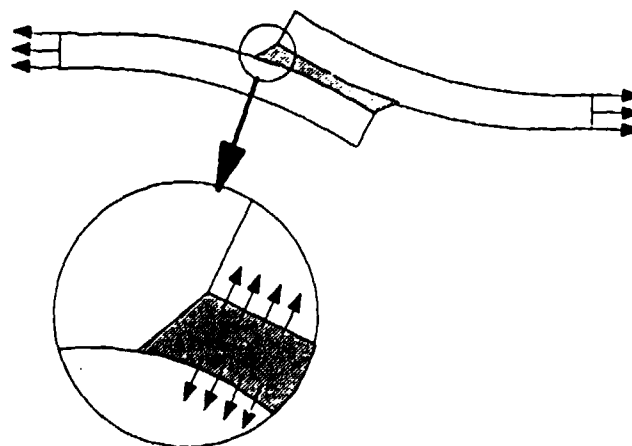
Data:

$E = 10^7$ psi	$G_b = 2 \times 10^5$ psi
$\nu_b = 0.4$	$h = 0.005$ "
$\beta = 0.1$	$t = 0.040$ "
$L = 3$ "	
τ = Shear stress in bond	
σ_y = Tensile stress in upper skin	
σ = Applied load	

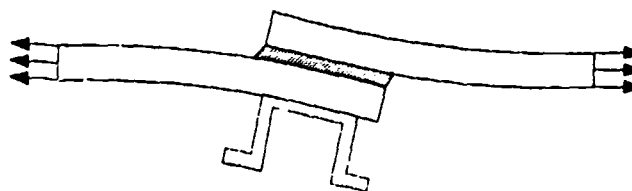
Figure 4-33. Load transfer in a bonded lap splice.

The peel stress is lower in splices tied to stringers because the stringer torsional stiffness partially restrains the splice against eccentric bending, as shown in Figure 4-34(b).

The fail-safe built into a fastened splice is sometimes taken for granted. However, close attention should be paid to the fatigue characteristics, especially for crosswise splices. When



(a) Eccentric bending reduces offset



(b) Edge of bend stresses in tension

Figure 4-34. Eccentric bending effects in a lap splice

fastener bearing loads are high, as they must be in a splice across a major load path, subtle effects of fretting and/or corrosion can lead to widespread cracking early in the airframe life.

In the 1930s and early 1940s, load-bearing splices in many airframes were fastened by clearance rivets, i.e., the fastener hole diameters were such that some clearance between the skin and rivet shank remained after driving. The resulting loose fit allowed the faying surfaces and rivets to slide back and forth against each other when the airframe was subjected to gusts and other flight loads.

The motion is called fretting and is revealed by the presence of metal oxide dust, some of which migrates to the exposed skin surface. Fretting fatigue life is typically less than half the fatigue life of plain specimens subjected to the same alternating stress without the fretting action. The result in the old airframes was unexpected early fatigue cracking.

As a consequence of the experience with clearance rivets, airplane manufacturers switched to interference-fit rivets, in order to eliminate the fretting problem, at about the time that high-altitude transports began to be built in large numbers. Interference fit refers to the condition achieved when a rivet shank is expanded against the surrounding skins during driving. The resulting pressure maintains a more nearly uniform bearing stress distribution under load and eliminates the opportunity for large fretting motion (Figure 4-35). However, there are still some circumstances in which interference-fit fasteners may not prevent fretting (see Section 4.4).

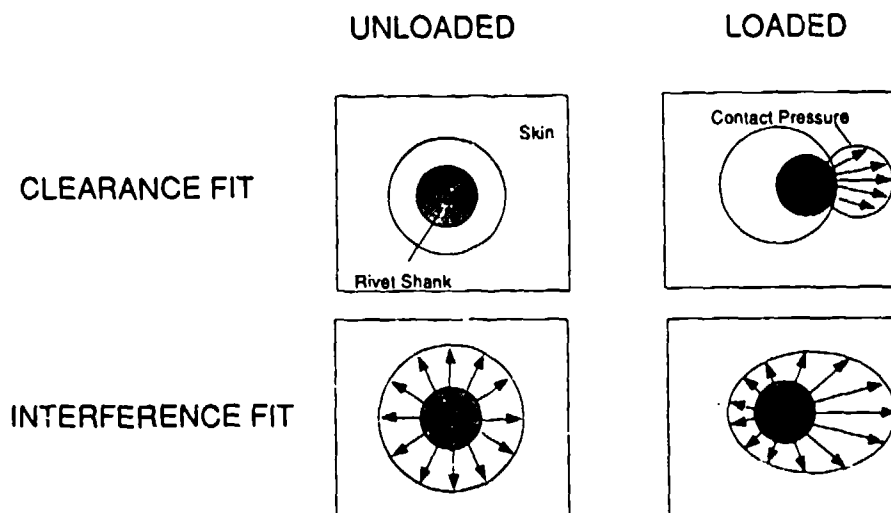


Figure 4-35. Effect of interference fit.

Corrosion is normally viewed as a maintenance problem because its most common effects are visibly evident, gradual reductions of skin thickness which can be discovered and repaired well before any significant loss of airframe strength. If liquids can reach fastener details, however, the effects of corrosion can be concentrated at the thin edges of countersunk holes. Even atmospheric moisture can provide a good corrosive medium in this case, because different metals in contact can act like a small galvanic battery in the presence of ordinary water. The effect of the battery circuit is to transport metal ions from one surface to another (Figure 4-36). The surface which loses the ions is pitted, and the pits develop into a crack.

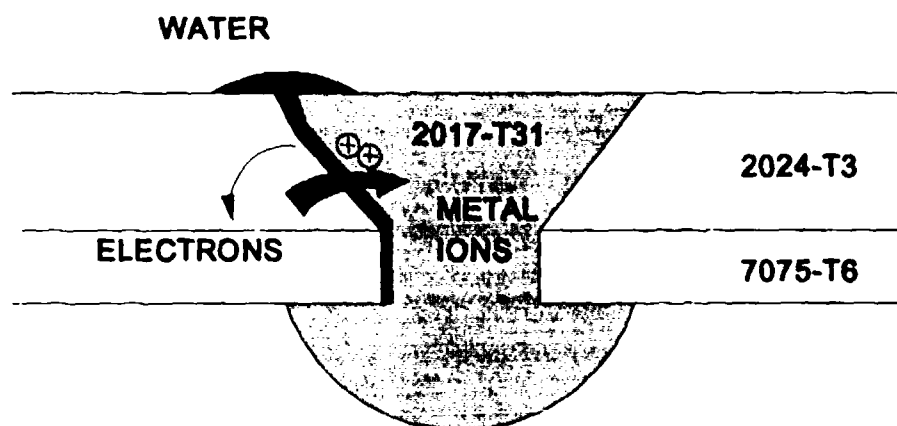


Figure 4-36. Galvanic corrosion.

The effects of fretting and corrosion can be insidious in splices which carry major loads. When either effect is present, small cracks may form within a short period at large numbers of adjacent ligaments between fastener holes. The critical crack length must be small because the ligaments are short. Thus, large numbers of ligaments can fail within a short time, robbing the splice of its fail-safety. Due to the load concentration effect discussed earlier, the outer fastener rows are generally the critical rows in such situations.

4.3.4 Repairs

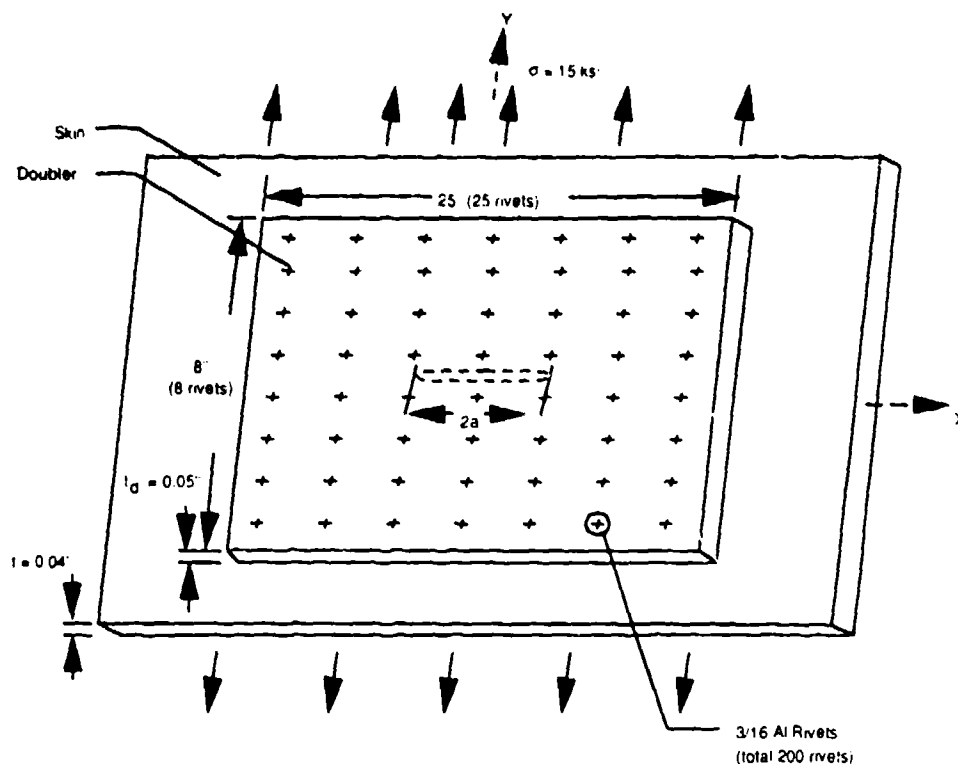
Airframe repairs are often designed as rivetted doubler patches on skin areas which have either been damaged or are being reinforced to avoid or delay cracking. Repair doublers transfer load in the same way as doublers at splices, i.e., the bearing loads are concentrated toward the outer fastener rows. However, the bearing loads in a repair patch are less than those in a crosswise splice because the skin underneath the repair is still stressed. Another difference between patches and splices is that most patches are subject to Poisson effects because they do not span the full width of the skin. As a result, the fastener bearing loads also tend to concentrate toward the corners of a patch.

Older repair doubler designs were generally based on static strength considerations. The doubler skin thickness, number and size of fasteners, number of rows, and fastener pitch were selected to provide sufficient strength for the doubler to carry the entire load in its area. However, fatigue and damage tolerance considerations suggest that some doubler designs are better than others, even though they may have identical static margins. The following example illustrates these points [4-3].

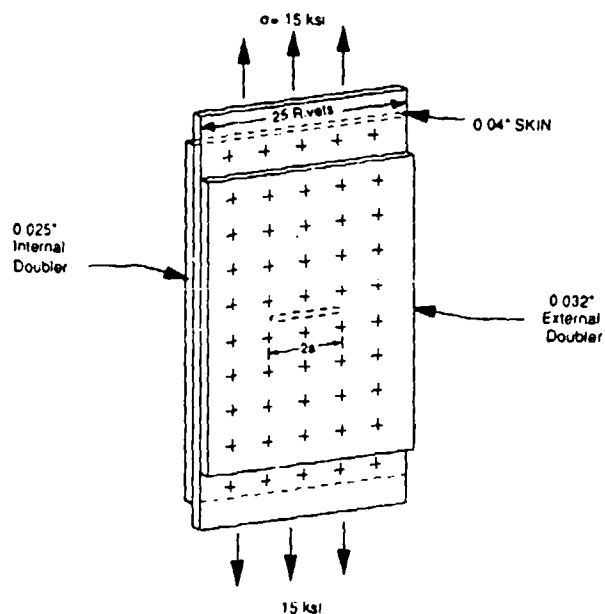
Figure 4-37 illustrates two alternative but statically comparable repair designs for a 0.04-inch thick damaged skin with a nominal stress of 15 ksi. Design (a) is a 0.05-inch thick conventional single doubler patch with four rows of rivets on each side of the damage. The 8x25-inch doubler covers a skin area where damage has been cut out. The effect of the cutout on the ability of the underlying skin is represented by a crack (length = $2a$) in the numerical analysis model. Design (b) is a patch consisting of two doublers: a 0.025-inch thick internal doubler which extends to a fifth fastener row on each side, and a 0.032-inch thick external doubler.¹³

A finite element stress analysis was performed for each of the designs shown in Figure 4-37, in order to determine the fastener bearing loads. The underlying skin damage was

¹³Design (b) has the same 8x25-inch dimensions; the sketch stops at a typical section to show the doubler arrangement.



(a) Conventional single doubler.



(b) Stepped inside/outside doubler.

Figure 4-37. Damaged skin with repair patch.

represented by a 2-inch crack. The results for the conventional repair are shown in Figure 4-38. The plot at the right compares the bearing load component parallel to the applied stress with results obtained from a compatibility model solution by Swift [4-4]. Swift's model considered only one-dimensional behavior (no Poisson effect). The concentration of bearing load toward the outer rows is evident and, near the center of the patch, the results agree with Swift's results. The finite element results, which do include the Poisson effect, show an additional concentration of load toward the lateral edges of the patch. The component parallel to the applied stress is 227 lb. (18 percent higher than the 187 lb. load on the interior upper and lower fasteners). There is also a 76-lb. lateral force component acting on the corner fasteners, i.e., their total bearing load is 239 lb.

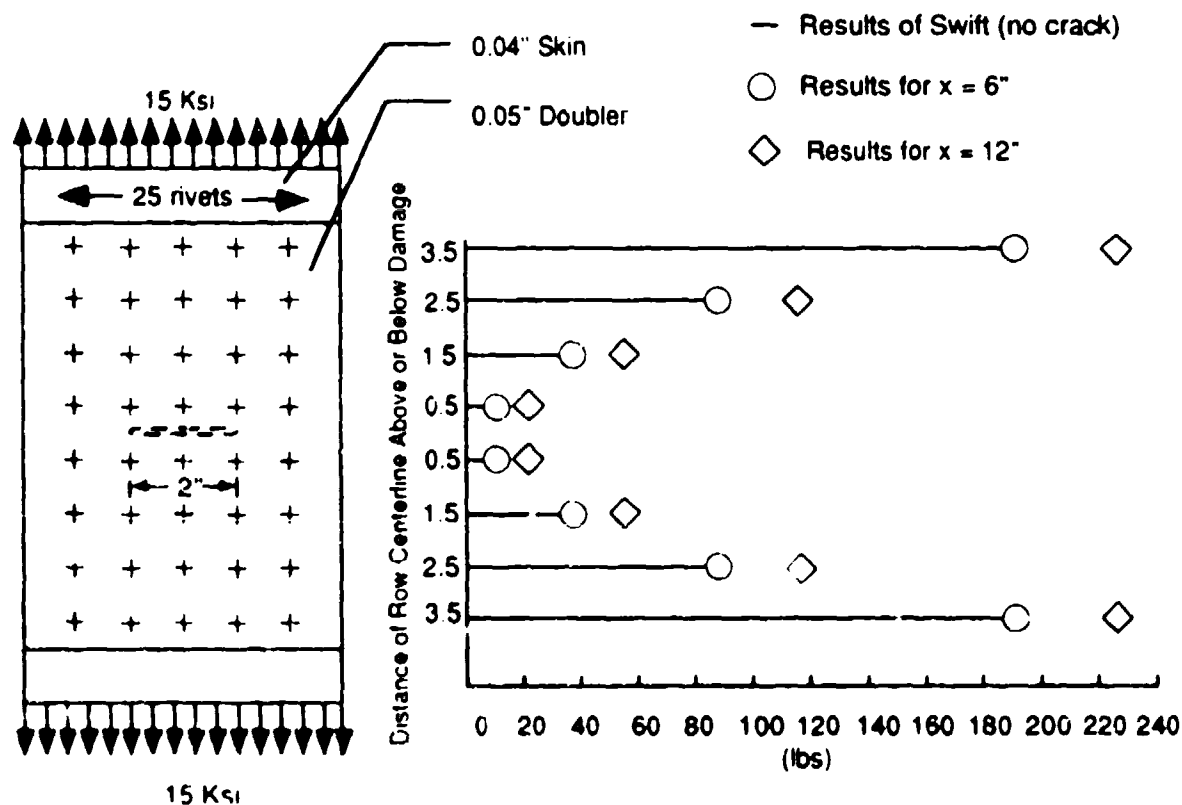


Figure 4-38 Rivet load distribution in a single doubler.

Figure 4-39 compares the finite element solutions for the fastener bearing loads at the lateral edges of the two alternative repair designs. (As in the preceding figure, only the force component parallel to the applied stress is plotted.) The stepped doubler reduces the corner fastener bearing load by about 20 percent.

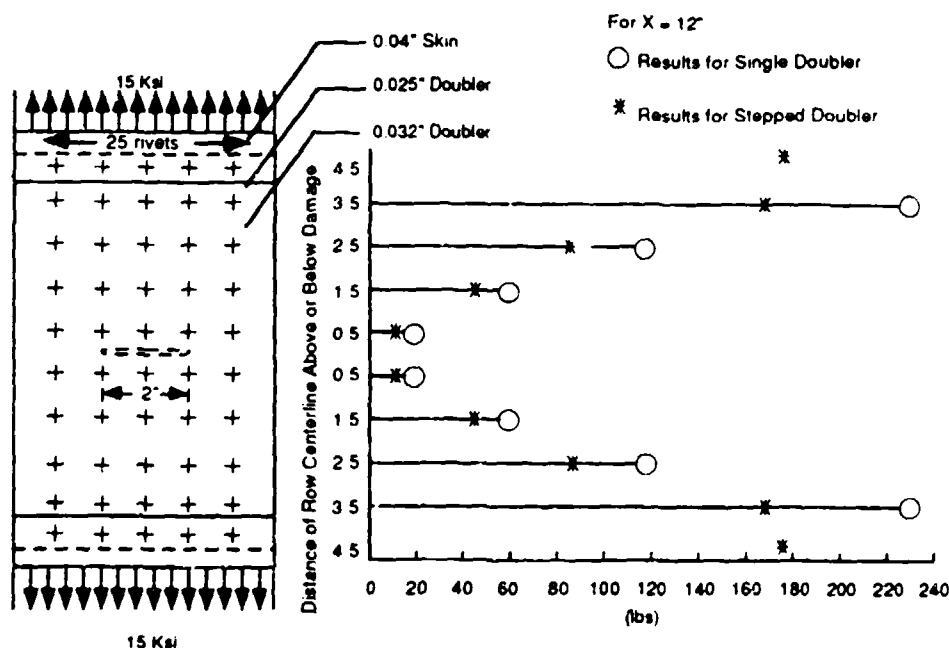


Figure 4-39. Comparison of rivet load distributions in stepped and single doublers.

A conventional fatigue analysis using open hole data (stress concentration factor of 3) for 2024-T3 aluminum skins and assuming $R=0$ gives a safe-life of 160,000 cycles for the basic structure. Similar analyses for the doublers give much shorter safe lives because of the fastener bearing load concentrations. The life was estimated to be 39,000 cycles for the single doubler, but improved to 55,000 cycles for the stepped doubler.

Another lesson to be learned from the foregoing example is that one should expect recurring damage at repair patch sites. If the example is considered as an approximate model for a fuselage repair, the estimated safe lives represent numbers of flight cycles that could easily be accumulated on the patch. Thus, it would be a good idea to evaluate the damage tolerance of such repairs as multiple patch structure (keeping in mind the possibility of widespread cracking).

4.4 MATERIAL CONSIDERATIONS

Materials are selected for airframes based on a wide variety of criteria. Most of the criteria were evolved to meet other goals, before the advent of damage tolerance requirements. The other goals involve practical considerations of economics and manufacturing, as well as other parts of the airworthiness standards. Some of these criteria contribute to damage tolerance, whereas others tend to detract from it.

The engineer responsible for damage tolerance evaluation should recognize the fact that material selection involves a series of compromises to balance competing requirements. Material selection should be reviewed for: (1) possible sacrifice of damage tolerance characteristics; (2) effect of selections on damage sources; (3) use of appropriate damage assumptions and material properties; and (4) requirements for supporting tests.

Table 4-3 summarizes some typical metal selection criteria and their associated goals. Following the table are several examples of the ways in which selection decisions can affect damage tolerance.

It is unlikely that future selections for major materials in primary structure will be made at the sacrifice of damage tolerance. Nevertheless, it is worthwhile to understand how such decisions were arrived at in the past, before much attention was paid to damage tolerant design.

The tendency to overemphasize static strength criteria has been a recurring theme.¹⁴ The pressure to save weight has sometimes led to increased allowable stresses based on higher static strength, but the stronger material was neither tougher nor more resistant to crack growth than the material it replaced.

¹⁴This was discussed with regard to repair patches in the preceding section.

Table 4-3. Metal selection criteria.

Yield strength	Static margins (FAR 23.305, FAR 25.305)
Ultimate strength	High strength/weight ratio for light structure Bearing strength and resistance to FOD
Elongation	Machinability Malleability (sheet metal forming, cold heading) Ability to accommodate assembly misalignment Redistribution of load from local damage site
Elastic modulus	Buckling and flutter resistance High stiffness/weight ratio for light structure
Fatigue strength	Low notch sensitivity; durability
High-temperature properties	Ability to take hot work without tearing (forgings) Strength retention at elevated service temperature
Hardness	Resistance to wear and FOD
Microstructure	Good casting properties (low discard) Machinability; weldability Good properties in secondary directions Resistance to pit/crevice corrosion Resistance to stress corrosion cracking
Fracture toughness	Reliability (repeatability) of properties
R-curve properties	Large critical crack size
Crack growth rate	Slow growth; high threshold
Alloy class and composition	Cost and availability Low weight Good tempering characteristics Resistance to oxidation (area corrosion) Galvanic compatibility Frictional compatibility

One example was the widespread use of 7178-T6 in place of 2024-T3 in the lower wing skins of some military airplanes built in the 1950s and 60s. The fracture toughness of 7178-T6 was also later found to be unreliable, based on the lack of repeatability in tests of samples from existing airframes.

Materials that are sensitive to pit or crevice corrosion should be treated as potential sources of multiple site damage. The 2014-T6 forgings often used for wheels are in this category. Also of concern are the precipitation hardened (PH) stainless steels when aged¹⁵ to high strength levels.

A circumstance which can affect the type of damage is lack of improvement in secondary properties. For example, some of the Ti-6Al-4V titanium alloy used in the early 1970s was later found to have poor stress corrosion cracking resistance (K_{ISCC}) in the TL and TS orientations. The secondary stresses in titanium spar cap reinforcements led to early cracking, which revealed the problem.

Fastener selection can have subtle but important effects on damage tolerance. On one hand, making fasteners more flexible relative to the joint stack thickness reduces the concentration of bearing loads in the outer rows of splices (Section 4.3.3). On the other hand, the extra flexibility decreases tear strap effectiveness (Section 4.3.2) and may promote fretting.

The change from clearance to interference-fit rivets to take care of fretting fatigue and widespread cracking was mentioned in Section 4.3.3, but interference fit is just one of three equally important factors. The other two are clamping pressure and flexibility. In general, the more flexible the fastener, the more interference-fit pressure and/or clamping pressure are required to suppress fretting motion.

When a rivet is driven, the cold heading process simultaneously expands the shank against the fastener hole and creates clamping pressure between the heads and stack. Both interference and clamping pressure are limited, especially in thin-sheet stacks, in order to avoid excessive distortion of the skin surrounding the fastener hole. This restriction is generally enforced by selection of a rivet material somewhat softer than the skin material.

¹⁵Heat treated according to a specified temperature-time profile to agglomerate the precipitates into particles of certain size and spacing in the microstructure.

Another general area of concern is dissimilar metal contact in joint stacks. Steel or titanium plate is frequently interleaved with aluminum to provide additional strength and bearing capacity where load is gathered into a major transfer point (wing/fuselage attachments), and titanium sheet is sometimes used for fuselage tear straps. Inboard wing boxes generally have skins or webs thick enough to require bolts at some connections, and the fasteners are usually steel.

Common drilling of dissimilar metals is an accepted practice to meet dimensional tolerances in a joint stack. In such cases, it is important to examine the stacking sequence in relation to the drilling direction, since chips from hard, high strength metals can create damage when dragged out through overlying layers of softer metals (Figure 4-40).

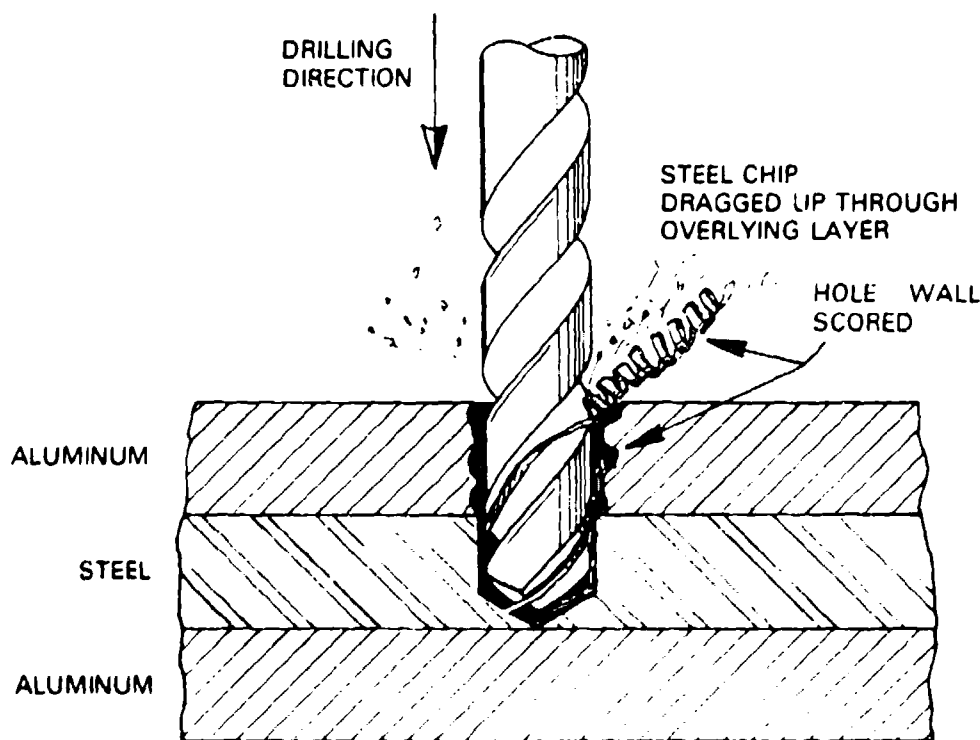


Figure 4-40 Chip-drag damage in dissimilar metal stack

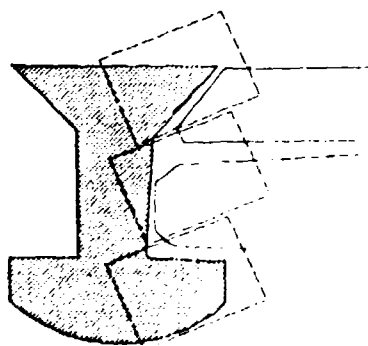
Debris from drilling operations is another topic worth mentioning at this point, even though strictly speaking, drilling involves shop practice rather than material selection. Debris from countersinking and/or deburring can migrate in between faying surfaces when common drilling practice is employed on unbonded splices. An example is illustrated in Figure 4-41. Debris reduces clamping effectiveness and degrades fastener hole quality.

Any opportunity for dissimilar metals to come into contact in the presence of moisture is an opportunity for galvanic corrosion and cracking. Zinc chromate treatment of skin and stringer surfaces and cadmium plating of bolts have been used for many years to protect aluminum structure. However, parts are chromated before fastener holes are drilled, and cadmium plating can be scratched through when a fastener is installed. Better measures (bonded/sealed joints with anodized fasteners) are now beginning to replace the older practice.

The damage tolerance evaluator should still remain alert to the possibility of galvanic corrosion in stacks that are not thoroughly protected. A useful indication of the potential for corrosion is how far apart the contacting metals are located in a galvanic series (Table 4-4). Stacks with high potential should be further examined for their ability to act as moisture traps.

4.5 TYPE AND EXTENT OF DAMAGE

It is accepted practice to assume certain standard crack shapes and sizes for the purpose of damage tolerance analysis. Well known stress intensity factor formulas represent the standard cracks, which establish a common baseline for evaluation of different airframes. The specifications for the standard cracks are based on the experience gained from studies which supported the development of the Air Force damage tolerance requirements and from the general experience acquired by industry specialists who have analyzed the propagation paths of numerous cracks in structure removed from civil as well as military airplanes.



(The specimen was encased in a clear plastic before sectioning to keep cutting debris from contaminating the experiment. Specimen was not produced to aircraft quality specifications.)

Left: schematic of details in above photograph.

Figure 4-41. Section through rivet showing debris between faying surfaces.

[From Professor R. Pelloux, MIT, by permission]

Table 4-4. Galvanic series in sea water.

[Reprinted from J.H. Brophy, R.M. Rose, and J. Wulff, The Structure and Properties of Materials, Volume II, Thermodynamics of Structure, Copyright © 1964, by permission of John Wiley and Sons, New York, N.Y.] [4-5]

CORRODED END

Magnesium
Magnesium alloys
Zinc
Galvanized steel or galvanized wrought iron
Aluminum (52SH, 4S, 3S, 2S 53ST in this order)
Alclad
Cadmium
Aluminum (A17ST, 17ST, 24ST in this order)
Mild steel
Wrought iron
Cast iron
Ni-Resist
13% Cr stainless steel Type 410 (active)
50-50 lead-tin solder
18-8 stainless steel Type 304 (active)
18-8-3 stainless steel Type 316 (active)
Lead
Tin
Muntz metal
Manganese bronze
Naval brass
Nickel (active)
Inconel (active)
Yellow brass
Admiralty brass
Aluminum bronze
Red brass
Copper
Silicon bronze
Ambrac
70-30 copper-nickel
Composition G bronze
Composition M bronze
Nickel (passive)
Inconel (passive)
Monel
18-8 stainless steel Type 304 (passive)
18-8-3 stainless steel Type 316 (passive)

PROTECTED END

The most important elements are the specifications for the cracks which are assumed to exist in the airframe when it enters service. These are called initial cracks, and their shapes and sizes are based on Air Force studies of manufacturing damage. Realistic initial crack specifications are so important because a small change in the assumed crack size can make a big difference in the estimate for crack growth life.

Therefore, there are two separate specifications for initial cracks. The first represents average manufacturing quality, i.e., the kind of small nicks and scratches one would expect to find at numerous locations in any airframe. The second (sometimes called the "rogue flaw"¹⁶) represents occasional shop-work errors which do not conform to production quality standards but, for some reason, go undetected. For the purposes of a damage tolerance evaluation, one rogue flaw is assumed to exist in the structure for each analysis case.

The specification for the average quality initial crack is based on a study conducted for the Air Force by McDonnell-Douglas in the 1970s. An aging F-4 airframe was torn down, and the primary structure components were closely inspected for cracks. Fasteners were removed, parts were stripped of paint and primer, and the clean metal at every fastener hole and other stress raiser was examined in bright light with 20X or 40X hand-held optical microscopes. For practical purposes, this search revealed every initial damage site in the study airframe.

The damage had, of course, turned into growing cracks long before the inspection, so that additional work was needed to derive the initial crack sizes. Some of the cracked parts were taken to the laboratory, where the crack surfaces were exposed and examined at high magnification (1000X to 10000X) under an electron microscope. At such high magnifications, fatigue crack surfaces in aluminum have a clearly rippled appearance (called striation). Striations begin to appear after the fatigue crack growth process gets underway; they are associated with the

¹⁶ The term was borrowed from sailing ship captains' descriptions of voyages in rough weather. One of their main concerns, when running before a heavy sea with swells coming from two different directions, was to watch for the occasional arrival of an abnormally large "rogue wave," which could swamp the ship if not detected in time for evasive action.

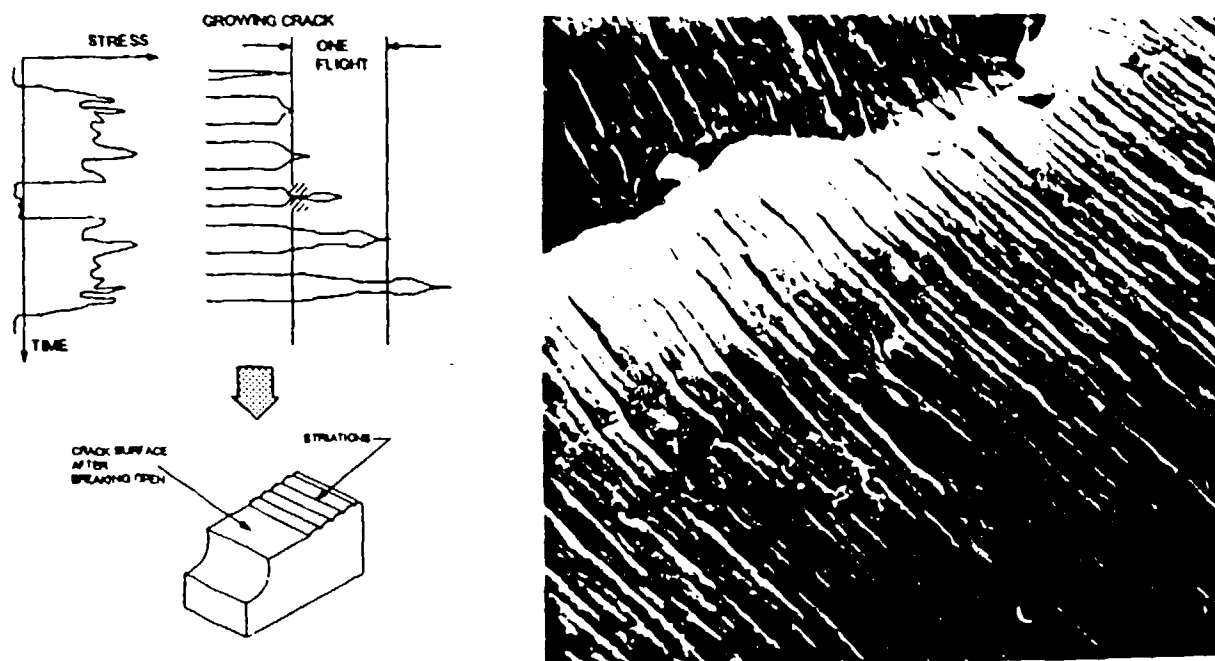


Figure 4-42. Striation mechanism and appearance.

[From Professor R. Pelloux, MIT, by permission.]

repeated opening and closing of the crack in response to the major stress changes in a flight (Figure 4-42).

Striations can be correlated with flight hours by comparison with flight recorder data, and striation counts can then be used to trace the fatigue crack back in time. This is not an exact science, but reasonable estimates are possible if the observations are further correlated with a crack growth analysis based on a da/dN equation which fits the specimen material properties. This was done for the F-4 cracks, and the da/dN equation was also used to extrapolate the crack size from the earliest visible striations back to zero time on the airframe. For the other cracks which were not examined in the laboratory, the da/dN was used to extrapolate from the time of the teardown inspection back to zero time.

The study results consisted of 104 derived values for initial crack size. The data was plotted on a cumulative probability graph, and a statistical analysis was made to evaluate the results (Figure 4-43). As can be seen from the plot, about 99% of the initial crack sizes in this sample were

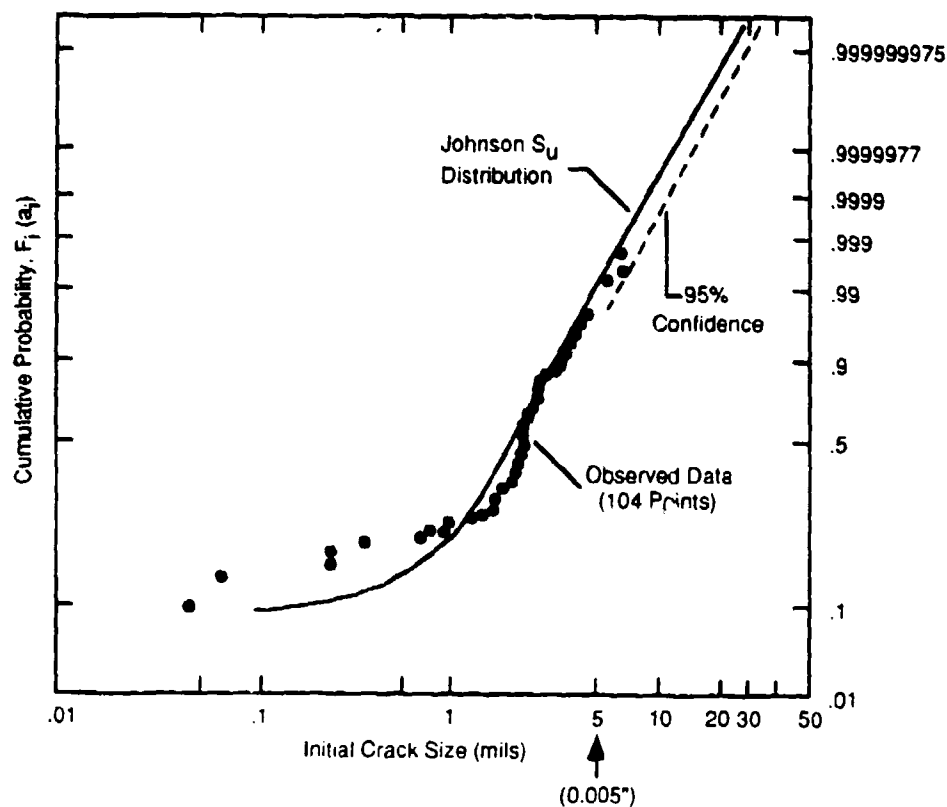


Figure 4-43. Derived initial size distribution for average quality cracks.

[Reprinted from Case Studies in Fracture Mechanics, AMMRC MS 77-5, June 1977, Fig. 1, with permission of McDonnell Douglas Corporation for use of their data.]

smaller than 0.005 inch. Also, the statistical analysis results suggest that, with 95% confidence, 90 to 95% of the cracks in any similar sample should be less than this size.¹⁷

Based on the foregoing results, the initial size for average quality cracks was conservatively specified as 0.005 inch. Most such cracks result from nicks or scratches caused by inadvertent angling of a tool against the edge of a sheet or fastener hole. Therefore, the initial shape was specified as a quarter circular corner crack for sections thicker than 0.005 inch, or a through-crack for thinner sheets (Figure 4-44).

The Air Force conducted a similar but much broader study to establish a specification for the rogue flaw. In reality, rogue flaws do not occur very often, and chances are that none would be

¹⁷The statistical statement means that, if similar surveys were made on 100 F-4 airframes, then the initial sizes of 90 to 95% of the cracks would be less than 0.005 inch in 95 of those airframes.

found in a teardown inspection of one airframe picked at random. Therefore, the rogue flaw study was based on collection from numerous airframes of components which had failed or were found to have large visible cracks during maintenance inspections. Conservative judgement in this case led to a specification for an initial crack ten times larger than the average quality crack (Figure 4-45).

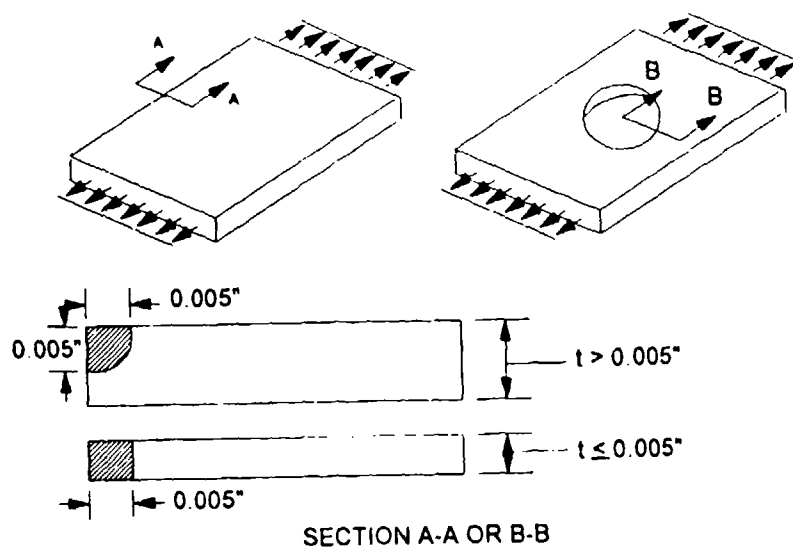


Figure 4-44. Specifications for average quality initial crack.

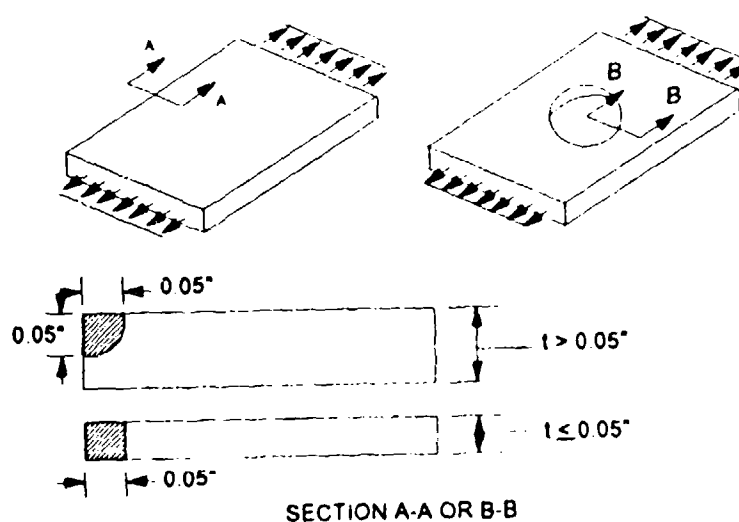


Figure 4-45. Specifications for rogue initial crack.

One or two initial cracks per analysis case are assumed for most purposes. (Average quality cracks at a number of adjacent fastener holes should be assumed to represent multiple site damage.) Figure 4-46 summarizes the initial crack type and location as a function of the analysis objective.

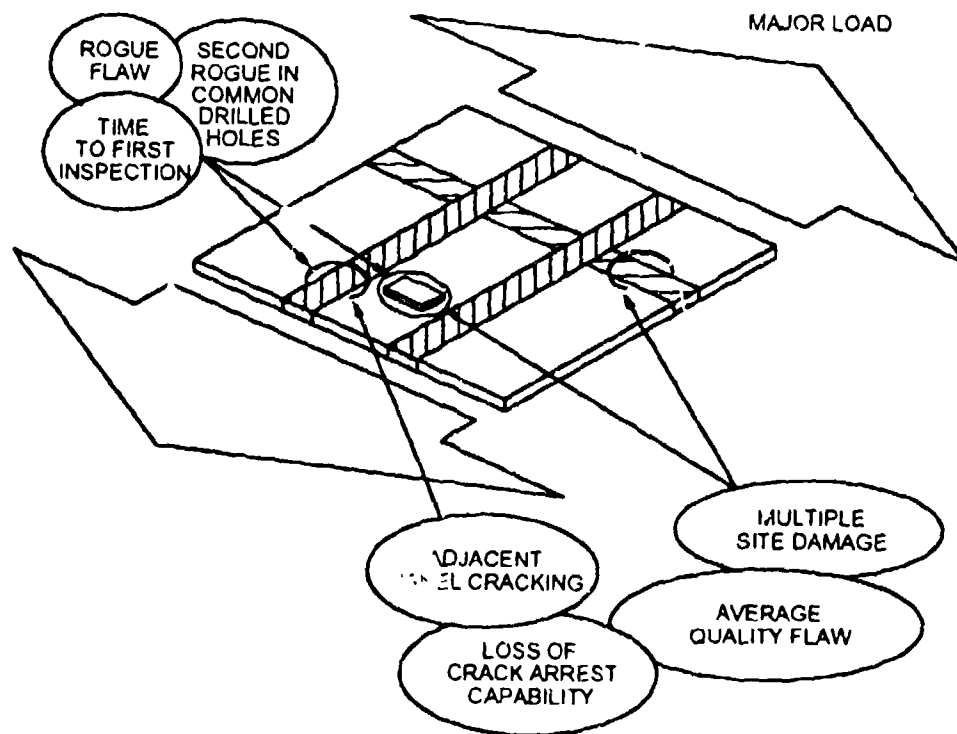


Figure 4-46 Uses of initial crack specifications.

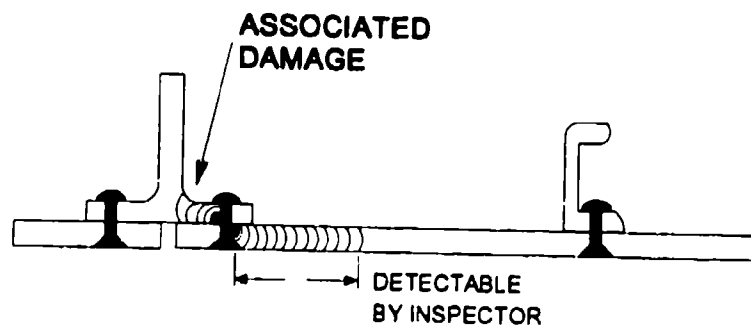
Cracks do not become detectable to maintenance inspectors until they have grown larger than the initial sizes discussed above. How much larger depends on the configuration of the structure, type of inspection, access, and work environment. These factors must be considered as general guidelines for the definition of a detectable crack in each analysis case prepared in support of inspection interval specifications. A detectable crack of appropriate size must be assumed for each analysis case used to derive an inspection interval. The following examples and checklists illustrate how the guidelines can be applied.

Figure 4-47 shows how the configuration of the structure might affect the detectable crack size assumed for inspection of a spanwise wing skin splice. The examples are the same butt and ship-lap splices which were discussed in Section 4.3.1 (see Figures 4-16 and 4-17). Visual inspection from a position under the wing is assumed.

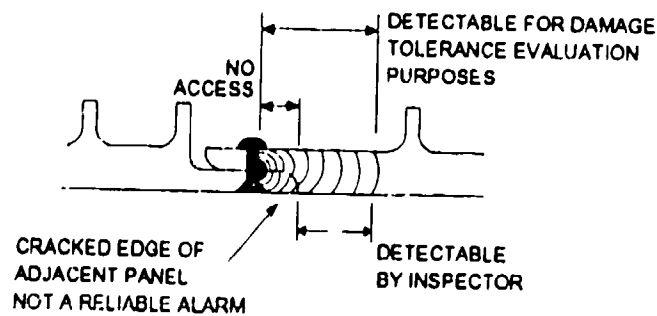
Definition of the detectable size for the butt splice in example (a) requires only a judgement about what the inspector should be able to find reliably in the given environment.¹⁸ However, note that associated damage should also be assumed in the stringer in this case. The extent of the stringer damage would be determined by the relative growth rates of the two initial cracks, to be conservative, both assumed to be rogue flaws.

Conversely, in the scenario assumed for example (b), rogue flaws are located on the same side of the hole in both planks of the ship-lap splice. The lower flaw is assumed to grow out to the edge of the left-hand plank, but even if detectable, this crack should not necessarily be assumed to be present or to enhance the detectability of the crack in the right-hand plank. In this case, it has been assumed that the inspector is able to detect the same length of crack on either surface (a) or (b). The consequence is that a longer crack must be assumed as the "detectable" crack in the ship-lap plank for the purpose of the damage tolerance analysis.

¹⁸The work environment in this case would include factors such as overhead position, distance between eyes and surface being inspected, hand-held light source to dispel shadows, etc.



(a) Butt splice.



(b) Ship-lap splice.

Figure 4-47. Effect of access on detectable size.

Access has similar effects on doubler repairs. Recall that the outer rows are usually the critical fastener rows in a doubler (see Section 4.3.4). The skin is the critical component, since it has more bypass stress in it than does the doubler at the outer row. Therefore, a skin crack should be

analyzed to establish the inspection interval, and the detectable size should reflect the accessibility for external inspection (Figure 4-48).

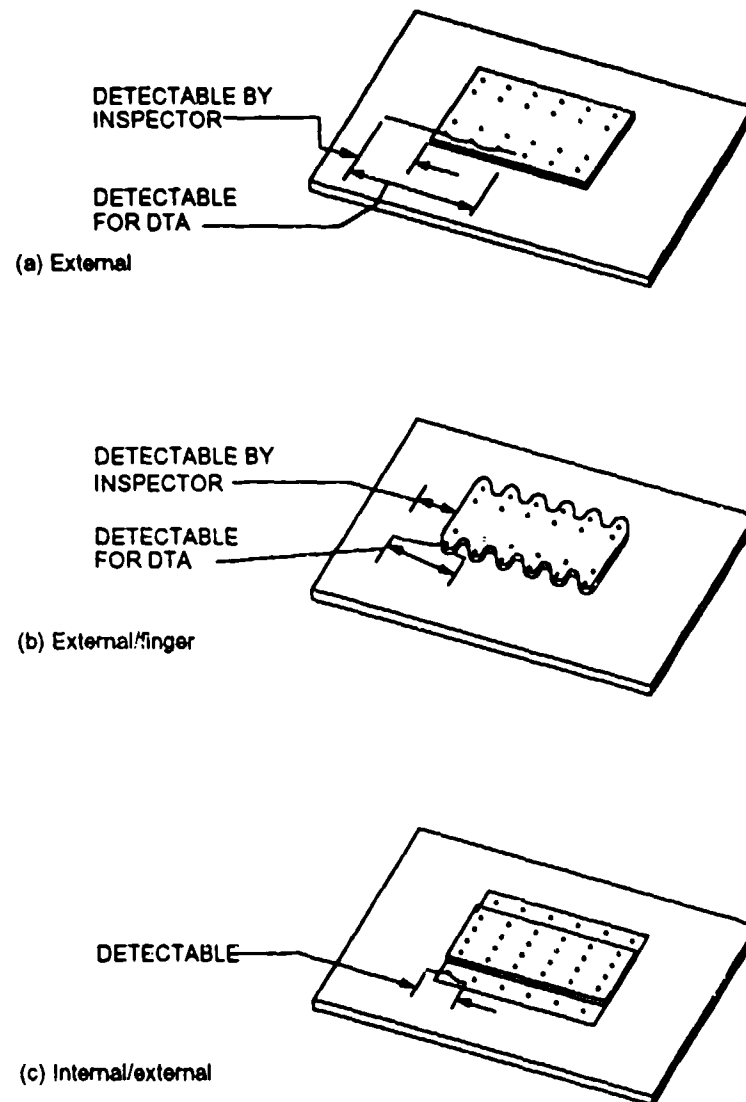


Figure 4-48 Track detectability for different doubler designs.

There is a growing recognition of the need to inspect for multiple site damage, and that such inspections require technical (as opposed to purely visual) methods because the critical crack sizes are small. Tables 4-5 and 4-6 summarize, respectively, the current state of the art and the near-term improvements expected in nondestructive inspection (NDI) technology. Figure 4-49 compares the detection capabilities of some of the currently available methods. The damage tolerance evaluator should be familiar with the general capabilities of different NDI methods and with the requirements for demonstration of adequate reliability, as depicted by detection probability curves like the examples shown in Figure 4-49.

Table 4-5. Currently available NDI methods.

[Reprinted from a presentation by D.J. Hagemaijer to FAA Inspection Authorized Meeting, San Jose, CA, March 1990. By permission of the Douglas Aircraft Co.] [4-6]

NONDESTRUCTIVE TESTING METHODS APPLICATION'S, ADVANTAGES, AND DISADVANTAGES









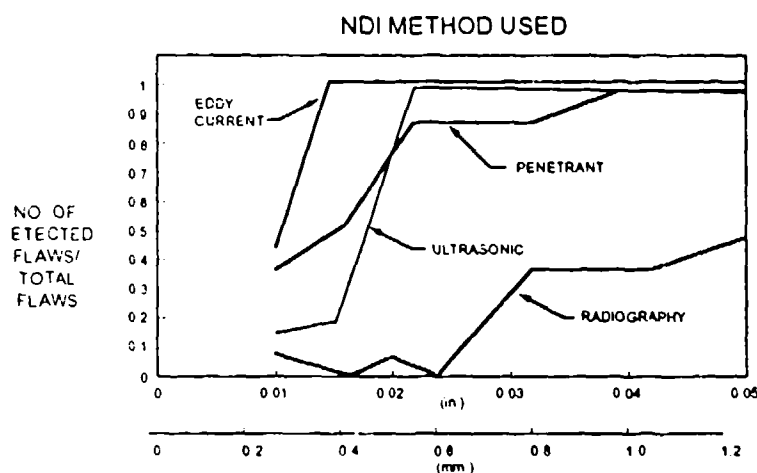
TYPE OF METHOD EMPLOYED	APPLICATION	ADVANTAGES	DISADVANTAGES
VISUAL OPTICAL 	DETECTION OF SURFACE DEFECTS OR STRUCTURAL DAMAGE IN ALL MATERIALS	SIMPLE TO USE IN AREAS WHERE OTHER METHODS ARE IMPRACTICAL. OPTICAL AIDS FURTHER ENHANCE THIS METHOD	RELIABILITY DEPENDS UPON THE ABILITY AND EXPERIENCE OF THE USER. ACCESSIBILITY REQUIRED FOR DIRECT VISIBILITY OR BORE SCOPE
PENETRANT 	DETECTION OF SURFACE CRACKS IN ALL METALS, CASTINGS, FORGINGS, MACHINED PARTS, WELDMENTS	SIMPLE TO USE. ACCURATE, FAST, EASY TO INTERPRET	DEFECT MUST BE OPEN TO SURFACE AND ACCESSIBLE TO OPERATOR. DEFECT MAY BE COVERED BY SMEARED METAL. PART MUST BE CLEANED BEFORE AND AFTER CHECK
HIGH-FREQUENCY EDDY CURRENT 	DETECTION OF SURFACE CRACKS IN METALLIC SURFACES, CRACKS, PITS, INTERGRANULAR CORROSION, AND HEAT TREAT CONDITION. CONDUCTIVITY FOR MEASUREMENT FOR DETERMINING FIRE DAMAGED AREA	USEFUL FOR CHECKING ATTACHMENT HOLES FOR CRACKS NOT DETECTABLE BY VISUAL OR PENETRANT METHODS. FAST, SENSITIVE, PORTABLE	TRAINED OPERATOR REQUIRED. SENSITIVE COMBINATIONS AND VARIATIONS IN MATERIAL. SPECIAL PROBES REQUIRED FOR EACH APPLICATION. REFERENCE STANDARDS REQUIRED
LOW-FREQUENCY EDDY CURRENT 	DETECTION OF SUBSURFACE DEFECTS IN METALLIC MATERIALS, CORROSION THINNING, AND SPACING	USEFUL FOR CHECKING FOR CRACKS WITHOUT REMOVAL OF FASTENERS OR DISASSEMBLY OF SUBSTRUCTURE	TRAINED OPERATOR REQUIRED. LARGER PROBES NEEDED, OR LOWER FREQUENCY USAGE. SPECIAL PROBES REQUIRED FOR EACH APPLICATION. REFERENCE STANDARDS REQUIRED
SONIC 	DETECTION OF DELAMINATIONS, DEBONDS, VOIDS, AND CRUSHED CORE IN COMPOSITE AND HONEYCOMB MATERIALS	CAN BE ACCOMPLISHED FROM ONE SURFACE. DIRECT READING. DOES NOT REQUIRE PAINT REMOVAL OR SPECIAL SURFACE PREPARATION	LOSES SENSITIVITY WITH INCREASING MATERIAL THICKNESS. ELECTRICAL SOURCE REQUIRED
X-RAY 	DETECTION OF INTERNAL FLAWS AND DEFECTS SUCH AS CRACKS, CORROSION, INCLUSIONS, AND THICKNESS VARIATIONS	ELIMINATES MANY DISASSEMBLY REQUIREMENTS. HAS HIGH SENSITIVITY AND PROVIDES A PERMANENT RECORD ON FILM	RADIATION HAZARD. TRAINED OPERATORS AND FILM PROCESSING EQUIPMENT REQUIRED. CRACK PLANE MUST BE NEARLY PARALLEL TO X-RAY BEAM TO BE DETECTED. ELECTRICAL SOURCE REQUIRED. SPECIAL EQUIPMENT REQUIRED TO POSITION X-RAY TUBE AND FILM
MAGNETIC PARTICLE 	DETECTION OF SURFACE OR NEAR-SURFACE DEFECTS IN FERROMAGNETIC MATERIALS OF ANY SHAPE OR HEAT TREAT CONDITION	SIMPLE IN PRINCIPLE, EASY, PORTABLE. FAST METHOD IS POSITIVE	TRAINED OPERATOR REQUIRED. PARTS MUST BE CLEANED BEFORE AND DEMAGNETIZED AFTER CHECK. MAGNETIC FLUX MUST BE NORMAL TO PLANE OF DEFECT TO YIELD INDICATIONS
ULTRASONIC 	DETECTION OF SURFACE AND SUBSURFACE DEFECTS, CRACKS, DEBONDS, LAMINAR FLAWS, AND THICKNESS GAUGING IN MOST METALS BY PULSE ECHO TECHNIQUES	FAST, DEPENDABLE, EASY TO OPERATE. RESULTS ARE IMMEDIATELY KNOWN. HIGHLY ACCURATE, HIGH SENSITIVITY, AND PORTABLE	TRAINED OPERATOR REQUIRED. ELECTRICAL SOURCE REQUIRED. CRACK PLANE ORIENTATION MUST BE KNOWN TO SELECT WAVE MODE TO BE USED. TEST STANDARDS REQUIRED TO ESTABLISH INSTRUMENT SENSITIVITY

Table 4-6. Expected advances in nondestructive inspection technology.

Method	Principle	Application
Shearography	Interferometry	Fuselage and wings for bond integrity and composites screening
Magneto-optic imaging	Faraday effect	Visualization of eddy current detection of cracks
Advanced ultrasonics	Reflection of sonic energy from internal anomalies	Focussed ultrasound for detection of defects in aerospace materials (titanium)
Advanced image processing	Computerized enhancement	X-ray, ultrasonics, eddy current



DEPTH OF THIN SPECIMEN FLAWS, a
PROPORTION AS A FUNCTION OF DEPTH IN THIN
ALUMINUM SPECIMENS, COMBINED DATA

Figure 4-49. Examples of crack detection probability curves.

[Reprinted from a presentation by D.J. Hagemaier to FAA Inspection Authorized Meeting, San Jose, CA, March 1990. By permission of the Douglas Aircraft Co.] [4-6]

4.6 ANALYSIS AND TESTS

The objectives of damage tolerance evaluation are to establish: (1) time to first inspection and safe inspection interval (or safe crack growth life for single path structure); (2) ability to arrest and contain isolated component fractures (fail-safety); and (3) retention of fail-safety over the economic life of the airframe (continued airworthiness). Full-scale testing is the preferred method for demonstrating compliance with the damage tolerance criteria. However, full-scale testing is subject to the constraints of cost, time, availability of structure, and service load simulation. Thus, analysis must be used to cover many cases. However, analysis is subject to modeling error and must be validated by comparison with test results.

4.6.1 Load Specification and Stress Analysis

The airworthiness standards specify limit and ultimate load factors for the major components of an airframe. Except for fuselage pressurization and some asymmetrical maneuvers, the specifications are based on airplane load factor. The airplane load factor n_x is the acceleration of the airplane's center of gravity, expressed as a dimensionless multiple of the earth's acceleration of gravity $g \approx 32.2 \text{ ft/sec}^2$, at right angles to the airplane's platform. Thus, $n_x = 1$ for straight and level flight. For accelerated conditions, the airplane's gross weight W_G is replaced by $n_x W_G$ to calculate balancing loads. The airplane load factor is also the primary basis for estimation of fatigue loads.

Figure 4-50 illustrates the most common accelerated condition characterized by airplane load factor: a steady angle of bank established for a coordinated level turn. The graph at the right, showing the relation between n_x and bank angle, suggests two key observations about the character of fatigue loads due to turning maneuvers. First, such loads are always positive excursions from the 1g condition. (Negative excursions are discussed later.) Second, the expected usage of a transport involves load factors well below limit load.

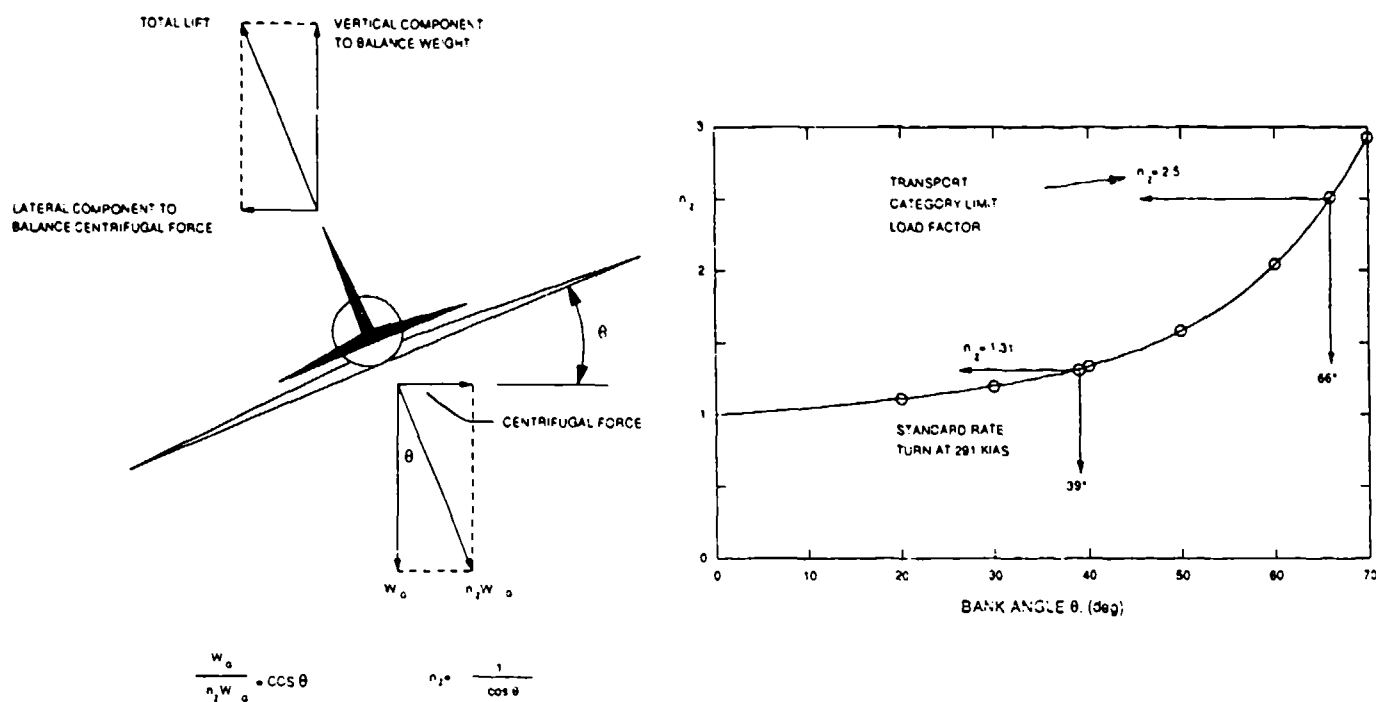


Figure 4-50. Airplane load factor for coordinated level turns.

The second point arises from consideration of how airplanes are supposed to be operated. For example, FAR 91.117 restricts all aircraft to speeds not exceeding 250 KIAS at altitudes below 10,000 ft MSL (about 291 KIAS at 10,000 MSL in the standard atmosphere). These low altitudes are also where aircraft make turns most frequently and at the highest rates. However, transports making high-rate turns would not normally exceed the standard IFR rate of 3 deg/sec, and would turn at lower rates in most cases [4-7]. A standard rate turn at 291 KIAS requires a bank angle close to 39 degrees, and the corresponding airplane load factor is about 1.3 (see Figure 4-50). Thus, transport usage for turning maneuvers is expected to consist of some excursions up to $n_z = 1.3$ and frequent smaller excursions.

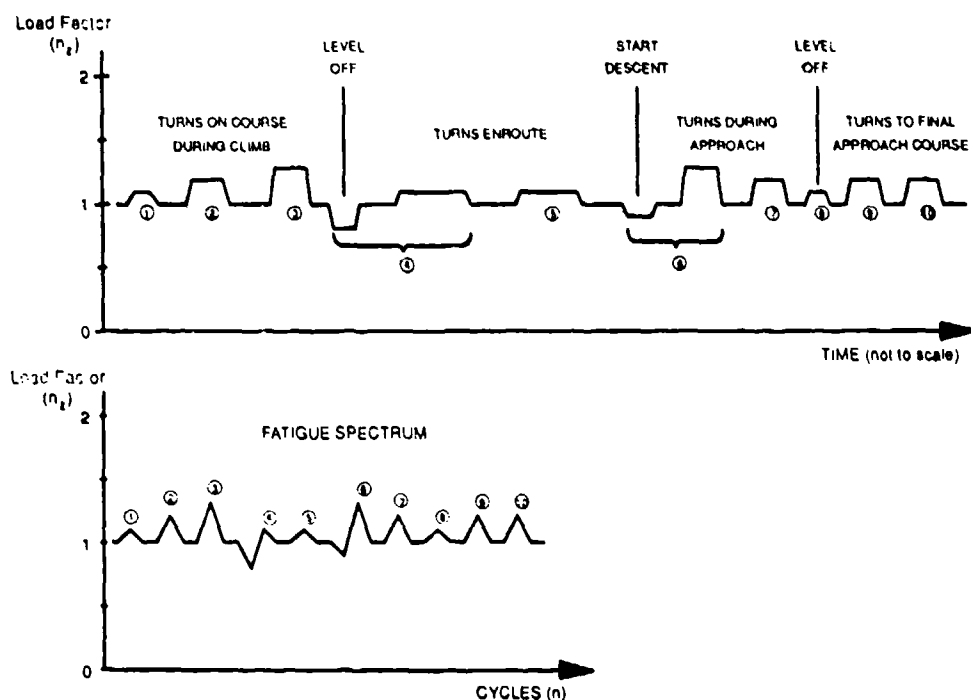
Pitch maneuvers also affect the airplane load factor by curving the flight path in the vertical plane. Nose-up pitch to start a climb or to level off after descent creates a positive excursion. Nose-down pitch to start a descent or to level off after a climb creates a negative excursion. These maneuvers typically take 10 to 20 seconds at load factors between 0.8 and 1.2 under normal conditions.

Figure 4-51 illustrates a hypothetical sequence of maneuvers during the climb, enroute, descent, and approach phases of a flight. The fatigue load spectrum is obtained by counting only the positive and negative peak excursions and grouping them into cycles, as shown in the lower graph. The table at the right summarizes the number of cycles per flight (n) for each block of cycles having the same range and ratio, based on the minimum and maximum load factors. After conversion to stress, the summary could be used to estimate crack growth life by the direct sum (block), direct sum (spectrum), or equivalent S-N methods (see Section 3.4). The sequenced spectrum would be useful to have if the crack growth rates are expected to be influenced by load interaction (Section 3.5). However, only the spectrum summary or its equivalent may be available, and the evaluation of load interaction effects in such cases requires reconstruction of a sequence based on conservative judgement.

The fatigue load spectrum must be converted to a stress spectrum in order to establish crack growth rates by testing design details or to calculate crack growth life. The conversion is usually based on a stress analysis of the airframe for the straight and level flight condition.

The airplane load factor is treated, with certain important exceptions, as a scale factor to be applied to the 1g stresses. For example, the stress ranges are given by:

$$\Delta S = S_k \Delta n_i \quad (4-18)$$



SUMMARY OF A HYPOTHETICAL SPECTRUM

LOAD FACTOR n_z		Δn_z	R	CYCLES PER FLIGHT (n)
min	max			
0.9	1.3	0.4	0.69	1
1.0	1.3	0.3	0.77	1
0.8	1.1	0.3	0.73	1
1.0	1.2	0.2	0.83	4
1.0	1.1	0.1	0.91	3

Figure 4-51. Example of construction of maneuver spectrum from time history.

and the stress ratios are the same as those in the load spectrum summary. The exceptions are the fuselage crown and keel areas, wing bending stress as a function of flight configuration, and the ground-air-ground (GAG) cycle.

For most areas of the fuselage, the hoop stress due to pressurization is the dominant factor, and the "spectrum" reduces to one pressure cycle per flight. However, axial bending stress can be a significant factor in the crown and keel areas near the wing/fuselage attachments (see Section 4.2.2). For these areas, the axial tension due to pressure combined with the bending stresses increases the flight cycle stress ratios, and also affects the GAG cycle.

Wing bending is affected by the spanwise lift distribution, which depends on the position of flaps and slats. The lift distribution is concentrated more inboard, and the 1g stresses are lower, when the aircraft is configured for approach and landing with flaps and slats deployed. Lower S_{1g} means lower stress range, and the effect can be accounted for in the spectrum by analyzing maneuver time histories as a function of flap setting.

The GAG cycle represents the effect of transition from the landing gear to the wing, and back to the landing gear, as the support for the aircraft weight. The wing bending distribution when the aircraft is on the ground differs from the distribution in flight. Therefore, the relation between airplane load factor and bending stress is also different, and must be accounted for by stress analysis of the aircraft on the ground. Figure 4-52 shows how these differences make the ground part of the stress spectrum a function of wing station. The figure also shows how the GAG cycle is defined: a stress range from the minimum ground stress to the maximum stress in the next flight.¹⁹

¹⁹For the fuselage crown and keel areas, the ground part of the spectrum is changed by both depressurization and a change in fuselage bending moment distribution.

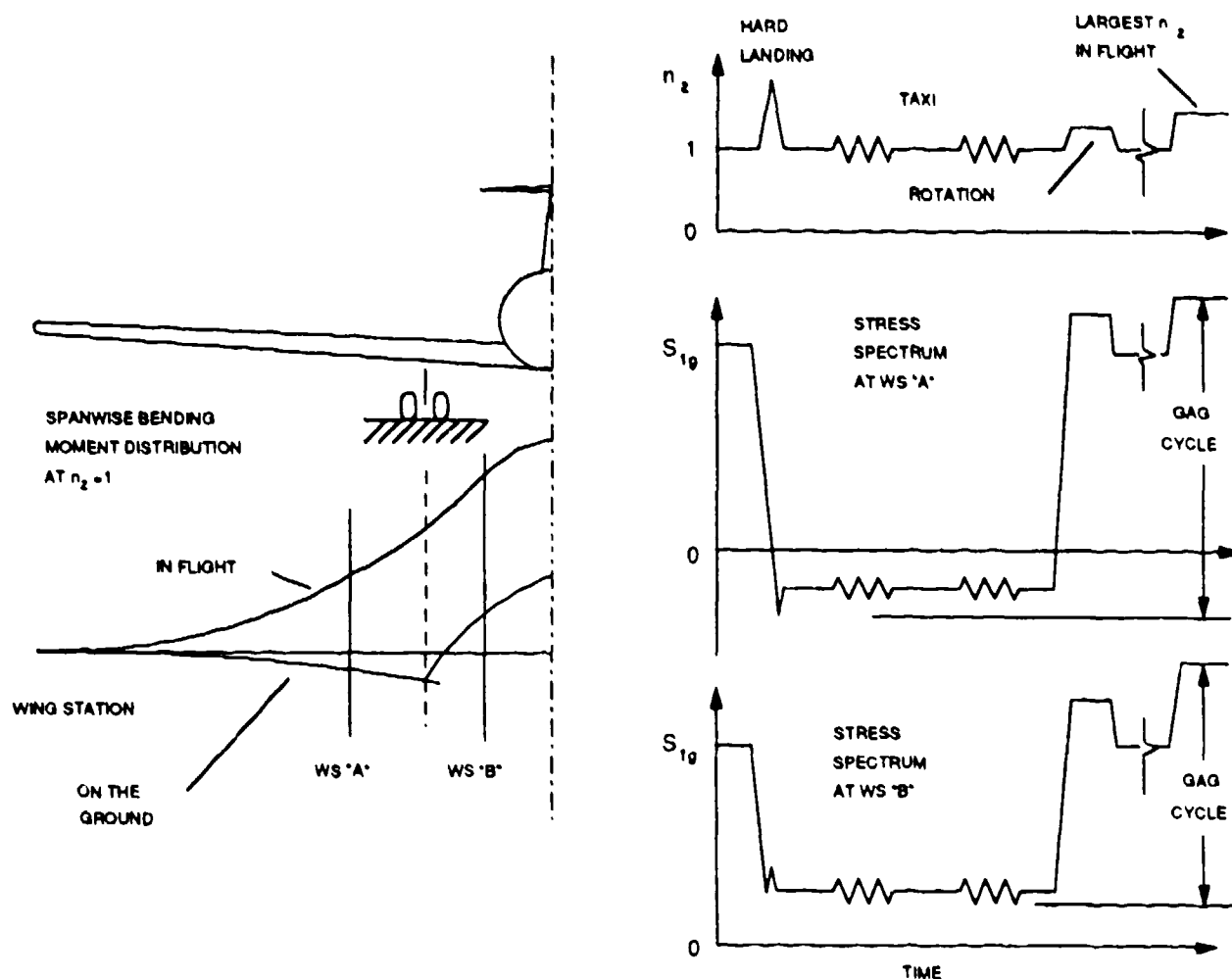


Figure 4-52. Effect of spanwise location on ground-air-ground cycle.

The foregoing examples illustrate the general character of maneuver load spectra but do not present a reliable quantitative picture. The sequence of maneuvers and the magnitudes of their associated load factors vary from flight to flight. Therefore, hundreds to thousands of flight hours of data must be recorded to obtain reliable quantitative characteristics.²⁰

²⁰Such analyses often reveal correlation between airplane usage and altitude or length of flight. For example, transport manufacturers generally define separate spectra to represent typical short, medium, and long flights.

Air turbulence is another important contributor to fatigue load spectra. Gust load cycles typically consume 50% of the fatigue life or crack growth life in large transport airplanes, and the proportion can exceed 70% in light twin-engine commuter aircraft. The rest of the life is consumed by maneuver loads, landing, taxiing, etc. Although there is a reliable empirical method for calculating the airplane load factor due to a gust of defined magnitude, an airplane in flight encounters gusts of random magnitude at random times. The airplane load factors associated with gusts generally have excursions symmetrically distributed above and below the 1g condition. Aside from this general feature, the description of gust contributions to fatigue load spectra requires analysis of flight data.

4.6.1.1 Gust Load Factors (FAR 23.231 and FAR 25.341)

The empirical formula for calculation of gust load factors is given by:

$$n_z = 1 + \frac{K_g U_e V_a}{498(W/S)} \quad (4-19)$$

where

$$K_g = \frac{0.88\mu_g}{5.3 + \mu_g} \quad (\text{gust alleviation factor}) \quad (4-20)$$

$$\mu_g = \frac{2(W/S)}{\rho C a g} \quad (\text{airplane mass ratio}) \quad (4-21)$$

U_e = derived gust velocity (ft/sec)

ρ = air density (slugs/ft³)

W/S = wing loading (psf)

C = mean geometric chord (ft)

g = acceleration of gravity (32.2 ft/sec²)

V = airplane equivalent speed (knots)

α = slope of the airplane normal force coefficient curve $C_{N\alpha}$ per radian, if the gust loads are applied to the wings and horizontal tail surfaces simultaneously by a rational method. The wing lift curve slope C_L per radian may be used when the gust load is applied to the wings only and the horizontal tail gust loads are treated as a separate condition.

The derived gust velocity is specified in FAR 23.333(c) and FAR 25.341(a) for various performance and strength requirements. For transports and commuter airplanes, the derived gust velocity for rough air (66 fps to 20,000 MSL, decreasing linearly to 38 fps at 50,000 MSL) can be used together with the airplane design maneuvering speed V_A to estimate the gust load factor for fatigue.

Gust and maneuver loads are interspersed in time, but frequency analysis of flight data can separate them. Gusts are typically high-frequency events that cause the airplane to vibrate at its own natural frequencies. The effect on airplane load factor appears mainly at the fundamental wing bending frequency, generally above 1 Hz for large transports and increasing for smaller aircraft. Conversely, maneuvers typically last from a few seconds to 2 minutes, i.e., their frequencies are well below 1 Hz. Figure 4-53 illustrates a typical sample of L-1011 flight data, with the 1g bias removed. The top graph shows the full record. The middle graph shows the same record after processing through a low-pass filter to isolate the maneuver loads. In the bottom graph, the same record has been processed through a high-pass filter to isolate the gust loads. This plot also illustrates one other general characteristic of gust loads: they tend to occur in patches, with the magnitudes roughly in a low-high-low sequence for each patch.

Analyzing hundreds or thousands of flight hours requires automated counting. Automated counting requires specific rules to identify events which should be counted. The rules must be either expressed in data acquisition hardware or programmed into data processing software.

Flight load data acquisition and analysis procedures were developed well before the advent of transistors, integrated circuits, and high-speed digital microprocessor chips. The counting methods which came into wide use reflect what the instrumentation engineer of the 1950s could

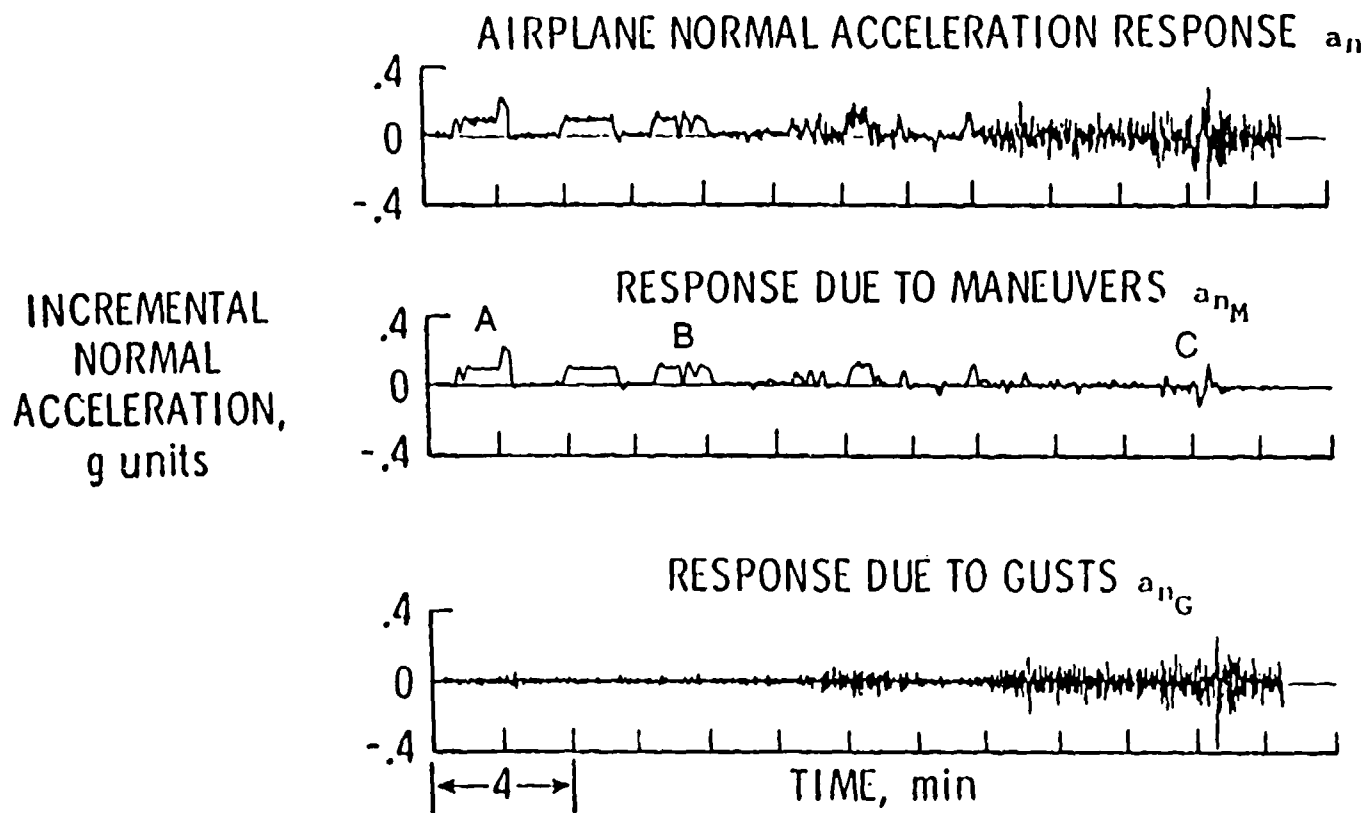


Figure 4-53. L-1011 airplane load factor record.

[Reprinted from The NASA Digital VGH Program - Exploration of Methods and Final Results, Volume I: Development of Methods, DOT/FAA-CT-89/36-I, December 1989.] [4-8]

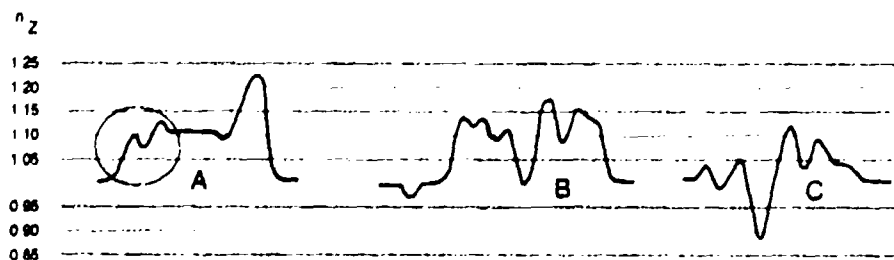
design into light-weight, low-power hardware that would preserve the data from numerous flights without the need for continuous power. The typical counting accelerometer from this era could store cumulative counts of half a dozen different kinds of events on mechanical dials, which had to be periodically read and reset.

The most common procedure with equipment of this type was to define the countable events as crossings of preselected acceleration levels. (Only positive crossings of levels above and negative crossings of levels below the 1g state are counted.) This basic level-crossing procedure, with some refinements, remains the most common form for reporting airplane load factor data.

Figure 4-54 compares four different counting methods used for various purposes. In the time history plot at the top, seven significant levels of airplane load factor have been selected, and three sets of events A, B, C have been sketched. These groups resemble the similarly labelled groups on the maneuver data sample in Figure 4-53.

The two tables below the graph in Figure 4-54 compare the counting of these groups by the level crossing and peak discrimination methods. In the basic level crossing method, a count is recorded for each positive level ($n_i > I$) each time the signal rises above that level, and a count is recorded for each negative level ($n_i < I$) each time the signal falls below that level.²¹ A plot of level crossing counts versus airplane load factor is called a level exceedance curve or, simply, an exceedance curve.

²¹ A refinement called level discrimination counting is normally used in practice. A positive level count is not accumulated until the signal falls below the next lower level; a negative level count is not accumulated until the signal rises above the next higher level. This strategy is adopted to prevent high-frequency noise in the signal from building up large spurious counts. This procedure is also referred to as the fatigue meter method.



LEVEL CROSSING COUNTS

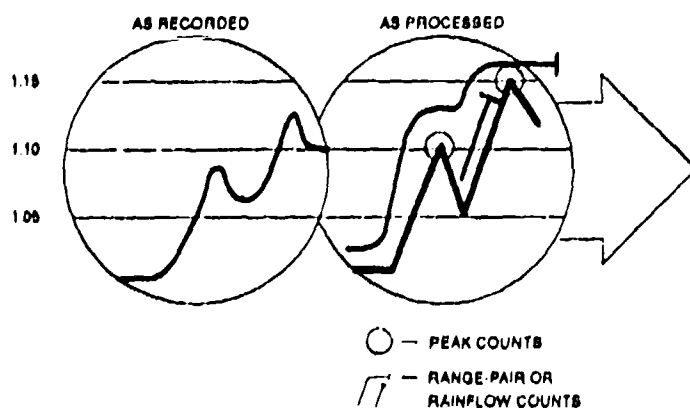
LEVEL	A	B	C	TOTAL	PEAKS (*)
1.25					1
1.20	1			1	2
1.15	1	2		3	4
1.10	2	4	1	7	
1.05	1	2	2	5	
0.95			1	1	
0.90			1	1	
0.85					1

PEAK DISCRIMINATION COUNTS

TOTAL	A	B	C	PEAK
1	1			1.25
2		2		1.20
4	1	2	1	1.15
2	1		1	1.10
2			2	1.05
1		1		0.95
				0.90
1			1	0.85

*from level count differences

AS COUNTED OR
RECONSTRUCTED



PEAK DISCRIMINATION

min	max	Δn_z	R
1.00	1.10	0.10	0.91
1.00	1.15	0.15	0.87

RANGE-PAIR OR RAINFLOW

min	max	Δn_z	R
1.00	1.15	0.15	0.87
1.05	1.10	0.05	0.95

Figure 4-54. Comparison of different counting methods.

Peak occurrences are usually inferred from exceedance curves by taking differences. This is based on the idea that a signal which has risen across one level must either cross the next higher level or reach a peak between the two levels. Thus, the difference between the two exceedance counts is taken to indicate the number of peaks. The peaks are conservatively assumed to have a value just at the higher exceedance level. The right-hand column in the level crossing table indicates the peak count thus inferred from the total level crossing counts for the three event sets A, B, C. (Note that the difference procedure does not work if the crossing count is larger for the higher level, e.g., the 1.05g and 1.10g levels in the example.)

In the peak discrimination method, each positive and negative peak is sought directly by identifying significant reversals in the signal. The counts may be assigned to discrete load factor values, and reversals may be defined as valid at 1/2 or 3/4 of the discrete-value difference. In the present case, the preselected discrete values are the same as for the level crossing example (0.05g difference), and a reversal of 0.025g is taken as a peak indication.²² The left-hand column of the peak count table shows the total counts obtained from the three event sets A, B, C. Note that the peak method has produced somewhat more detail than the level crossing method.

One further comparison is shown at the bottom of Figure 4-54. The circled part of the event set A has been reproduced to illustrate the difference between peak counting and the range-pair or rainflow counting methods. (The two latter methods have become more popular as microelectronics has made it practical to build more sophisticated data acquisition hardware, and also as structures engineers have begun to pay increasing attention to damage tolerance.) The range-pair and rainflow counting methods tend to produce similar results. In the example shown here, both methods count this part of the signal as a range to the higher peak and a smaller range defined by the lower peak and following minimum. Reconstruction of ranges from the peak count data reproduces the large range but overestimates the size of the smaller range.

²²There is no problem in applying the peak discrimination method to the maneuver data shown in this example. If the method is applied to gust load data, however, some high-frequency filtering is required to remove noise before counting.

The most recent data on transport airplane loads was gathered in a flight survey program conducted for the FAA by the NASA Langley Research Center from 1978 to 1982. Several examples of exceedance plots derived from the NASA program are presented in Figures 4-55 and 4-56. The plots are presented in the form of level exceedance curves with the 1g bias removed.

In Figure 4-55 a series of plots for different altitude bands shows a gradually decreasing trend in gust loads as the test altitude approaches and then exceeds the height of the tropopause. (Some exceptions to the trend are also evident, probably due to clear air turbulence associated with jet stream winds.)

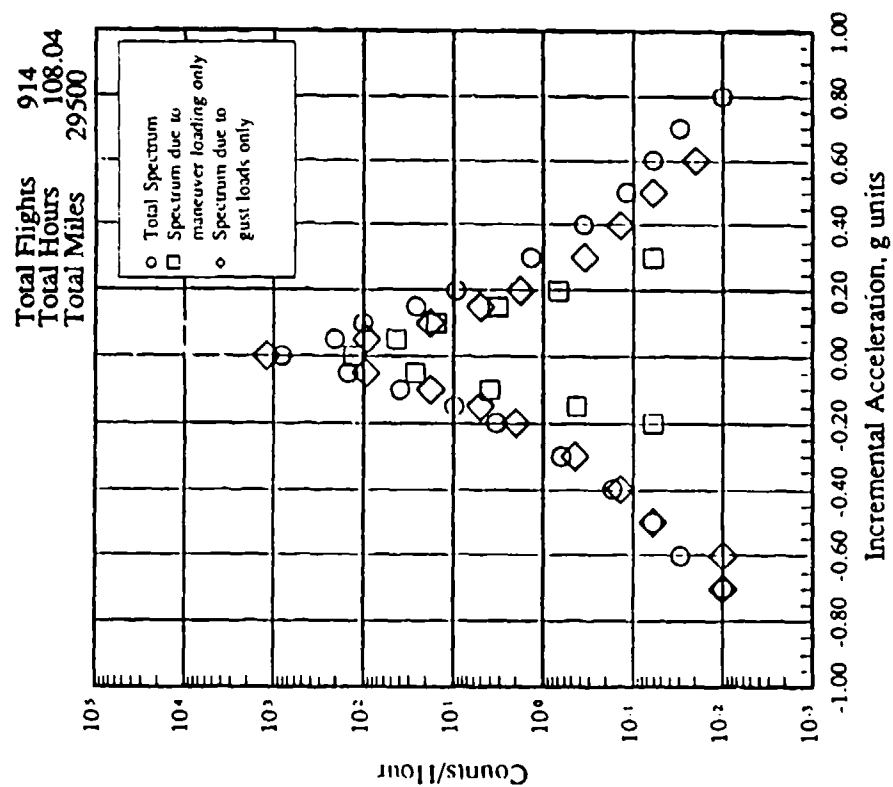
Figure 4-56 compares the composite (all altitudes) exceedance curves for the L-1011, B-727, B-747, and DC-10. Some differences in airplane usage appear. Note that the B-747 and DC-10 exceedance curves are somewhat less severe than the L-1011 and B-727 curves.²³

Two other general features are visible in these plots. First, most of the gust load exceedances are symmetrically distributed above and below the 1g state. (Some exceptions are evident at low count rates.) Second, the maneuver exceedances are generally asymmetrical, as discussed earlier.

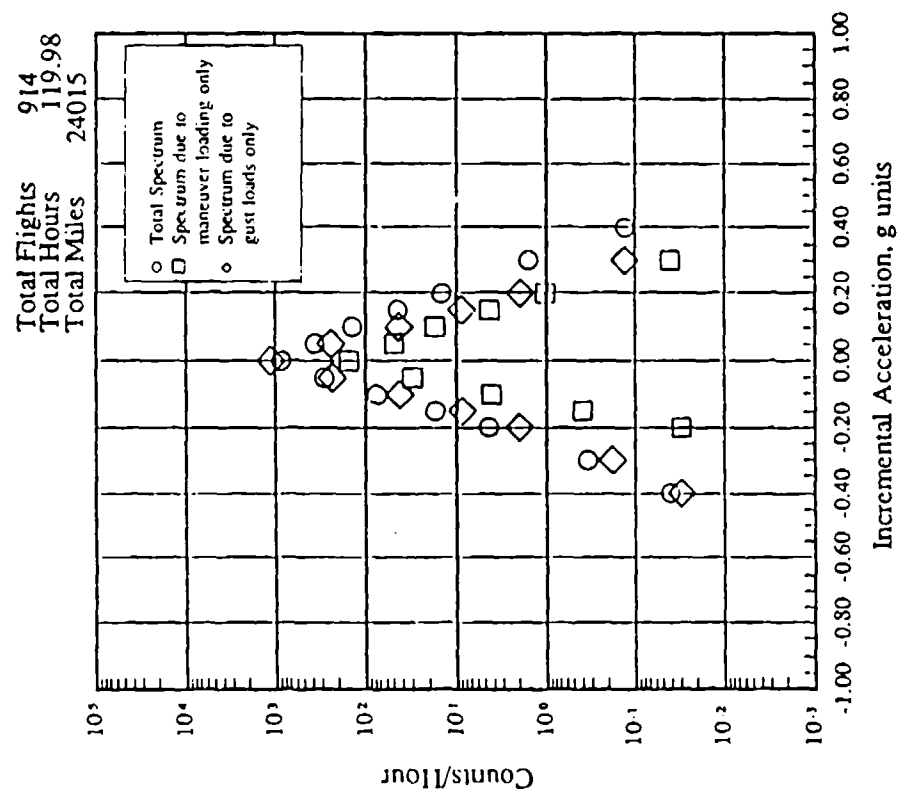
4.6.2 Residual Strength Evaluation

FAR 25.571(b)(5)(ii) requires that a pressurized fuselage be able to contain discrete source damage under 1g loads combined with 1.1 times the normal operating cabin pressure differential. Containment is usually demonstrated by a full-scale test on a production-hardware fuselage section long enough to properly simulate the energy release from the pressurized air. A crack longer than the critical crack length for the applied load is suddenly introduced by an explosively propelled "guillotine" blade. The test result is unambiguous: the structure either does or does not arrest the running crack. If the crack is arrested, judgement of compliance reduces to verification of the hardware and test conditions.

²³The DC-10 comparison should not be accepted at face value because of the difference in sample size (129 hours of DC-10 data, as compared with over 1600 hours for each of the other airplanes).

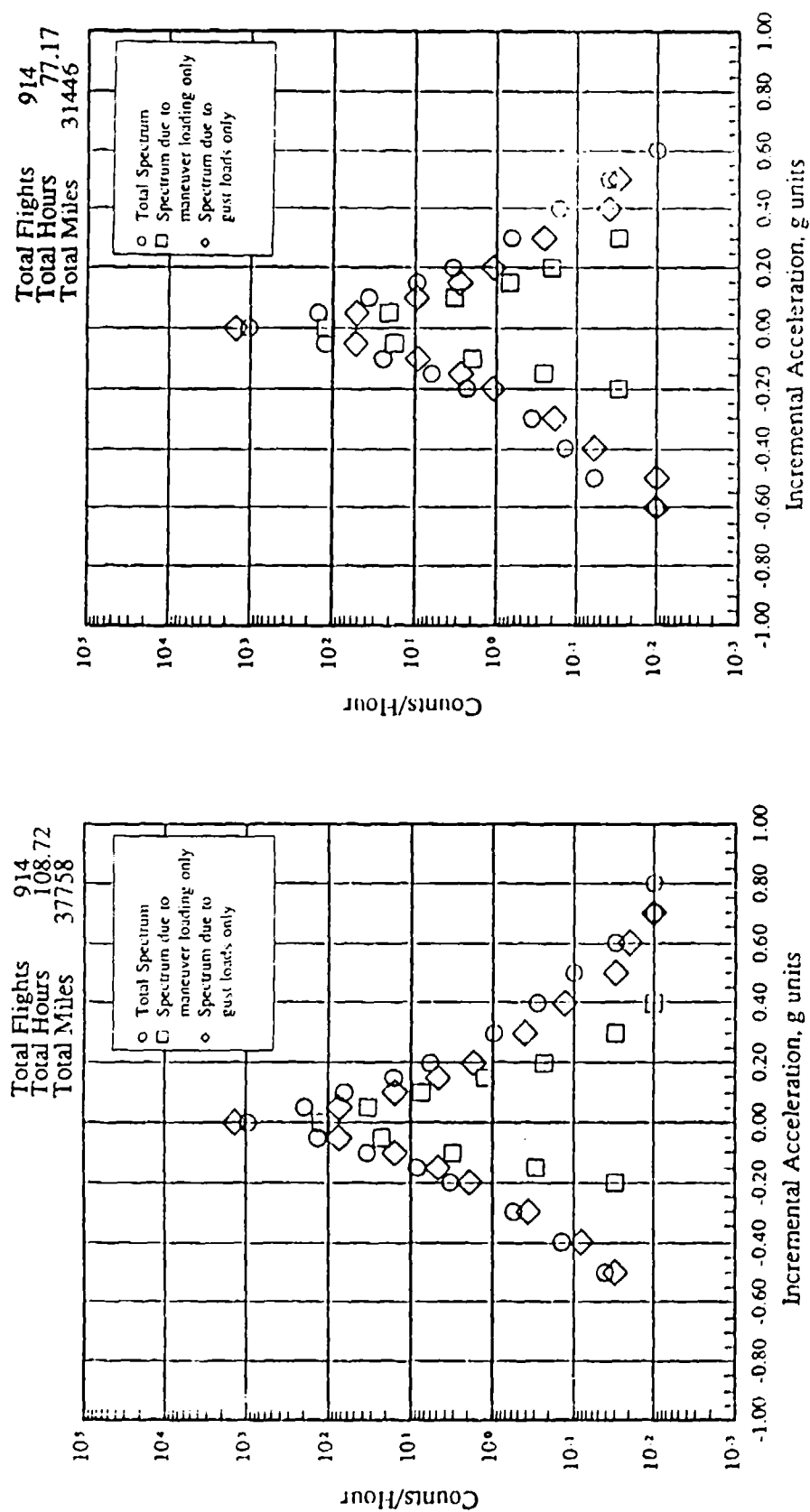


(a) 4500 to 9500 MSL.



(b) 500 to 4500 MSL.

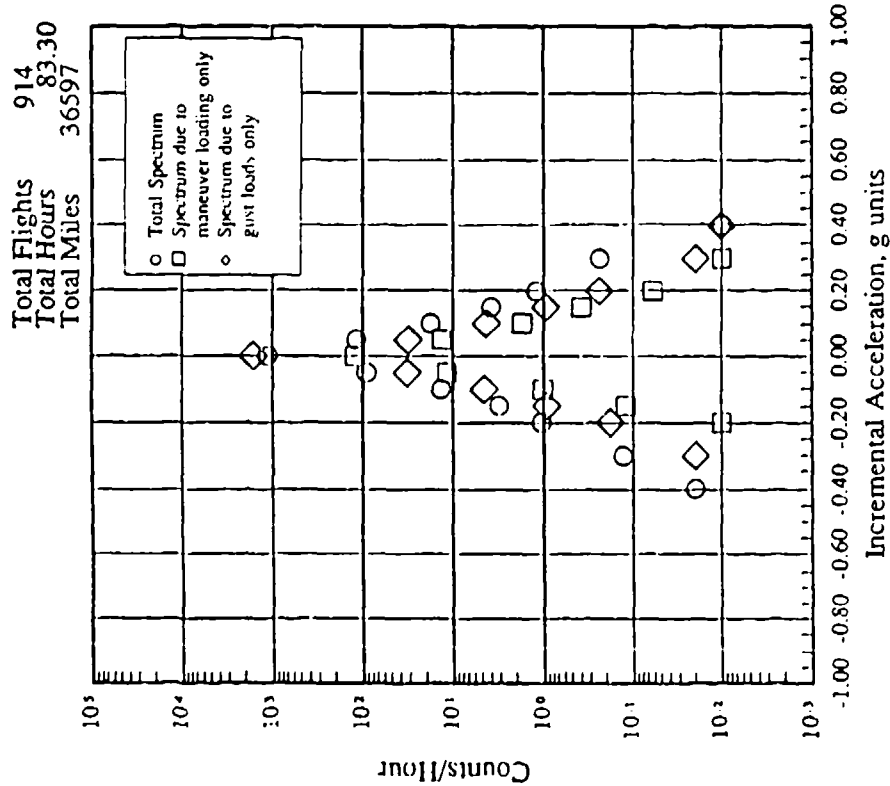
Figure 4-55. L-1011 exceedance curves for different altitude bands. [Reprinted from ref. 4-8]



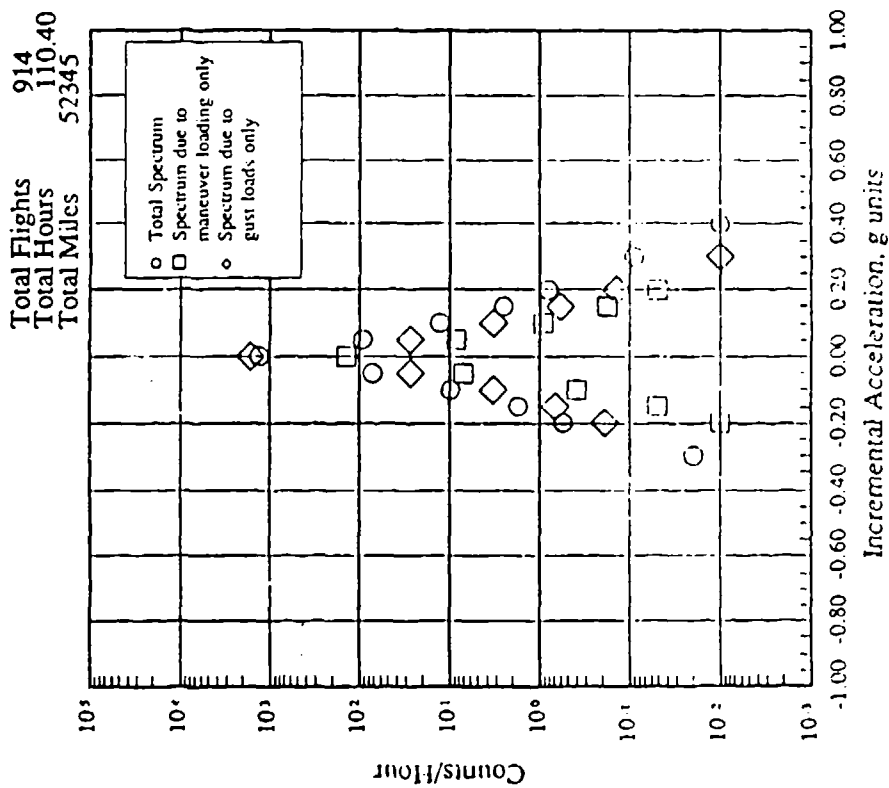
(c) 9500 to 14500 MSL.

(d) 14500 to 19500 MSL.

Figure 4-55 (continued). L-1011 exceedance curves for different altitude bands. [Reprinted from ref. 4-8]

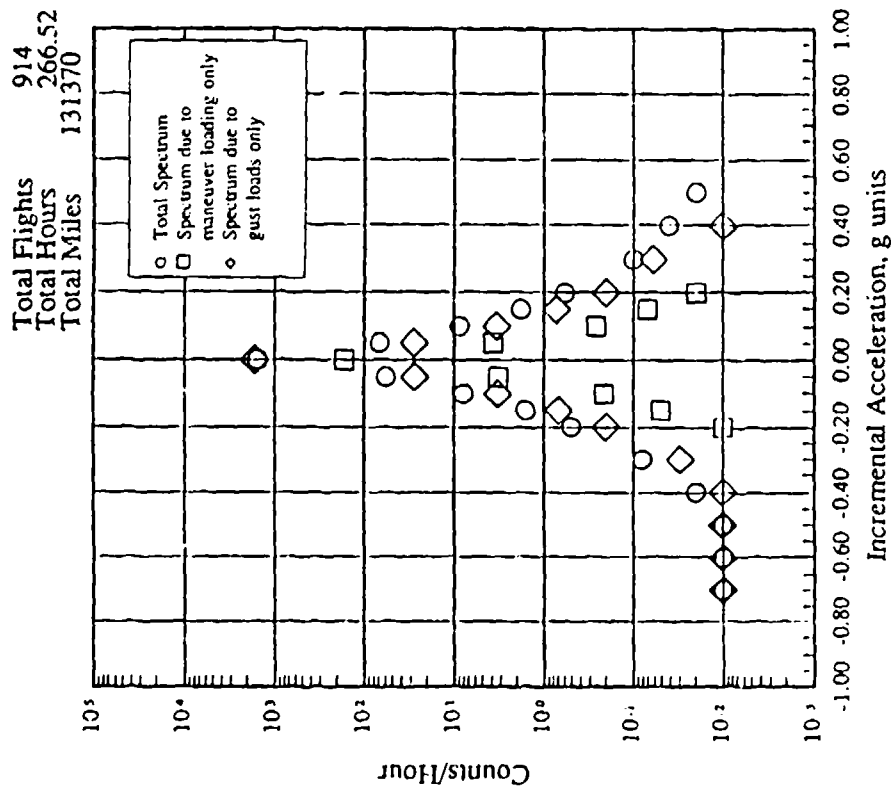


(e) 19500 to 24500 MSL.

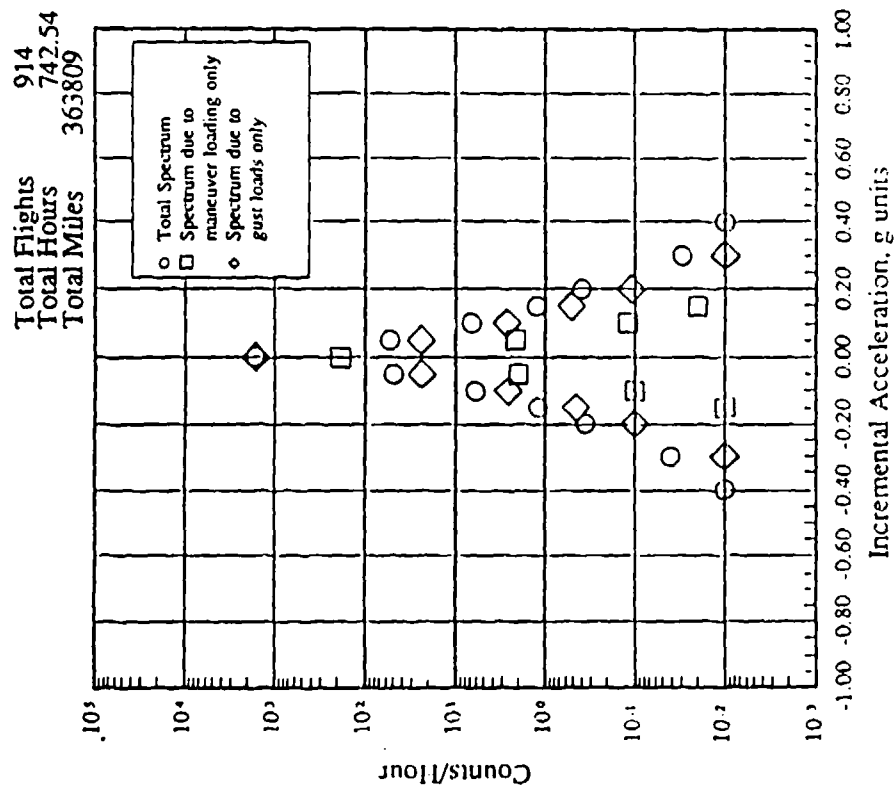


(f) 24500 to 29500 MSL.

Figure 4-55 (continued). L-1011 exceedance curves for different altitude bands. [Reprinted from ref. 4-8]

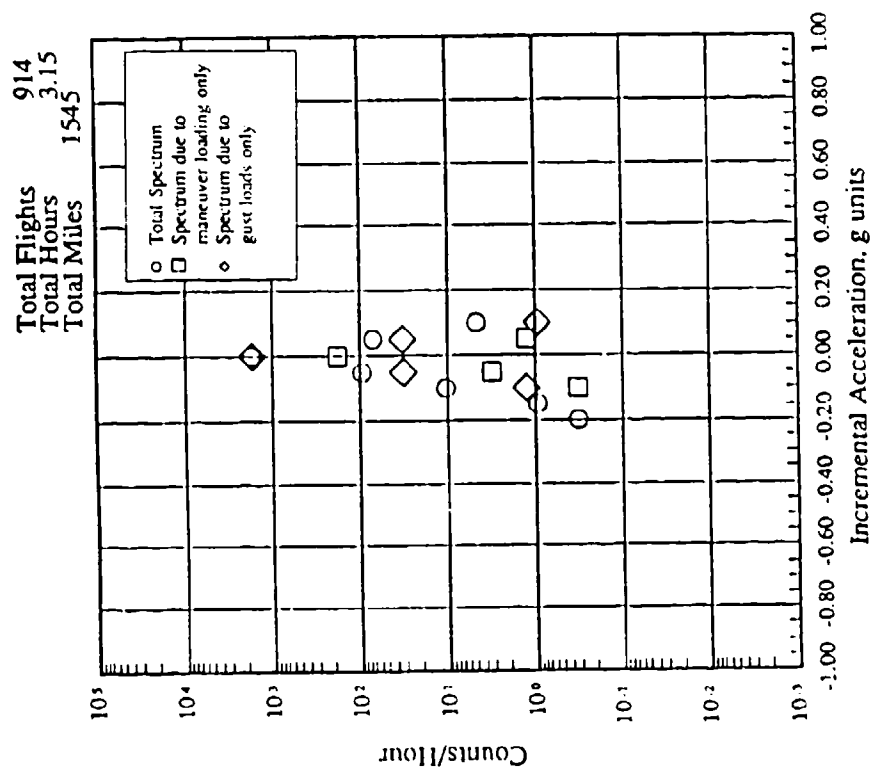


(g) 295(X) to 345(X) MSL.



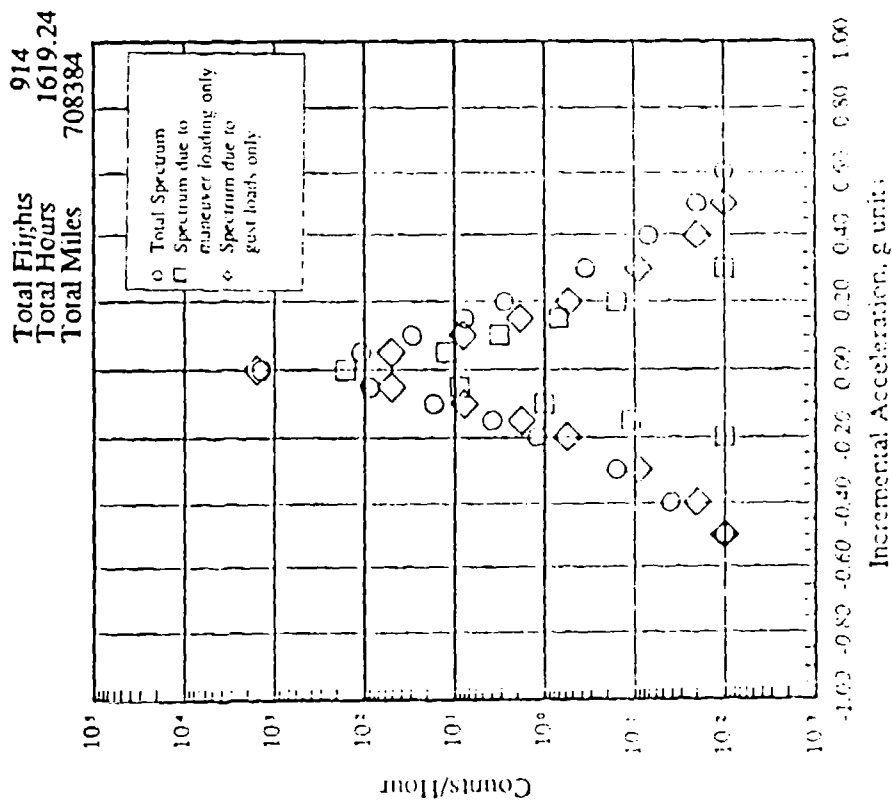
(h) 345(X) to 395(X) MSL.

Figure 4-55 (continued). L-1011 exceedance curves for different altitude bands. [Reprinted from ref. 4-8]

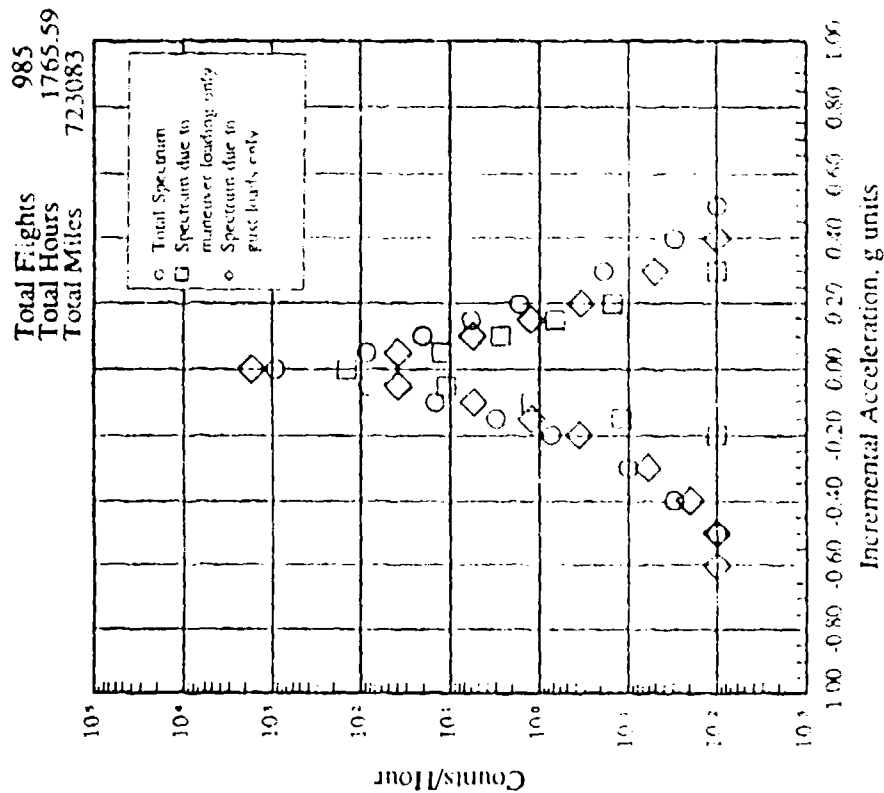


(i) 39500 to 44500 MSL.

Figure 4-55 (continued). L-1011 exceedance curves for different altitude bands. [Reprinted from ref. 4-8]

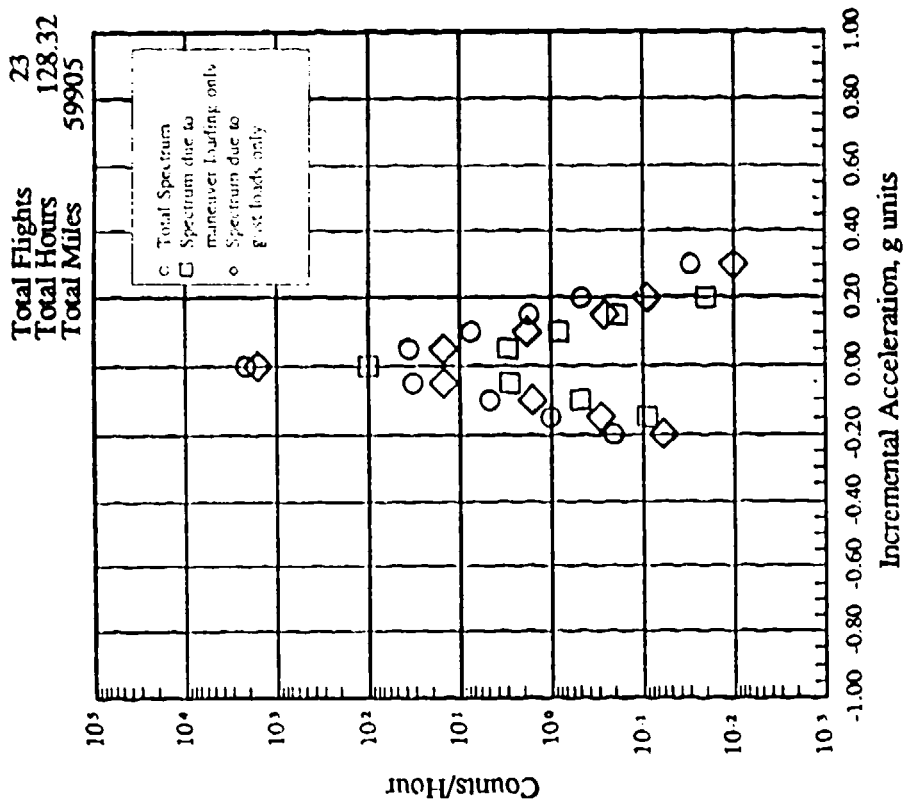


(a) L-1011.

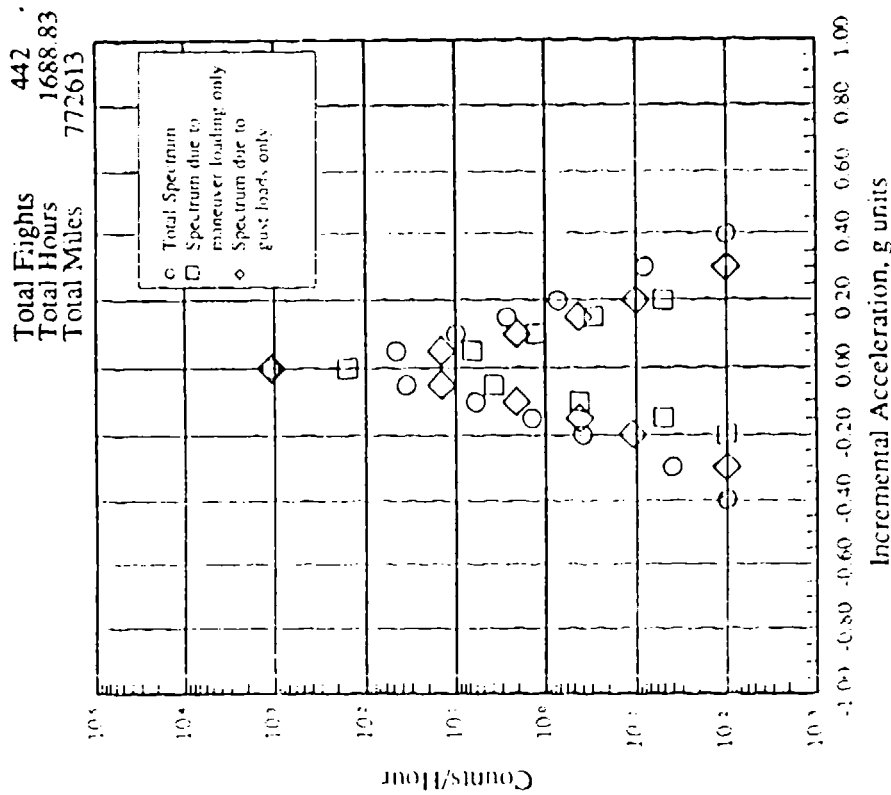


(b) B-727.

Figure 4-56. Comparison of composite exceedance curves from four airplanes (all altitudes).
[Reprinted from ref. 4-8]



(c) B-747.



(d) DC-10.

Figure 4-56 (continued). Comparison of composite exceedance curves from four airplanes (all altitudes).
[Reprinted from ref. 4-8]

Conversely, a manufacturer may offer analysis based on tests to support other damage tolerance certification requirements which involve residual strength. For example, areas not normally tested for discrete source damage (e.g., the fuselage crown and wing box panels) must still be able to tolerate fatigue damage; the time to first inspection and inspection interval must also be established. The last two criteria require a specification of critical crack length. If fail-safety depends on crack arrest within a continuous skin, then the arrest capability at certain limit load conditions must be demonstrated. The supporting test data generally comes from the manufacturer's design development program, in which neither test conditions nor hardware may precisely represent the airframe.²⁴ Therefore, the flight standards engineer should understand how panel strength analysis is correlated with test results, in order to understand the logic underlying certification support documents and to identify weak points which may require further support.

Figure 4-57 illustrates the modeling and stress analysis process for a panel with an assumed crack. The structure is considered to be uniformly loaded by the reference stress S , which is a product of the whole airframe stress analysis (e.g., S_g for a wing box panel).²⁵ A central crack of length $2a$ has been assumed, and in this case it has also been assumed that the central stringer is broken.

One quarter of the panel is modeled, as indicated by the shaded region on the drawing of the structure. This is a common procedure to take advantage of symmetries. The symmetry criteria in this case can be expressed in terms of conditions on the model's edge deflections under load: (1) the centerline remains on the y -axis; and (2) the intact part of the section along the x -axis remains on the x -axis. The structure is represented by a compatibility model or a finite element model. Numerical analysis of the model produces three key results for the damage tolerance evaluation: (1) the stress intensity factor K_I , for the skin crack; (2) the maximum stress

²⁴The cost of repeated full-scale tests to demonstrate every aspect of damage tolerance would be prohibitive. Also, it would be extremely difficult for a manufacturer to schedule large numbers of major components out of the production line for such testing.

²⁵ S is also called a nominal or gross area stress, since the total load on the panel is the product of S and the panel's total (skin plus stringer) cross section area.

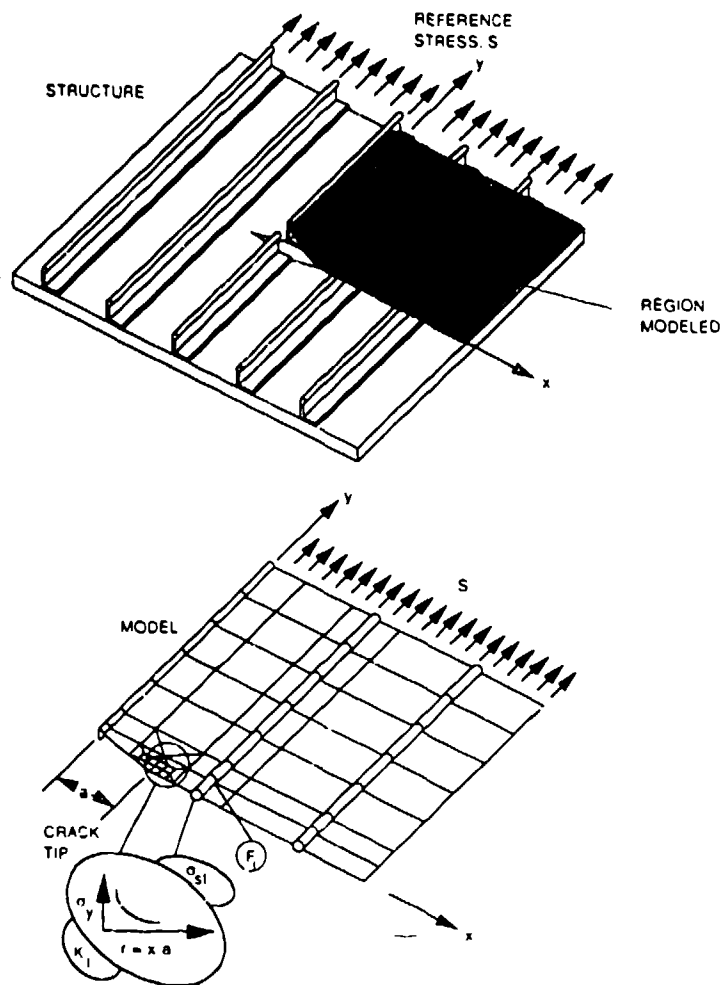


Figure 4-57. Panel stress analysis.

σ_{sl} in the stringer near the crack tip; and (3) the bearing force F_1 acting on the fastener closest to the crack tip ("first fastener"). The values obtained for K_I , σ_{sl} , and F_1 correspond to the assumed crack length $2a$ and the reference stress S .

The panel stress analysis is repeated for different crack lengths, including cracks long enough to extend past the first intact stringer on each side. The complete set of results is then used to prepare a panel strength diagram. The panel strength diagram is basically a comparison of the nominal stress level at which each component would fail, assuming that the other components do not fail. Evidently, the failure mode is determined by whichever component has the lowest strength. The diagram is constructed as follows.

The results for the skin are plotted as a curve of applied stress intensity factor versus half crack length, and an R-curve analysis is performed as indicated in Figure 4-58 (a). This is the same as the procedure discussed in Section 2.4.1, except that the applied K_I curve has a dip in this case, due to the presence of the stringer. The result of the R-curve analysis is a curve of critical nominal stress S_c for skin fracture, Figure 4-58(b).

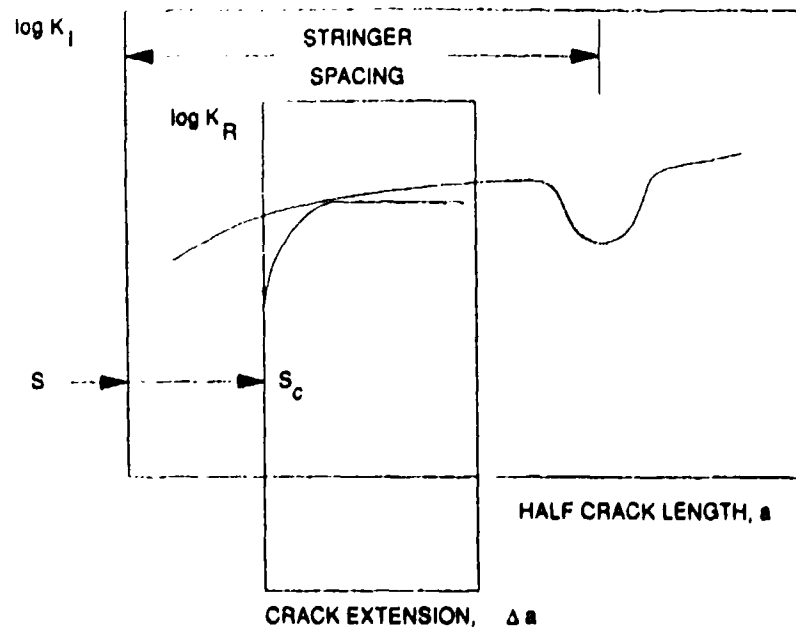
The results for the maximum stringer stress are compared directly with a conventional strength property, e.g., the yield strength Y for the stringer material. If the reference panel stress S has produced the stringer stress σ_{st} , then it follows that the stringer would yield at the critical value:

$$S_c(a) = \frac{Y}{\sigma_{st}} S \quad (4-22)$$

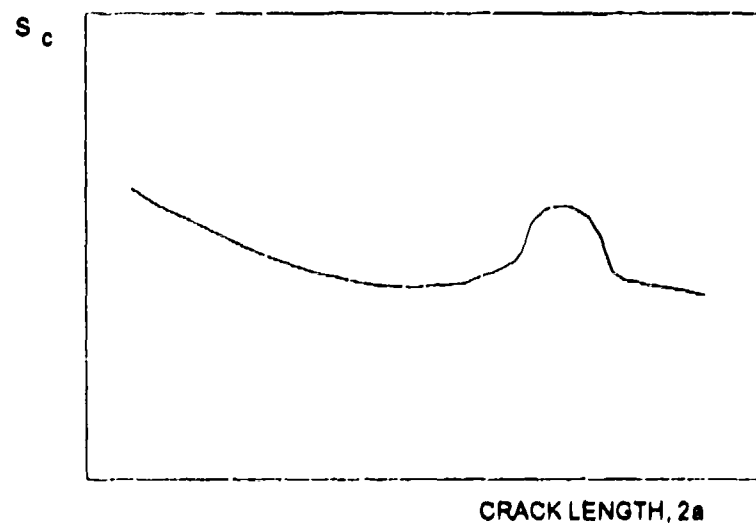
In a similar manner,

$$S_c(a) = \frac{F_{\max}}{F_1} S \quad (4-23)$$

is the critical stress for first fastener failure, where F_{\max} is the product of fastener shear strength and effective shear area. The panel strength diagram is then completed by superimposing the stringer and first fastener critical stress curves on the skin fracture strength plot (Figure 4-59).



(a) R-curve analysis.



(b) Strength plot.

Figure 4-58. Construction of skin fracture strength plot.

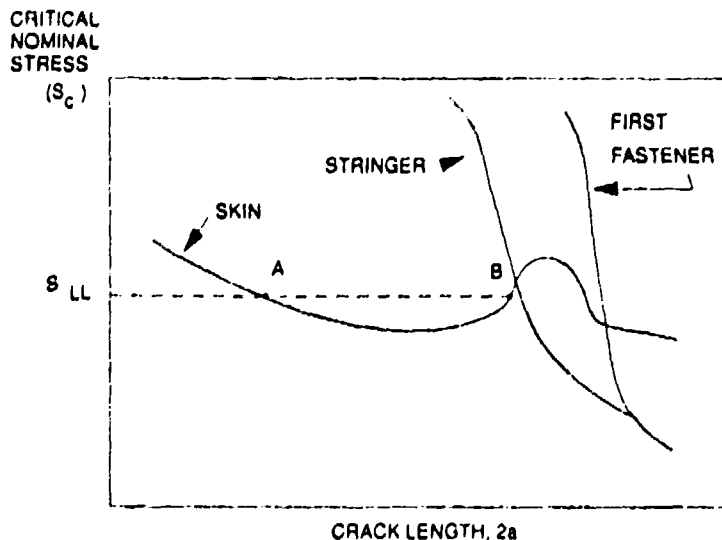


Figure 4-59. Panel strength diagram.

The panel strength diagram is the basis for the residual strength damage tolerance analysis. As shown in Figure 4-59, the analysis is completed by plotting the nominal panel stress at limit load, S_{LL} , and reading across. At the first intersection (point A), the limit-load stress is equal to the skin fracture strength and is a decreasing function of crack length. This defines the critical crack length for later use in crack growth life estimation. If the panel actually contained a crack this long, application of limit load would start a running skin fracture. However, the fracture would be arrested at a crack length corresponding to the second intersection (point B). This establishes the fail-safe character of the panel.

The significance of the stringer and first fastener curves in this example is that both components maintain a safe margin above the applied stress for all crack lengths up to and including the arrest length. This should always be the case for certifiable structure, but test panel failures may occur during development of the airframe design. The results of such failures can be accepted for the purpose of validating the panel strength analysis method, provided that the strength diagram is properly interpreted and each link in the chain of logic supporting the applicant's statement of compliance is verified.

Figure 4-60 shows what might happen, for example, if fasteners with greater strength and stiffness had been used. In this case, the first fastener failure stress would increase, but the stringer failure stress would be decreased by the more efficient transfer of overload through the fasteners. As the crack runs, the stringer is overloaded to failure (point C) before the crack can be arrested. The stringer failure effectively decreases the skin fracture strength to a value near that for an unstiffened panel, i.e., the capability for crack arrest has been lost.²⁶

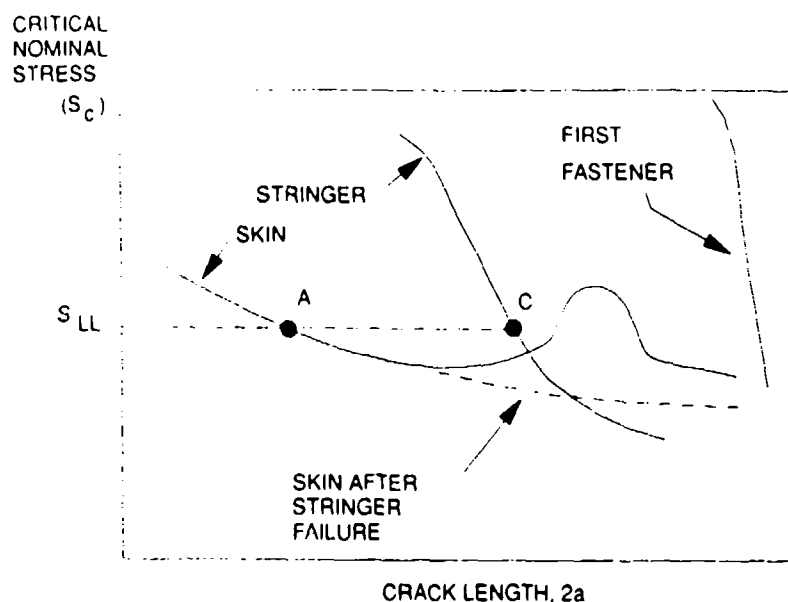


Figure 4-60. Panel failure due to stringer overload.

Figure 4-61 illustrates the kind of situation which calls for close scrutiny of an application for certification. Suppose that this strength diagram is submitted in support of certification, and that the diagram has been prepared by means of analysis. The supporting data consists of strengths diagrams for somewhat different panel details, prepared by the same analysis procedure, but also correlated with design development test results. The nature of the correlation is that, for the crack lengths actually tested, the predicted critical stress is close to the measured failure load divided by the panel cross section area. Note that the diagram in Figure 4-61 predicts crack arrest at the limit-load panel stress, but also that there is only a small margin in the stringer. Is the analysis reliable enough to justify certification of the production panel as multiple path structure?

²⁶ A similar effect might be produced by weaker, more flexible fasteners, i.e., loss of crack-arrest capability caused by fastener failure. This phenomenon is sometimes called "unzipping" but occurs only infrequently in practice.

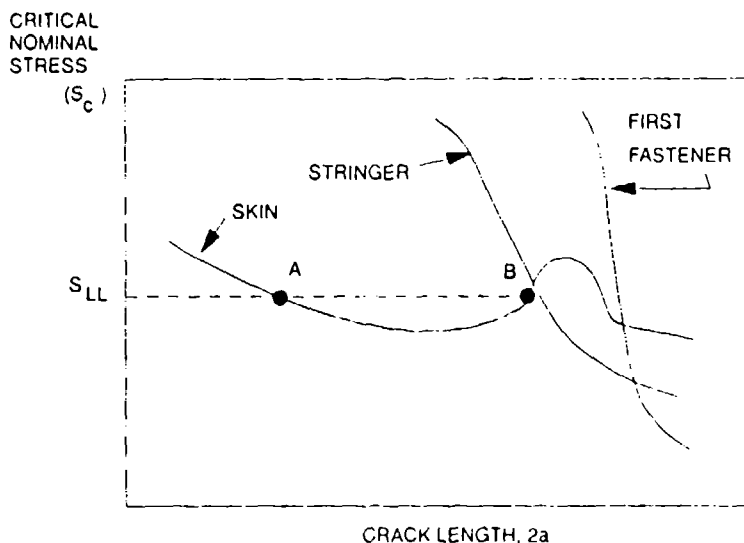


Figure 4-61. Panel strength diagram indicating marginal fail-safety.

The above question can only be answered by examining the uncertainties associated with the model validation and its subsequent application. If there are such uncertainties, they may be either conservative or unconservative and so may either increase or decrease confidence in the analysis. The review should consider two general questions:

- (1) Regarding the panel tests used to correlate the analysis, did the tests omit covering any key aspect of material or mechanical behavior that could affect the actual structure in a significant way?
- (2) Regarding the model itself, were there any assumptions, inputs, or levels of detail required for analysis of the actual structure that were not exercised when the analysis was correlated?

Some specific examples are discussed in the following paragraphs.

Skin fracture resistance, as characterized by R-curve and net section behavior, is a key material property. However, the results of a panel test program may sometimes be used to establish a thin-section fracture toughness K_{IC} as an apparent material property. Adopting a constant K_{IC} value based on test correlation is a convenient way to simplify the analysis procedure, as long as

the selected value is conservative. This short cut may be justified if the actual K_C (as determined by R-curve analysis) does not change much over the range of critical to arrest crack length for both the test panels and the actual structure.

The applicability of the R-curve should be verified. Does it correspond to the actual skin thickness? If not, was it obtained by interpolation from tests which closely bracket the actual thickness? Is LT oriented data being applied to a TL crack orientation in the actual structure?

Even a full R-curve analysis may be unconservative if the skin is net section critical. For an isolated long crack (the situation represented in Figure 4-57), the skin is generally fracture critical, and the R-curve analysis is applicable. This is easily established by verifying that the significant part of the skin strength curve belongs to the middle segment of the Feddersen diagram. (Multiple site damage along a fastener row in a crosswise splice is an important exception; the ligaments between fastener holes are usually net section critical.)

Stringer and fastener flexibility are two other key properties. In the earlier discussion, these components were implicitly assumed to be elastic, in order to simplify the description of the analysis procedure. The elastic assumption is valid for the stringer if yield strength or a flow stress a few percent above yield strength is the failure criterion (a conservative approach), but the elastic assumption is not valid if the stringer failure criterion is ultimate strength or a flow stress approaching ultimate strength. The elastic assumption for the fastener is generally not valid for rivets, but is conservative in that it penalizes the stringer with more than the actual overload stress. If this penalty is too conservative, then the elastic-plastic flexibility obtained from fastener tests should be used in the analysis. In this case, the tests should represent the actual fastener type, diameter, and stack thickness (Figure 4-62).

Nonlinear panel stress analysis is required if either the stringer or fasteners are represented by elastic-plastic flexibility. In this type of analysis, the nominal panel stress is applied in a series of small load steps. After each step, the states of the stringer and fasteners are checked, and

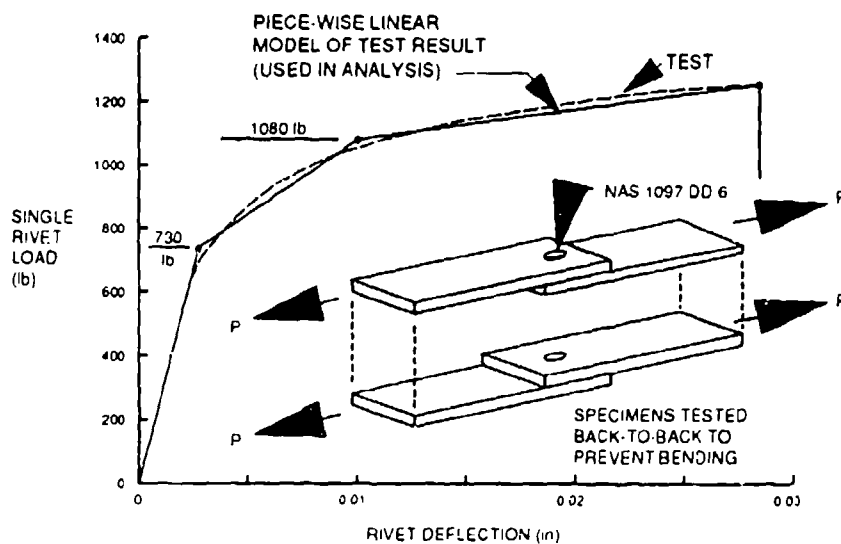


Figure 4-62. Simulated rivet load-displacement curve.

their flexibilities are adjusted to approximate the stress-strain or load versus displacement curve with a tangent. The load steps should be small enough to allow the series of tangents to follow the actual material property curve without appreciable lag error.

Proper development of the crack arrest region of the panel strength diagram requires that the applied load steps be continued up to the point of stringer or fastener failure, whichever occurs first for the assumed crack length being analyzed. This procedure involves much more computation than required by the elastic scaling rules discussed earlier.

Local stringer bending is a key mechanical property. Since the neutral axis of the stringer is offset from the skin, the stringer is locally stressed in bending by the fastener bearing load as the crack approaches. Combined bending and tension overload can stress the stringer to its failure point at a lower nominal applied stress value than the value corresponding to pure tensile overload. As depicted in Figure 4-57, most panel stress analysis models represent the stringer as a pure tension member. This is unconservative, especially for situations where the stringer strength curve has a steep slope and crosses the skin fracture curve near the predicted crack arrest point (Figure 4-61).

Bulging is another key mechanical property for curved panels in pressurized structure. As depicted in Figure 4-57, however, most panel stress analysis models are based on a flat panel under uniform tension. The skin stress intensity factors calculated with such models are modified by empirical factors to represent the effects of pressure and bulging. For example, the factor proposed by Swift (ref. [4-9]).

$$K_I(\text{curved}) = \left[1 + \frac{5W}{4R} \left\{ 1 + \cos \pi \left(1 + \frac{2a}{W} \right) \right\} \right] K_I(\text{flat}) \quad (4-24)$$

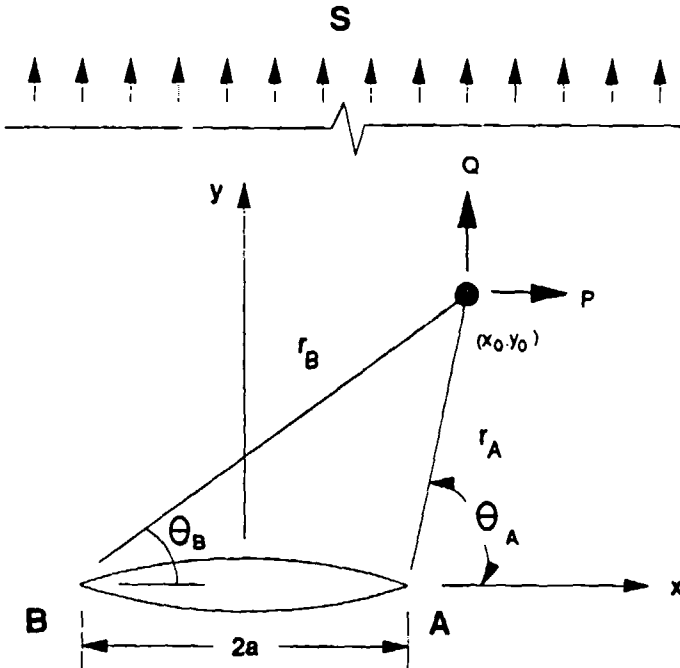
where W is the frame spacing and R is the panel radius of curvature, is often used to represent the bulging effect.²⁷ The applicability of such factors should be demonstrated by correlation with pressurized curved panel fracture tests.

The flat panel stress analysis is based on either a compatibility model or a finite element model. In either case, the first objective is to determine the fastener bearing load values that match the difference in skin and stringer deflection to fastener shear at each fastener location. The two methods differ in the way they represent the skin displacement.

Compatibility models are based on exact elasticity solutions for an unbounded skin with a crack. In addition to the original Irwin solution ($K_I = S\sqrt{\pi a}$), the solutions for point loads P , Q shown in Figure 4-63 are used to represent the effect of each fastener. The corresponding skin displacement equations are used to express the total skin displacement in terms of the unknown fastener bearing loads P_1 , Q_1 , P_2 , Q_2 , \dots , P_J , Q_J , and similar expressions are constructed for the deflection of each stringer. The loads are determined from the displacement matching conditions, and then the skin stress intensity is calculated by summing the contributions:

$$K_I = S\sqrt{\pi a} + \sum_{j=1}^J [K_I(P_j) + K_I(Q_j)] \quad (4-25)$$

²⁷ Another scaling factor is usually included to represent the nonlinear stiffening effect (a reduction of K_I) due to large skin deflections.



$$\phi = \frac{\theta_A - \theta_B}{2}$$

$$\Psi = \frac{\theta_A + \theta_B}{2}$$

$$K_I = S\sqrt{\pi a}$$

$$K_I(P) = \frac{(k-1)\left[1 - \sqrt{\frac{r_B}{r_A}} \cos \phi\right] - \frac{2y_0}{\sqrt{r_A r_B}} \left[\sin \Psi - \frac{r_B}{r_A} \sin(\phi + \theta_A) + \frac{a}{r_A} \sin(\Psi + \theta_A)\right]}{2(k+1)\sqrt{\pi a}} \quad P$$

$$K_{II}(Q) = \frac{(k+1)\sqrt{\frac{r_B}{r_A}} \sin \phi + \frac{2y_0}{\sqrt{r_A r_B}} \left[\cos \Psi - \frac{r_B}{r_A} \cos(\phi + \theta_A) + \frac{a}{r_A} \cos(\Psi + \theta_A)\right]}{2(k+1)\sqrt{\pi a}} \quad Q$$

at point A

$$(k = \frac{3 - \nu}{1 + \nu} \text{ for plane stress})$$

Figure 4-63. Basic stress intensity factors used in compatibility model.

[Source: Ref. 4-10]

The procedure requires simultaneous solution of as many equations as there are fastener bearing load components included in the model,²⁸ but the principle of the method is the same as in the lap splice example discussed in Section 4.3.3.

²⁸Only the central and two adjacent stringers are represented in the model. Enough fasteners must be modeled along each stringer to reach a distance at which the stringers and skin closely approach the condition of uniform nominal stress S .

Finite element models came into wide use for airframe gross stress analysis in the 1960s and are now beginning to be used for panel stress analysis. The basic concept of the finite element method is to represent a continuous body by an assembly of pieces ("elements") with simple shapes. Instead of exact elasticity solutions, the stresses and displacements in each element are approximated in a way such that continuity between adjacent elements is automatically maintained when the assemblage is loaded. Figure 4-64 shows how the method is applied to a simple bar element. Under the tensile load P , the bar stretches as shown in Figure 4-64(a) by an amount ΔL related to the load by:

$$P = \frac{EA}{L} \Delta L \quad (4-26)$$

One purpose of the finite element method is to make it convenient to deal with problems in which several such bars might be connected at different angles. As shown in Figure 4-64(b), this is done by viewing the bar in a "global" reference frame (the XY coordinate system). The ends of the bar are assigned displacement components u_i , which are related to ΔL by:

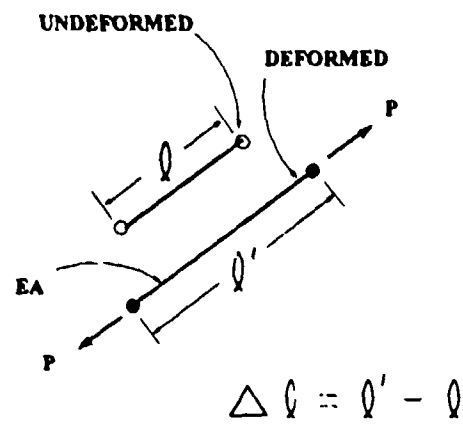
$$\Delta L = (u_3 - u_1)\cos\theta + (u_4 - u_2)\sin\theta = \begin{bmatrix} -\cos\theta & -\sin\theta & \cos\theta & \sin\theta \end{bmatrix} \begin{Bmatrix} u_1 \\ u_2 \\ u_3 \\ u_4 \end{Bmatrix} \quad (4-27)$$

In a similar manner, the force components f_i in the reference frame are:

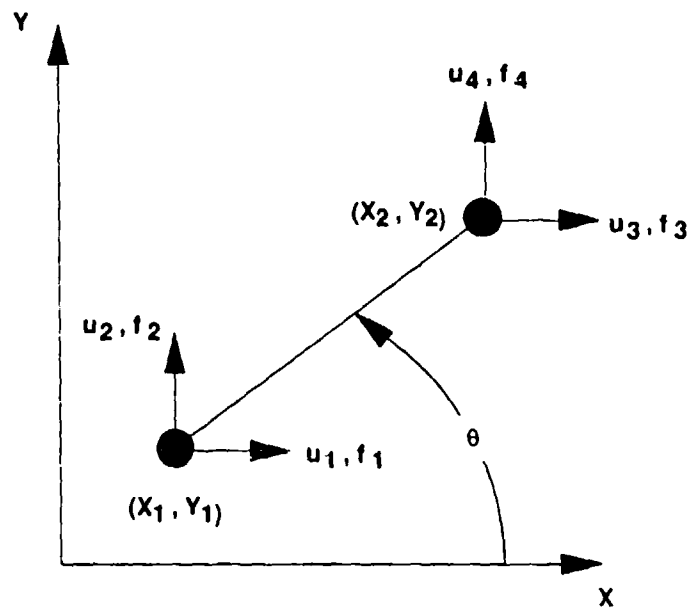
$$f_1 = -P \cos\theta \quad f_2 = -P \sin\theta \quad f_3 = P \cos\theta \quad f_4 = P \sin\theta \quad (4-28)$$

or

$$\begin{Bmatrix} f_1 \\ f_2 \\ f_3 \\ f_4 \end{Bmatrix} = \begin{Bmatrix} -\cos\theta \\ -\sin\theta \\ \cos\theta \\ \sin\theta \end{Bmatrix} P \quad (4-29)$$



(a) Bar viewed in natural reference frame.



(b) Bar viewed in global reference frame.

Figure 4-64. Finite element concept.

Substituting these equations into the P versus ΔL relation then leads to:

$$\begin{Bmatrix} f_1 \\ f_2 \\ f_3 \\ f_4 \end{Bmatrix} = \frac{EA}{L} \begin{bmatrix} \cos^2\theta & \sin\theta \cos\theta & -\cos^2\theta & -\sin\theta \cos\theta \\ \sin\theta \cos\theta & \sin^2\theta & -\sin\theta \cos\theta & -\sin^2\theta \\ -\cos^2\theta & -\sin\theta \cos\theta & \cos^2\theta & \sin\theta \cos\theta \\ -\sin\theta \cos\theta & -\sin^2\theta & \sin\theta \cos\theta & \sin^2\theta \end{bmatrix} \begin{Bmatrix} u_1 \\ u_2 \\ u_3 \\ u_4 \end{Bmatrix} \quad (4-30)$$

The matrix in the above equation represents the bar's stiffness in the global reference frame. The stiffness matrix is completely described by the material and section properties (EA) and the end coordinates, since:

$$L = \sqrt{(X_2 - X_1)^2 + (Y_2 - Y_1)^2}$$

$$\sin\theta = \frac{Y_2 - Y_1}{L} \quad \cos\theta = \frac{X_2 - X_1}{L} \quad (4-31)$$

Bar elements like the one in Figure 4-64 can be joined end-to-end to represent stringers, each joint being a place where a fastener can be attached. Similar elements with triangle and quadrilateral shapes are used to represent the skin. The stiffness matrices for these elements are determined by the coordinates of the corners. The lower part of Figure 4-57 illustrates an assembly of skin elements joined at their corners, stringer elements joined at their ends, and (not shown) springs between skin and stringer junction points to represent the fasteners.

In mathematical terms, the assembly is equivalent to summing the stiffness coefficients of all the elements connected to each attachment point. Some of these points represent the ends of the panel, and forces are applied to those points to represent the uniform gross stress. The resulting system of equations must then be solved simultaneously to find the displacement components at each attachment point. After the displacements have been found, other equations can be used to calculate the stresses in each element.

Figure 4-65 shows how the skin stress intensity factor is estimated. When conventional finite elements are used in the model, there is no direct representation of the Irwin crack-tip stress field. Instead, the linear distribution of stress along the element edges between corners must be relied

upon to follow the concentration of stress near the crack tip. As shown in the lower part of the figure, K_I can be estimated by plotting (on a logarithmic scale) σ_y versus $2\pi r$ (where $r = x - a =$ distance from the crack tip) for the corner points along the line ahead of the crack. If the numerical solution accurately followed the Irwin stress distribution, the data would plot along a straight line with a slope of $-1/2$, and the intercept at $2\pi r = 1$ would define K_I . However, an extremely fine grid of elements must be used to obtain an accurate solution. In practice, some approximation is usually accepted in order to keep the size of the model reasonable, and the data points do not fall neatly on a line of the proper slope. A best-fit line is then used to estimate K_I , but the result may be unconservative.

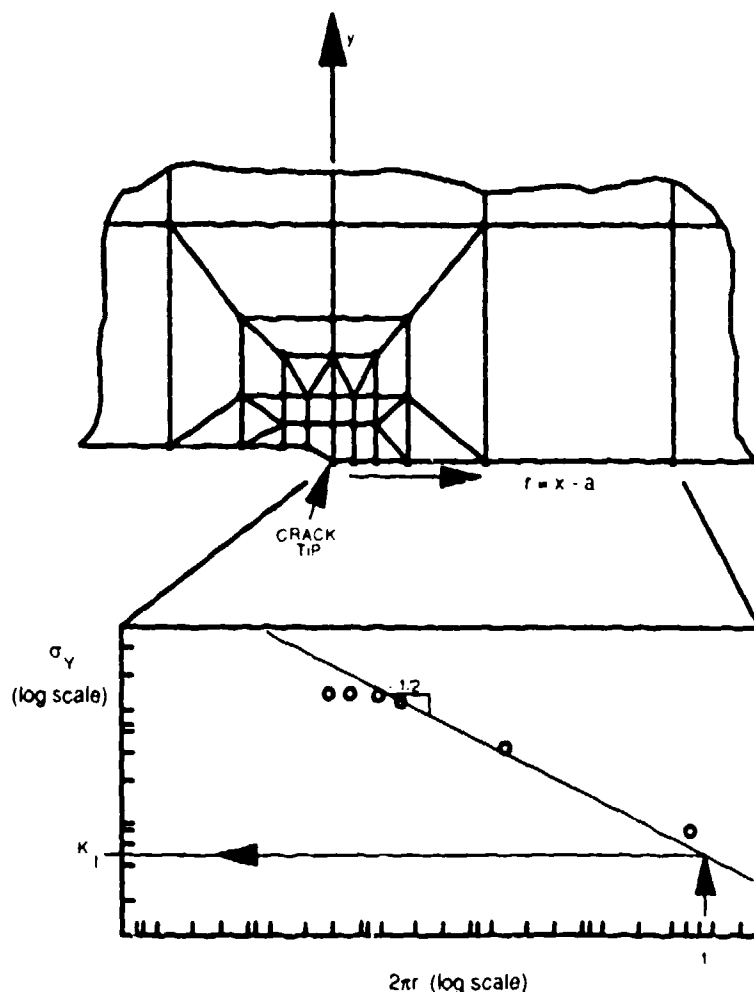


Figure 4-65. Finite element estimate for skin stress intensity factor.

Advanced finite element methods can be used to avoid the above problem. In the advanced methods, special elements are used around the crack tip to better approximate the stress gradient (ref. [4-11]) or to incorporate the Irwin stress solution exactly (ref. [4-12]). However, these methods have not yet been widely applied to panel stress analysis.

Each manufacturer of transport airplanes has developed its own compatibility model for panel stress analysis. A manufacturer's model consists of software dedicated to the specific residual strength analysis task, together with procedures for translating structural details and dimensions into input data. The reliability of the model is established by a long history of correlation with panel test results. Compatibility models are also inherently difficult to reconfigure because even simple changes (e.g., from a one-bay crack to a two-bay crack) require extensive reprogramming under the supervision of an experienced airframe stress analyst. Although this characteristic is sometimes cited as a criticism, it actually enhances reliability by forcing a slow pace of model evolution and frequent rechecking of correlation with test results.

Conversely, there is a wide variety of general-purpose commercial finite element software which is suitable for panel stress analysis. It is likely that the finite element option will become more and more popular in the future because finite element models can be reconfigured quickly and easily by changing input data. Also, many advanced options such as elastic-plastic analysis, curved panel geometry, and stiffening effects due to large deflections are already available in commercial software. Future options may provide the capability to analyze panels assumed to contain widespread cracking, e.g., for the purpose of establishing a critical adjacent or multiple-site crack length as a basis for estimating time to loss of fail-safety. Although the basic software is generally reliable, its "user friendly" character can obscure the risk that rapid evolution may compromise the reliability of a panel stress analysis model. Therefore, the flight standards engineer should pay close attention to such models, in order to assure that they are correlated and documented to the same standards of practice as the compatibility models.

4.6.3 Crack Growth Life Evaluation

For the purpose of damage tolerance evaluation, crack growth life is defined as the time (number of flights or flight hours) required to grow a crack from a specified initial length to a critical length determined by a specified limit load condition. The life is based on expected fatigue loads derived from the airplane service spectrum. In order to account for uncertainties in the evaluation, a factor of safety is applied to the unfactored crack growth life to establish the corresponding safe-life or time. The basis for the crack length assumptions depends on the purpose of the specific evaluation. Table 4-7 lists five possible evaluation criteria and their associated initial and critical crack lengths. Examples of each type of evaluation are discussed in Sections 4.6.3.1 through 4.6.3.4. Verification of crack growth models is discussed in Section 4.6.3.5.

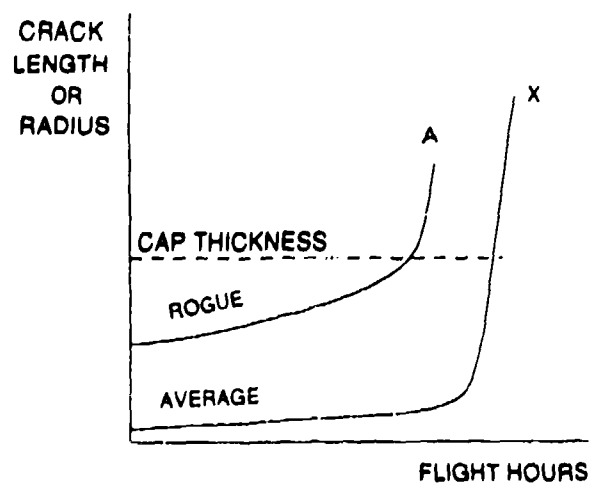
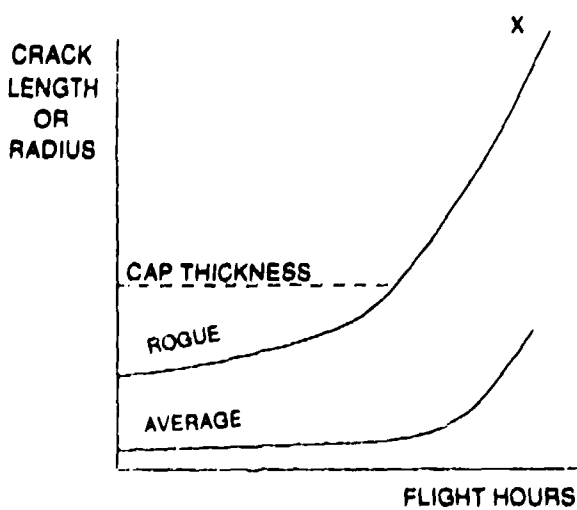
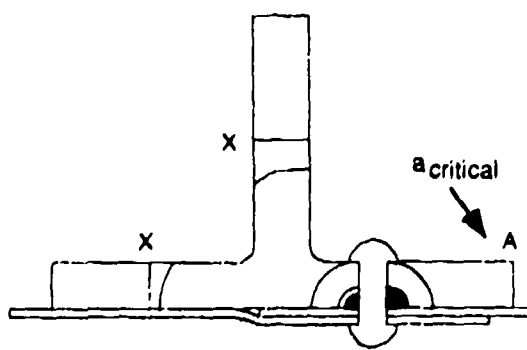
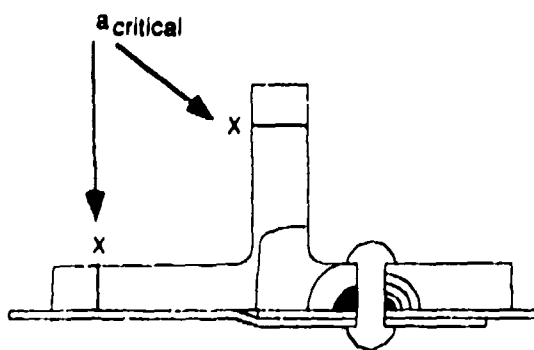
4.6.3.1 Modified Safe-life Based on Crack Growth

The safe-life of single path structure is based on the time required to grow a rogue flaw to the length that would be a critical crack at limit load. One evaluation of crack growth life, with a rogue flaw assumed in the worst location, is sufficient for most cases. In some cases, however, the worst location is not immediately obvious because continuing damage must be considered in order to evaluate the life.

Figure 4-66 illustrates a hypothetical example. The structure is a heavy spar cap, which is assumed to carry all of the tension due to bending of an aerodynamic surface. Thin skins, assumed to be ineffective in tension, are lapped over the cap and attached to it via a spanwise rivet row. The rivets bear only secondary loads, but the fastener holes are damage sites for the cap. This type of construction might be found in empennage or in the wing of a light twin engine commuter airplane.

Table 4-7. Crack growth life evaluation criteria.

Type of structure	Purpose of the crack growth life evaluation (subsection)	Basis for crack length	
		Initial	Critical
Single path	Modified safe-life, based on crack growth (4.6.3.1)	Rogue (plus average if required for continuing damage)	Design limit load
Multiple path	Time to first inspection (4.6.3.2.2)	Rogue (plus common hole rogue and average for continuing damage)	Design limit load
	Safe inspection interval (4.6.3.2.2)	Detectable by specified inspection procedure	Design limit load and adjacent noninspectable component failed from crack at common hole
	Safe flight time after discrete source damage (4.6.3.3)	Demonstrated length at crack arrest	Reduced limit load and continuing slow growth from arrested crack
	Time to loss of fail-safety (4.6.3.4)	Average	Design limit load and adjacent inspectable component failed



(a) Rogue flaw in a long ligament.

(b) Rogue flaw in a short ligament.

Figure 4-66. Use of continuing damage to evaluate safe crack growth life in single path structure.

Since access to the cap would require tearing down the wing, the cap is considered to be noninspectable. The cap is also classified as single path structure, even though the fastener hole divides it into two ligaments, because the lack of access prevents detection of partial failures.

The life of the cap might be evaluated by assuming a rogue flaw in the longer ligament. As shown in example (a), a rogue flaw would grow to critical length (indicated by the X symbols) well before an average initial crack assumed to co-exist in the shorter ligament could affect the outcome. However, this is not necessarily the minimum safe crack growth life. In example (b), the locations of the rogue flaw and the average initial crack have been exchanged. In this scenario, the rogue flaw first breaks the short ligament (symbol A), and the continuing damage from the average flaw is accelerated. Eventually, the continuing damage reaches critical length (symbol X), which is less than the length in example (a) because the short ligament is already broken. Both scenarios represented in Figure 4-66 must be evaluated to determine the safe crack growth life for this case.

4.6.3.2 Damage Tolerance Evaluations Requiring Inspection

4.6.3.2.1 General Considerations for Nondestructive Inspection (NDI) Methodologies and the Inspection Intervals [Reference 4-13]

Proper maintenance and inspection are keys for ensuring the safety of airframes especially with multiple site damage (MSD) potential. MSD must be detected at smaller crack lengths and in much shorter time than an isolated crack if MSD is to be found and repaired ahead of linkup and fracture.

The issue of inspection involves both inspection techniques and inspection interval.

The requirements of detecting small cracks preclude reliance on visual inspection only. The only alternative which is in common usage in the airline industry involves the use of hand-held eddy current probes. The eddy current method is technically reliable but tedious to apply, leading to

excessive downtime and human factors problems. Some of the new NDI technologies under consideration include infrared imaging and shearography, which have the potential to inspect a large area at a time.

Adhesive bonding is utilized in modern aircraft fuselages, frequently in combination with rivets. As aircraft age, bond failure becomes a major problem, since it may promote fatigue cracking, moisture intrusion, and subsequent corrosion. The shearographic method of detecting disbonds depends on the deformation of the aircraft skin under varying pressurization. When illuminated by coherent light, the phase relationship and intensity of the light reflected from any two points of the skin changes as a result of this deformation. Surface changes down to 0.00025 millimeter can be detected and displayed as a real-time image of the field of view. Comparison of successive images as the pressure changes permits interpretation of the condition of a bond.

One key element of a successful inspection program is the interval between inspections. Too short an interval becomes economically burdensome, while too long an interval increases the possibility that a critical crack will go undetected. The selection of inspection interval (or strategy) should be made very carefully.

4.6.3.2.2 Time to First Inspection and Safe Inspection Interval

Figure 4-67 illustrates a hypothetical example of a continuous-skin lower wing panel, together with a typical crack growth scenario that might be used as a basis for evaluating time to first inspection and safe inspection interval. Similar scenarios could be employed to evaluate fuselage panels, with the frames playing the role of the wing panel stringers.²⁹ Also, similar scenarios should be evaluated for damage at lateral edges, i.e., at splices parallel to the major load axis (see Figures 4-16 and 4-17).

²⁹If the frames were offset and supplemented by tear straps, then the tear straps would play the role of the stringers, and the central frame could be assumed to remain intact.

The first schematic in Figure 4-67 shows the initial crack assumptions and the first stage of crack growth. Common drilling is assumed, and so a rogue flaw has been placed in the stringer as well as the skin. Also, an average flaw has been placed in the skin, on the opposite side of the fastener hole, to represent continuing damage. Successive crack front positions are indicated, up to the point at which the stringer crack reaches its critical length (symbol A). At this point, the rogue flaw in the skin has already become a through crack, but the average flaw is still growing as a corner crack.

A conservative short cut is taken at this point to define the second stage of crack growth. Continuing damage in the stringer is not specifically evaluated; it is simply assumed instead that failure of the short ligament coincides with failure of the long ligament (symbol A). The second schematic shows an intermediate stage, in which the central stringer is broken, and the two skin cracks grow until the continuing damage is about to become a through crack (symbol B).

Another conservative short cut is taken at this point by neglecting the time required for transition of the continuing damage. As shown in the third schematic, the final stage of crack growth is assumed to begin with both skin cracks treated as through cracks, the lengths of which are combined with the fastener hole diameter to define a single tip-to-tip crack length $2a$. The center of this crack will likely be offset from the stringer centerline, as shown in the schematic. However, the effect of the fastener hole will increase the stress intensity factor for a while at the right crack tip, and the offset will thus tend to decrease as the crack grows. Therefore, it is reasonable to base the critical length on a panel strength diagram such as Figure 4-59, where the skin crack was assumed to be centered on the stringer. The critical crack length from this diagram is interpreted as the critical tip-to-tip length in Figure 4-67 (symbol X) for the purpose of the life evaluation.³⁰

³⁰This approximation introduces some error in the critical crack length. However, the effect on crack growth life is quite small. Crack growth life is extremely sensitive to the initial crack length assumption but is relatively insensitive to the critical crack length assumption.

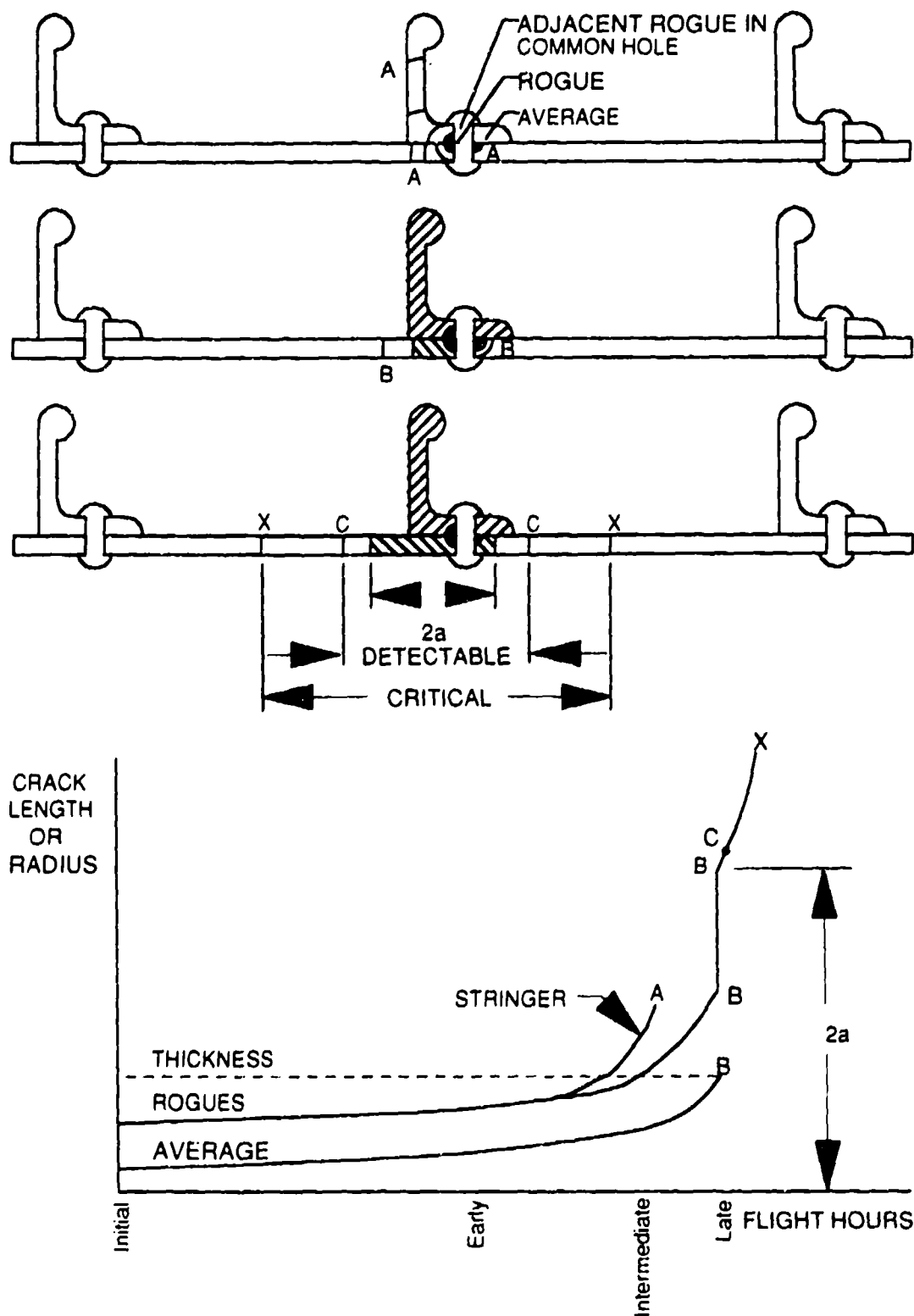


Figure 4-67. Evaluation of bases for time to first inspection and safe inspection interval for multiple path structure.

The final stage schematic also includes a detectable crack length (symbol C) which has been established based on close visual inspection underneath the wing. Note also that the life evaluation for safe inspection interval is thus based on the assumption that the adjacent noninspectable component (the central stringer) is broken. This assumption is the accepted practice for evaluation of visual inspection intervals under FAR 25.571.

The sizes of the various cracks are plotted versus flight hours in the graph below the schematics (Figure 4-67). The total crack growth life is the sum of the three stages: (1) zero time to central stringer failure at point A; (2) continuing damage to linked through crack, point A to point B; and (3) linked through crack to critical length, point B to point X. This is the basis for the time to first inspection. The life during which the crack can be detected by the specified inspection procedure is the time from point C to point X. This is the basis for the safe inspection interval.

4.6.3.3 Safe Flight Time After Discrete Source Damage

Figure 4-68 summarizes the relation between the panel strength diagram and post-accident considerations for evaluation of tolerance to discrete source damage. Hypothetical accident damage (e.g., from an uncontained engine rotor fragment) might be assumed to be a critical fuselage skin crack with the central frame and tear strap broken. (The frame and tear strap failures are assumed to have been caused by the penetrating rotor fragment.) Note that, as indicated in the figure, the damage is assumed to be located in a mid-bay position on the circumference, with the skin crack along a line that bypasses the fastener holes. Rapid fracture and arrest are represented by the dashed line AB in the panel strength diagram. The critical ($2\alpha_{CR}$) and arrest ($2\alpha_{ARREST}$) crack lengths correspond to the nominal stress for the limit load condition specified for discrete source damage.³¹

³¹Maximum normal operating pressure, multiplied by a 1.1 factor of safety, plus the external aerodynamic pressure and flight loads for straight and level flight.

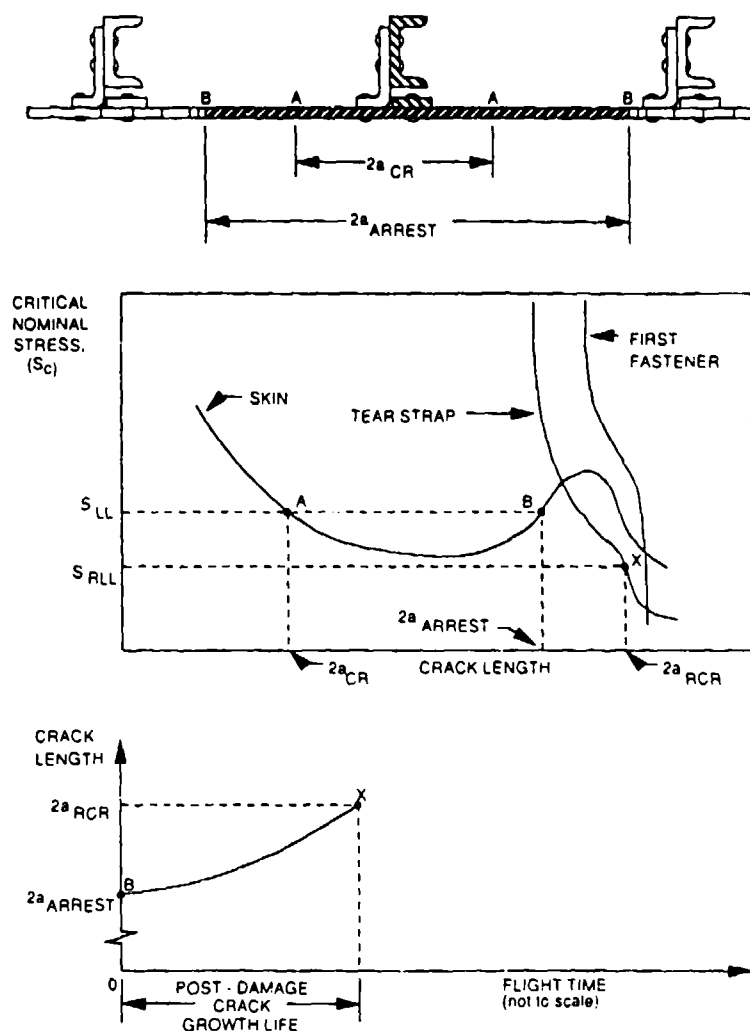


Figure 4-68. Evaluation of safe crack growth life after discrete source damage.

The life evaluation in this case addresses the issue of safe flight from just after the accident until the airplane can be landed. In accordance with AC 25.571-1A para. 8, the presumption is allowed that the flight crew will act to limit maneuvers and avoid excessive gust loads during this time. The AC prescribes a corresponding reduced limit load condition (referred to as an "ultimate condition") for the purpose of this evaluation: 70% of design limit maneuvering load and, separately 40% of design limit gust velocity (vertical or lateral) at specified airspeeds, each combined with the maximum appropriate cabin differential pressure including external aerodynamic pressure.

The reduced limit load condition is represented by the nominal stress S_{RLL} on the panel strength diagram in Figure 4-68. Reading across the diagram to the strength curve of the next critical component (the tear strap in this case) defines the intersection point X and the critical crack length at reduced limit load ($2a_{RCR}$).

The safe post-accident flight time is based on the crack growth life of the skin crack from its arrest length (point B) to its critical length at reduced limit load (point X). For consistency with the discrete source damage provisions of the AC, it is appropriate to base this crack growth life evaluation on a modified flight loads spectrum: (1) maneuver and gust load exceedances truncated above 70% and 40% of design limit, respectively; and (2) GAG cycle eliminated. In some cases, it may also be appropriate to consider two stages of post-accident crack growth. For example, the fuselage panel in Figure 4-68 would be subject to hoop stress from cabin pressurization for a short period during the blowdown³², but this stress would be relieved during the much longer time required to complete a descent to a landing. Thus, the evaluation might be based on critical crack lengths defined by reduced limit loads before and after blowdown, as indicated in Figure 4-69.

4.6.3.4 Time to Loss of Fail-safety

Under most circumstances, multiple path structure should retain its fail-safe character at least until an airplane reaches the economic design goal for the airframe. Therefore, evaluation of time to loss of fail-safety is not normally considered in the type certification process. However, such evaluations are an important part of the FAA's continued airworthiness program for aging fleets as they approach and exceed the original design goal. Fail-safety can be lost in either of two basic ways, depending on the structure: (1) adjacent panel cracking; or (2) loss of crack arrest capability. Fail-safety may also degrade much sooner if the structure is subject to multiple site damage.

³²The blowdown time should be substantiated by test or calculation.

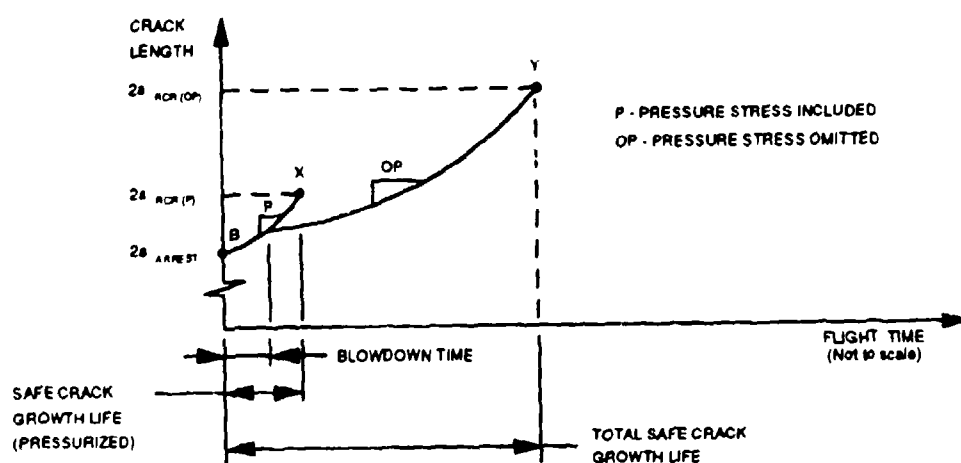
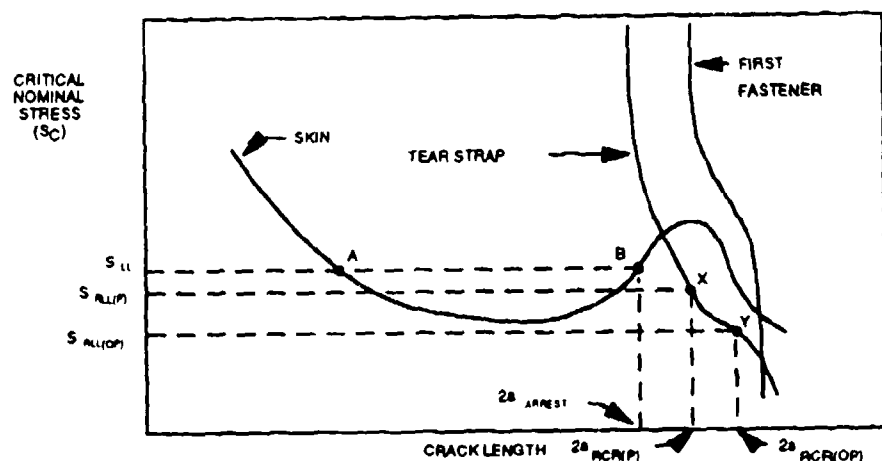


Figure 4-69. Two-stage evaluation of pressurized structure.

Adjacent panel cracking was mentioned in Section 4.3.1, in connection with the discussion of different approaches to the design of splices parallel to the major load axis. Although the examples there were based on damage assumed to be located in edge details, adjacent panel cracking can also result from mid-panel damage. Multiple panel designs with marginal internal crack arrest capability or designs which rely totally on the crack arrest capability at the splices should be evaluated for susceptibility to adjacent panel cracking. In such cases, the pertinent

crack growth life is the time required for average initial cracks to grow until they coalesce and form a skin crack of critical length. The critical crack length is determined from the skin fracture curve in the normal manner, except that the nominal stress at design limit load should be multiplied by the peak overload factor (Section 4.3.1) to represent the effect of the first panel failure on the adjacent panel. Assurance of continued airworthiness by means of a special supplemental inspection document (SSID) may be justified if the adjacent panel critical crack length exceeds the detectable crack length. Otherwise, the minimum necessary action should be skin replacement before the time in service exceeds the time to loss of fail-safety.

Panels designed to rely on internal crack arrest are not normally subject to the adjacent panel cracking limit. Instead, the critical condition is loss of crack arrest capability. Loss of fail-safety in this manner is typically associated with average initial flaws growing in noninspectable components, e.g., the stringers or tear straps in a continuous-skin panel. The critical crack length for this case is determined by reference to the basic panel strength diagram that was used to establish the fail-safe character of the design. The schematic in Figure 4-70 represents this diagram, except that the first fastener failure curve has been omitted for clarity. Instead, a family of stringer strength curves is shown. The curve marked "0" corresponds to an intact outer stringer (part of the original diagram). The curves marked "1" and "2" represent the stringer with different length cracks. The larger crack, represented by curve "2", is just sufficient to precipitate stringer failure before the skin crack can be arrested. This stringer crack defines the critical length for the purpose of evaluating time to loss of fail-safety.³³

A long crack in one or two bays should be arrested and contained by the fuselage structure, provided that there is no additional damage in adjacent bays. If the long crack was produced by a link-up of multiple site damage (MSD) type cracks, however, there may be additional MSD cracks in the adjacent bays at the time when the long crack becomes critical. The additional MSD cracks are also likely to be located on the same fastener row as the long crack.

³³The schematic has been simplified for clarity. Strictly speaking, the skin fracture curve should be modified to reflect the loss of stiffening associated with each assumed stringer crack length. The corresponding critical crack length would then be somewhat shorter.

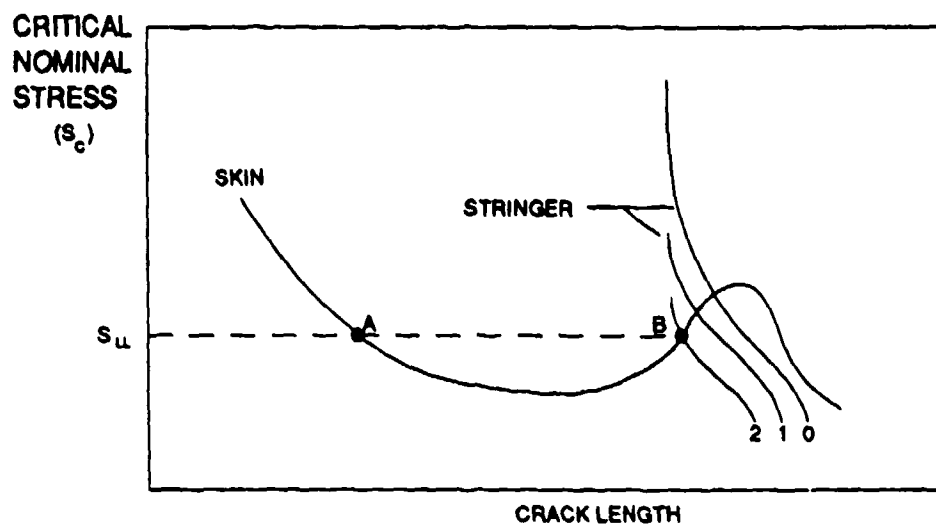


Figure 4-70. Determination of critical crack length for time to loss of crack arrest capability.

In such cases, the panel strength diagram must be modified as indicated in Figure 4-71 in order to estimate the time to loss of fail-safety. Here the curve marked "0" represents the skin fracture strength of a structure that is intact except for the long crack. The curves marked "1" and "2" represent the reduced skin fracture strength corresponding to different MSD crack lengths in the adjacent bays, with curve "2" corresponding to the larger cracks which are just sufficient to precipitate stringer failure and continuing skin fracture.

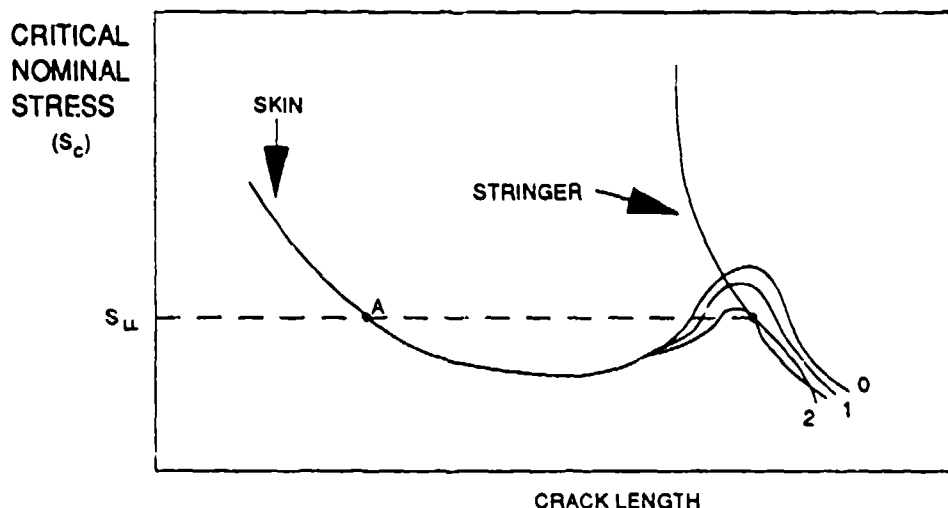


Figure 4-71. Determination of critical adjacent-bay MSD crack length for time to loss of crack arrest capability.

4.6.3.5 Verification of Crack Growth Life

The foregoing examples have been discussed from the viewpoint of analysis. In fact, most demonstrations of compliance with specific safe crack growth life objectives rely on analysis because it is impractical to conduct tests which accurately represent all of the specific damage tolerance requirements applicable to every PSE and CSE in production hardware. Thus, the model used for life evaluation must be validated by correlation with test results, just as is done for the panel stress analysis models discussed in the preceding section.

The basic elements of a crack growth life model are: (1) the stress intensity factor formulas to represent each stage of crack growth; (2) the flight loads spectrum, in terms of nominal stress; and (3) a crack growth rate equation to represent the basic material properties, together with a load-interaction model to account for spectrum effects on the basic crack growth rate. Each of these elements contains explicit and implicit assumptions which must be checked.

It is generally impractical to fully represent the geometry and load transfer details which affect an airframe crack and, at the same time, to calculate the stress intensity factor K with an arbitrarily small error. Either certain details are judged to have negligible effects in order to justify the use of K formulas based on simplified models of the structure (see Section 2.4.5), or an approximate

numerical model of the actual structure (Section 4.6.2) is used to calculate K for a set of specified crack lengths. In either case, additional error may be introduced by interpolating to find K for intermediate crack lengths. An error in K has a magnified effect on calculated crack growth life. A useful rule of thumb is that the life error is the product of the K error and the crack growth rate exponent. For example, a 10% error in K means a 40% error in calculated life if the basic material crack growth rate is proportional to $(\Delta K)^4$.

Therefore, the procedures actually used in the crack growth life calculation should be checked for analysis and interpolation error. Life calculations should also be correlated with test data to establish confidence that the stress intensity factor model reliably represents the airframe crack. The correlation is often accomplished in two phases. First, design development specimens are tested at constant stress amplitude (slowly rising K), to calibrate the detail stress intensity factor formulas. Second, life data obtained from airframe cracks are used together with the calibrated K formulas to correlate the spectrum crack growth rate model.

It is reasonable to assume that load interaction effects are negligible in a test performed at constant stress amplitude. Therefore, it should be possible to infer the stress intensity factor for a crack in a design development specimen by solving the basic material rate equation (see Chapter 3) for ΔK and dividing by the test stress range ΔS to scale to a unit value. However, the inference can be complicated by crack geometry effects.

Figure 4-72 illustrates one way in which such complications can arise. In this example, a coupon specimen is prepared in three steps for testing symmetrically positioned corner cracks at an open hole:

- (1) A small pilot hole is drilled, and a small circular saw is used to cut in corner notches. The initial notches are represented by the black areas in the upper section A-A diagram.
- (2) The coupon is subjected to fatigue loads which sharpen the notches into cracks and grow them to a larger size. The crack growth is represented by the cross-hatched areas in the middle section diagram.

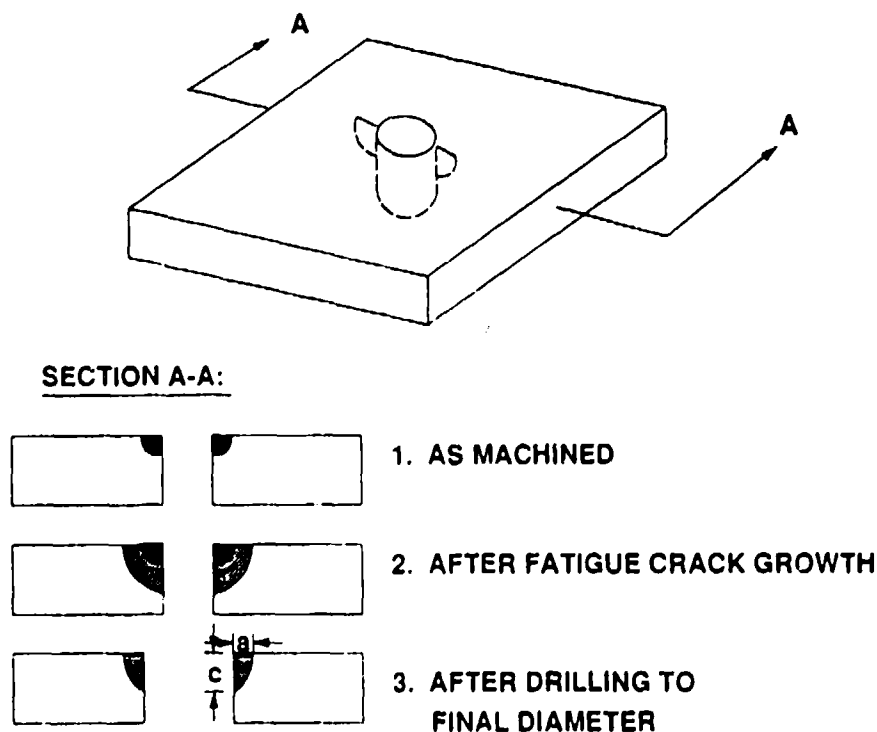


Figure 4-72. Preparation of corner crack test coupon.

- (3) As shown in the lower section diagram, the pilot hole is drilled out to a larger diameter. The drilling removes the notched regions and leaves "natural" corner cracks.

The coupon is now ready for the K calibration test, which is conducted by applying additional fatigue loads at constant stress amplitude, with a few overload cycles inserted occasionally to mark the crack front position.³⁴ The dimensions a and c can be determined for each position, including the initial crack size. Thus, the growing crack might be approximated by a series of quarter ellipses to facilitate interpolation of the results to different crack sizes and aspect ratios a/c . Additional tests with different hole radii r might also be conducted to allow interpolation to different a/r ratios.

³⁴The brief period of retardation which follows an overload can be identified in a scanning electron micrograph of the crack propagation surface when the coupon is broken open for examination after the test.

However, the crack aspect ratio will generally change as the crack grows. Also, neither the initial nor the later crack front positions necessarily have quarter ellipse shapes. Thus, any interpolation of test results based on a quarter-ellipse model of the crack should be treated with caution. How large are the correction factors needed to adjust the model K formula to conform to the test results? Do these factors exhibit consistent and smooth trends with respect to the variables (a/c , a/r , etc.)?

Correlating the spectrum crack growth aspects of the model potentially poses similar problems involving local stress distribution effects. Design development specimens are intended to simulate actual details, but the stress gradients in such specimens can deviate from the gradients near similar details in the actual structure. In theory, these problems could be resolved by conducting K calibration tests of cracks in an airframe or in major subassemblies. In practice, however, the hardware and load fixtures are too expensive to justify anything less than spectrum testing.

A typical problem might involve a K (based on a design development test) that overestimates K for small cracks and underestimates K for large cracks in the actual structure. If a calculation with the model matches test crack growth life over the entire range of crack size, the correlation could be the result of error cancellation. If inspection intervals corresponding to the larger size range were then established on the basis of model predictions for similar cracks, the results would be unconservative.

Similar errors can arise from other differences between test specimens and the actual structure, for example, residual stresses from fabrication, or load interaction effects that change as a function of stress level. The best way to guard against the effects of all such errors is to verify that spectrum life has been correlated over appropriate ranges of crack size. These ranges should approximate the ranges of initial to critical crack size for the damage tolerance evaluations in support of the correlation being presented.

Design evolution creates the potential for airframe crack growth to deviate from correlated test results on which inspection intervals have been based. There is an inherent conflict between the

need for information early in the design cycle, to allow time for changes before production, and the need for information late in the production cycle, to assure that what is tested corresponds to what is being flown. A compromise between these needs determines where the fatigue test airframe is positioned in the production run.

Since full-scale spectrum fatigue tests typically require more than a year to run, the manufacturer tends to select an early airframe, generally one produced not long after the airframes for the flight test aircraft. Consequently, the fatigue test is often well underway before flight test data can be fed back into the design cycle. This feedback may lead to structural modifications in the bulk of the production run. These modifications are not represented in the fatigue test and may or may not be represented in the crack growth test, depending on the time and resources available to modify the test airframe between the two phases of testing.

Fatigue and crack growth test results are generally not available to feed back until significant numbers of airframes have been built and placed in service. Nothing more may be needed than some modifications of the inspection program, but some cases may require minor structural modifications. Since there will generally be no opportunity to incorporate these modifications in the full-scale fatigue and crack growth test, the manufacturer monitors crack occurrence in the fleet and uses failure analysis techniques to back-track propagating cracks in order to establish times to initiation and safe crack growth lives. Such results may be offered in support of proposed ADs, or in support of certification of a new airframe design with a similar construction detail.

Test duration and costs are generally kept under control by means of accelerated testing procedures. The smallest, most frequently occurring loads in the service spectrum are omitted from the test spectrum, so that one test hour can be used to represent on the order of ten flight hours. The remainder of the test spectrum is also generally reduced to a simplified block sequence. Both the truncation point and the sequence should be checked to make sure that the test spectrum is not unconservative.

Truncating a spectrum for accelerated testing is based on the idea that stress cycles below some amplitude or range do not cause damage. The limiting amplitude in fatigue is associated with the material's endurance strength (see Chapter 1), but the actual limit is generally lower because of the load interaction effects which occur in spectrum fatigue. In a similar manner, the limiting stress intensity factor range in spectrum fatigue crack propagation can be associated with the material's threshold stress intensity factor (see Chapter 3). Depending upon the crack size(s) being tested, the corresponding threshold stress range may be above or below the range equivalent to endurance strength. Therefore, the certification review should include some checks to verify that the test spectrum was truncated below the more conservative range. This may require inclusion of more frequent cycles with lower stress ranges in the fatigue crack propagation phase of an airframe test.

Test spectrum sequences are generally reconstructed from exceedance curves, under the assumption that positive and negative exceedances with equal occurrence frequencies can be paired (see Section 4.6.1). A realistic assumption must also be made about the sequence in which the different load ranges appear in the load-time history, since load interaction effects are sensitive to sequence. An ideal test spectrum would be arranged in real sequence order, but in practice the real order will vary from flight to flight, and the best that can be done in the test spectrum is to represent average conditions. Reasonable results are generally obtained if the test spectrum is arranged to simulate individual flights by introducing a GAG cycle periodically. (From one to several different flight durations may be simulated, depending upon the type of service for which the aircraft has been designed.) Within each flight, the gust and maneuver cycles are generally aggregated, and the sequence arrangement should be either high-low or low-high-low (Figure 4-73).

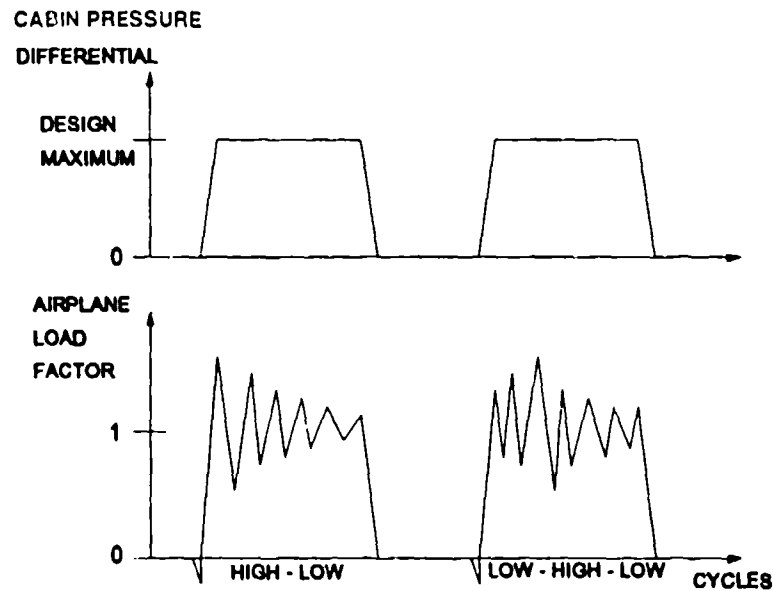


Figure 4-73. Test spectrum sequences.

Neither truncation nor sequence effects can be predicted with confidence when load interaction is present. Therefore, the choices made for the airframe test spectrum should be supported with coupon test data comparing the effects of different truncation points and sequences.

4.6.3.5.1 Approximate Estimation of Spectrum Truncation Points

The following approximate method can be used to make quick estimates of spectrum truncation points appropriate for crack propagation tests. Suppose that the crack under consideration is described by the stress intensity factor:

$$K = S\sqrt{\pi a} F(a) \quad (4-32)$$

where the crack geometry function $F(a)$ is known. Also, suppose that the material crack growth properties in the threshold region can be modeled with a conventional sharp cutoff:

$$\frac{da}{dN} = 0 \quad \text{for} \quad \Delta K \leq (1 - R)K_{TH} \quad (4-33)$$

For any given stress ratio R , the threshold stress range can then be expressed as:

$$\Delta S_{TH} \sqrt{\pi a} F(a) = (1 - R)K_{TH} \quad (4-34)$$

Now rearrange the above equation into the more convenient form:

$$\frac{\Delta S_{TH}}{1 - R} = \frac{K_{TH}}{\sqrt{\pi a} F(a)} \quad (4-35)$$

Note that all the stress parameters have been isolated on the left side of the last equation, while the right side contains all the factors involving crack length. Thus, the quantity $\Delta S_{TH}/(1 - R)$ can be plotted as a function of crack length.

The conventional assumptions for reconstructing a spectrum can be applied to derive a similar expression for the exceedance curve. For example, gust spectra are commonly assumed to consist of pairs of equal positive and negative excursions from straight and level flight, as indicated in Figure 4-74 (a). The Figure 4-74 (b) illustrates the equivalent contribution to the stress spectrum at a point in the airframe where the nominal stress is S_{1g} in straight and level flight.

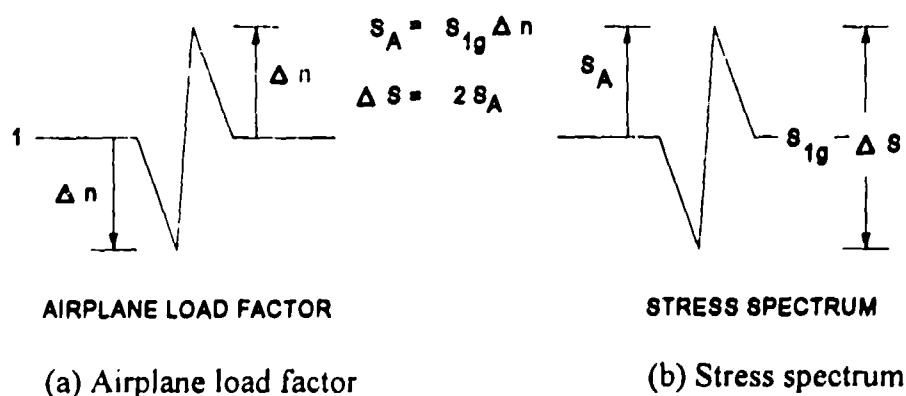


Figure 4-74. Airplane load factor and the stress spectrum.

From the definition of the stress ratio, it then follows that:

$$R = \frac{S_{\min}}{S_{\max}} = \frac{S_{lg} - S_A}{S_{lg} + S_A} = \frac{1 - \Delta n}{1 + \Delta n} \quad (4-36)$$

It is then easy to show that exceedances of $\Delta S/(1 - R)$ equivalent to the conventional exceedance diagram can be expressed as:

$$\frac{\Delta S}{1 - R} = (1 + \Delta n)S_{lg} \quad (4-37)$$

Thus the quantity $\Delta S/(1 - R)$ can be graphed as a function of frequency by plotting $(1 + \Delta n)S_{lg}$ versus the frequency N (per flight hour) corresponding to the exceedance Δn .

The two plots can be superimposed and used as indicated in the schematic illustration, Figure 4-75. For any crack length a under consideration, enter on the crack length scale (point A) and read down to the threshold curve (point B). Then, read across to the $\Delta S/(1 - R)$ exceedance curve (point C). Finally, read down to the frequency scale (point D) to find the truncation frequency estimate. The corresponding load truncation point is determined by reentering the conventional airplane load exceedance curve at this frequency.

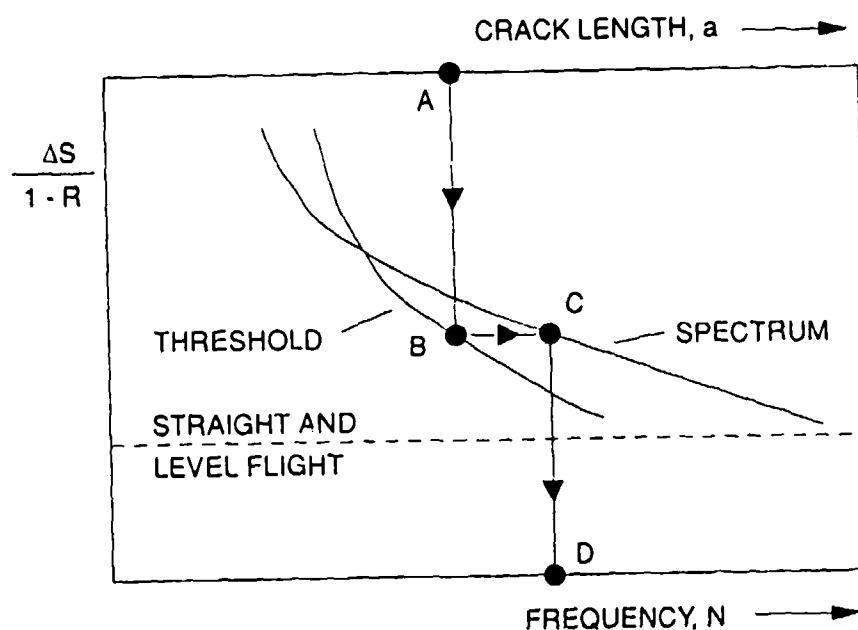


Figure 4-75. Truncation frequency estimation.

The foregoing estimation procedure does not account for load interaction effects. Therefore, the actual truncation point selected should be at a higher frequency (lower excursion Δ_n). The graphical procedure can be used to make quick estimates of truncation points as a function of crack length. For example, one might want to estimate points corresponding to the initial, critical, and one intermediate crack length for any given damage tolerance evaluation case.

REFERENCES FOR CHAPTER 4

- 4-1. Swift T., Damage Tolerance Technology, A Course in Stress Analysis Oriented Fracture Mechanics, Phase I & II, Federal Aviation Administration.
- 4-2. Timoshenko, S. and Woinowski-Krieger S., Theory of Plates and Shells, McGraw-Hill, New York, 1959.
- 4-3. Tong, P., Greif, R., and Chen, L., "Application of Hybrid Finite Element Method to Aircraft Repairs," XXII National Congress on Fracture Mechanics, Atlanta, GA, June 1990.
- 4-4. Swift, T., "Repair to Damage Tolerant Aircraft," Structural Integrity of Aging Airplanes, Springer Verlag, 433, 1991.
- 4-5. Brophy, J.H., Rose, R.M., and Wulff, J., The Structure and Properties of Materials Volume II, Thermodynamics of Structure, Wiley, New York, 1964.
- 4-6. Hagemaiier, D.J., Douglas Aircraft Company, Long Beach, CA, presentation to FAA Inspection Authorized Meeting, San Jose, CA, March 1990.
- 4-7. Airman's Information Manual, paragraph 347j (2) and (6) (b).
- 4-8. Crabill, N.L., The NASA Digital VGH Program - Exploration of Methods and Final Results: Vol. I - Development of Methods/Vol II - L 1011 Data 1978-1979: 1619 Hours/Vol. III - B 727 Data 1978-1980: 1765 Hours/Vol. IV - B 747 Data 1978-1980: 1689 Hours/Vol. V - DC 10 Data 1981-1982: 129 Hours, Eagle Engineering, Inc., Hampton, VA, DOT/FAA-CT-89/36-I, December 1989.
- 4-9. Swift, T., "Design of Redundant Structures," published in Fracture Mechanics Design Methodology, AGARD-LS-97, 1979.
- 4-10. Isida, M., "Data on Crack Tip Stress Intensity Factors," Journal of the Japan Society of Mechanical Engineers, Vol. 75, No. 642 (1972), pp. 1127-1135.
- 4-11. Pu, S.L., Hussain, M.A., and Lorensen, W.E., "The Collapsed Cubic Isoparametric Element as a Singular Element for Crack Problems," International Journal for Numerical Methods in Engineering 12, 1727-1742 1978.
- 4-12. Tong, P., Pian, T., H.H., and Lasry, S.J., "A Hybrid Element Approach to Crack Problems in Plane Elasticity," International Journal for Numerical Methods in Engineering 7, 297-308, 1973.

- 4-13. Tong, P., Arin, K., Jeong, D., Greif, R., Brewer, J., Bobo, S., and Sampath S., "Current DOT Research on the Effect of Multiple Site Damage on Structural Integrity," Proceedings of the 1991 International Conference on Aging Aircraft and Structural Airworthiness, Washington, DC, November 19-21, 1991.

APPENDIX A:

SELECTED

STRESS INTENSITY FACTOR

FORMULAE

[Pages A-1 — A-6 reprinted from J.P. Gallagher, F.J. Giessler, and A.P. Berens, USAF Damage Tolerant Design Handbook: Guidelines for the Analysis and Design of Damage Tolerant Aircraft Structures, Flight Dynamics Laboratory, Air Force Wright Aeronautical Laboratories, Wright-Patterson Air Force Base OH, AFWAL-TR 82-3073, May 1984. (for the references indicated, please see original document)]

Pages A-7 — A-13 reprinted from Y. Murakami (ed.) Stress Intensity Factors Handbook, pp. 187, 188, 194, 210, 291, 909, 910, 916, 917, 931, and 933, 1e, ©1987, by permission of Pergamon Press Ltd., Headington Hill Hall, Oxford OX3 OBW, U.K.

Pages A-14 — A-15 reprinted by permission from G. C. Sih, Handbook of Stress Intensity Factors Handbook, Lehigh University, Bethlehem, PA, 1973]

(Section, table and figure numbers are from the references indicated)

1.7 SELECTED STRESS-INTENSITY FACTOR CASES

This section will present a catalog of stress-intensity factor solutions for relatively simple crack geometries in plates. The remote loading solutions are typically presented in the form

$$K = \delta \sqrt{a} \quad (1.7.1)$$

where the coefficient δ is expressed as a function of geometry. Other solution forms also include

$$K = \frac{P}{BW} f(a) \quad (1.7.2)$$

for wedge force loading. Some of the cases considered can be used to develop more complex solutions through the methods of superposition and compounding. Many of the solutions are directly useful for obtaining approximate solutions to isolate local effects.

1.7.1 Through-Thickness-Internally Cracked Type Geometries

Table 1.7.1 presents a series of twelve solutions which are primarily of the center cracked geometry configuration. The table first presents the remotely loaded cases and then the wedge and point loaded cases. Each geometry and loading condition in Table 1.7.1 is graphically defined and given a case number, e.g. Case 1.7.1.10 is the case where the point loading is applied off the crack face along the perpendicular bisector of the crack.

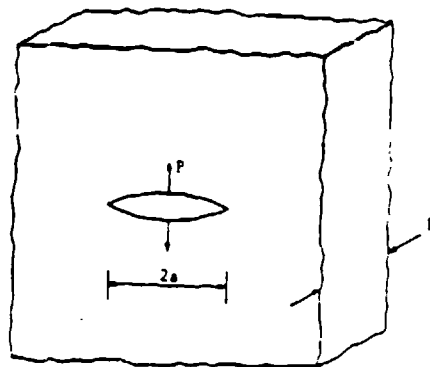
TABLE 1.7.1 (Continued)

CASE NO.

WEDGE LOADED CENTER
CRACKED GEOMETRIES

STRESS-INTENSITY FACTOR

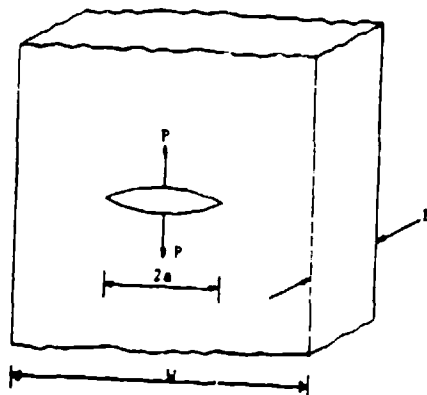
1.7.1.4



INFINITE WIDTH-LOAD AT
CENTER OF CRACK

$$K = \frac{(P/B)}{\sqrt{\pi a}}$$

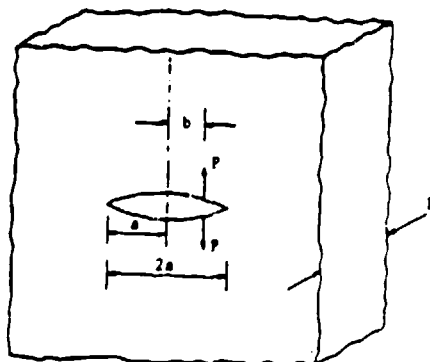
1.7.1.5



FINITE WIDTH-LOAD AT
CENTER OF CRACK

$$K = \frac{(P/B)}{\sqrt{\pi a}} \sqrt{\frac{1}{\frac{W}{2\pi a} \sin \frac{2\pi a}{W}}}$$

1.7.1.6



INFINITE WIDTH-LOAD OFFSET
FROM CRACK CENTER

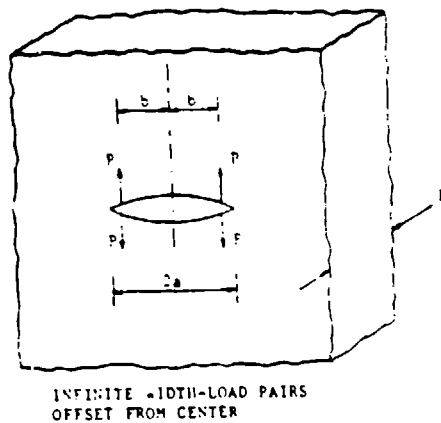
$$K = \frac{(P/B)}{\sqrt{\pi a}} \sqrt{\frac{a+b}{a-b}}$$

1.7.3

TABLE 1.7.1 (Continued)

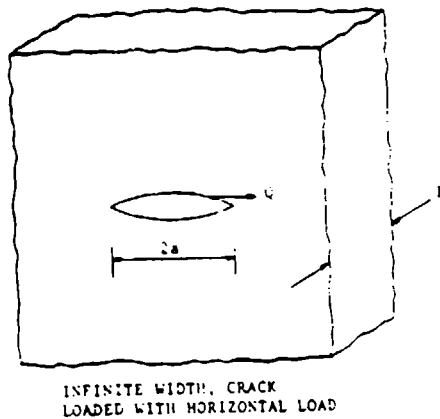
CASE NO. WEDGE AND POINT LOADED
CENTER CRACKED GEOMETRIES STRESS-INTENSITY FACTOR

1.7.1.7



$$K = 2(P/B) \frac{a}{b} \cdot \frac{1}{\sqrt{a^2 - b^2}}$$

1.7.1.8



$$K = \frac{Q}{2\sqrt{\pi a}} \left(\frac{\kappa - 1}{\kappa + 1} \right)$$

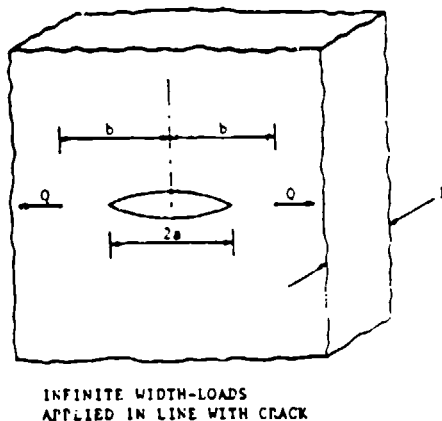
Where

$\kappa = 3 - 4\nu$ Plane Strain

$$\kappa = \frac{3 - \nu}{1 + \nu}$$

and ν = Poisson's ratio
Reference 55

1.7.1.9



$$K \begin{cases} = 0 & \text{if } b < a \\ \text{or} \\ = \frac{-Q(\kappa - 1)\sqrt{a}}{\sqrt{\pi}(\kappa + 1)\sqrt{b^2 - a^2}} \end{cases}$$

κ defined for case 1.7.1.8
Reference 55

1.7.4

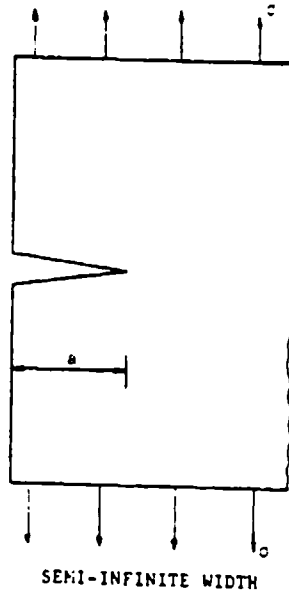
TABLE 1.7.2
STRESS-INTENSITY FACTORS FOR CRACKS STARTING
AT THE EDGE OF A STRUCTURE

CASE NO.

REMOTELY LOADED AND
EDGE CRACKED GEOMETRIES

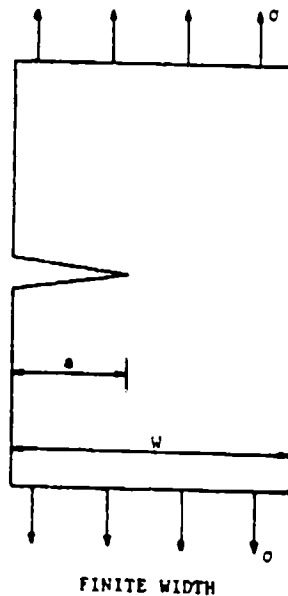
STRESS-INTENSITY FACTOR

1.7.2.1



$$K = 1.12 \sigma \sqrt{\pi a}$$

1.7.2.2



$$K = \sigma B \sqrt{\pi a}$$

$$B = 1.12 - 0.23 \left(\frac{a}{W}\right) + 10.6 \left(\frac{a}{W}\right)^2$$

$$- 21.7 \left(\frac{a}{W}\right)^3 + 30.4 \left(\frac{a}{W}\right)^4$$

$$\frac{a}{W} \leq 0.6$$

Reference 58

1.7.7

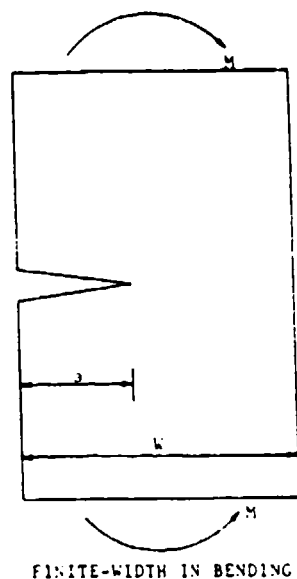
TABLE 1.7.2 (Continued)

CASE NO.

EDGE CRACKED GEOMETRY
AND LOADING

STRESS-INTENSITY FACTOR

1.7.2.3



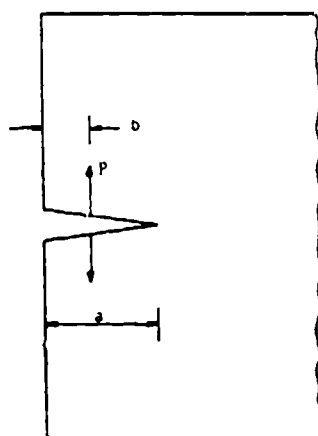
$$K = \frac{6(M/B) \sqrt{a}}{W^2} \cdot E$$

$$E = 1.12 - 1.39 \left(\frac{a}{W}\right) + 7.32 \left(\frac{a}{W}\right)^2 \\ - 13.1 \left(\frac{a}{W}\right)^3 + 14.0 \left(\frac{a}{W}\right)^4;$$

$$\frac{a}{W} \leq 0.6$$

Reference 58

1.7.2.4



POINT LOADING ON EDGE CRACK
IN SEMI-INFINITE PLATE

$$K = \frac{2}{\pi} \frac{1 + F\left(\frac{b}{a}\right)}{\sqrt{a^2 - b^2}} \cdot \frac{P \sqrt{a}}{B}$$

$$F\left(\frac{b}{a}\right) = \left(1 - \left(\frac{b}{a}\right)^2\right) \left[0.2945 - 0.3912 \left(\frac{b}{a}\right)^2 \right. \\ \left. + 0.7685 \left(\frac{b}{a}\right)^4 - 0.9942 \left(\frac{b}{a}\right)^6 \right. \\ \left. + 0.5094 \left(\frac{b}{a}\right)^8 \right]$$

References 59, 16

$$K = \frac{P}{B} \cdot \sqrt{\frac{2}{\pi(a-b)}} \cdot \left[1 + 0.6147 \left(1 - \frac{b}{a}\right) \right. \\ \left. + 0.2502 \left(1 - \frac{b}{a}\right)^2 \right]$$

Reference 20

1.7.8

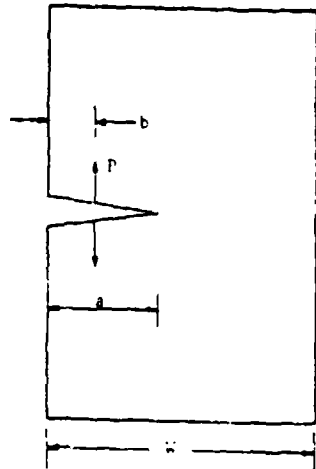
TABLE 1.7.2 (Concluded)

CASE NO.

EDGE CRACKED GEOMETRY
AND LOADING

STRESS-INTENSITY FACTOR

1.7.2.5



POINT LOADING ON EDGE CRACK
IN FINITE WIDTH PLATE

$$K = \frac{P}{B} \cdot \sqrt{\frac{2}{\pi(a-b)}} \left[1 + m_1 \left(1 - \frac{b}{a} \right) + m_2 \left(1 - \frac{b}{a} \right)^2 \right]$$

Where $a < 0.5w$ and

$$m_1 = 0.6147 + 17.1844 \left(\frac{a}{w} \right)^2 + 8.7822 \left(\frac{a}{w} \right)^6$$

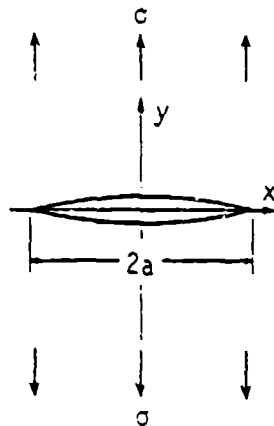
$$m_2 = 0.2502 + 3.2899 \left(\frac{a}{w} \right)^2 + 70.0444 \left(\frac{a}{w} \right)^6$$

Reference 43

1.7.9

SINGLE CRACK SUBJECTED TO TENSION

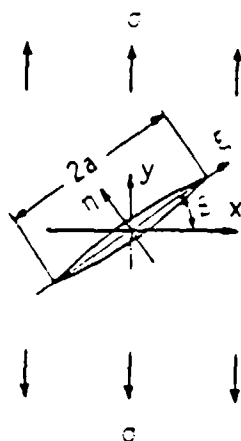
[Source: Ref. A-1]



$$K_I = \sigma \sqrt{\pi a}$$

A SINGLE CRACK INCLINED TO TENSILE AXIS

[Source: Ref. A-1]

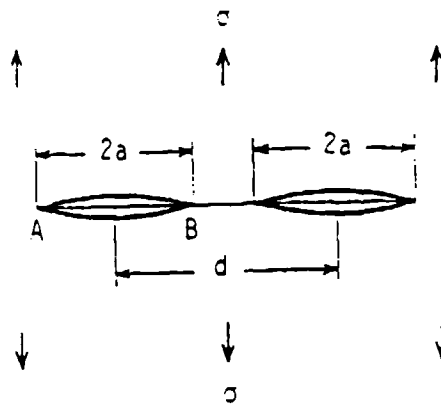


$$K_I = \sigma \sqrt{\pi a} \cos^2 \theta$$

$$K_{II} = \sigma \sqrt{\pi a} \sin \theta \cos \theta$$

TWO COLLINEAR CRACKS WITH THE SAME LENGTH

[Source: Ref. A-2]



$$K_I = F_{I,0} \sqrt{\pi a}$$

$$F_{I,A} = \frac{d+2a}{d} \left(\frac{d+2a}{d} \right)^{\frac{1}{2}} \left[1 - \frac{E(k)}{K(k)} \right]$$

$$F_{I,B} = \frac{d-2a}{d} \left(\frac{d-2a}{d} \right)^{\frac{1}{2}} \left[\left(\frac{d+2a}{d-2a} \right)^2 \frac{E(k)}{K(k)} - 1 \right]$$

$$k = \left[1 - \left(\frac{d-2a}{d+2a} \right)^2 \right]^{\frac{1}{2}}$$

$$K(k) = \int_0^{\frac{\pi}{2}} (1 - k^2 \sin^2 \theta)^{-\frac{1}{2}} d\theta, \quad E(k) = \int_0^{\frac{\pi}{2}} (1 - k^2 \sin^2 \theta)^{\frac{1}{2}} d\theta$$

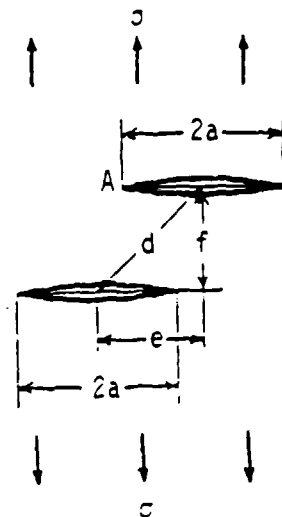
$$F_{I,A} = (1 - 0.0037 \lambda + 0.1613 \lambda^2 - 0.1628 \lambda^3 + 0.1560 \lambda^4)$$

$$F_{I,B} = (1 - 0.0426 \lambda + 0.5461 \lambda^2 - 1.1654 \lambda^3 + 1.2368 \lambda^4)$$

$$\lambda = 2a/d, \quad 0 \leq \lambda \leq 0.8$$

TWO PARALLEL CRACKS NOT ALIGNED TO TENSILE STRESS

[Source: Ref. A-3]



$$K_{I,A} = F_{I,A} \sigma \sqrt{\pi a}$$

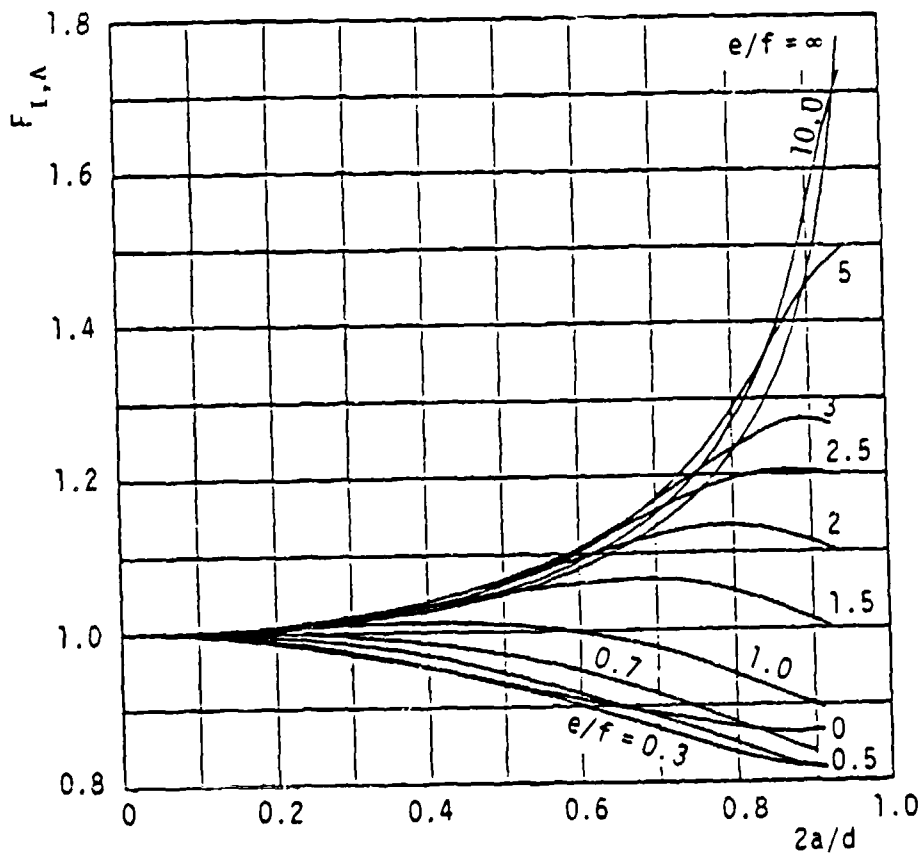
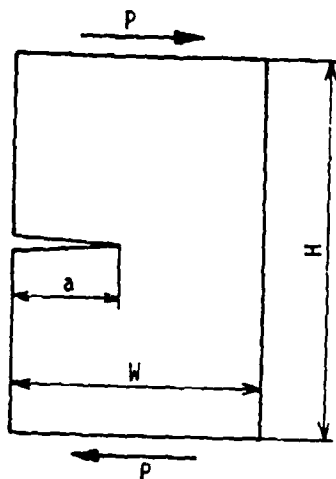


Fig. $F_{I,A}$ versus $2a/d$

SINGLE EDGE CRACKED RECTANGULAR PLATE SUBJECTED TO SHEAR LOADING

[Source: Ref. A-4]



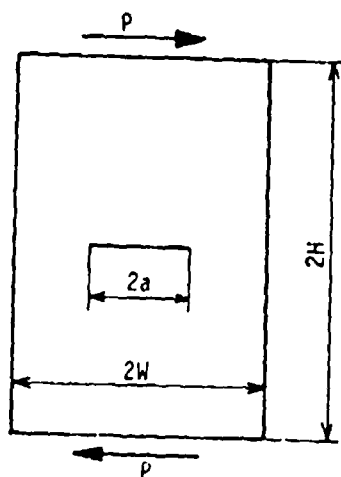
$$H/W = 2.8$$

$$K_{II} = F_{II}(\alpha) \tau_o \sqrt{\pi a}, \quad \tau_o = \frac{P}{Wt}, \quad \alpha = \frac{a}{W}$$

$$F_{II}(\alpha) = 4.886\alpha - 11.383\alpha^2 + 28.198\alpha^3 - 38.563\alpha^4 + 20.555\alpha^5$$

CENTER CRACKED RECTANGULAR PLATE SUBJECTED TO SHEAR LOADING

[Source: Ref. A-4]



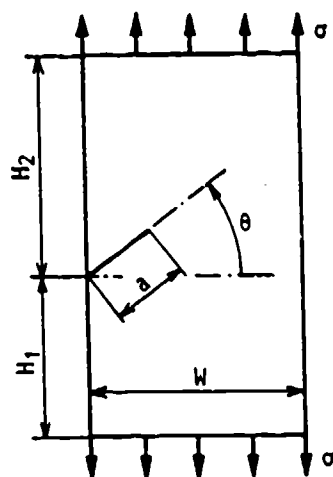
$$H/W = 2.8$$

$$K_{II} = F_{II}(\alpha) \tau_o \sqrt{\pi a}, \quad \tau_o = \frac{P}{2Wt}, \quad \alpha = \frac{a}{W}$$

$$F_{II}(\alpha) = 1.50 + 0.569\alpha - 6.282\alpha^2 + 25.01\alpha^3 - 38.157\alpha^4 + 21.013\alpha^5$$

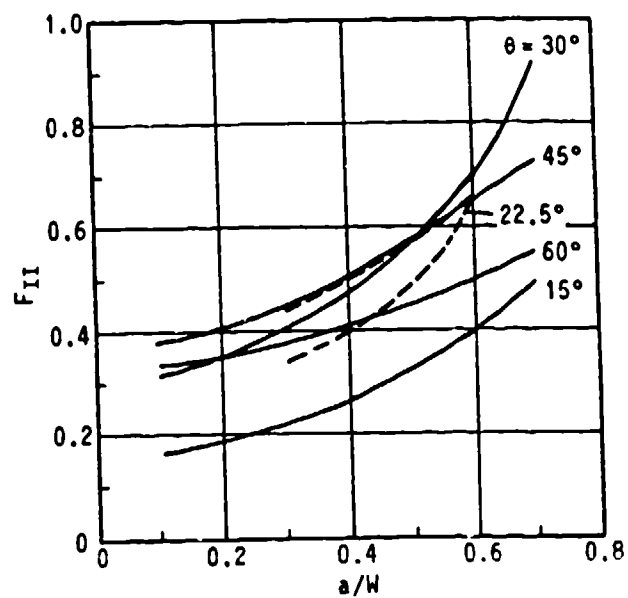
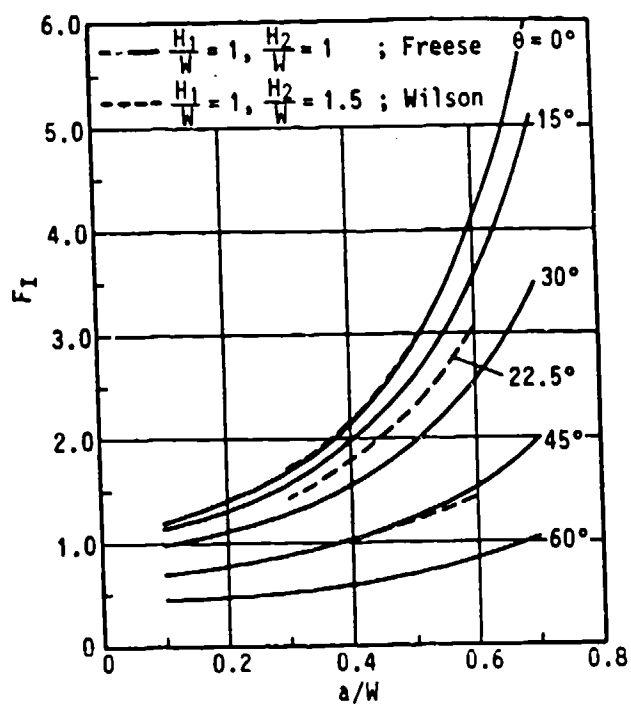
EDGE SLANT CRACKED RECTANGULAR PLATE SUBJECTED TO UNIFORM UNIAXIAL TENSILE STRESS

[Source: Ref. A-5, A-6]

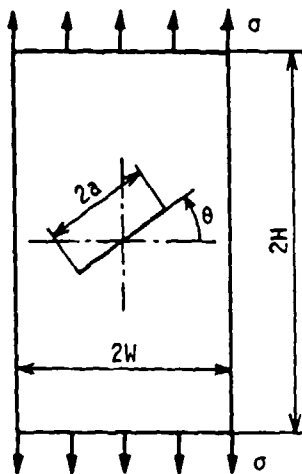


$$K_I = F_I \sigma \sqrt{\pi a}$$

$$K_{II} = F_{II} \sigma \sqrt{\pi a}$$



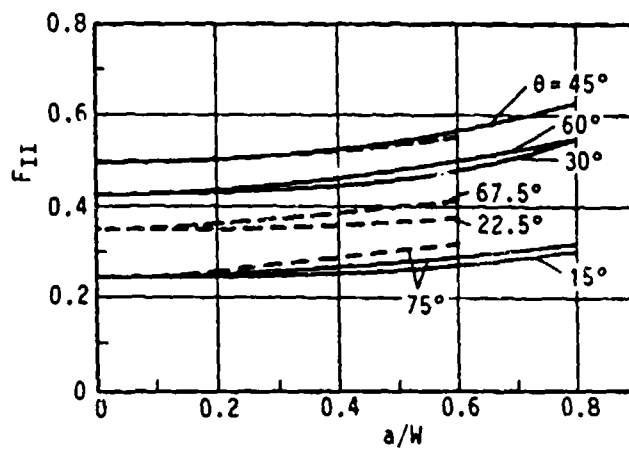
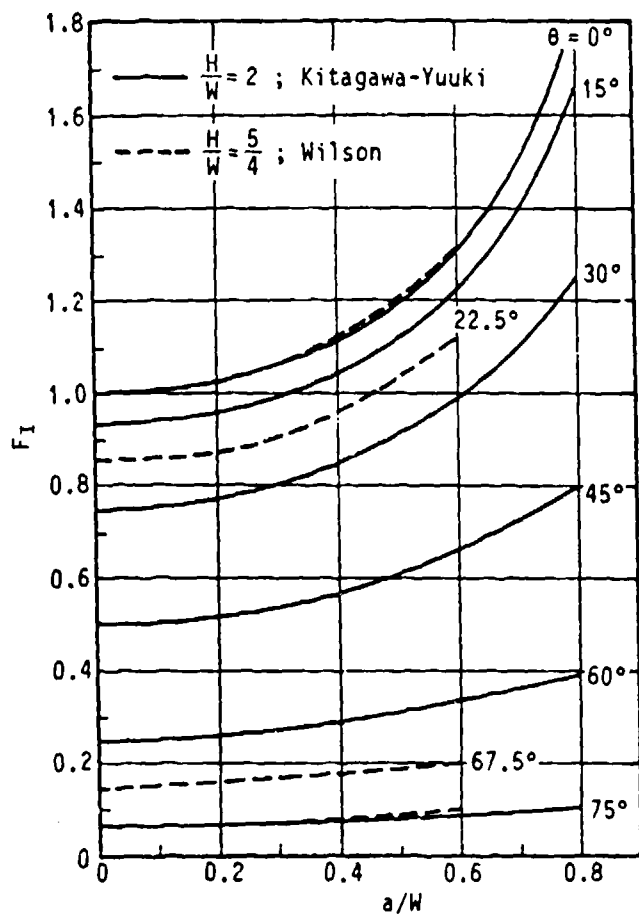
CENTER SLANT CRACKED RECTANGULAR PLATE SUBJECTED TO UNIFORM UNIAXIAL TENSILE STRESS



[Source: Ref. A-7, A-8]

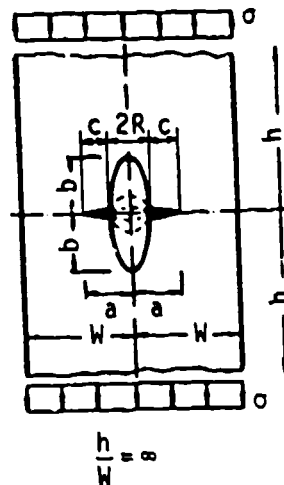
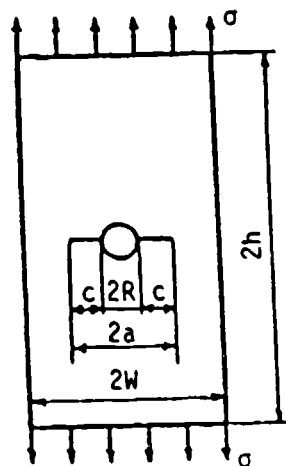
$$K_I = F_I \sigma \sqrt{\pi a}$$

$$K_{II} = F_{II} \sigma \sqrt{\pi a}$$



CRACKS EMANATING FROM A HOLE IN A RECTANGULAR PLATE UNDER TENSION

[Source: Ref. A-9, A-10, A-11]



$$K = F \cdot \sigma \sqrt{\pi a}$$

$$F = \varphi \cdot \psi \quad \alpha = \frac{a}{W}, \quad \bar{\alpha} = \frac{\pi}{2} \alpha, \quad \delta = \frac{b}{R}, \quad \gamma = \frac{R}{W}, \quad \beta = \frac{\alpha - \gamma}{1 - \gamma}$$

$$\varphi = \frac{\pi \left[\sqrt{\frac{1}{\bar{\alpha}} (\tan \bar{\alpha} + g \cdot \sin 2\bar{\alpha})} \cdot \left(1 + \frac{\epsilon^2 (2 - \epsilon^2)}{1 - \epsilon} \right) \right] - \sqrt{1 + 2g}}{\pi - 1}$$

$$g = 0.13 \left(\frac{2}{\pi} \cdot \arctan \delta \right)^2$$

$$\epsilon = \alpha \cdot \frac{2}{\pi} \cdot \arctan (0.6 \sqrt[3]{\delta})$$

$$\psi = \xi \cdot (3 \cdot \beta^{2/3 P} - 2 \cdot \sqrt{\xi} \beta^P)$$

$$P = \log (\xi^{-3/2}) / \log \beta^*$$

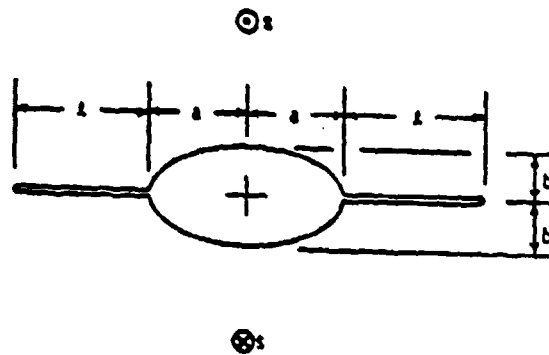
$$\beta^* = \frac{\gamma \cdot \delta}{\gamma (2\delta - 1) + 1}$$

$$\xi = 1 + \frac{2}{\pi} \cdot \arctan (1.5 \cdot \sqrt{\delta})$$

Range of	$0 \leq \delta \leq 10$	Accuracy : $\pm 5\%$
Application	$0.1 \leq \gamma \leq 0.8$	if $F \geq 1.0$
	$\gamma \leq \alpha \leq 0.95$	

Two Cracks Extending from an Elliptic Hole

[Source: Ref. A-12]



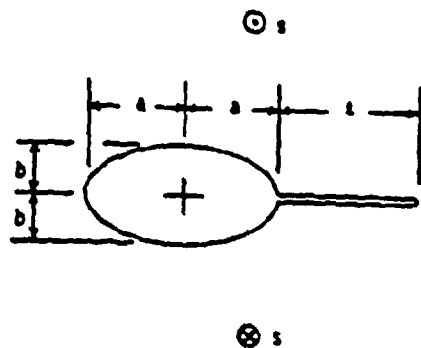
$$k_3 = s\sqrt{a+b}/\sqrt{2E} [(\xi^2-1)/(\xi^2 - \frac{a-b}{a+b})]^{1/2}$$

where (*)

$$\xi = [a + z + \sqrt{(a+z)^2 - (a^2-b^2)}]/(a+b)$$

Crack Extending from an Elliptic Hole

[Source: Ref. A-13]



$$k_3 = s\sqrt{a+b} \frac{\xi+1}{2\sqrt{E}} [(\xi^2-1)/(\xi^2 - \frac{a-b}{a+b})]^{1/2}$$

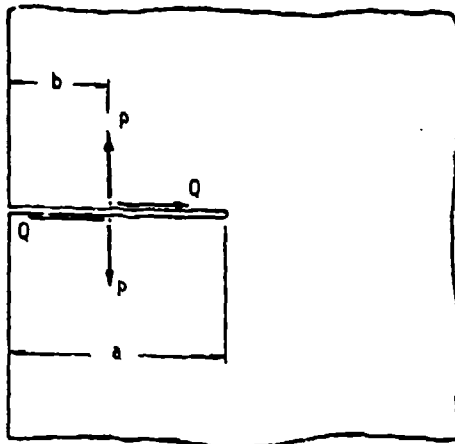
where (*)

$$\xi = [a + z + \sqrt{(a+z)^2 - (a^2-b^2)}]/(a+b)$$

(*) $K = \sqrt{\pi}k$

An Edge Crack in a Semi-Infinite Plane Subjected to Concentrated Forces

[Source: Ref. A-14]



$$k_1 = \frac{2}{\pi} \left[\frac{1+F(\frac{b}{a})}{\sqrt{a^2-b^2}} \right] P\sqrt{a}$$

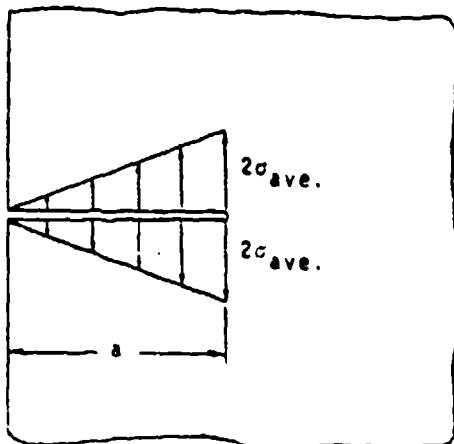
$$k_2 = \frac{2}{\pi} \left[\frac{1+F(\frac{b}{a})}{\sqrt{a^2-b^2}} \right] Q\sqrt{a}$$

where (*)

$$F\left(\frac{b}{a}\right) = \left(1 - \frac{b}{a}\right) \left[0.2945 - 0.3912\left(\frac{b}{a}\right)^2 + 0.7685\left(\frac{b}{a}\right)^3 - 0.9942\left(\frac{b}{a}\right)^4 + 0.5094\left(\frac{b}{a}\right)^5 \right]$$

An Edge Crack in a Semi-Infinite Plane Subjected to Linear Tensile Stress

[Source: Ref. A-14]



$$k_1 = 1.3660 \sigma_{ave.} \sqrt{a}$$

$$k_2 = 1.3660 \sigma_{ave.} \sqrt{a}$$

where (*)

(*) $K = \sqrt{\pi}k$

SOURCES FOR THE MATERIAL USED IN APPENDIX A, pp. A-7—A-15

- A-1. Irwin, G.R., "Analysis of Stresses and Strains Near the End of a Crack Transversing a Plate," Trans. ASME, Ser. E, J. Appl. Mech., Vol. 24, No. 3 (1957), pp. 361-364. Reprinted with permission.
- A-2. Erdogan, F., On the Stress Distribution in Plates with Collinear Cuts under Arbitrary Loads, Proc. 4th U.S. Nat. Congr. Appl. Mech., (1962), pp. 547-553. Reprinted with permission.
- A-3. Isida, M., "Analysis of Stress Intensity Factors for Plates Containing Randomly Distributed Cracks," Trans. Japan Soc. Mech. Engrs., Vol. 35, No. 277 (1969), pp. 1815-1822. Reprinted with permission.
- A-4. Ichikawa M. and Takamatsu, T., "Fracture Toughness Test for the Thin Plate under Mode II Loading," Trans. Japan Soc. Mech. Engrs., Vol. 51, No. 464 A(1985), pp. 1115-1121. Reprinted with permission.
- A-5. Bowie, O.L., Solutions of Plane Crack Problems by Mapping Technique, Mechanics of Fracture (Ed. G. C. Sih), Vol. 1 (1973), pp. 1.5.4, Noordhoff, Holland. Reprinted with permission.
- A-6. Wilson, W.K., Research Report 69-1E7-FMECH-R1, Westinghouse Research Laboratories, (Pittsburgh, 1969). Reprinted with permission.
- A-7. Kitagawa, H., and Yuuki, R., "Analysis of Arbitrarily Shaped Crack in a Finite Plate Using Conformal Mapping, 1st Report - Construction of Analysis Procedure and its Applicability," Trans. Japan Soc. Mech. Engrs., Vol. 43 No. 376 (1977), pp. 4354-4362. Reprinted with permission.
- A-8. Wilson, W.K., Numerical Method for Determining Stress Intensity Factors of an Interior Crack in a Finite Plate, Trans. ASME, Ser. D, J. Basic Engng., Vol. 93 (1971), pp. 685-690. Reprinted with permission.
- A-9. Fühling, H., "Approximation Functions for K-Factors of Cracks in Notches," Int. J. Frac., Vol. 9 (1973), pp. 328-331. Reprinted by permission of Kluwer Academic Publishers.
- A-10. Kitagawa H., and Yuuki, R., "Analysis of the Non-Linear shaped Crack in a Finite Plate by the Conformal Mapping Method," Trans. Japan Soc. Mech. Engrs., Vol. 43, No. 376 (1977), pp. 4354-4362. Reprinted with permission.
- A-11. Newman, J.C., Jr., An Improved Method of Collocation for the Stress Analysis of Cracked Plates with Various Shaped Boundaries, NASA Report TN D-6376 (1971).

- A-12. Yokobori, T. et al., (1971), Rep. Res. Inst. Strength and Fracture of Materials, Tohoku Univ., 7, 57. Reprinted with permission.
- A-13. Yokobori, T. et al., (1972), Rep. Res. Inst. Strength and Fracture of Materials, Tohoku Univ., 8, 1. Reprinted with permission.
- A-14. Hartranft, R.J. and Sih, G.C. (1973), Methods of Analysis and Solutions of Crack Problems, G.C. Sih, editor, Noordhoff, Holland. Reprinted with permission.

The following references are called out from pages A-3, A-4, A-5, and A-6. The numbering is that of J.P. Gallagher, F.J. Giessler, and A.P. Behrens, USAF Damage Tolerant Design Handbook: Guidelines for the Analysis and Design of Damage Tolerant Aircraft Structures, Flight Dynamics Laboratory, Air Force Wright Aeronautical Laboratories, Wright Patterson Air Force Base OH, AFWAL-TR82-3073, May 1984.

- 20. Parker, A.P., The Mechanics of Fracture and Fatigue, an Introduction (London: E.&F.N. Spon, Ltd., 1981). Reprinted with permission.
- 43. Bückner, H.F., "Weight Functions for the Notched Bar," Zeitschrift für Angewandte Mathematik und Mechanik, Vol. 51, (1971), pp. 97-109. Reprinted with permission.
- 55. Sih, G., Paris, P.C., and Erdogan, F., Application of Muskhelishvili's Methods to the Analysis of Crack Tip Stress-Intensity Factors for Plane Problems - Part II, Interim Report issued to Boeing Airplane Co. by Institute of Research, Lehigh University (7 January 1961). Reprinted with permission.
- 58. Brown, W.F., Jr. and Strawley, J., Plane Strain Fracture Toughness of High Strength Metallic Materials, ASTM STP 410, (Am. Society for Testing and Materials, 1966). Reprinted with permission.

APPENDIX B:

SELECTED

RESISTANCE CURVE (R-CURVE)

PLOTS

FOR AIRCRAFT MATERIALS

[Reprinted from M M. Ratwani and D.P. Wilhem, Development and Evaluation of Methods of Plane Strain Fracture Analysis, Northrop Corporation, AFFDL-TR-73-42, April, 1975]

(Figure numbers correspond to reference cited.)

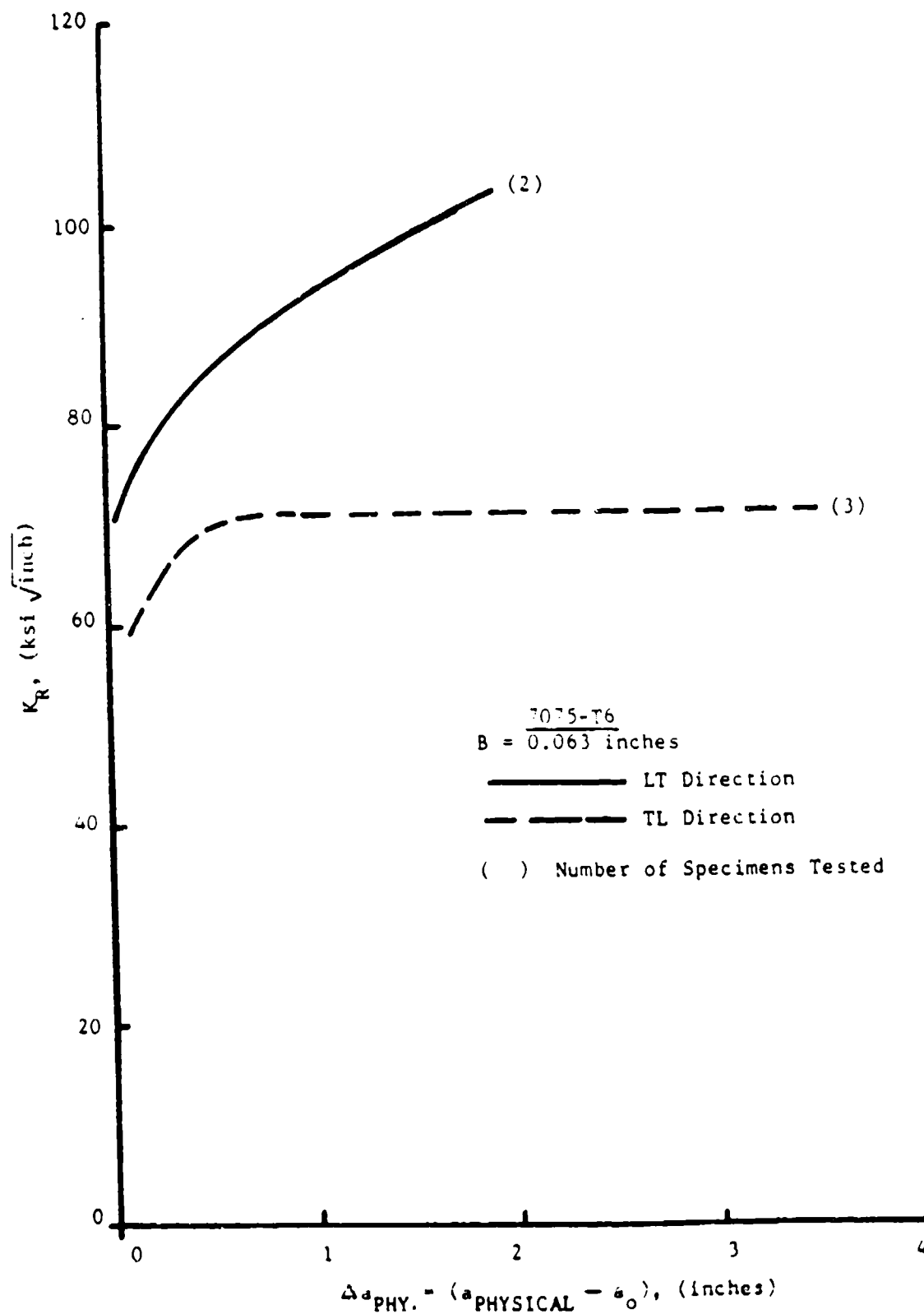


Figure 82. Average Crack Growth Resistance Curves - 0.063 Inch, 7075-T6

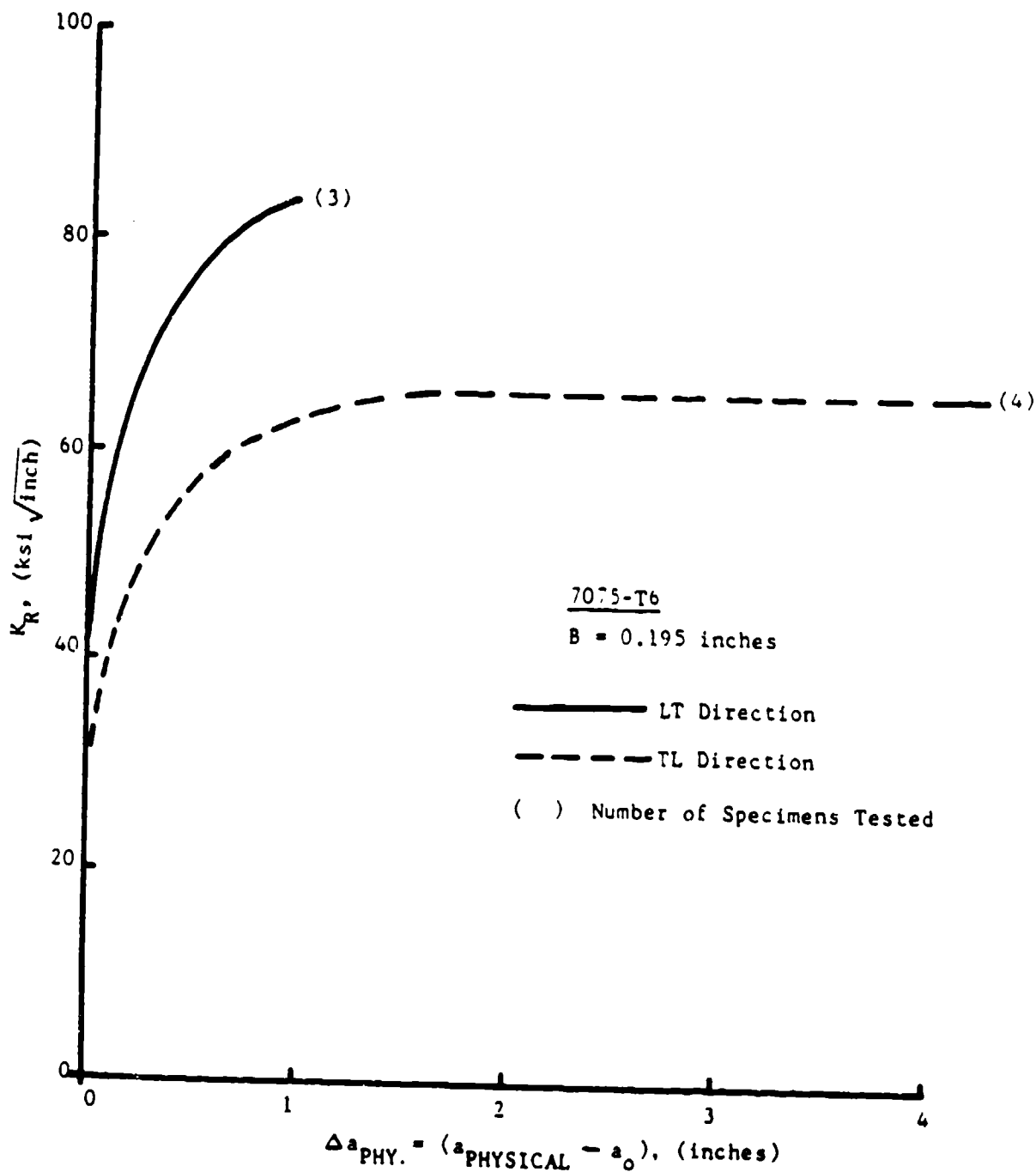


Figure 83. Average Crack Growth Resistance Curves - 0.195 Inch, 7075-T6

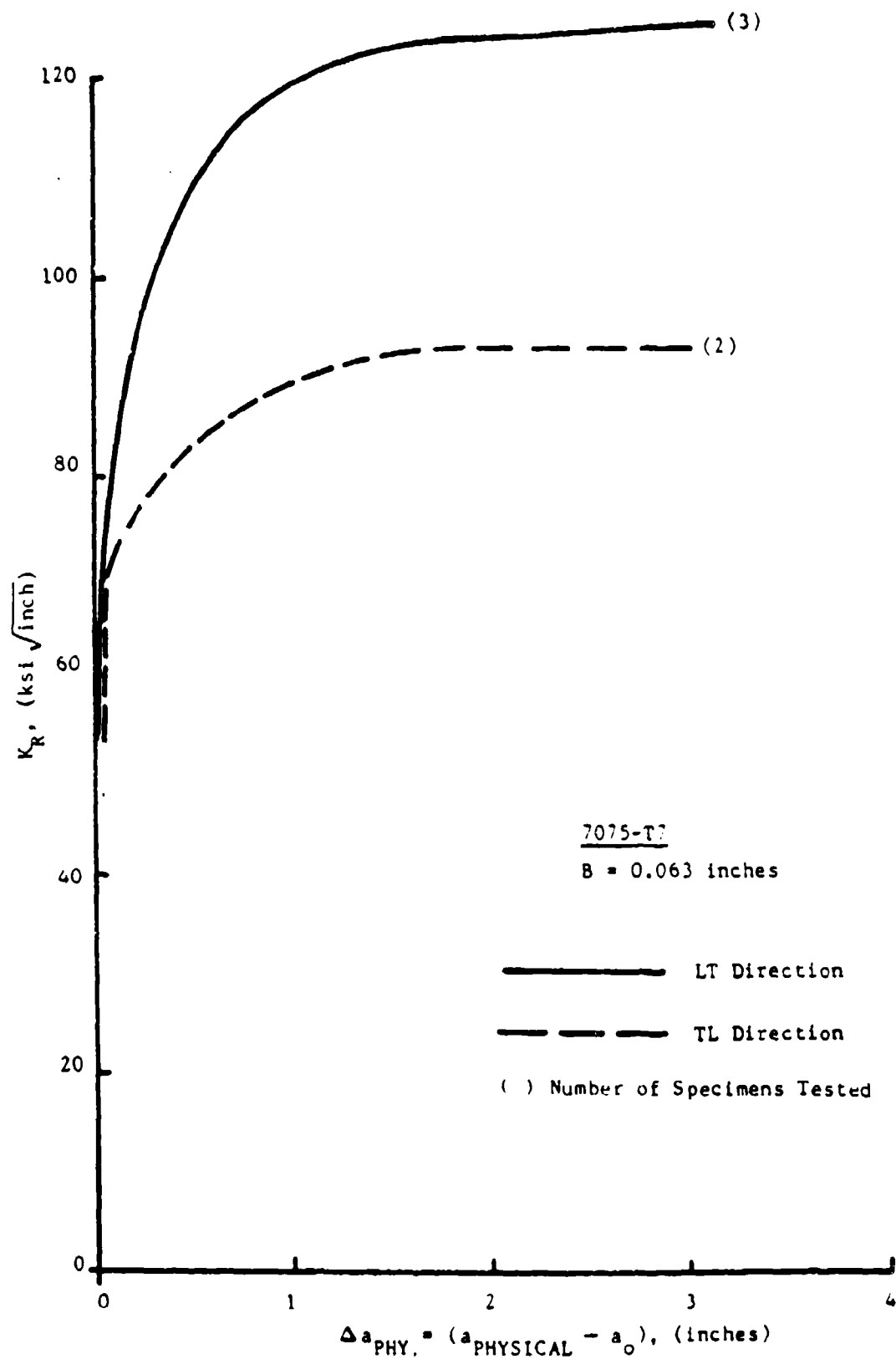


Figure 84. Average Crack Growth Resistance Curves - 0.063 Inch, 7075-T7

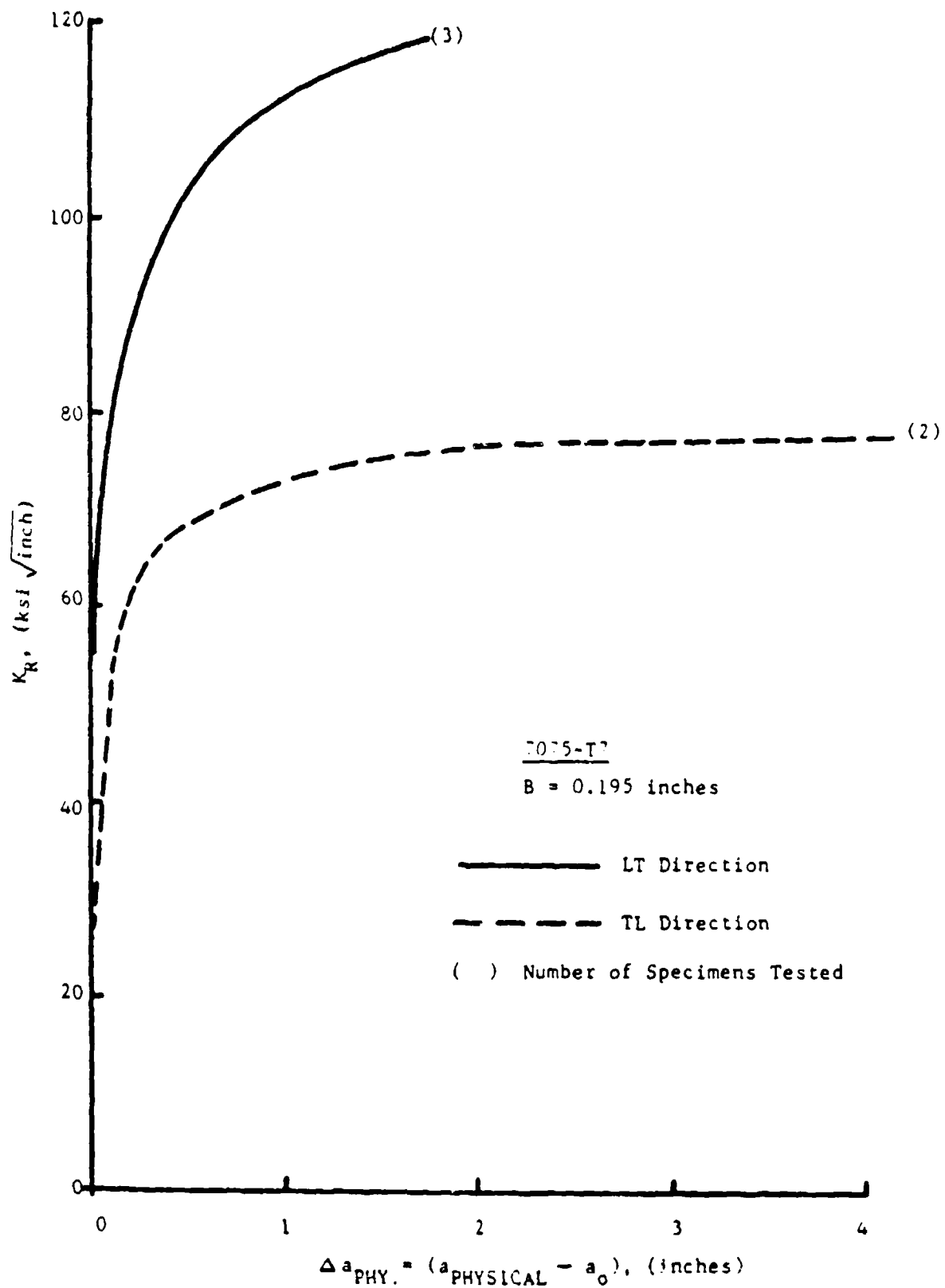


Figure 85. Average Crack Growth Resistance Curves - 0.195 Inch, 7075-T7

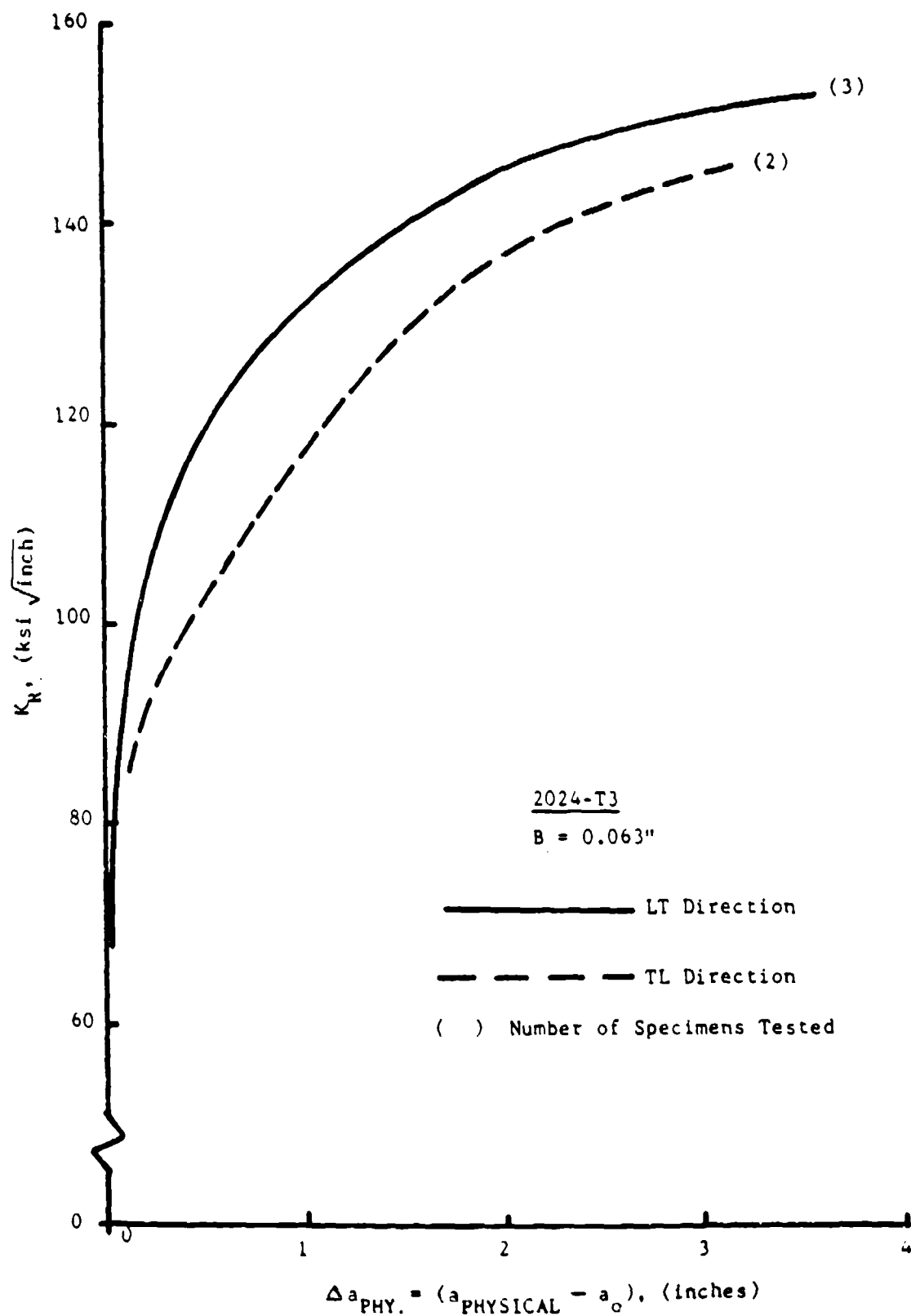


Figure 86. Average Crack Growth Resistance Curves - 0.063 Inch, 2024-T3

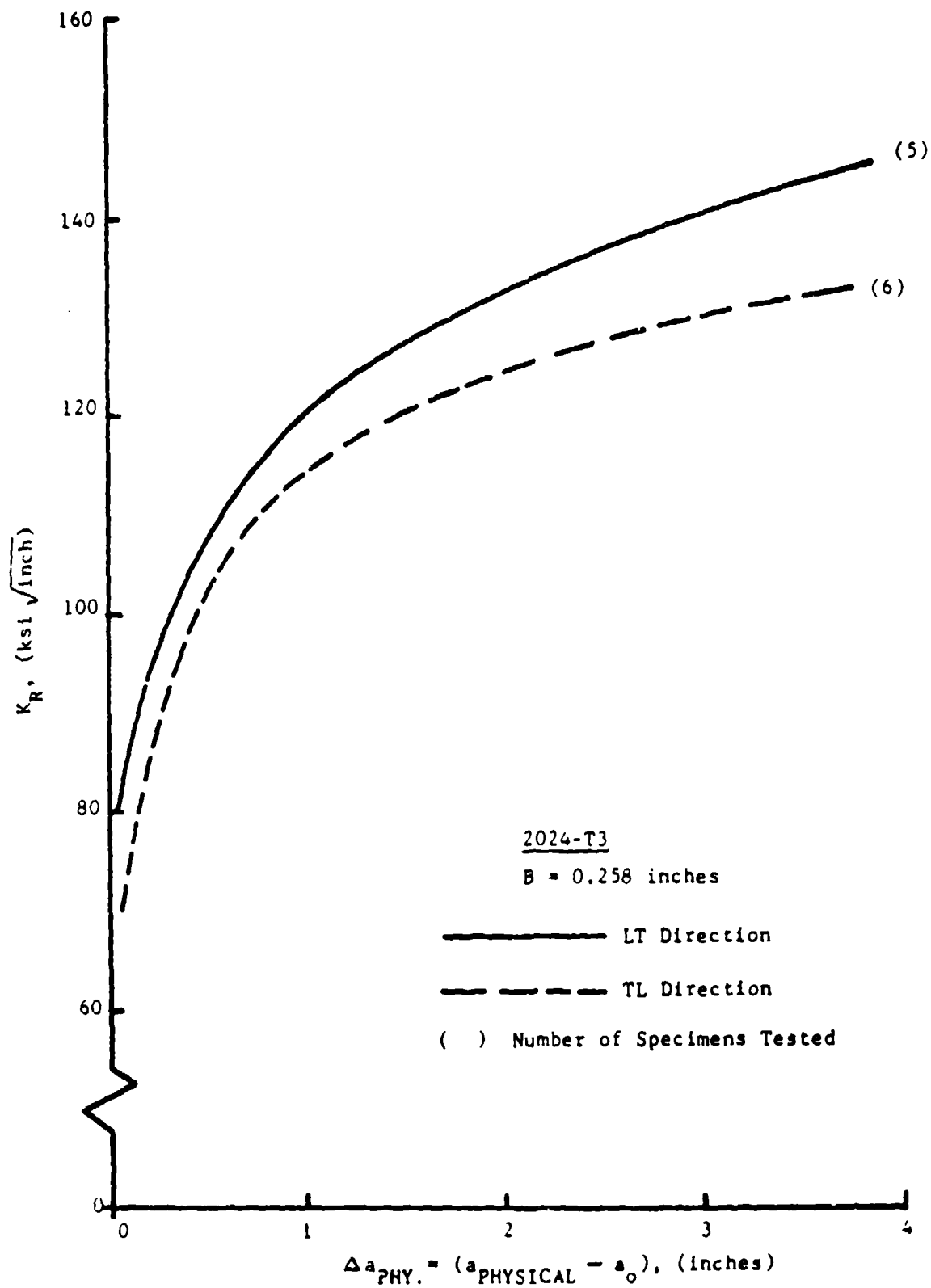


Figure 87. Average Crack Growth Resistance Curves - 0.258 Inch, 2024-T3

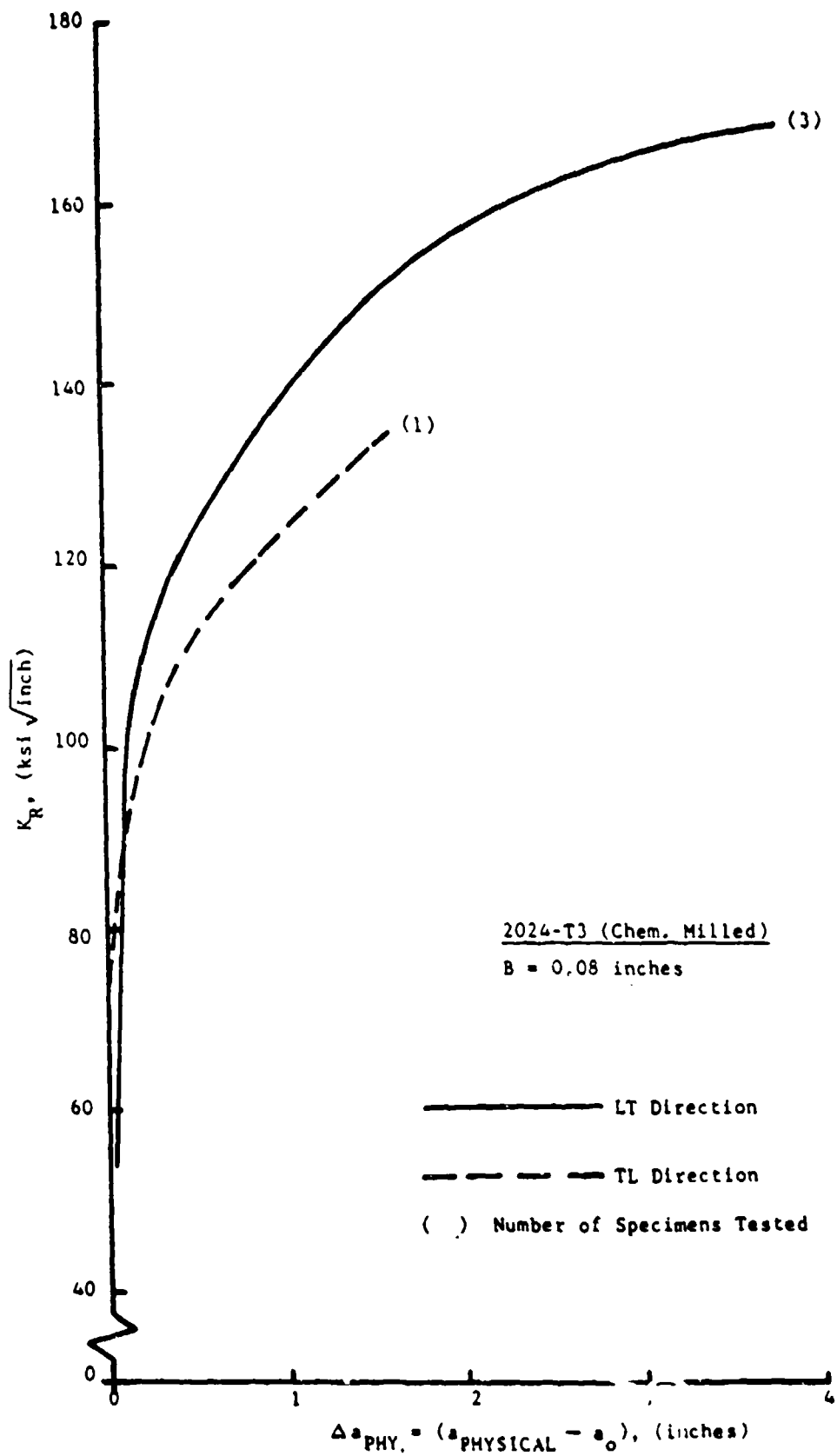


Figure 88. Average Crack Growth Resistance Curves - 0.08 Inch, Chem. Milled 2024-T3

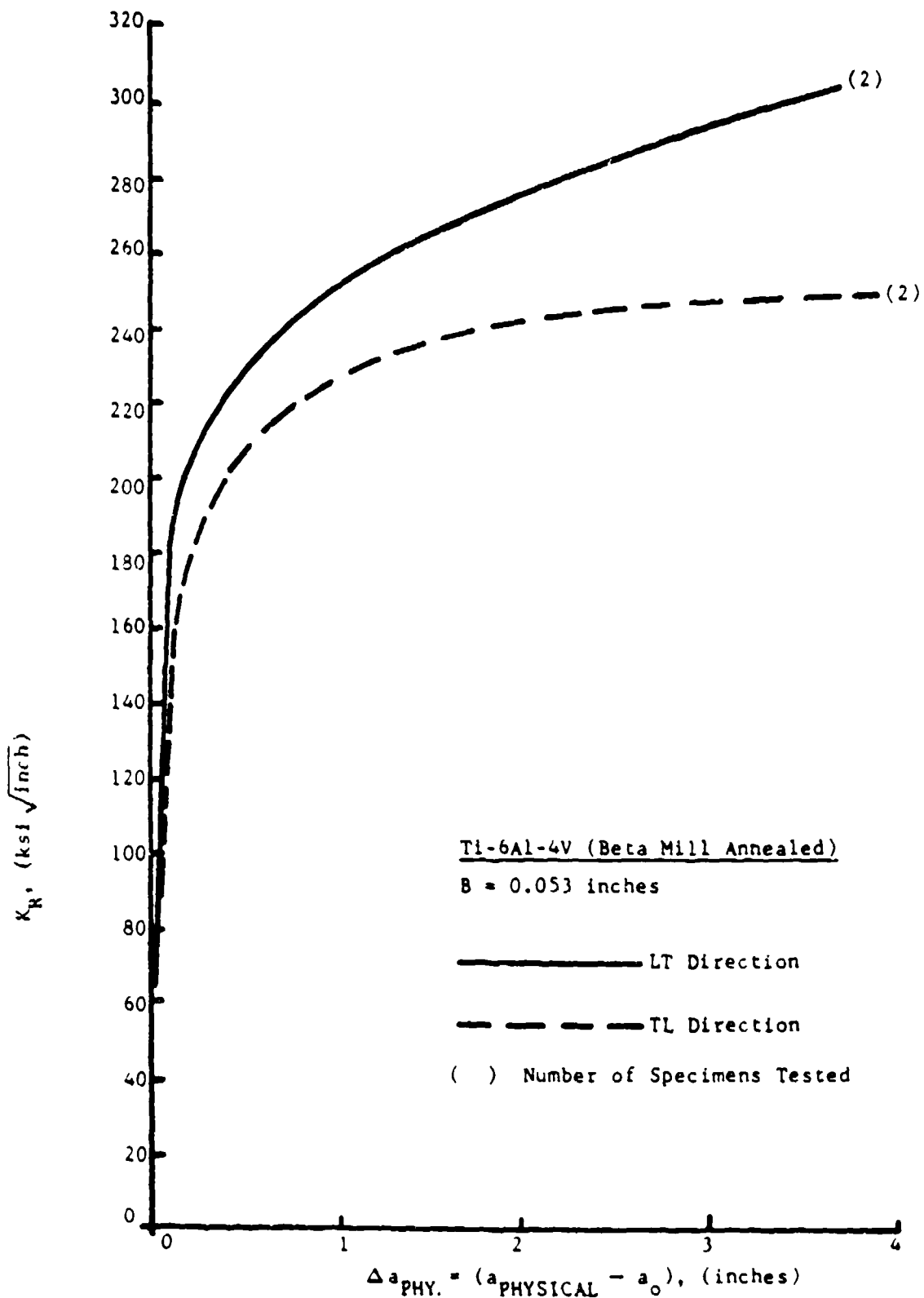


Figure 89. Average Crack Growth Resistance Curves - 0.053 Inch, Beta Mill Annealed Ti-6Al-4V

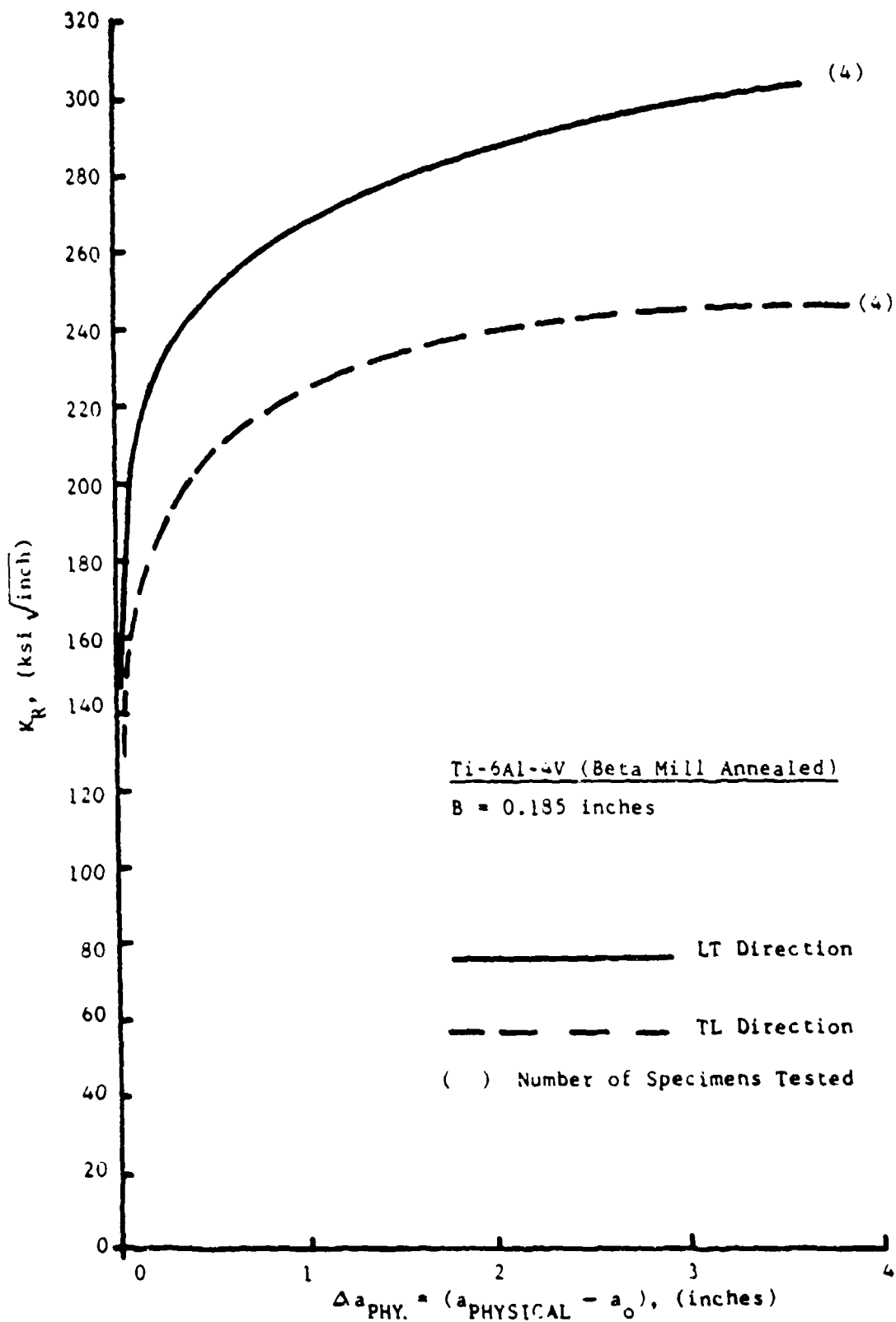


Figure 90. Average Crack Growth Resistance Curves - 0.185 Inch, Beta Mill Annealed Ti-6Al-4V

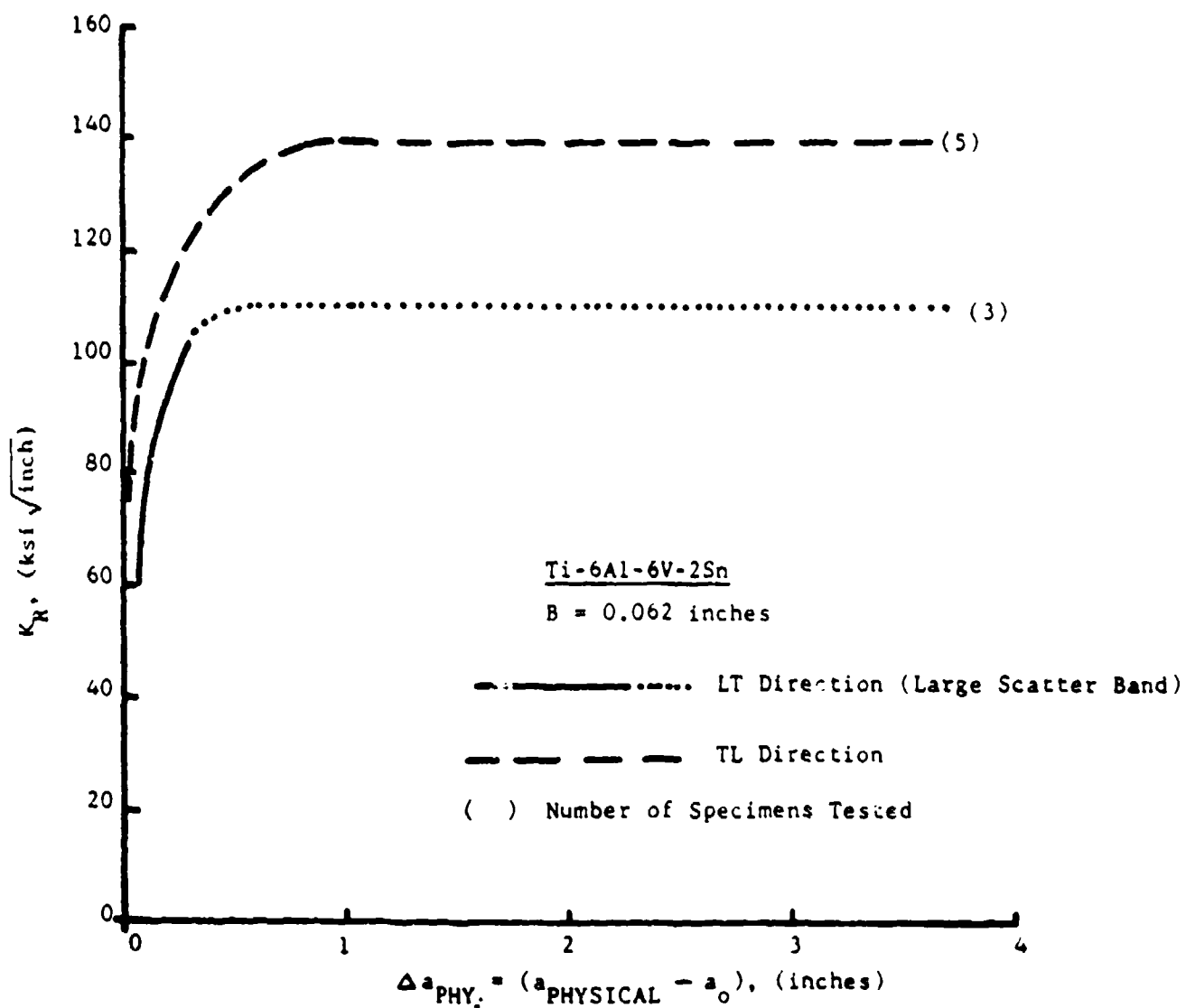


Figure 91. Average Crack Growth Resistance Curves - 0.062 Inch, Ti-6Al-6V-2Sn

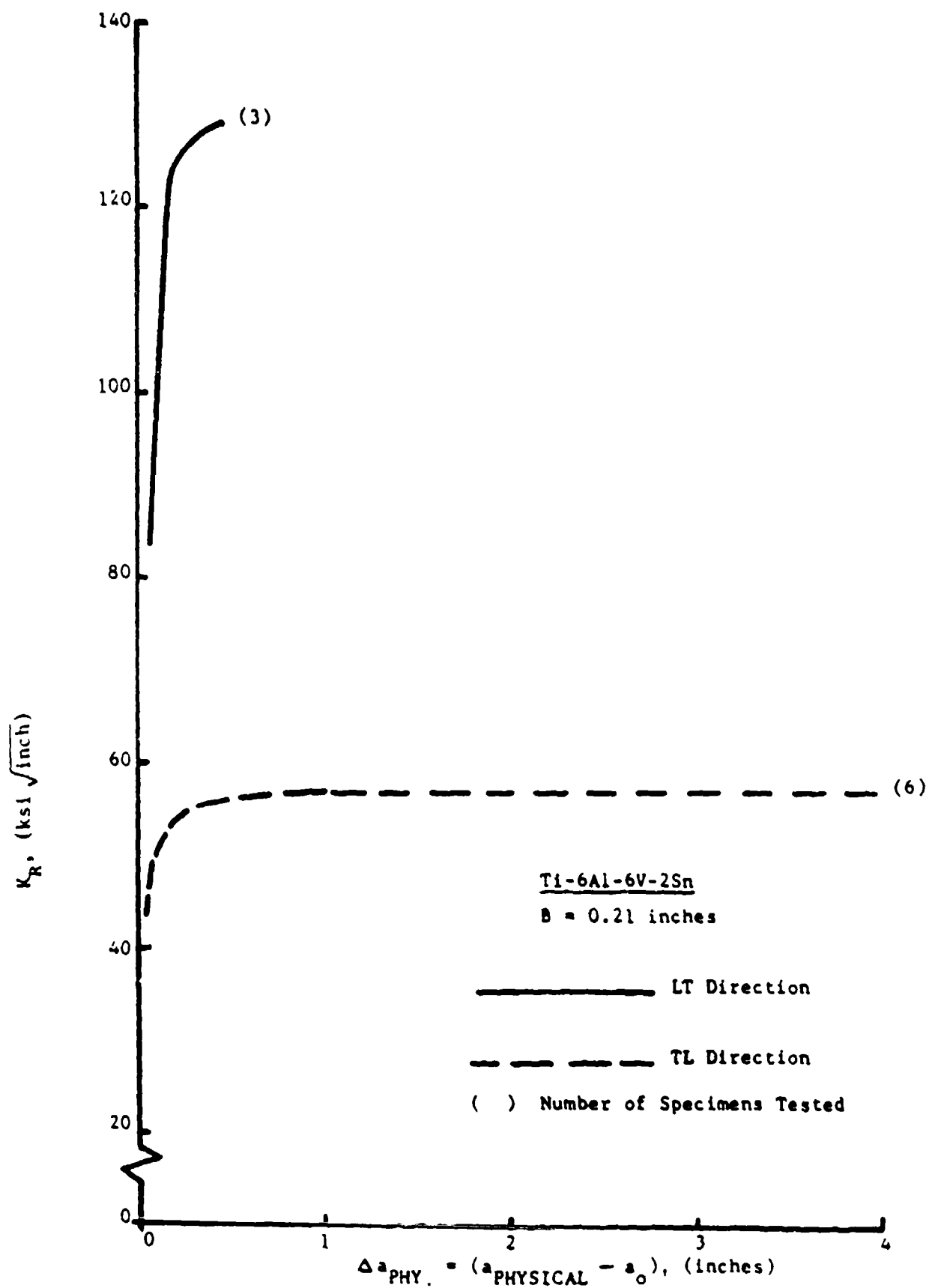


Figure 92. Average Crack Growth Resistance Curves - 0.21 Inch, Ti-6Al-6V-2Sn

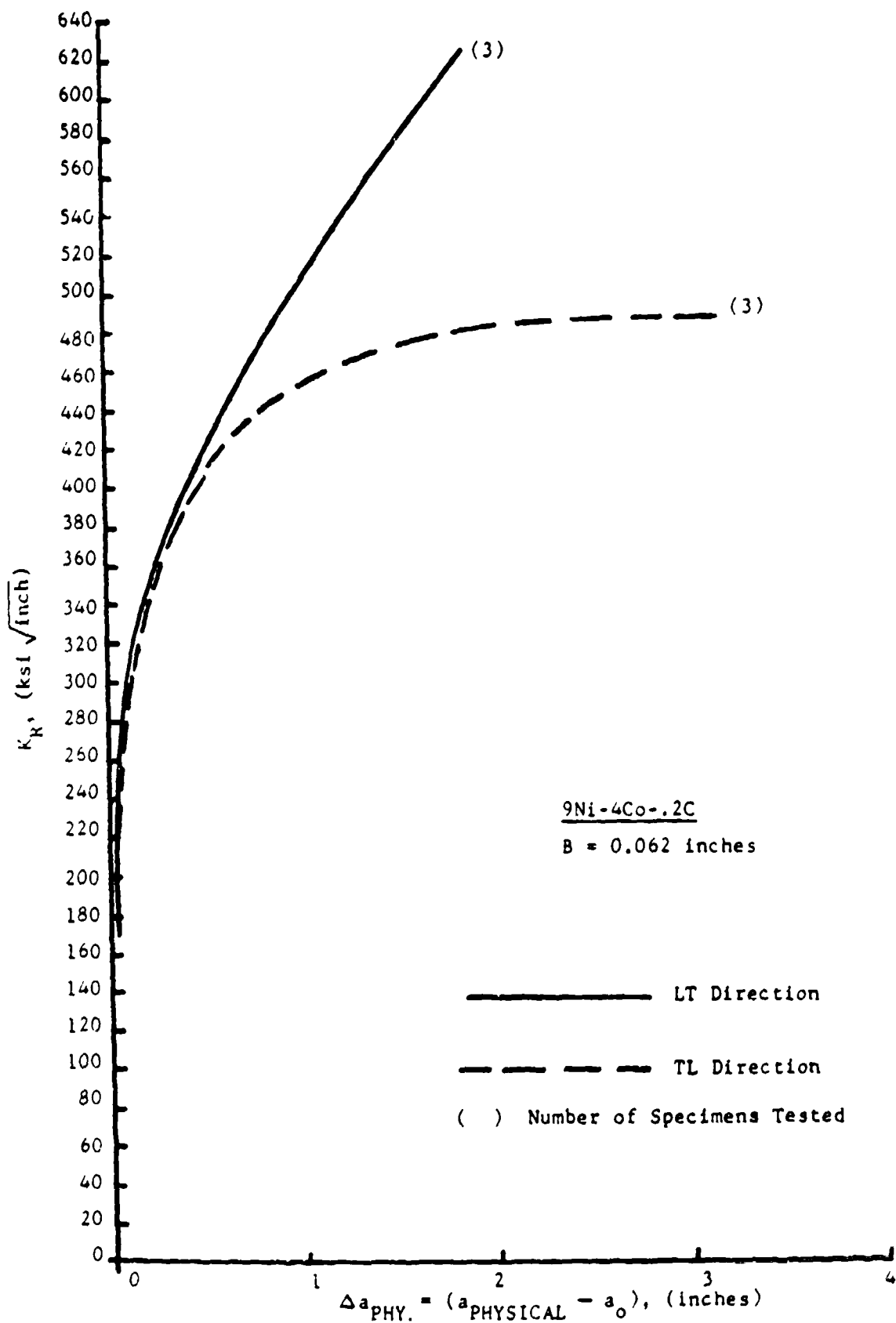


Figure 93. Average Crack Growth Resistance Curves - 0.062 Inch, 9Ni-4Co-.2C Steel

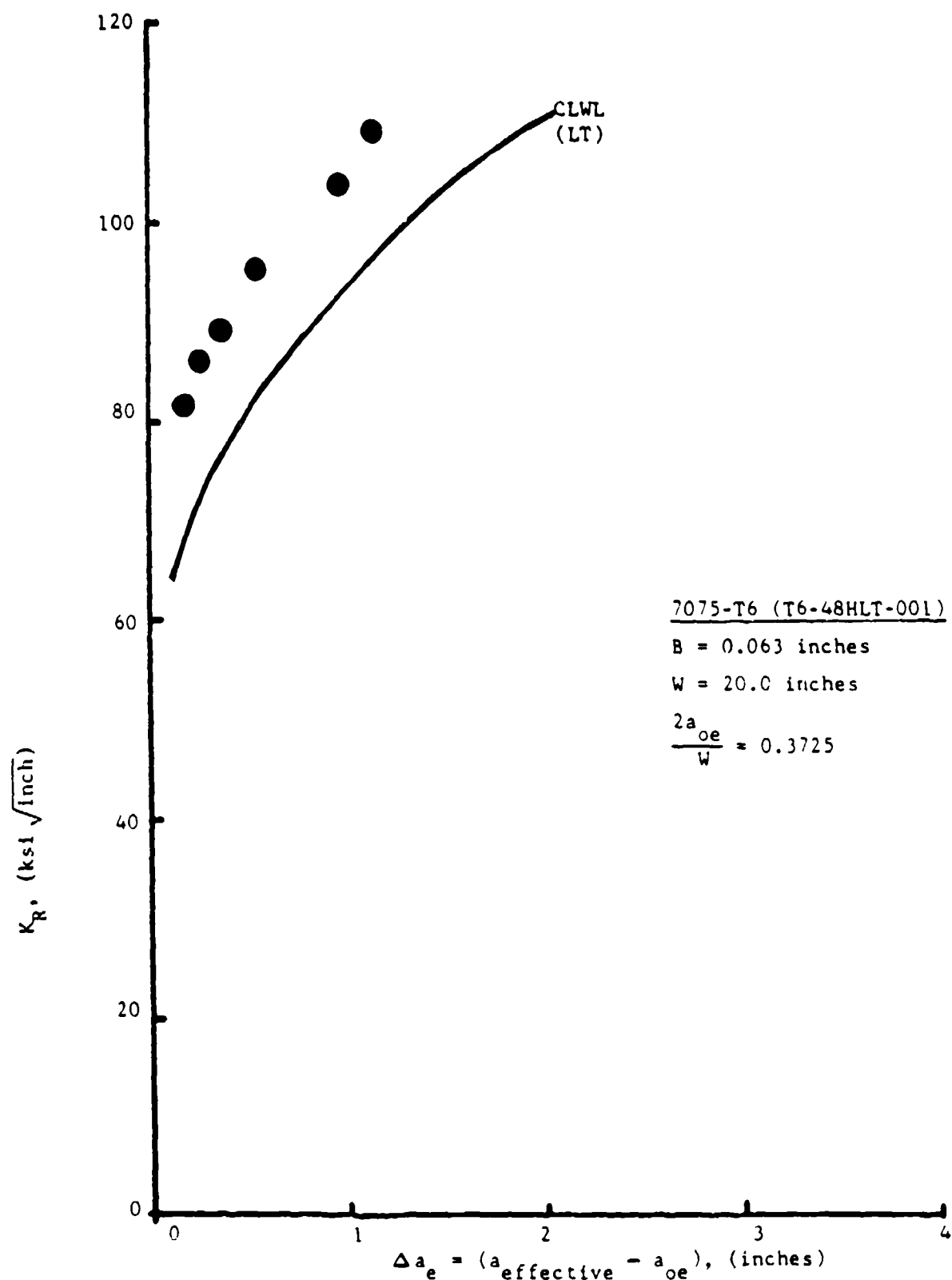


Figure 95. Comparison of CLWL and CCT Resistance Data - 0.063 Inch, 7075-T6

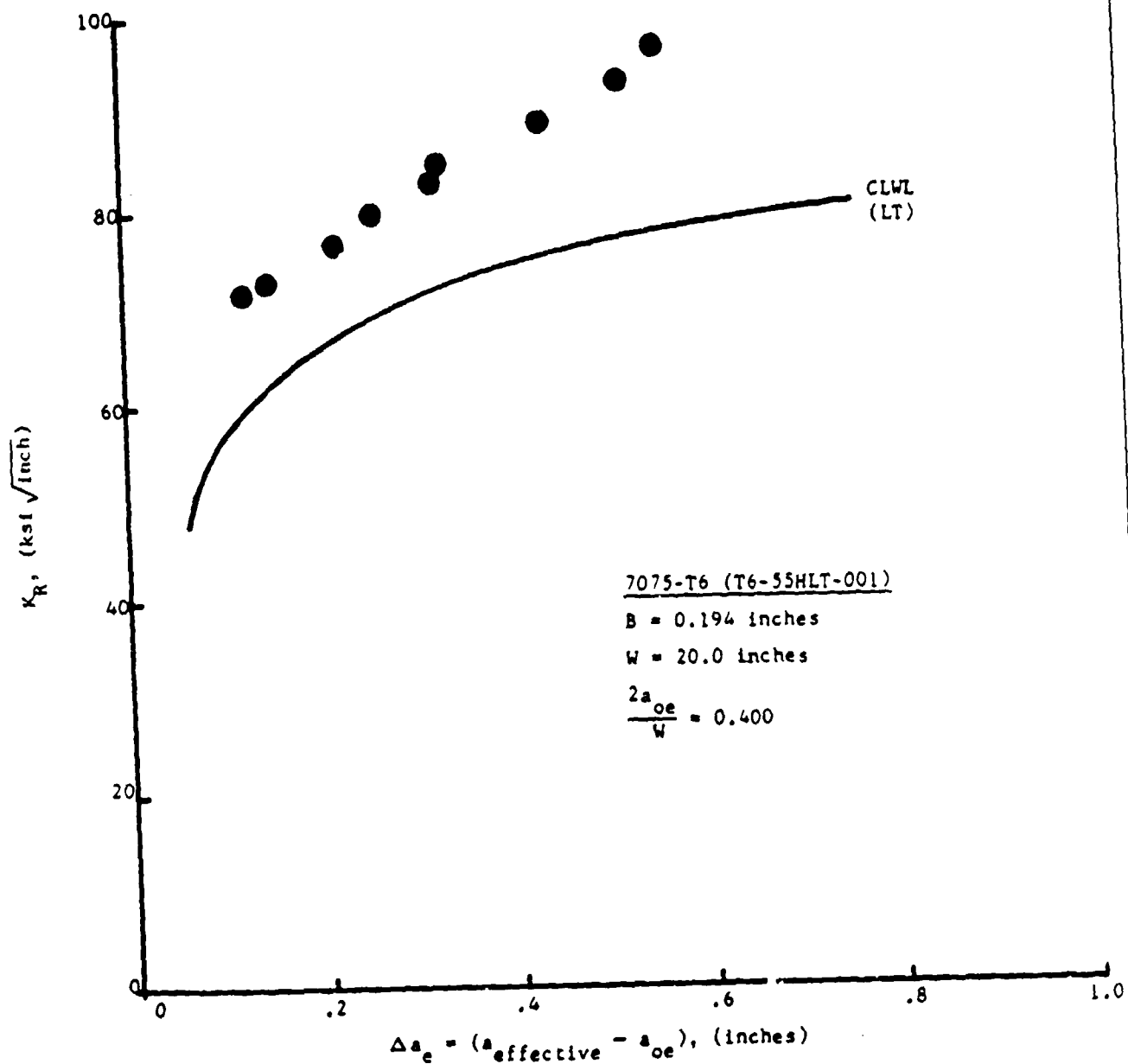


Figure 96. Comparison of CLWL and CCT Resistance Data - 0.194 Inch, 7075-T6

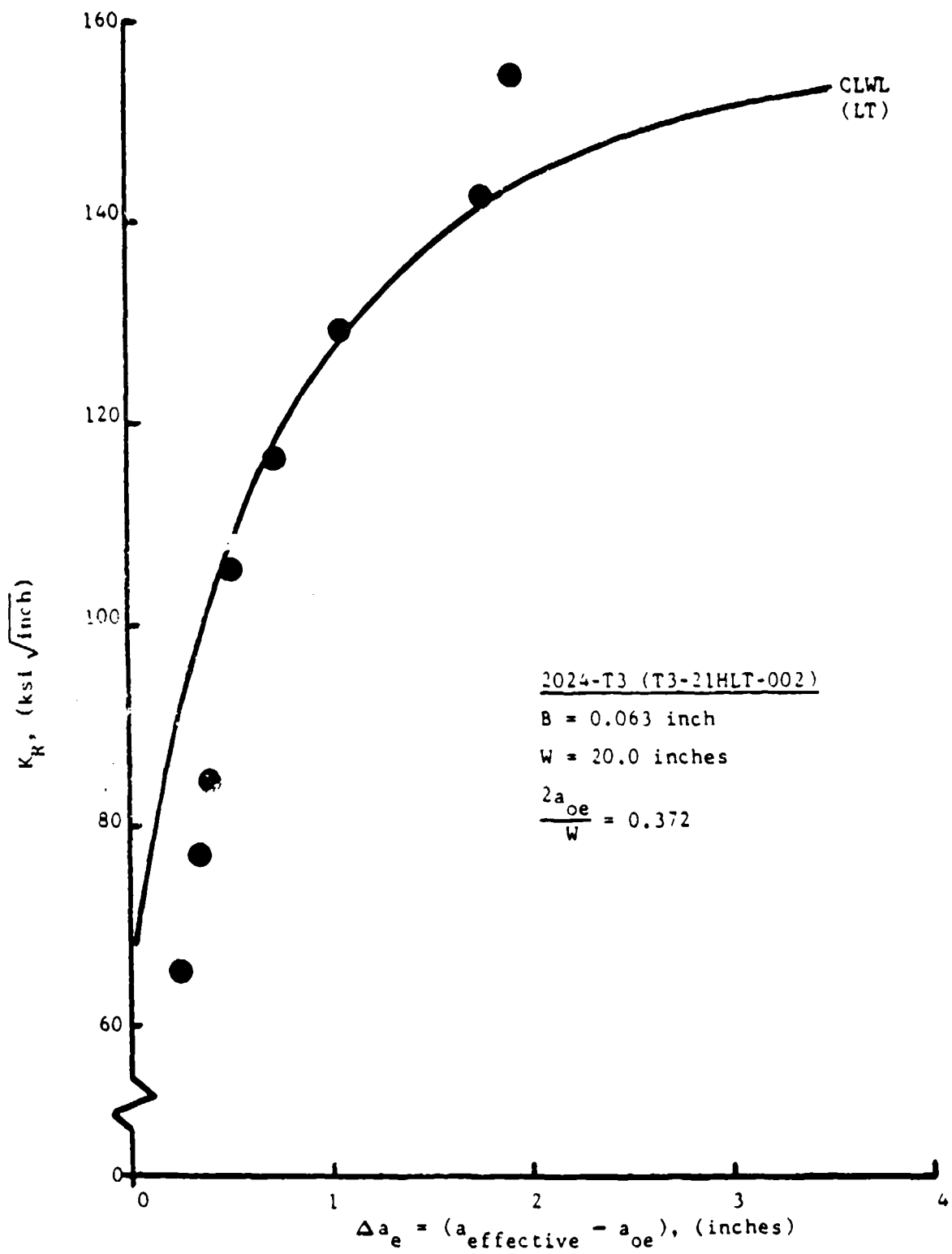


Figure 97. Comparison of CLWL and CCT Resistance Data - 0.063 Inch, 2024-T3

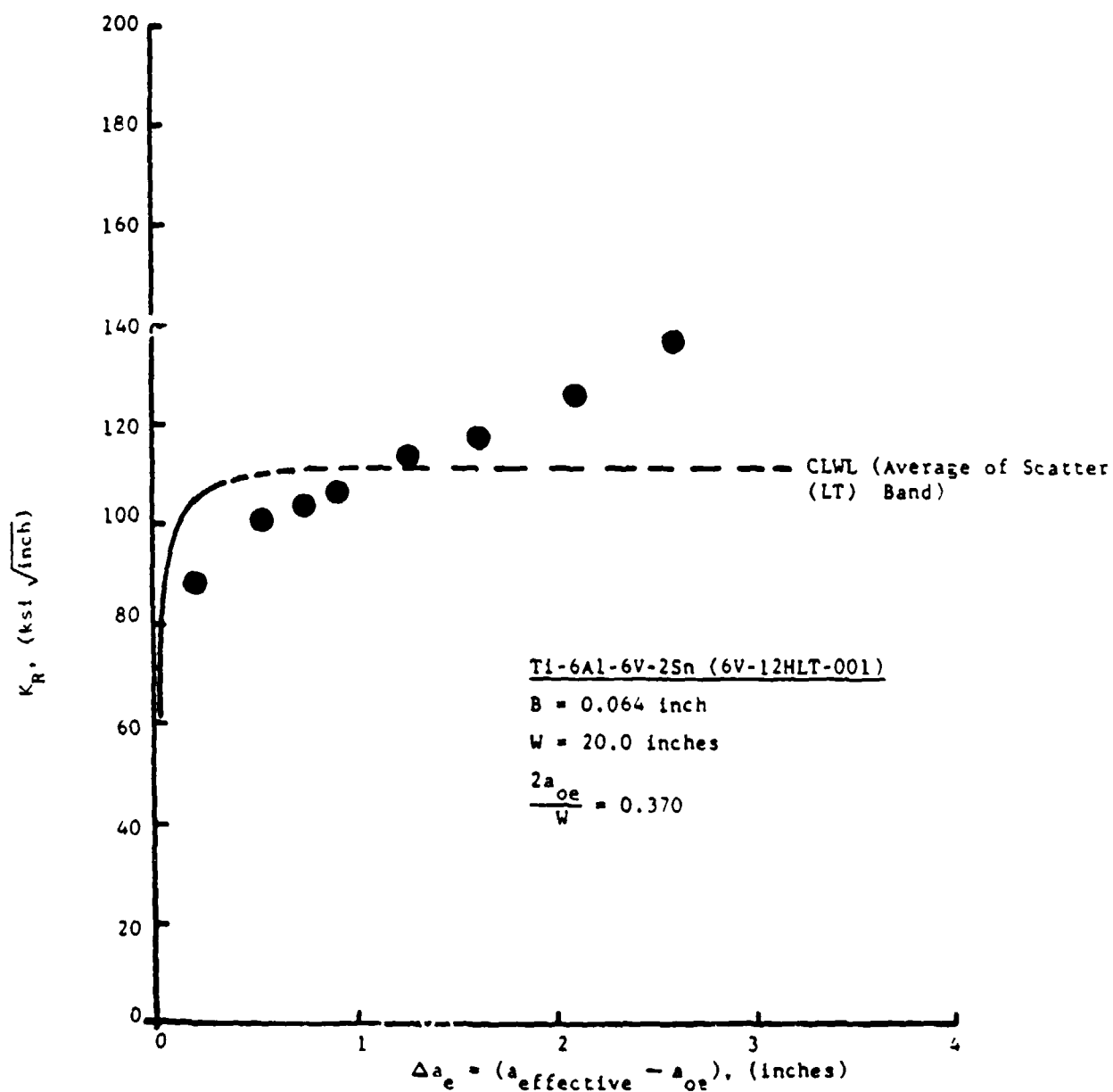


Figure 98. Comparison of CLWL and CCT Resistance Data - 0.064 Inch, Ti-6Al-6V-2Sn